ACTIVE VIBRATION CONTROL IN LINEAR TIME-INVARIANT AND NONLINEAR SYSTEMS

Thesis submitted in accordance with the requirements of
the University of Liverpool for the degree of
Doctor in Philosophy

by

Xiaojun Wei

June 2015

To my parents

ABSTRACT

Active vibration control techniques are widely used in linear time-invariant and nonlinear systems. However, there still exist many difficulties in the application of conventional active vibration control techniques, including the following: (1) In application, some of the degrees of freedom may not be physically accessible to actuation and sensing simultaneously; (2) large flexible structures are difficult in terms of isolating one substructure from the vibration of another; (3) the incomplete understanding of the effects of softening nonlinearity may put conventional active controllers at risk; and (4) global stability of under-actuated nonlinear aeroelastic systems, resulting from actuator failure or motivated by weight and cost constraints imposed on next-generation flight vehicles, is extremely challenging, especially in the case of uncertainty and external disturbances. These intellectual challenges are addressed in this research by linear and nonlinear active control techniques.

A new theory for partial pole placement by the method of receptances in the presence of inaccessible degrees of freedom is proposed. By the application of a new double input control and orthogonality conditions on the input and feedback gain vectors, partial pole placement is achieved in a linear fashion while some chosen degrees of freedom are free from both actuation and sensing. A lower bound on the maximum number of degrees of freedom inaccessible to both actuation and sensing is established.

A theoretical study is presented on the feasibility of applying active control for the purpose of simultaneous vibration isolation and suppression in large flexible structures by block diagonalisation of the system matrices and at the same time

assigning eigenvalues to the chosen substructures separately. The methodology, based on eigenstructure assignment using the method of receptances, is found to work successfully when the open-loop system, with lumped or banded mass matrix, is controllable.

A comprehensive study of the effects of softening structural nonlinearity in aeroelastic systems is carried out using the simple example of a pitch-flap wing, with softening cubic nonlinearity in the pitch stiffness. Complex dynamical behaviour, including stable and unstable limit cycles and chaos, is revealed using sinusoidal-input describing functions and numerical integration in the time domain. Bifurcation analysis is undertaken using numerical continuation methods to reveal Hopf, symmetry breaking, fold and period doubling bifurcations. The effects of initial conditions on the system stability and the destabilising effects of softening nonlinearity on aerodynamic responses are considered.

The global stability of an under-actuated wing section with torsional nonlinearity, softening or hardening, is addressed using a robust passivity-based continuous sliding-mode control approach. The controller is shown to be capable of stabilising the system in the presence of large matched and mismatched uncertainties and large input disturbance. With known bounds on the input disturbance and nonlinearity uncertainty, the continuous control input is able to globally stabilise the overall system if the zero dynamics of the system are globally exponentially stable.

The merits and performance of the proposed methods are exemplified in a series of numerical case studies.

ACKNOWLEDGEMENTS

I would like to express my sincere gratitude to my supervisor Prof. John Mottershead. I have been amazingly fortunate to have a supervisor who gave me the freedom to explore on my own and at the same time the guidance to recover when my steps faltered. His patience, kindness and support helped me overcome many difficult situations and finish this thesis. Also, I want to thank Prof. Yitshak Ram at Louisiana State University for his valuable help in the development of the theory of partial pole placement with inaccessible degrees of freedom.

I would also like to thank the Chinese Scholarship Council and the University of Liverpool for the award of a scholarship, which has supported me during my research.

I would like to thank my colleagues and academic members of Dynamics and Control Group at the University of Liverpool for their kind suggestions and support.

Finally, I would like to express my special thanks to my parents, sister and brother. They have been supportive and encouraging since I came to the University of Liverpool for PhD study.

LIST OF PUBLICATIONS

Journal papers

1. **X. Wei**, J.E. Mottershead, *Aeroelastic systems with softening nonlinearity*, AIAA Journal, 52 (2014) 1915-1927.

2. **X. Wei**, J.E. Mottershead, *Block-decoupling vibration control using eigenstructure assignment*, Mechanical Systems and Signal Processing, In press (2015). (doi: 10.1016/j.ymssp.2015.03.028)

3. **X. Wei**, J.E. Mottershead, Y.M. Ram, *Partial pole placement by feedback control with inaccessible degrees of freedom*, Mechanical Systems and Signal Processing, (submitted) (2015).

4. **X. Wei**, J.E. Mottershead, *Robust passivity-based continuous sliding-mode control for under-actuated nonlinear wing sections*, Journal of Guidance, Control, and Dynamics, (submitted) (2015).

Conference proceedings

1. **X. Wei**, J. Mottershead, *Limit cycle assignment in nonlinear aeroelastic systems using describing functions and the receptance method*, in: R. Allemang, J. De Clerck, C. Niezrecki, A. Wicks (Eds.) Topics in Modal Analysis, Volume 7, Springer New York, 2014, pp. 701-713.

2. **X. Wei**, J. Mottershead, *A Block Decoupling Control Algorithm for Vibration Suppression of Linear Structures*, in: J.K. Sinha (Ed.) Vibration Engineering and Technology of Machinery, Springer International Publishing, 2015, pp. 329-338

3. **X. Wei**, J.E. Mottershead, *Instability of aeroelastic systems with softening nonlinearity*, International Forum on Aeroelasticity and Structural Dynamics (IFASD), Bristol, UK, 2013.

4. **X. Wei**, *Aeroelastic systems with softening nonlinearity*, The Airbus Flight Physics Distributed R&T Partnership (DiPaRT), Bristol, UK, 2013.

5. **X. Wei**, A. Maha, Y.M. Ram, J.E. Mottershead, *The role of controllability and observability in partial pole placement by the method of receptance*, International Conference on Noise and Vibration Engineering (ISMA), Leuven, Belgium, 2014.

6. E. Papatheou, **X. Wei**, S. Jiffri, M. Prandina, M.G. Tehrani, S. Bode, K.V. Singh, J.E. S. Mottershead, J. Cooper, *Flutter control using vibration test data: theory, rig design and preliminary results*, International Conference on Noise and Vibration Engineering(ISMA), Leuven, Belgium, 2012.

7. S. Fichera, S. Jiffri. **X. Wei**, A. Da Ronach, N. Tantaroudas, J. E. Mottershead, *Experimental and numerical study of nonlinear dynamic behaviour of an aerofoil*, International Conference on Noise and Vibration Engineering(ISMA), Leuven, Belgium, 2014.

8. Fichera, S. Jiffri. **X. Wei**, J. E. Mottershead, *High bandwidth morphing aerofoil*, International Conference on Adaptive Structures and Technologies (ICAST), The Hague, The Netherlands, 2014.

CONTENTS

LIST OF FIGURES

NOMENCLATURE

AR	Aspect ratio of the wing
$\mathbf{B}$	Force distribution matrix
$\mathbf{b}$	Force distribution vector
b	Wing semi-chord
$\mathbf{C}$	Structural damping matrix
$\mathbf{C}_A$	Aerodynamic damping matrix
C_κ, C_θ, C_h	Structural damping coefficients in flap, pitch and plunge
C_{L_θ}, C_{M_θ}	Aerodynamic lift and moment coefficients due to the angle of attack
C_{L_β}, C_{M_β}	Aerodynamic lift and moment coefficients due to the deflection of trailing-edge control surface
c	Wing chord
$\mathbf{D}$	Acceleration feedback control gain matrix
$\mathbf{e}_k$	Unit vector at coordinate k
$\mathbf{F}$	Velocity feedback control gain matrix
$\mathbf{f}$	Velocity feedback control gain vector
$\mathbf{G}$	Displacement feedback control gain matrix
$\mathbf{g}$	Displacement feedback control gain vector
$\mathbf{H}$	Open-loop receptance matrix
$\hat{\mathbf{H}}$	Closed-loop receptance matrix
h	Displacement in plunge
$\mathbf{I}$	Identity matrix

I_κ , I_θ	Mass moments of inertia in flap and pitch
$I_{\kappa\theta}$	Product moment of inertia
$\mathbf{K}$	Structural stiffness matrix
$\Delta\mathbf{K}$	Structural stiffness uncertainty
$\mathbf{K}_A$	Aerodynamic stiffness matrix
K_κ , K_θ , K_h	Stiffness coefficients in flap, pitch and plunge
L	Aerodynamic lift about the elastic axis
$\mathbf{M}$	Structural mass matrix
M	Aerodynamic moment about the elastic axis
$\bar{m}$	Mass ratio of wing and air
m_w	Mass of wing
m_t	Total mass of wing and its supporting structure
n	Number of degrees of freedom
S	Sliding surface
s	Laplace variable
s_w	Wing span
$\mathbf{V}$	Matrix of open-loop eigenvectors
V	Free airflow speed
$\mathbf{v}$	Open-loop eigenvector
$\mathbf{W}$	Matrix of closed-loop right eigenvectors
$\mathbf{w}$	Closed-loop right eigenvector
$\mathbf{x}$	Vector of displacement in physical coordinate
β	Deflection of trailing-edge control surface
ε	Thickness of a boundary layer
$\zeta_\kappa, \zeta_\theta$	Structural viscous damping ratios in flap and pitch
θ	Pitch angle of the wing

κ	Flap angle of the wing
$\mathbf{\Lambda}$	Spectrum matrix
λ	Open-loop eigenvalue
$\lambda_{\min}(\bullet)$	Minimum eigenvalue of $(\bullet)$
$\lambda_{\max}(\bullet)$	Maximum eigenvalue of $(\bullet)$
μ	Closed-loop eigenvalue
ρ	Air density
$\mathbf{\Psi}$	Matrix of closed-loop left eigenvectors
$\boldsymbol{\psi}$	Closed-loop left eigenvector
$O(\bullet)$	Big O notation
$\mathbb{C}$	Field of complex numbers
$\mathbb{R}$	Field of real numbers
$\dot{}$	First derivative with respect to time t
$\ddot{}$	Second derivative with respect to time t
$\mathbf{null}(\bullet)$	Null space of $(\bullet)$
$(\bullet)^*$	Conjugate of a complex variable $(\bullet)$
$(\bullet)^T$	Transpose of $(\bullet)$
$(\bullet)^{-1}$	Inverse of $(\bullet)$
$\|(\bullet)\|_2$	Euclidean norm of $(\bullet)$
$\|(\bullet)\|_\infty$	Infinity norm of $(\bullet)$

Chapter 1

Introduction

1.1 Introduction

The subject of this thesis is vibration suppression in linear time-invariant (LTI) systems and nonlinear aeroelastic systems using active control techniques. The research will address several intellectual challenges in the development and application of active vibration control techniques.

Aircraft design is conservative for flight safety reasons. For example, a 15% margin of safety on the estimated flutter speed is regularly used to determine the useable flight envelope. As aircraft design moves toward lighter-weight material, to improve fuel efficiency and aircraft agility, it is anticipated that aircraft will operate closer to the flutter boundary. Also, nonlinear flutter, typically limit cycle oscillation (LCO), is not infrequently encountered by military and civil aircraft, such as those observed in the F-16 fighter [1, 2], F-18 fighter [2] and airbus A320 [3], leading to a reduction in aeroelastic performance, compromising the ability of pilots to perform critical mission-related tasks, structural fatigue and even failure of the vehicle. Furthermore, the requirements of next-generation flight vehicles place increasing and contradictory demands on designers, typically greater structural flexibility, improved manoeuvrability and greater operational safety in severe environmental conditions [4]. Therefore, developing advanced techniques to improve the flight safety and satisfy the contradictory requirements placed on next-generation flight vehicles is of

significant importance. Active vibration control, superior to passive modification, is a promising technique that can be helpful in the treatment of such aeroelastic problems.

Passive control methods have the advantage of guaranteed stability, but this is vastly outweighed by the flexibility of active methods to assign the dynamic of the system efficiently. For example, state feedback is capable theoretically of assigning all the eigenvalues of a system with a single input. On the other hand, structural modifications, such as the classical vibrations absorber, are awkward to use and must be tuned in an ad-hoc way. Also modifications in the form of added beams or masses are often impractical or too heavy. Much recent work has been carried out on nonlinear passive methods, including nonlinear vibration absorbers [5] and nonlinear energy sinks [6, 7]. Passive nonlinearities are difficult to design, may be difficult to retro-fit to existing hardware and in-situ modification to optimise performance may not be straightforward

Active feedback control for aircraft vibration suppression is a science in its infancy. There are examples of feed-forward control for vibration cancellation, mostly in rotorcraft, and some examples of active damping in fixed-wing aircraft. There are academic examples of flutter suppression in wind tunnels, but nonlinear active feedback control has never been applied to a production aircraft. There still exist many difficulties in the application of conventional active vibration control techniques, including the following: (1) In application, some of the degrees of freedom may not be physically accessible to actuation and sensing simultaneously; (2) large flexible flight vehicles are difficult in terms of isolating the aircraft cabin from unwanted vibrations, e.g., the vibration of engines; (3) the incomplete understanding

of the effects of nonlinearities, e.g., softening nonlinearity, may put conventional active controllers at risk; (4) there unavoidably exist uncertainty and external disturbances; and (5) global stability of under-actuated nonlinear aeroelastic systems, resulting from the failure of partial actuation or motivated by weight and cost constraints imposed on next-generation flight vehicles, is extremely challenging. These problems are addressed in this research by linear and nonlinear active control techniques.

In LTI systems, the method of receptances [8, 9] based on eigenvalue assignment will be further developed to cope with the first two challenges. Advantages include the following: (1) there is no need to know or to evaluate the **M**, **C**, **K** matrices usually determined from finite elements (FE) and containing errors due to modelling assumptions and approximations which must be corrected by model updating; and (2) there is no need for an observer or for model reduction - the receptance equations are complete for each sensor (output) measurement when the actuator inputs are measured. Generally there are a small number of actuators and the number of receptance equations is generally small. (3) By using the transfer function between actuator-input and sensor-output signals, any dynamic present in the actuation and sensing functions becomes included in the measurement so that mathematical modelling of the actuator/sensor dynamic becomes unnecessary. This is very advantageous in practical application since actuators (particularly) can possess unexpected modes not represented by the simple second order transfer functions often used in theoretical studies. In aeroelastic systems, the method of receptances, based on vibration tests carried out in-flight, is very advantageous in vibration suppression since unpredicted instabilities revealed during flight-tests will be controlled adaptively.

All systems in nature are inherently nonlinear. In aeroelastic systems, nonlinearity may lead to stable sustained periodic oscillation (stable LCO) in the vicinity of the linear flutter boundary. On the other hand, nonlinearity effects may result in wholly detrimental consequences. That is, a system that may be stable to a sufficiently small perturbation can become unstable due to a large disturbance [10]. Therefore, a good and complete understanding of the effects of nonlinearity in open-loop systems is crucial to effective active control design. Apparently, the presence of nonlinearity makes flutter suppression complicated. The problem becomes more difficult in nonlinear under-actuated aeroelastic systems with modelling errors and external disturbances.

The objective of the present work is to further develop the method of receptances for LTI systems with inaccessible degrees of freedom and those requiring the combination of active vibration suppression and active vibration isolation. Also, the present work aims to systematically understand aeroelastic systems with softening nonlinearity and design a robust passivity-based sliding mode controller for nonlinear under-actuated aeroelastic systems in presence of uncertainty and input disturbance.

1.2 Problem statement

In this section, the intellectual challenges considered in this thesis are described in detail. The challenges in LTI systems are ubiquitous and exist in linear aeroelastic systems. We begin with partial pole placement with inaccessible degrees of freedom.

1.2.1 Partial pole placement with inaccessible degrees of freedom

In practice, there may be a large number of eigenvalues but only a few that are undesirable. While reassigning some eigenvalues related to large vibrations, other

eigenvalues, which are not intended to be altered, are affected by the control input with full controllability. It frequently happens that some eigenvalues shift to the right hand side of the complex plane with full controllability. This is and effect of the spill-over phenomenon resulting in dynamical instability. Therefore, partial pole placement, where some eigenvalues are required to be relocated and the remaining poles are rendered unchanged, is of practical value in suppressing vibration and stabilising dynamic systems.

In the traditional application of active vibration control by partial pole placement with state feedback the input vectors are assumed to be given and the calculated vectors of the control gain are therefore in general fully populated. Consequently, to realise the control in practice it is required to sense the state at each degree of freedom. In applications, however, some of the degrees of freedom may not be physically accessible to actuation and sensing simultaneously. There exist some inaccessible degrees of freedom.

In order to overcome this difficulty it is possible to consider the input vectors to be unknown and to solve the partial pole assignment problem with the added constraint that certain prescribed elements of the input and control gain vectors vanish simultaneously. Such a problem would become a nonlinear problem due to the interaction between the unknowns in the input vectors and the unknowns of the control gains. The partial pole placement problem would thus be transformed from a linear to a nonlinear problem

In this research, a new theory for partial eigenvalue assignment by receptance-based active vibration control in the presence of inaccessible degrees of freedom is proposed. Both partial controllability and partial observability conditions are

exploited for maintaining the eigenvalues of open-loop system, intended to be unchanged. A new double input control involving position, velocity and acceleration feedback is proposed such that a linear system of constraints may be imposed causing chosen elements of the input vectors and the control gains to vanish. The methodology introduced in the research enables the input vectors and the vectors of control gains to be determined linearly while chosen degrees of freedom are rendered free from force excitation and state sensing. Hence, the nonlinear problem of determining input vectors and the control gains for partial pole placement with inaccessible degrees of freedom is converted into a linear one. A lower bound on the maximum number of degrees of freedom completely cleared of both sensing and actuation is then established using purely linear analysis.

1.2.2 Block decoupling vibration control using eigenstructure assignment

Active vibration isolation is a technique of vibration control by means of reducing transmitted forces between the isolated structure and its surroundings and its application is ubiquitous. It is well suited to industrial problems where a relatively massive piece of engineering hardware, such as an engine-block or a heavy machine tool is to be isolated from its surroundings. In the classic active vibration isolation methods, the isolated structure and its surroundings are assumed to be rigid and single degree of freedom models are used for analysis and design. Spacecraft structures, such as deployable antennae, space telescope or solar arrays, large flexible aircrafts and light-weight multi degree of freedom structures generally, are much more difficult in terms of isolating one substructure from the vibration of another since the rigid body assumption is invalid. The flexibility should be modelled, typically using finite element methods [11] or analytical impendence and mobility

[12-14]. In this research, experimentally measured receptances are used to represent the flexibility of large-scale flexible structures.

In practice, it frequently happens that the isolated system is excited by multiple disturbances. The active vibration isolator, designed for isolating one of the disturbances, might be invalid since the isolated structure might still be prone to large amplitude oscillation or instability in the presence of other disturbances. Therefore, for flexible structures subjected to multiple excitation sources, it is of importance to combine active vibration isolation and active vibration suppression such that the isolated structure is isolated from its surrounding structures and also its behaviours can be regulated subjected to other excitation sources. This problem appears to be one that has received very little attention in the vibrations control literature to date.

In this research, we consider from a purely theoretical point of view, the feasibility of decoupling multi degree of freedom systems to form substructures that are completely isolated from one another and with desired performances. The research reported in this article is a preliminary study, which might be deemed timely in view of contemporary interest in lightweight and deployable structures, piezo-based actuators and sensors with proven capability and a related literature on active input-output decoupling. In this research, a new block decoupling control algorithm based on eigenstructure assignment, simultaneous eigenvalue and eigenvector assignment, using measured receptances is proposed for the combination of structural vibration suppression and vibration isolation. Modal degree of freedom constraints are imposed such that the matrix of closed-loop right eigenvectors is block-diagonalised, leading to block diagonal matrices of the second-order system in physical

coordinates. For the purpose of simplicity, we limit the investigation in this thesis to the problem of block decoupling to form two independent substructures from a linear multi degree of freedom system. It is straightforward to show that the approach can be extended to the case of multiple independent substructures and also diagonal decoupling in physical coordinates.

1.2.3 Nonlinear analysis of aeroelastic systems with softening nonlinearity

It is well known that classical linear aeroelasticity is able to provide accurate predictions for comparison with flight test results, including aeroelastic response to gust, turbulence and external excitation as well as flutter boundary estimation. However, aeroelastic systems are inherently nonlinear. Structural nonlinearities typically arise from free-play at the inter-connections between different components, such as the wing-pylon-engine connections or the attachment of external stores to the wing. Other structural nonlinearities include geometric ones due to large wing deflections and nonlinear damping. Aerodynamic nonlinearities may be introduced by shock motion in transonic flow and flow separation [10, 15]. A good understanding of the effects of structural and aerodynamic nonlinearities on the stability of aeroelastic system is crucial to the efficient and safe design of aircraft wings and control surfaces. The complexity of dynamic behaviour of systems with softening structural nonlinearity is one of the least well understood aeroelastic phenomena. Although, softening nonlinearities might be less prevalent than hardening ones, they are not uncommon. They tend to occur in structures under compressive loads such as panel buckling [16]. Also, kinetic heating at high Mach numbers can produce large reductions in structural stiffness and softening

nonlinearity [15]. Therefore, the dynamics of aeroelastic systems with softening nonlinearity is a topic of practical engineering significance.

This research aims to investigate the presence of stable and unstable LCO and the conditions under which they may be found in aeroelastic systems with softening nonlinearity. LCO stability criteria, strictly applicable within the limitations of quasilinearisation by sinusoidal-input describing functions, are confirmed by numerical integration in the time domain. Excellent agreement is found at low steady-state amplitudes and even at higher amplitudes the approximation is found to be close to accurate time-domain predictions. The analysis confirms the existence of stable LCO, dependent upon initial conditions, and shows that a softening nonlinearity can destabilise LCO and chaos as well as prohibiting the occurrence of certain predicted LCO. Results are presented conveniently in the form of graphs of steady-state amplitude versus velocity and as basins of attraction with regions of stability, stable LCO, dynamic instability and static divergence. The boundaries separating the regions of different dynamic behaviour may be simple or non-simple depending upon the parameters of the aerofoil considered.

1.2.4 Robust flutter suppression of nonlinear aeroelastic systems

Nonlinear flutter may result in a reduction in vehicle performance, structural fatigue and even the failure of vehicle. Never-the-less the requirements of next-generation flight vehicles place increasing and contradictory demands on designers, typically greater structural flexibility, improved manoeuvrability and greater operational safety in severe environmental conditions [4]. Hence, active nonlinear flutter suppression becomes increasingly important in ensuring the safety and efficiency of future

aircraft [17] and presents intellectual challenges that have attracted the interest of researchers in aerospace and control communities for more than three decades.

Since linear active vibration control techniques have been proved to have limited success in the suppression of nonlinear flutter [18], nonlinear active vibration techniques should be used.

In the control community, mechanical systems which have fewer independent actuators than degrees of freedom to be controlled are known as under-actuated mechanical systems [19]. The control design of under-actuated aeroelastic systems is of importance, firstly for reasons of actuator failure and the need to rely on fewer actuators. Secondly, under-actuation might be motivated by weight and cost constraints imposed on next-generation flight vehicles. A typical under-actuated aeroelastic system is a two-dimensional nonlinear wing section with a single control surface in incompressible flow, which is the control objective of the present thesis.

Usually, for under-actuated systems, local asymptotic stability can be achieved by existing nonlinear control techniques. However, global asymptotic stabilisation for tracking control of under-actuated mechanical systems is considered to be extremely challenging [19, 20]. For example, by using feedback linearisation techniques, the stability of the zero dynamics only guarantees local stability of the system, global asymptotical stability can only be achieved if the internal dynamics is input-to-state stable [21]. Under-actuated nonlinear aeroelastic systems are even more complicated owing to the intrinsic uncertainty and/or softening nonlinearity.

This research is to develop a robust passivity-based continuous sliding-mode control approach, which can globally stabilise all the degrees of freedom of an under-actuated prototypical wing section with hardening or softening torsional nonlinearity

in the presence of nonlinearity uncertainty and input disturbance. The approach makes good use of the robustness of sliding-mode control to large matched uncertainty and large input disturbances. To deal with mismatched uncertainty in under-actuated systems, a robust passivity-based control method is used for the design of globally asymptotically (or exponentially) stable nonlinear sliding surfaces. Moreover, a proposed continuous sliding-mode control is able to alleviate the chattering which occurs in the process of discontinuous sliding-mode control. The sufficient conditions for global asymptotic stability and global stability of under-actuated two-degree-of-freedom nonlinear aeroelastic systems are provided. Compared with feedback linearisation or adaptive feedback linearisation, the proposed method relaxes the requirements for global asymptotical stability because it does not require the internal dynamics to be input-to-state stable. Bounds must be specified on the nonlinear uncertainty, but knowledge of the structure of the nonlinearity is not needed.

1.3 The scope of thesis

Chapter 2 reviews the literature on active vibration control in LTI systems and nonlinear aeroelastic systems and nonlinear aeroelastic analysis.

A new theory for partial eigenvalue assignment by receptance-based active vibration control in the presence of inaccessible degrees of freedom is proposed in Chapter 3. Also, the solvability conditions are discussed. Furthermore, a lower bound on the maximum number of degrees of freedom inaccessible to both actuation and sensing is established. For simplicity, distinct eigenvalues in both open and closed loops are assumed.

Chapter 4 reports a new block decoupling vibration control algorithm based on eigenstructure assignment using measured receptances. The investigation in this research is limited to the problem of block decoupling to form two independent substructures from a linear multi degree of freedom system. It is straightforward to show that the approach can be extended to the case of multiple independent substructures and also diagonal decoupling in physical coordinates. The eigenvalue assignment is limited to the case of distinct eigenvalues in both open and closed loops. The number of actuators and sensors required in the case of banded damping and stiffness matrices is considered. The research presented is a preliminary theoretical study.

Chapter 5 presents comprehensive nonlinear aeroelastic analysis of aeroelastic systems with softening nonlinearity using sinusoidal-input describing functions, numerical integration in the time domain and numerical continuation techniques. Complex dynamic behaviour is demonstrated using the illustration of a nonlinear binary flutter model with a cubic stiffness in the pitch degree of freedom.

Chapter 6 addresses the global stability of an under-actuated wing section with hardening or softening nonlinearity using a robust passivity-based continuous sliding-mode control approach. The controller is shown to be capable of stabilising the system in the presence of large matched and mismatched uncertainties and large input disturbance. With known bounds on the input disturbance and nonlinearity uncertainty, the continuous control input is able to globally stabilise the overall system if the zero dynamics of the system are globally exponentially stable.

Conclusions are drawn and the future work proposed in Chapter 7.

Chapter 2

Literature review

2.1 Introduction

The purpose of this chapter is to present an overview of literature on active vibration control in LTI systems and nonlinear aeroelastic systems. The literature of active vibration control in linear systems includes (i) eigenvalue assignment (ii) eigenstructure assignment and (iii) decoupling control.

The literature of active vibration control in nonlinear aeroelastic systems covers (a) nonlinear aeroelastic analysis and (b) active nonlinear flutter suppression.

2.2 Active vibration control in LTI systems

Active vibration control, by applying control forces to structures using actuators based on the signals perceived by sensors, enables desired performances to be achieved actively. Active vibration control strategies may be classified into two categories: feedback and feedforward control [22]. With the availability of disturbance signals, feedforward active vibration control methods can effectively alleviate unwanted vibrations due to the disturbances. When the disturbances are not available, feedback active vibration control approaches are widely used and also employed in this research. In feedback active vibration control, the feedback may affect the transmission path of disturbance such that unwanted oscillations are suppressed. A typical technique of transmission path control is active vibration

isolation. On the other hand, eigenvalue assignment is a commonly used active vibration suppression technique to affect disturbed structures directly by relocating eigenvalues. Apart from assigning eigenvalues, the use of multi-input feedback control allows to select closed-loop eigenvectors such that the closed-loop responses are reshaped. The simultaneous eigenvalue and eigenvector assignment is known as eigenstructure assignment. Decoupling vibration control is to decouple a structure into substructures such that the transmitted forces between substructures are eliminated and desired performances are achieved for each substructure, which may be viewed as the combination of active vibration isolation and active vibration suppression. We begin with reviewing the progress of active vibration control by using eigenvalue assignment.

2.2.1 Eigenvalue assignment

In LTI systems, eigenvalues determine the decay or growth rate of system's response. The problem of eigenvalue placement, relocating the eigenvalues of a linear system such that its behaviour is altered as desired, has received considerable attention from the active control and vibration communities over several decades [23]. The eigenvalue assignment problem has many potential applications in structural dynamics, including the improvement of the stability of dynamic systems, avoidance of the damaging large-amplitude vibrations close to resonance, and adaptive changes to system behaviour. Wonham [24] stated that the closed-loop poles may be assigned arbitrarily by complete state feedback if the system is controllable. Davison [25] generalised Wonham's results for the case of incomplete state feedback and demonstrated that a subset of closed-loop poles can be assigned but nothing was said about the remaining poles of the system. Kimura [26] improved Davison's results

and showed that if the system is controllable and observable, then under certain conditions an almost arbitrary set of distinct closed-loop poles is assignable by gain output feedback. Constrained output feedback in the form of fixed zeros within the feedback matrix [27] can lead to inexact assignment to desired locations [28]. Fletcher and Magni [29], Fletcher [30] and Magni [31] investigated and proved that exact assignment of distinct poles using real output feedback is possible in any controllable and observable LTI multivariable system in which the number of inputs plus the number of outputs exceeds the number of states. By virtue of multi-input feedback control, the robust pole assignment problem, featured by the requirement that the assigned poles should be insensitive to perturbations, was studied by researchers, such as Byers and Nash [32], Kautsky et al. [33, 34], Chu and Datta [35] and Chua [36].

In practice, there may be a large number of eigenvalues but only a few that are undesirable. Therefore, partial pole placement, where some eigenvalues are required to be relocated and the remaining poles are rendered unchanged, is of practical value in suppressing vibration and stabilising dynamic systems. Saad [37] proposed a projection algorithm for the partial eigenvalue assignment for first-order systems. Datta et al. [38] developed an closed-form solution to the partial pole assignment problem by state feedback control in systems represented by second order differential equations. The method has been generalised for the case of multi-input control [39, 40]. Chu [36] also proposed a partial pole assignment method with state feedback for second-order systems. The robust partial pole placement problem was investigated in [41-44]. The problem of optimising control efforts in the partial eigenvalue assignment problem was addressed by Guzzardo et al. [45]. The problem of partial pole placement with time delay was considered in [46-48].

Recently, Ram and Mottershead [8] developed a new theory known as the receptance method for eigenvalue assignment in active vibration control using measured receptances. The receptance method has a wealth of advantages. There is no need to estimate or know the mass, stiffness and damping matrices, which are usually obtained from a finite element model. While by conventional methods force equations are formed using dynamic stiffness and the algorithms are based on the assumption that the dimension of the system is finite and measurable at every degree of freedom, in the receptance method the motion of system is represented by displacement equations. It can be seen that a complete displacement equation is formed for each measured degree of freedom provided each of the external forces applied by a small number of actuators is measured. Therefore, there is no need to estimate the unmeasured state using an observer or a Kalman filter and no need for model reduction. A series of experimental tests using collocated accelerometers and inertial actuators on a T-shaped plate were carried out to demonstrate the capability of the receptance method in active vibration suppression [49]. Ghandchi Tehrani et al. [50] developed the theory of partial pole placement using measured receptance for single-input and multi-input state feedback control. For multi-input control case, partial pole assignment was implemented by the sequential assignment of poles, ensuring at each step that previously assigned eigenvalues were unaffected by spillover of the most recently assigned pair of poles. Experimental implementation included (1) a lightweight glass-fibre beam with MFC sensors and actuators and (2) a heavy modular test structure in two configurations using electromagnetic actuators and piezoelectric accelerometers. The terminology “receptance” has become generalised to the ratio of inputs and outputs, for example input and output voltage signals to the actuators and from sensors, so that the sensor and actuator dynamics

were embedded in the measured data. The application of the receptance method to the vibration control of large industrial scale structures [51] and flutter suppression in aeroelastic systems [52-54] have been described. Very recently, Ram and Mottershead [9] developed a new theory of pole placement in active vibration control using the receptance method, which allows for multi-input state feedback partial pole assignment in a single application of the routine and is superior to the sequential application of single-input control.

2.2.2 Eigenstructure assignment

In LTI systems, the right eigenvectors fix the shape of the mode while the product of initial conditions and the left eigenvectors determines the amount each mode is excited in the response. By the use of multi-input feedback control, the closed-loop system cannot be uniquely determined by only assigning eigenvalues. That is, in addition to the eigenvalue assignment, there exists a freedom to assign eigenvectors. Eigenstructure assignment, simultaneous assignment of eigenvalues and eigenvectors, brings out design freedom beyond eigenvalue assignment. Moore [55] identified for the first time this freedom offered by state feedback beyond pole assignment in the case where the prescribed poles are distinct. Klein and Moore [56] presented an eigenstructure assignment method in the case of non-distinct closed-loop eigenvalues. Fahmy and O'Reilly [57] introduced a parametric approach of eigenstructure assignment using state feedback, in which the assignable set of eigenvectors is dependent upon arbitrarily chosen parameters. Srinathkumar [58] investigated the eigenstructure assignment problem using output feedback. He derived sufficient conditions for the maximum number of assignable eigenvalues via output feedback and also determined the maximum number of eigenvectors which can be partially

assigned with certain number of entries arbitrarily chosen. To preserve the symmetry and sparseness of system matrices of second-order mechanic systems, some eigenstructure assignment techniques were developed for second-order mechanic systems. Inman and Kress [59] developed an eigenstructure assignment approach using inverse eigenvalue methods for mechanical systems represented by second-order systems of differential equations. Datta et al. [60] presented a partial eigenstructure assignment algorithm for systems modelled by a set of second order differential equations such that certain eigenpairs of a vibrating system may be assigned while the other eigenpairs remain unchanged. Ram and Mottershead [9] proposed a multi-input partial pole placement method based on measured receptances of open-loop systems, in which some modal constraints may be imposed on closed-loop right eigenvectors.

A judicious choice of a right eigenvector may be useful in reshaping closed-loop responses while a judicious choice of a left eigenvector may prevent a mode from being excited. Simultaneous assignment of eigenvalues and right eigenvectors is known as right eigenstructure assignment. By contrast, simultaneous assignment of eigenvalues and left eigenvectors is known as left eigenstructure assignment. Right and/or left eigenstructure assignment has been widely applied for active vibration control.

Disturbance decoupling, which aims to make the disturbance have no effects on controlled output, was considered in [61] by right eigenstructure assignment. Sobel et al. [62, 63] employed eigenstructure assignment to obtain some decoupled aircraft motions in flight control systems. Specifically, some modes are decoupled by specifying some entries of the corresponding right eigenvectors to be zero. Song and

Jayasuriya [64] proposed an algorithm primarily for modal localisation by prescribing the entries associated with certain areas of closed-loop right eigenvectors to relatively small values. Therefore, the vibration of these areas is relative small and the vibrational energy is restricted to the other areas. Shelley and Clark [65] presented an eigenvector assignment algorithm for modal localisation in mass-spring systems. The closed-loop eigenvalues were kept the same as their open-loop values. The closed-loop eigenvectors were given by scaling the entries, related to isolated areas, of the complete set of open-loop eigenvectors with a small factor while the entries related to localised areas with a big factor. Therefore, the displacements in the isolated areas would be proportionally smaller than the displacements in the localised portions of the system. An experimental implementation of their algorithm was presented in [66]. Also, they generalised the idea of modal localisation to distributed parameters systems [67, 68]. It was also shown that the performance of modal localisation depends on the number of actuators.

Zhang et al. [69] used left eigenstructure assignment to reject undesired inputs to a vibrating flexible beam by orthogonalising left eigenvectors to the disturbance input matrix. Orthogonalising left eigenvectors to disturbance input matrix may degrade the controllability of the system. Both controllability and the disturbance rejection using left eigenstructure assignment were considered simultaneously in [70]. In [69, 70], zeros were prescribed to the entries of the desired left eigenvectors corresponding to nonzero entries of the forcing vector. Alternatively, Wu and Wang [71] minimised the inner product of each left eigenvector and each forcing vector such that each left eigenvector was as closely orthogonal to each forcing vector as possible. It is understandable that the simultaneous assignment of right and left eigenstructure may improve the control performance or achieve multiple control

objectives. However, the assignment of left eigenstructure conflicts with that of right eigenstructure because they are coupled with each other. Choi [72] proposed an algorithm for simultaneous approximate assignment of left and right eigenstructure such that disturbance rejection and the disturbance decoupling are approximately achieved. Wu and Wang [73] presented a simultaneous left and right eigenstructure assignment method for active vibration isolation. Specifically, the left eigenvectors were prescribed to be as closely orthogonal to the forcing vector of the system as possible and the entries associated with the concerned region of the right eigenvectors are constrained to relatively small values. A performance index was minimised such that simultaneous assignment left and right eigenstructure was approximately achieved.

2.2.3 Decoupling vibration control

Decoupling vibration control is to decouple a structure into substructures such that the transmitted forces between substructures are eliminated and desired performances are achieved for each substructure.

A related, but different problem is that of input-output decoupling in LTI multivariable control. The purpose of input-output decoupling is simplification to form a number of single variable systems by the elimination of cross-couplings between the variables of the system. There is an extensive literature on this topic spanning several decades using state feedback (Morgan [74], Falb and Wolovich [75], Gilbert [76] and Descusse et al. [77]) and output feedback (Paraskevopoulos and Koumboulis [78], Howze [79], Denham [80] and Descusse [81]). The combined problem of simultaneous decoupling and pole placement in LTI multivariable systems was addressed by several authors [75, 82-84] and the block decoupling

problem was investigated [85-91]. A transfer function matrix approach with block-decoupling was proposed by Hautus and Heymann [92] and Commault et al. [93] and unity-output feedback systems with decoupling and stability was investigated using a transfer function matrix approach [94-97], especially for vibration control of industrial-scale structures. Q.-G. Wang provides a detailed account of input-output decoupling control in the research monograph [98].

Although there are considerable volumes of literature devoted to the development of theoretical input-output decoupling methods, far less attention has been paid to the application of decoupling to structural vibration control. Zacharenakis [99, 100] investigated the decoupling problems of civil engineering structures via state/output feedback with the assumption that the number of inputs is equal to the number of outputs. Li et al. [101] proposed decoupling control law for vibration control of multi-story building using a diagonal mass matrix and tri-diagonal damping and stiffness matrices. The control laws were based on the second-order matrix differential equations directly.

Almost all the existing input-output decoupling algorithms are developed based on first-order state space formulation. In structure dynamics, it is preferable to deal with dynamic equations in the second-order form rather than in the first order state-space form. This is due to the fact that converting the equations of motion into a first-order state-space formulation, the bandedness, definiteness and symmetry, of the mass damping and stiffness matrices are lost [102]. Also, anther obvious drawback of a first-order realisation is that the system matrices become $2n \times 2n$, which is computationally expensive if the order of the system n is large [103]. The transfer function matrix approach, which requires much algebraic manipulation of rational

functions, becomes increasingly complicated as the dimension of the system increases.

2.3 Active vibration control in nonlinear aeroelastic systems

All aeroelastic systems in nature are nonlinear. It is known that linear analysis and active vibration control methods have limited performances in nonlinear aeroelastic systems. Therefore, the modelling and performance of systems can be improved by applying nonlinear analysis methods. A good understanding of open-loop nonlinear aeroelastic systems is crucial to nonlinear control design. In what follows, the literature starts with nonlinear aeroelastic analysis, followed by nonlinear active flutter suppression.

2.3.1 Nonlinear aeroelastic analysis

It is well known that classical linear aeroelasticity is able to provide accurate predictions for comparison with flight test results, including aeroelastic response to gust, turbulence and external excitation as well as flutter boundary estimation. However, aeroelastic systems are inherently nonlinear. Structural nonlinearities typically arise from free-play at the inter-connections between different components, such as the wing-pylon-engine connections or the attachment of external stores to the wing. Other structural nonlinearities include geometric ones due to large wing deflections and nonlinear damping. Aerodynamic nonlinearities may be introduced by shock motion in transonic flow and flow separation [10, 15]. A good understanding of the effects of structural and aerodynamic nonlinearities on the stability of aeroelastic system is crucial to the efficient and safe design of aircraft wings and control surfaces. The complexity of dynamic behaviour of systems with softening structural nonlinearity is one of the least well understood aeroelastic

phenomena and forms one of the topics in the thesis. Although, softening nonlinearities might be less prevalent than hardening ones, they are not uncommon. They tend to occur in structures under compressive loads such as panel buckling [16]. Also, kinetic heating at high Mach numbers can produce large reductions in structural stiffness and softening nonlinearity [15]. Therefore, the dynamics of aeroelastic systems with softening nonlinearity is a topic of practical engineering significance.

Although there are great volumes of literature devoted to nonlinear aeroelastic analysis of hardening nonlinearity, far less attention has been paid to aeroelastic systems with softening nonlinearity. Woolston et al. [16] studied the effects of cubic nonlinearities on the flutter of a two-degree-of-freedom system using an analogue computer. They discovered that the softening spring had a destabilising effect on flutter. In particular, flutter could be induced below the linear flutter speed and oscillations above the flutter boundary were found to be highly divergent. Lee et al. [104] studied the flutter characteristics of a two-dimensional aerofoil in an incompressible flow with a cubic structural restoring force. Their numerical results, obtained using a fourth-order Runge-Kutta scheme, showed that the divergent flutter boundary was dependent upon on initial conditions when a softening nonlinearity was present. The system stability close to equilibrium was presented using a plot similar to the bifurcation diagram. They discovered that the motion was stable when the initial displacement was less than a threshold value at the flutter boundary. Beyond the flutter boundary the system diverged rapidly. Liu and Chan [105] investigated the limit cycle behaviour of a rigid sweptback wing with a tip mass connected by a tri-linear spring and aerodynamic forces determined using a doublet lattice method. Analysis was carried out using the harmonic balance method and a

fourth order Runge-Kutta procedure. Using the harmonic balance method they predicted stable, semi-stable and unstable LCO for hardening and softening nonlinearities and confirmed the predicted stable LCO by numerical integration. Unfortunately, the numerical integration did not show the predicted unstable and semi-stable LCO. Dimitriadis et al. [106] employed the extended centre manifold technique to predict bifurcation conditions and limit cycle oscillation amplitudes for simple aeroelastic systems with hardening or softening cubic stiffness nonlinearities. In the case of the hardening cubic nonlinearity, the extended centre manifold linearisation produced very good predictions of the LCO amplitudes in the nonlinear degree of freedom. In the case of the softening cubic nonlinearity the same method produced a so-called 'worst-case' stability boundary - a combination of the predicted static divergence and dynamic instability boundaries - which was found to be significantly narrower than the stability envelope predicted by numerical integration. LCO was not predicted for the case of softening cubic nonlinearity. Ghadiri and Razi [107] investigated the nonlinear aeroelastic analysis of rectangular flexible cantilever wings with cubic nonlinearity. As for hardening nonlinearity, they used a higher-order harmonic balance method to predict the amplitude and frequency of LCO. A better agreement between frequency and time domain results was achieved by using the higher-order harmonic balance method. For the wings containing softening cubic nonlinearity, LCO was found not to occur in the vicinity of the linear flutter. According to [108], subcritical LCO induced by softening nonlinearity is unstable but turns into a stable large-amplitude LCO due to the existence of higher-order hardening nonlinearities.

The reported nonlinear responses of aeroelastic systems with softening nonlinearity can be classified into two categories. First, in the presence of softening nonlinearity,

the aeroelastic responses are reported to be dependent upon initial conditions and to take the form of divergent flutter well below the linear flutter boundary. Secondly, there may exist stable, semi-stable and unstable LCO in softening nonlinear aeroelastic systems. In terms of stable LCO, contradictory comments can been found in references [105] and [108]. Stable LCO are predicted for aeroelastic systems with tri-linear stiffness in [105]. However, according to comments in [108], the same system will only result in unstable LCO because of the absence of higher-order hardening nonlinearity. Although it is recognised that unstable LCO exist in softening nonlinear aeroelastic systems, as predicted by frequency-domain methods in reference [105], the reporting of numerical or experimental results that show the presence of unstable LCO is very limited. This is usually explained by the statement that unstable LCO are sensitive to small perturbation. Stable LCO are not always reported in aeroelastic system with softening nonlinearities and ambiguous explanations for the destabilising effects of softening nonlinearity are present in the literature. It can be seen that the literature on softening stiffness nonlinearity in aeroelastic systems is not definitive, contains partial explanations and even conflicting results.

At this point a small clarification regarding concepts of divergence and flutter (static and dynamic instability) will be helpful to the understanding of later discussion in this article. Whereas, flutter of a linear system is a dynamic instability characterised by an exponential growth of the oscillation with time, the flutter of a nonlinear system may be amplitude limited, neutrally stable and referred to as LCO. Use of the term ‘divergence’ will be reserved for the non-oscillatory static instability with dramatically increasing magnitude.

2.3.2 Nonlinear active flutter suppression

Nonlinear flutter, typically limit cycle oscillation, is not infrequently encountered by military and civil aircraft [1, 3, 109-112] and can have catastrophic consequences as discussed previously. Never-the-less the requirements of next-generation flight vehicles place increasing and contradictory demands on designers, typically greater structural flexibility, improved manoeuvrability and greater operational safety in severe environmental conditions [4]. Hence, active nonlinear flutter suppression becomes increasingly important in ensuring the safety and efficiency of future aircraft [17] and presents intellectual challenges that have attracted the interest of researchers in aerospace and control communities for more than three decades.

In the control community, mechanical systems which have fewer independent actuators than degrees of freedom to be controlled are known as under-actuated mechanical systems [19]. The control design of under-actuated aeroelastic systems is of importance, firstly for reasons of actuator failure and the need to rely on fewer actuators. Secondly, under-actuation might be motivated by weight and cost constraints imposed on next-generation flight vehicles. A typical under-actuated aeroelastic system is a two-dimensional nonlinear wing section with a single control surface in incompressible flow, which is the control objective of the present thesis.

Linear control techniques, namely pole placement [53], the linear quadratic regulation [18] and linear quadratic Gaussian methods [113], have been employed for nonlinear flutter suppression in two-dimensional wing sections with a single control surface, but with limited success [18]. Hence, nonlinear control methodologies are required for flutter suppression in nonlinear aeroelastic systems,

e.g. Ko et al. [114, 115] employed feedback linearisation techniques to control a prototypical wing section with torsional nonlinearity.

In practice, there unavoidably exist unmodelled dynamics, parameter uncertainty, and external disturbances in nonlinear control systems. Adaptive and robust control are two of the leading techniques for uncertainty compensation. Several adaptive control algorithms have been proposed for control of typical wing sections with structural nonlinearity using a single trailing-edge control, namely adaptive feedback linearisation [116], structured model reference adaptive control [117], output-feedback adaptive control [118] and backstepping-based adaptive control [119]. Alternatively, Lyapunov-based robust control is considered in [120] for an under-actuated nonlinear wing section. A robust controller in the form of state feedback control in conjunction with a proportional-integral observer, is used for active flutter suppression of a nonlinear two-dimensional wing-flap system [121]. Usually, robust constant-gain feedback control allows for the handling small uncertainties, while adaptive control is applicable for a wider range of parameter variation but is sensitive to unstructured uncertainty [19].

In recent years, sliding-mode control (SMC), a variable-structure controller, has been developed for control design of dynamic systems under uncertainty conditions. The idea of sliding-mode control is to design a high-frequency switching (discontinuous) control law to drive the system onto a specified sliding surface in state space and maintain it there for all subsequent time. The resultant sliding mode is claimed to be insensitive to matched model uncertainties and disturbances which do not steer the system away from the specified surface. The advantage of sliding-mode control is its tolerance of large matched uncertainty and large input disturbance.

Continuous sliding-mode control [122], second-order sliding-mode control [123, 124] and dynamic sliding-mode control [125] have been applied to suppress flutter instability in two-dimensional nonlinear wing sections with leading- and trailing-edge control surfaces, i.e. fully actuated aeroelastic systems. Very little research appears to have been carried out on the use of sliding-mode control for under-actuated aeroelastic systems. Examples include the robust control of supersonic three degree-of-freedom aerofoils using sliding-mode control [126]. Gujjula and Singh [127] designed a discontinuous sliding-mode controller for the pitch angle trajectory control of an unsteady aeroelastic system with a single control surface. Of course control of under-actuated systems is more complicated than the control of fully-actuated ones, requiring the consideration of globally stability and the presence of mismatched uncertainty.

Usually, for under-actuated systems, local asymptotic stability can be achieved by existing nonlinear control techniques. However, global asymptotic stabilisation for tracking control of under-actuated mechanical systems is considered to be extremely challenging [19, 20]. For example, by using feedback linearisation techniques, the stability of the zero dynamics only guarantees local stability of the system, global asymptotical stability can only be achieved if the internal dynamics is input-to-state stable [21]. Under-actuated nonlinear aeroelastic systems are even more complicated owing to the intrinsic uncertainty and/or softening nonlinearity.

2.4 Conclusion

In this chapter an overview of active vibration control in LTI systems and nonlinear aeroelastic systems is provided. The survey of active vibration control in LTI systems covers eigenvalue assignment, eigenstructure assignment and decoupling

vibration control. Progress in nonlinear aeroelastic analysis of aeroelastic systems with softening nonlinearity and active vibration control for under-actuated nonlinear aeroelastic systems is discussed in detail.

Chapter 3

Partial pole placement with inaccessible degrees of freedom

3.1 Introduction

This chapter presents a new theory of partial pole placement by the receptance method with inaccessible degrees of freedom [128]. The classical theory of partial pole placement problem [38] is reviewed, which aims to show that, in the presence of inaccessible degrees of freedom, the partial pole placement problem becomes nonlinear. It is shown that this nonlinear active vibration control problem is rendered linear by the application of a new double input control methodology implemented in conjunction with a receptance-based scheme where full pole placement is achieved while some chosen degrees of freedom are free from both actuation and sensing. The necessary equations for partial pole placement with inaccessible actuators and sensors represented by zero terms in the input vector and the control-gain vectors are established. The solvability conditions that enable lower bounds on the maximum numbers of inaccessible actuators and sensors to be determined are established. A lower bound on the maximum number of degrees of freedom inaccessible to both actuation and sensing is achieved. Simplification provides a solution to the natural frequency modification problem with inaccessible degrees of freedom. Eventually, a series of numerical examples are used to demonstrate the working of the proposed theory.

3.2 Motivation

The motion of the n degree of freedom system

$$\mathbf{M}\ddot{\mathbf{x}} + \mathbf{C}\dot{\mathbf{x}} + \mathbf{K}\mathbf{x} = \mathbf{0} \tag{3.1}$$

where $\mathbf{M}$, $\mathbf{C}$ and $\mathbf{K}$ are real symmetric $n \times n$ matrices and where $\mathbf{M}$ is positive-definite and $\mathbf{C}$ and $\mathbf{K}$ are positive-semidefinite, may be altered by state feedback control,

$$\mathbf{M}\ddot{\mathbf{x}} + \mathbf{C}\dot{\mathbf{x}} + \mathbf{K}\mathbf{x} = \mathbf{b}u(t) \tag{3.2}$$

where

$$u(t) = \mathbf{f}^T\dot{\mathbf{x}} + \mathbf{g}^T\mathbf{x} \tag{3.3}$$

and where $\mathbf{b}$, $\mathbf{f}$ and $\mathbf{g}$ are real vectors denoting force-distribution and control-gain terms.

It is well known that (3.1) has exponential solutions of the form

$$\mathbf{x}(t) = \mathbf{v}e^{\lambda t} \tag{3.4}$$

for certain values of λ and constant vectors $\mathbf{v}$. Substituting (3.4) in (3.1) gives

$$\left(\lambda^2\mathbf{M} + \lambda\mathbf{C} + \mathbf{K}\right)\mathbf{v} = \mathbf{0}. \tag{3.5}$$

The quadratic eigenvalue problem (3.5) of the open loop system has a self-conjugate set of $2n$ poles, $\{\lambda_k\}_{k=1}^{2n}$, with corresponding eigenvectors $\{\mathbf{v}_k\}_{k=1}^{2n}$ that satisfy (3.5).

Similarly exponential solutions of the form

$$\mathbf{x}(t) = \mathbf{w}e^{\mu t} \tag{3.6}$$

applied to the closed loop system (3.2) lead to the eigenvalue problem

$$\left(\mu^2\mathbf{M} + \mu\left(\mathbf{C} - \mathbf{b}\mathbf{f}^T\right) + \mathbf{K} - \mathbf{b}\mathbf{g}^T\right)\mathbf{w} = \mathbf{0}. \tag{3.7}$$

The self-conjugate set of $2n$ poles, $\{\mu_k\}_{k=1}^{2n}$, with corresponding eigenvectors $\{\mathbf{w}_k\}_{k=1}^{2n}$ that satisfy (3.7) are the eigenpairs of the closed loop system. The eigenvalues of both the open- and closed-loop systems are assumed to be distinct, the case of repeated roots and defective systems to be considered in further work beyond the scope of the present thesis.

To regulate the dynamic of the open loop system (3.1) it is frequently required to alter a subset of eigenvalues. Since the eigenvalues may be ordered arbitrarily, without loss of generality we may assume that the $2m \le 2n$ poles of the self-conjugate set $\{\lambda_k\}_{k=1}^{2m}$ associated with (3.5) are required to be changed to a predetermined self-conjugate set $\{\mu_k\}_{k=1}^{2m}$ by the applied control force. To avoid spillover it is further requested that $\{\mu_k\}_{k=2m+1}^{2n} = \{\lambda_k\}_{k=2m+1}^{2n}$. These conditions may be thus written in the form

$$\mu_k = \begin{cases} \mu_k & k = 1, 2, ..., 2m \\ \lambda_k & k = 2m+1, 2m+2, ..., 2n. \end{cases} \tag{3.8}$$

The classical problem of partial pole placement by state feedback control is formulated as follows.

Problem 1: *Partial pole assignment by state feedback control*

> **Given:** $\mathbf{M}$, $\mathbf{C}$, $\mathbf{K}$, $\mathbf{b}$ and a self-conjugate set $\{\mu_k\}_{k=1}^{2m}$
>
> **Find:** $\mathbf{f}$, $\mathbf{g}$ such that the poles of (3.7) form the closed-conjugate set (3.8).

Datta, Elhay and Ram [38] gave the following closed form solution to Problem 1,

$$\mathbf{f} = \mathbf{M}\mathbf{V}_m\mathbf{\Lambda}_m\boldsymbol{\beta}, \tag{3.9}$$

$$\mathbf{g} = -\mathbf{K}\mathbf{V}_m\boldsymbol{\beta} \tag{3.10}$$

and

$$\beta_i = \frac{1}{\mathbf{b}^T\mathbf{v}_i}\frac{\mu_i - \lambda_i}{\lambda_i}\prod_{\substack{k=1\\k\neq i}}^{2m}\frac{\mu_k - \lambda_i}{\lambda_k - \lambda_i},\quad i = 1,2,...,2m \tag{3.11}$$

where

$$\boldsymbol{\Lambda}_m = diag\left(\lambda_k,\quad k = 1,2,...,2m\right), \tag{3.12}$$

$$\mathbf{V}_m = \begin{bmatrix}\mathbf{v}_1 & \mathbf{v}_2 & \cdots & \mathbf{v}_{2m}\end{bmatrix} \tag{3.13}$$

and

$$\boldsymbol{\beta} = \begin{pmatrix}\beta_1 & \beta_2 & \cdots & \beta_{2m}\end{pmatrix}^T. \tag{3.14}$$

We note in passing that it follows from (3.11) that if $\mathbf{v}_k^T\mathbf{b} = 0$, $k \le 2m$, the k-th pole is not movable by a finite control force. It is invariant regardless of $\mathbf{f}$ and $\mathbf{g}$.

By inspection of the solution we realize that in general we may choose for example $\mathbf{b} = \mathbf{e}_1$, where $\mathbf{e}_k$ is the k-th unit vector of appropriate dimension, and solve Problem 1. The solution however would generally lead to fully populated vectors of control gains $\mathbf{f}$ and $\mathbf{g}$. The physical meaning is that the state feedback control may be implemented in general by one actuator and n sensors measuring the complete state of the system in real time. In practice, however, some of the degrees of freedom may not be accessible to both sensing and actuation. For brevity we will refer to such degrees of freedom as the *inaccessible degrees of freedom.*

Since the degrees of freedom may be numbered arbitrarily, without loss of generality we may assume that the last p degrees of freedom are inaccessible. Let

$$\sigma_k = \left(\mathbf{e}_k^T\mathbf{b}\right)^2 + \left(\mathbf{e}_k^T\mathbf{f}\right)^2 + \left(\mathbf{e}_k^T\mathbf{g}\right)^2, \tag{3.15}$$

then the condition

$$\sum_{k=n-p+1}^{n} \sigma_k = 0, \tag{3.16}$$

implies that there is no need to sense or actuate the last p degrees of freedom since every term in (3.16) is non-negative and therefore $b_k = f_k = g_k = 0$ for $k = n-p+1, n-p+2, ..., n$.

In addressing the problem of state feedback control with inaccessible degrees of freedom we may thus attempt to modify Problem 1 to the problem of finding $\mathbf{b}$, $\mathbf{f}$ and $\mathbf{g}$ subject to the constraint (3.16). Problem 1, which is linear, would then be changed to a non-linear problem since the unknowns elements of $\mathbf{b}$ interact with the unknown elements of $\mathbf{f}$ and $\mathbf{g}$ nonlinearly.

It will be shown in this chapter that with a new double-input controller taking form

$$\mathbf{M}\ddot{\mathbf{x}} + \mathbf{C}\dot{\mathbf{x}} + \mathbf{K}\mathbf{x} = \mathbf{b}_1 u_1(t) + \mathbf{b}_2 u_2(t) \tag{3.17}$$

where,

$$u_1(t) = \mathbf{f}^T \ddot{\mathbf{x}} + \mathbf{g}^T \dot{\mathbf{x}} \tag{3.18}$$

$$u_2(t) = \mathbf{f}^T \dot{\mathbf{x}} + \mathbf{g}^T \mathbf{x} \tag{3.19}$$

it is possible to solve in a linear fashion the partial pole placement with inaccessible degrees of freedom. In (3.17) the vectors $\mathbf{b}_1$ and $\mathbf{b}_2$ represent the distributions of control forces. The magnitudes of individual terms denote amplification factors to be applied to the inputs u_1 and u_2. The closed loop quadratic eigenvalue problem associated with (3.17) in conjunction with (3.18) and (3.19) then becomes

$$\left(\mu^2\mathbf{M} + \mu\mathbf{C} + \mathbf{K}\right)\mathbf{w} = \left(\mu^2\mathbf{b}_1\mathbf{f}^T + \mu\left(\mathbf{b}_1\mathbf{g}^T + \mathbf{b}_2\mathbf{f}^T\right) + \mathbf{b}_2\mathbf{g}^T\right)\mathbf{w} \tag{3.20}$$

or

$$\left(\mu^2\left(\mathbf{M} - \mathbf{b}_1\mathbf{f}^T\right) + \mu\left(\mathbf{C} - \mathbf{b}_1\mathbf{g}^T - \mathbf{b}_2\mathbf{f}^T\right) + \left(\mathbf{K} - \mathbf{b}_2\mathbf{g}^T\right)\right)\mathbf{w} = \mathbf{0} \tag{3.21}$$

The control force on the right-hand-side of (3.20) may be rewritten as

$$\left(\mu^2\mathbf{b}_1\mathbf{f}^T+\mu\left(\mathbf{b}_1\mathbf{g}^T+\mathbf{b}_2\mathbf{f}^T\right)+\mathbf{b}_2\mathbf{g}^T\right)\mathbf{w}=\left(\mu\mathbf{b}_1+\mathbf{b}_2\right)\left(\mu\mathbf{f}^T+\mathbf{g}^T\right)\mathbf{w} \tag{3.22}$$

so that the eigenvalue problem (3.20) becomes

$$\left(\mu^2\mathbf{M}+\mu\mathbf{C}+\mathbf{K}\right)\mathbf{w}=\left(\mu\mathbf{b}_1+\mathbf{b}_2\right)\left(\mu\mathbf{f}^T+\mathbf{g}^T\right)\mathbf{w} \tag{3.23}$$

and the condition (3.16), with

$$\sigma_k=\left(\mathbf{e}_k^T\mathbf{b}_1\right)^2+\left(\mathbf{e}_k^T\mathbf{b}_2\right)^2+\left(\mathbf{e}_k^T\mathbf{f}\right)^2+\left(\mathbf{e}_k^T\mathbf{g}\right)^2 \tag{3.24}$$

ensures that there is no need to actuate or sense the last p degrees of freedom of the controlled system (3.17).

The problem under consideration is thus

Problem 2: *Partial pole assignment with inaccessible degrees of freedom*

Given: $\mathbf{M}$, $\mathbf{C}$, $\mathbf{K}$, $\{\mu_k\}_{k=1}^{2m}$ and $0<p<n$

Find: $\mathbf{b}_1$, $\mathbf{b}_2$, $\mathbf{f}$ and $\mathbf{g}$ such that the poles of (3.23) form the set (3.8) and the condition (3.16), in conjunction with (3.24), is satisfied.

3.3 Immovable and assigned eigenvalues

We begin by writing the open-loop and closed-loop eigenvalue problems, (3.5) and (3.23), as

$$\left(\lambda_k^2\mathbf{M}+\lambda_k\mathbf{C}+\mathbf{K}\right)\mathbf{v}_k=\mathbf{0}, \qquad k=1,2,...,2n \tag{3.25}$$

and

$$\left(\mu_k^2\mathbf{M}+\mu_k\mathbf{C}+\mathbf{K}\right)\mathbf{w}_k=\left(\mu_k\mathbf{b}_1+\mathbf{b}_2\right)\left(\mu_k\mathbf{f}^T+\mathbf{g}^T\right)\mathbf{w}_k, \quad k=1,2,...,2n \tag{3.26}$$

with the understanding that

$$\mu_k=\lambda_k, \qquad k=2m+1,2m+2,...,2n \tag{3.27}$$

and $\{\mu_k\}_{k=1}^{2m}$ are assumed to be distinct from $\{\lambda_k\}_{k=1}^{2n}$.

It is apparent that the matrix $\left(\mu_k \mathbf{b}_1 + \mathbf{b}_2\right)\left(\mu_k \mathbf{f}^T + \mathbf{g}^T\right)$ is asymmetric, so that the closed-loop eigenvalue problem may be expressed in terms of the left eigenvector $\boldsymbol{\psi}_k$,

$$\boldsymbol{\psi}_k^T \left(\mu_k^2 \mathbf{M} + \mu_k \mathbf{C} + \mathbf{K}\right) = \boldsymbol{\psi}_k^T \left(\mu_k \mathbf{b}_1 + \mathbf{b}_2\right)\left(\mu_k \mathbf{f}^T + \mathbf{g}^T\right), \quad k = 1, 2, ..., 2n \tag{3.28}$$

It follows from (3.26) that $\mu_k = \lambda_k$ and $\mathbf{w}_k = \mathbf{v}_k$ whenever

$$\left(\lambda_k \mathbf{f}^T + \mathbf{g}^T\right)\mathbf{v}_k = 0 \tag{3.29}$$

and from (3.28) that $\mu_k = \lambda_k$ and $\boldsymbol{\psi}_k = \mathbf{v}_k$ when

$$\mathbf{v}_k^T \left(\lambda_k \mathbf{b}_1 + \mathbf{b}_2\right) = 0 \tag{3.30}$$

We now partition the set of unchanged eigenvalues $\{\mu_k\}_{k=2m+1}^{2n} = \{\lambda_k\}_{k=2m+1}^{2n}$, closed under conjugation, so that those eigenvalues with indices $k = 2m+1, \ldots, 2\tau$, rendered unchanged by virtue of (3.29), are separated from those with $k = 2\tau+1, \ldots, 2n$, given by satisfaction of (3.30) and $m \le \tau \le n$. To summarise, there are $2m$ eigenvalues to be assigned arbitrarily, $2(\tau - m)$ that are unchanged due to (3.29) and $2(n - \tau)$ unchanged due to (3.30) as shown in Fig. 3.1

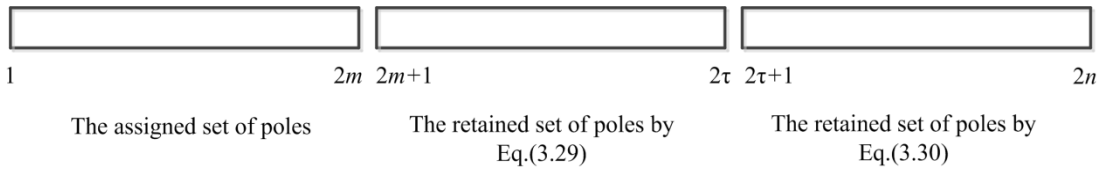

Fig. 3.1 Eigenvalues assigned and retained

To ensure that $\{\mu_k\}_{k=2m+1}^{2\tau} = \{\lambda_k\}_{k=2m+1}^{2\tau}$ we re-write equation (3.29) in the form

$$\mathbf{Q}\begin{pmatrix}\mathbf{f}\\ \mathbf{g}\end{pmatrix} = \mathbf{0} \tag{3.31}$$

where

$$\mathbf{Q}=\begin{bmatrix}\lambda_{2m+1}\mathbf{v}_{2m+1}^T & \mathbf{v}_{2m+1}^T\\ \lambda_{2m+2}\mathbf{v}_{2m+2}^T & \mathbf{v}_{2m+2}^T\\ \vdots & \vdots\\ \lambda_{2\tau}\mathbf{v}_{2\tau}^T & \mathbf{v}_{2\tau}^T\end{bmatrix} \tag{3.32}$$

Likewise equation (3.30) may be recast to ensure $\{\mu_k\}_{k=2\tau+1}^{2n}=\{\lambda_k\}_{k=2\tau+1}^{2n}$

$$\mathbf{\Phi}\begin{pmatrix}\mathbf{b}_1\\ \mathbf{b}_2\end{pmatrix}=\mathbf{0} \tag{3.33}$$

where

$$\mathbf{\Phi}=\begin{bmatrix}\lambda_{2\tau+1}\mathbf{v}_{2\tau+1}^T & \mathbf{v}_{2\tau+1}^T\\ \lambda_{2\tau+2}\mathbf{v}_{2\tau+2}^T & \mathbf{v}_{2\tau+2}^T\\ \vdots & \vdots\\ \lambda_{2n}\mathbf{v}_{2n}^T & \mathbf{v}_{2n}^T\end{bmatrix}, \tag{3.34}$$

The rows of **Q** and **Φ** are independent when the retained eigenvalues of the open-loop system are distinct.

The assignment of $2m$ eigenvalues $\{\mu_k\}_{k=1}^{2m}$ is achieved as in [9] by the satisfaction of characteristic equations arranged in the form,

$$\mathbf{P}\begin{pmatrix}\mathbf{f}\\ \mathbf{g}\end{pmatrix}=\tilde{\mathbf{e}} \tag{3.35}$$

where

$$\mathbf{P}=\begin{bmatrix}\mu_1\mathbf{r}_1^T & \mathbf{r}_1^T\\ \mu_2\mathbf{r}_2^T & \mathbf{r}_2^T\\ \vdots & \vdots\\ \mu_{2m}\mathbf{r}_{2m}^T & \mathbf{r}_{2m}^T\end{bmatrix},\qquad \mathbf{r}_k=\left(\mu_k^2\mathbf{M}+\mu_k\mathbf{C}+\mathbf{K}\right)^{-1}\left(\mu_k\mathbf{b}_1+\mathbf{b}_2\right),\qquad \tilde{\mathbf{e}}=\begin{pmatrix}1\\ 1\\ \vdots\\ 1\end{pmatrix}\in\mathbb{R}^{2m}. \tag{3.36}$$

The rows of $\mathbf{P}$ are independent when the assigned eigenvalues $\{\mu_k\}_{k=1}^{2m}$ are distinct.

3.4 Degrees of freedom free of actuation and sensing

Let us assume that the number of inaccessible actuators is $p_1, 0 < p_1 < n$, the number of inaccessible sensors is $p_2, 0 < p_2 < n$ and zero entries are placed in the last p_1 terms of $\mathbf{b}_1$ and $\mathbf{b}_2$ and in the last p_2 terms of $\mathbf{f}$ and $\mathbf{g}$. Since there is no restriction on the choice of degrees of freedom to be assigned zero entries, we may write

$$\mathbf{E}\begin{pmatrix}\mathbf{b}_1\\ \mathbf{b}_2\end{pmatrix} = \mathbf{0} \tag{3.37}$$

where

$$\mathbf{E} = \begin{bmatrix}\mathbf{E}_{n-p_1+1}\\ \mathbf{E}_{n-p_1+2}\\ \vdots\\ \mathbf{E}_n\end{bmatrix} \tag{3.38}$$

In addition,

$$\bar{\mathbf{E}}\begin{pmatrix}\mathbf{f}\\ \mathbf{g}\end{pmatrix} = \mathbf{0}. \tag{3.39}$$

where

$$\bar{\mathbf{E}} = \begin{bmatrix}\mathbf{E}_{n-p_2+1}\\ \mathbf{E}_{n-p_2+2}\\ \vdots\\ \mathbf{E}_n\end{bmatrix} \tag{3.40}$$

and $\mathbf{E}_k$ is a $2\times 2n$ matrix

$$\mathbf{E}_k = \begin{bmatrix}\mathbf{e}_k^T\\ \mathbf{e}_{k+n}^T\end{bmatrix}. \tag{3.41}$$

The rows of $\mathbf{E}$ and $\bar{\mathbf{E}}$ are by definition independent.

3.5 Lower bounds on the maximum numbers of inaccessible actuators and sensors

In this section conditions are established that determine lower bounds on the maximum numbers of inaccessible actuators and sensors. These include the existence of nontrivial solutions for the force-distribution terms $\left(\mathbf{b}_1^T \quad \mathbf{b}_2^T\right)^T$ and that such solutions are always admitted when $p_1 \le (\tau - 1)$. Then the conditions under which exact solutions are admitted for the control gains $\left(\mathbf{f}^T \quad \mathbf{g}^T\right)^T$ are established. It is shown that certain identical exact solutions are available for $p_2 \le (n - \tau)$ to guarantee at least $(n - \tau)$ null terms in $\mathbf{f}$ and $\mathbf{g}$. Thus the lower bounds on the maximum numbers of inaccessible actuators and sensors are found to be $p_1 = \breve{p}_1 = (\tau - 1)$ and $p_2 = \breve{p}_2 = (n - \tau)$ respectively.

We begin by establishing the necessary systems of equations. Thus, by combining equations (3.33) and (3.37),

$$\begin{bmatrix} \mathbf{\Phi} \\ \mathbf{E} \end{bmatrix} \begin{pmatrix} \mathbf{b}_1 \\ \mathbf{b}_2 \end{pmatrix} = \begin{pmatrix} \mathbf{0} \\ \mathbf{0} \end{pmatrix} \tag{3.42}$$

and also equations (3.31), (3.35) and (3.39),

$$\begin{bmatrix} \mathbf{P} \\ \mathbf{Q} \\ \bar{\mathbf{E}} \end{bmatrix} \begin{pmatrix} \mathbf{f} \\ \mathbf{g} \end{pmatrix} = \begin{pmatrix} \tilde{\mathbf{e}} \\ \mathbf{0} \\ \mathbf{0} \end{pmatrix} \tag{3.43}$$

The inaccessible actuators and sensors are denoted by vanishing entries placed in the last p_1 terms of $\mathbf{b}_1$ and $\mathbf{b}_2$ and in the last p_2 terms of $\mathbf{f}$ and $\mathbf{g}$ respectively. Thus,

$$\begin{pmatrix}\mathbf{b}_1\\ \mathbf{b}_2\end{pmatrix}=\begin{pmatrix}\tilde{\mathbf{b}}_1\\ \mathbf{0}_{(p_1\times 1)}\\ \tilde{\mathbf{b}}_2\\ \mathbf{0}_{(p_1\times 1)}\end{pmatrix};\quad \begin{pmatrix}\mathbf{f}\\ \mathbf{g}\end{pmatrix}=\begin{pmatrix}\tilde{\mathbf{f}}\\ \mathbf{0}_{(p_2\times 1)}\\ \tilde{\mathbf{g}}\\ \mathbf{0}_{(p_2\times 1)}\end{pmatrix} \tag{3.44}$$

Then equations (3.31), (3.33) and (3.35) may be recast in the form,

$$\begin{bmatrix}\boldsymbol{\Phi}_1 & \boldsymbol{\Phi}_2\end{bmatrix}\begin{pmatrix}\tilde{\mathbf{b}}_1\\ \tilde{\mathbf{b}}_2\end{pmatrix}=\mathbf{0};\quad \boldsymbol{\Phi}_1=\boldsymbol{\Phi}_{(:,1:n-p_1)};\quad \boldsymbol{\Phi}_2=\boldsymbol{\Phi}_{(:,n+1:2n-p_1)} \tag{3.45}$$

$$\begin{bmatrix}\mathbf{P}_1 & \mathbf{P}_2\\ \mathbf{Q}_1 & \mathbf{Q}_2\end{bmatrix}\begin{pmatrix}\tilde{\mathbf{f}}\\ \tilde{\mathbf{g}}\end{pmatrix}=\begin{pmatrix}\tilde{\mathbf{e}}\\ \mathbf{0}\end{pmatrix};\quad \begin{matrix}\mathbf{P}_1=\mathbf{P}_{(:,1:n-p_2)};\quad \mathbf{P}_2=\mathbf{P}_{(:,n+1:2n-p_2)}\\ \mathbf{Q}_1=\mathbf{Q}_{(:,1:n-p_2)};\quad \mathbf{Q}_2=\mathbf{Q}_{(:,n+1:2n-p_2)}\end{matrix} \tag{3.46}$$

where,

$$\dim\begin{bmatrix}\boldsymbol{\Phi}_1 & \boldsymbol{\Phi}_2\end{bmatrix}=2(n-\tau)\times 2\left(n-p_1\right);\quad \dim\begin{bmatrix}\mathbf{P}_1 & \mathbf{P}_2\\ \mathbf{Q}_1 & \mathbf{Q}_2\end{bmatrix}=2\tau\times 2\left(n-p_2\right) \tag{3.47}$$

Lemma 3.1: There exists a non-trivial solution $\left(\mathbf{b}_1^T \quad \mathbf{b}_2^T\right)^T$ to equation (3.42) if and only if $\operatorname{rank}\begin{bmatrix}\boldsymbol{\Phi}_1 & \boldsymbol{\Phi}_2\end{bmatrix}<2\left(n-p_1\right)$.

Proof: The necessary and sufficient condition for the existence of a nontrivial solution to a homogeneous system of linear equations is that the rank of the coefficient matrix is smaller than the number of unknowns.

□

Corollary 3.1: There always exists a non-trivial solution $\left(\mathbf{b}_1^T \quad \mathbf{b}_2^T\right)^T$ to equation (3.42) when $p_1\le\tau-1$.

Proof: From (3.47), if $p_1\le\tau-1$ then $\operatorname{nullity}\left(\begin{bmatrix}\boldsymbol{\Phi}_1 & \boldsymbol{\Phi}_2\end{bmatrix}\right)\ge 2$.

Therefore, a nontrivial solution is available from,

$$\begin{pmatrix}\tilde{\mathbf{b}}_1\\ \tilde{\mathbf{b}}_2\end{pmatrix} = \mathbf{N}\boldsymbol{\alpha};\quad \mathbf{N} = \text{null}\begin{bmatrix}\boldsymbol{\Phi}_1 & \boldsymbol{\Phi}_2\end{bmatrix} \tag{3.48}$$

where $\boldsymbol{\alpha}$ is an arbitrarily chosen parameter vector and $p_1 \le \tau - 1$ denotes the number of null entries in $\begin{pmatrix}\mathbf{b}_1^T & \mathbf{b}_2^T\end{pmatrix}^T$.

□

Corollary 3.2: The lower bound on the maximum number of inaccessible actuators is given by $\breve{p}_1 = \tau - 1$.

Proof: If $p_1 = \tau - 1$ and $2\ell_1$ of the $2(n-\tau)$ rows of $\begin{bmatrix}\boldsymbol{\Phi}_1 & \boldsymbol{\Phi}_2\end{bmatrix}$ are redundant then $\text{nullity}\left(\begin{bmatrix}\boldsymbol{\Phi}_1 & \boldsymbol{\Phi}_2\end{bmatrix}\right) = 2 + 2\ell_1$ and a further ℓ_1 inaccessible actuators may be admitted while still ensuring that $2(n-\tau)$ eigenvalues remain unchanged. Therefore the lower bound on the maximum number of inaccessible actuators is given when $\ell_1 = 0$ so that $p_1 = \breve{p}_1 = \tau - 1$.

□

Lemma 3.2: There always exists one or more identical exact solutions $\begin{pmatrix}\mathbf{f}^T & \mathbf{g}^T\end{pmatrix}^T$ to equation (3.43) for different $p_2 \le (n-\tau)$ when $\text{rank}\begin{bmatrix}\mathbf{P}_1 & \mathbf{P}_2\\ \mathbf{Q}_1 & \mathbf{Q}_2\end{bmatrix}_{p_2=n-\tau} = \text{rank}\begin{bmatrix}\mathbf{P}_1 & \mathbf{P}_2 & \tilde{\mathbf{e}}\\ \mathbf{Q}_1 & \mathbf{Q}_2 & \mathbf{0}\end{bmatrix}_{p_2=n-\tau}$, and any other solution requires a greater number of sensors.

Proof: One or more exact solutions exist when $\text{rank}\begin{bmatrix}\mathbf{P}_1 & \mathbf{P}_2\\ \mathbf{Q}_1 & \mathbf{Q}_2\end{bmatrix}_{p_2\le n-\tau} = \text{rank}\begin{bmatrix}\mathbf{P}_1 & \mathbf{P}_2 & \tilde{\mathbf{e}}\\ \mathbf{Q}_1 & \mathbf{Q}_2 & \mathbf{0}\end{bmatrix}_{p_2\le n-\tau}$ so the right-hand-side of equation

(3.46) is given by a linear combination of the columns of $\begin{bmatrix} \mathbf{P}_1 & \mathbf{P}_2 \\ \mathbf{Q}_1 & \mathbf{Q}_2 \end{bmatrix}_{p_2 \le n-\tau}$. However, any exact solution when $p_2 = (n-\tau)$ is also a solution when $p_2 < (n-\tau)$ because the columns of $\begin{bmatrix} \mathbf{P}_1 & \mathbf{P}_2 \\ \mathbf{Q}_1 & \mathbf{Q}_2 \end{bmatrix}_{p_2 = n-\tau}$ are included in $\begin{bmatrix} \mathbf{P}_1 & \mathbf{P}_2 \\ \mathbf{Q}_1 & \mathbf{Q}_2 \end{bmatrix}_{p_2 \le n-\tau}$. Other solutions exist when $p_2 < (n-\tau)$ but are given by the linear combination of a greater number of columns, therefore requiring a greater number of sensors.

□

Corollary 3.3: If $\text{rank}\begin{bmatrix} \mathbf{P}_1 & \mathbf{P}_2 \\ \mathbf{Q}_1 & \mathbf{Q}_2 \end{bmatrix}_{p_2 = n-\tau} = \text{rank}\begin{bmatrix} \mathbf{P}_1 & \mathbf{P}_2 & \tilde{\mathbf{e}} \\ \mathbf{Q}_1 & \mathbf{Q}_2 & \mathbf{0} \end{bmatrix}_{p_2 = n-\tau}$ then the lower bound on the maximum number of inaccessible sensors is given by $\breve{p}_2 = n - \tau$.

Proof: If $2\ell_2$ of the 2τ rows of $\begin{bmatrix} \mathbf{P}_1 & \mathbf{P}_2 \\ \mathbf{Q}_1 & \mathbf{Q}_2 \end{bmatrix}_{p_2 = n-\tau}$ are redundant then $\text{nullity}\left(\begin{bmatrix} \mathbf{P}_1 & \mathbf{P}_2 \\ \mathbf{Q}_1 & \mathbf{Q}_2 \end{bmatrix}_{p_2 = n-\tau}\right) = 2\ell_2$ and a further ℓ_2 inaccessible sensors may be admitted while still ensuring that $2(\tau - m)$ eigenvalues remain unchanged and $2m$ eigenvalues are assigned. Therefore the lower bound on the maximum number of inaccessible sensors is given when $\ell_2 = 0$ so that $p_2 = \breve{p}_2 = n - \tau$.

□

The solution of equation (3.43) is dependent upon the solution of (3.42) in that the eigenvalues to be assigned must be controllable. This imposes a condition on the solution of (3.42) that,

$$\begin{bmatrix} \lambda_k \mathbf{v}_k^T & \mathbf{v}_k^T \end{bmatrix} \begin{pmatrix} \mathbf{b}_1 \\ \mathbf{b}_2 \end{pmatrix} \neq 0; \quad k = 1, 2, \cdots, 2m \tag{3.49}$$

or,

$$\begin{bmatrix} \lambda_k \tilde{\mathbf{v}}_k^T & \tilde{\mathbf{v}}_k^T \end{bmatrix} \begin{pmatrix} \tilde{\mathbf{b}}_1 \\ \tilde{\mathbf{b}}_2 \end{pmatrix} \neq 0; \quad \tilde{\mathbf{v}}_k = \left(\mathbf{v}_k \right)_{(1:n-p_1)} \tag{3.50}$$

Lemma 3.3*:* The eigenvalues to be assigned in (3.43) are controllable when the $\boldsymbol{\alpha}$ is chosen so that

$$\begin{bmatrix} \lambda_k \tilde{\mathbf{v}}_k^T & \tilde{\mathbf{v}}_k^T \end{bmatrix} \mathbf{N}\boldsymbol{\alpha} \neq 0; \quad k = 1, 2, \cdots, 2m \tag{3.51}$$

Proof:

Equation (3.50) may be obtained by the combination of equation (3.51) with (3.48).

□

3.6 Lower bound on the maximum number of inaccessible degrees of freedom

The numbers of degrees of freedom inaccessible to actuation and sensing are p_1 and p_2 respectively. Our objective is to have equal values for p_1 and p_2 so that the number of inaccessible degrees of freedom is maximised. It was already shown that the lower bound on the maximum numbers of inaccessible actuators is $\breve{p}_1 = \tau - 1$ and if equation (3.43) is satisfied for $p_2 = \breve{p}_2 = n - \tau$, the lower bound on the maximum numbers of inaccessible sensors is $\breve{p}_2 = n - \tau$. Therefore, under the solvability condition, a lower bound on the maximum inaccessible degrees of freedom may be achieved by equating $\breve{p}_1 = \tau - 1$ and $\breve{p}_2 = n - \tau$.

We have already established that the eigenvalues can be separated into three groups:

- $2m$ eigenvalues to be assigned
- $2(\tau - m)$ eigenvalues to be unchanged due to equation (3.29) and
- $2(n - \tau)$ eigenvalues to be unchanged due to equation (3.30).

where $n \geq \tau \geq m$.

Equal numbers of degrees of freedom without sensing and actuation can be achieved when $\breve{p}_1 = \breve{p}_2$, so that $\tau - 1 = n - \tau$ and is possible when n is odd and $m \leq \frac{n+1}{2}$, in which case $\tau = \frac{n+1}{2}$. This case is illustrated in Fig. 3.2 where it is seen that it corresponds to an optimal maximum solution $p = \breve{p}_1 = \breve{p}_2 = \frac{n-1}{2}$ of equations (3.42) and (3.43).

When n is even and $m \leq \frac{n+1}{2}$ a sub-optimal solution is obtained as shown in Fig. 3.3. This results in two solutions $\tau = \frac{n}{2}$ or $\tau = \frac{n}{2} + 1$ corresponding to $p = \frac{n}{2} - 1$. In practice, $\tau = \frac{n}{2} + 1$ is preferable because it requires fewer actuators than sensors.

When $m > \frac{n+1}{2}$ and $\tau \geq m$ then the only solution available is that denoted by the thick line in Fig. 3.4. We are free to choose any value of $p = n - \tau$ on the thick line and the best available solution is $\tau = m$. This solution results in fewer degrees of freedom free of sensing than those free of actuation and, as such, is a practical solution because fewer actuators are required than sensors.

To summarise:

Case 1 - n is an odd number and $m \leq \frac{n+1}{2}$:

$$\tau = \frac{n+1}{2}; \quad p = \frac{n-1}{2} \tag{3.52}$$

Case 2 - n is an even number and $m \leq \frac{n+1}{2}$:

$$\tau = \frac{n}{2} \quad \text{or} \quad \tau = \frac{n}{2} + 1; \quad p = \frac{n}{2} - 1 \tag{3.53}$$

Case 3 - $m > \frac{n+1}{2}$:

$$\tau = m; \quad p = n - m \tag{3.54}$$

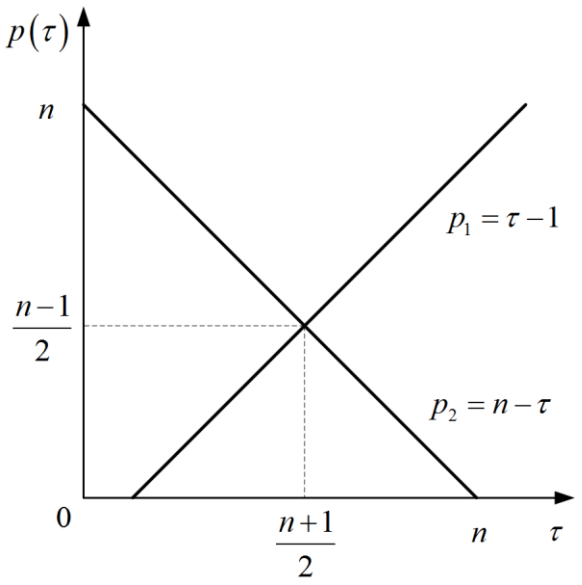

Fig. 3.2 Number of inaccessible degrees of freedom (Case 1)

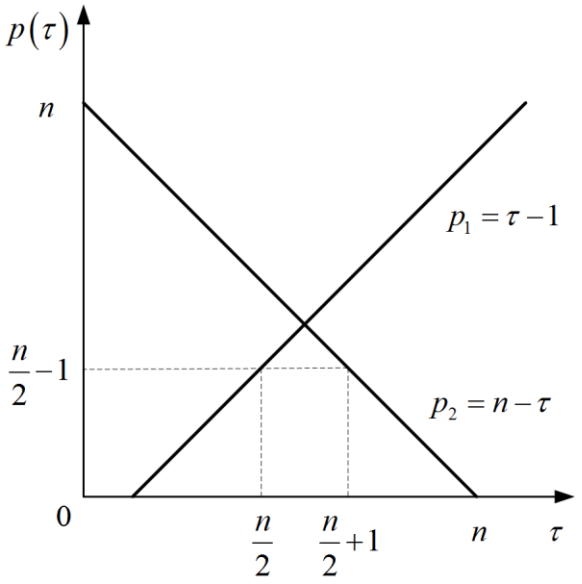

Fig. 3.3 Number of inaccessible degrees of freedom (Case 2)

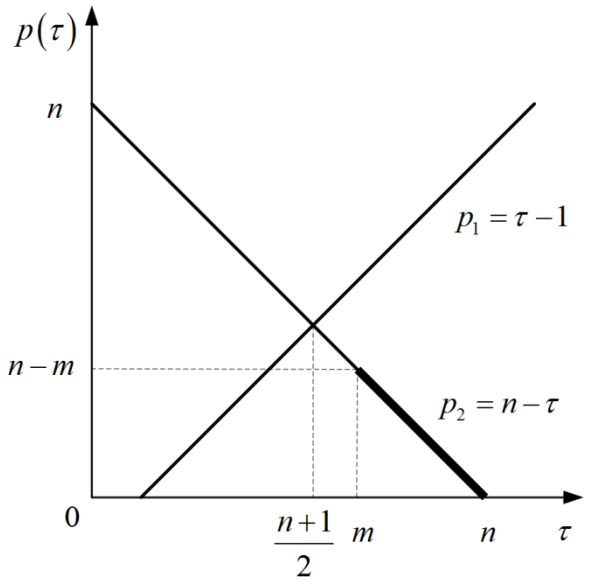

Fig. 3.4 Number of inaccessible degrees of freedom (Case 3)

The procedure for partial pole placement with inaccessible degrees of freedom may be summarised as follows:

1. Determine τ such that the lower bound on the maximum number of inaccessible degrees of freedom is achieved;
2. Choose $p_1 = \tau - 1$ and $p_2 = n - \tau$ and check the solvability of equation (3.43);
3. Solve equations (3.42) and (3.43).

Sufficient conditions for achieving the lower bound of the maximum number of inaccessible degrees of freedom are:

1. The force distribution vector should not be orthogonal to the first $2m$ modes (by choice of vector $\boldsymbol{\alpha}$);
2. $$\operatorname{rank}\begin{bmatrix}\mathbf{P}_1 & \mathbf{P}_2 \\ \mathbf{Q}_1 & \mathbf{Q}_2\end{bmatrix}_{p_2=n-\tau} = \operatorname{rank}\begin{bmatrix}\mathbf{P}_1 & \mathbf{P}_2 & \tilde{\mathbf{e}} \\ \mathbf{Q}_1 & \mathbf{Q}_2 & \mathbf{0}\end{bmatrix}_{p_2=n-\tau}.$$

3.6.1 Example 3.1

Consider the open loop system with

$$\mathbf{M}=\begin{bmatrix}3 & & & \\ & 10 & & \\ & & 20 & \\ & & & 12\end{bmatrix},\ \mathbf{C}=\begin{bmatrix}2.3 & -1 & & \\ -1 & 2.2 & -1.2 & \\ & -1.2 & 2.7 & -1.5 \\ & & -1.5 & 1.5\end{bmatrix},$$

$$\mathbf{K}=\begin{bmatrix}40 & -30 & & \\ -30 & 60 & -30 & \\ & -30 & 90 & -30 \\ & & -30 & 30\end{bmatrix}.$$

The open-loop eigenvalues are

$$\lambda_{1,2}=-0.0108\ \pm\ 0.8736\text{i}$$
$$\lambda_{3,4}=-0.0809\ \pm\ 1.6766\text{i}$$
$$\lambda_{5,6}=-0.1336\ \pm\ 2.5280\text{i}$$
$$\lambda_{7,8}=-0.3980\ \pm\ 4.0208\text{i}.$$

We wish to assign the first two pairs of eigenvalues while the remaining eigenvalues are unchanged

$$\mu_{1,2}=-0.03\pm 1\text{i}$$
$$\mu_{3,4}=-0.1\pm 2\text{i}.$$

Following the analysis given in Section 3.6 the system has $p=1$ degree of freedom inaccessible when either $\tau=2$ or $\tau=3$. Here we choose $\tau=2$ and then $p_1=1$ and $p_2=2$. Equation (3.43) is found to be solvable. The vector $\begin{pmatrix}\mathbf{b}_1^T & \mathbf{b}_2^T\end{pmatrix}^T$ is required to be orthogonal to the last two pairs of open-loop eigenvectors

$$\mathbf{\Phi}\begin{pmatrix}\mathbf{b}_1\\ \mathbf{b}_2\end{pmatrix}=\mathbf{0}$$

where

$$\mathbf{\Phi}=\begin{bmatrix}\lambda_5\mathbf{v}_5^T & \mathbf{v}_5^T\\ \lambda_6\mathbf{v}_6^T & \mathbf{v}_6^T\\ \lambda_7\mathbf{v}_7^T & \mathbf{v}_7^T\\ \lambda_8\mathbf{v}_8^T & \mathbf{v}_8^T\end{bmatrix}$$

$$\mathbf{v}_5^T = \begin{bmatrix} -0.0941 + 0.2578\mathrm{i} & -0.0829 + 0.1727\mathrm{i} & 0.1056 - 0.2807\mathrm{i} & -0.0738 + 0.1775\mathrm{i} \end{bmatrix}$$
$$\mathbf{v}_7^T = \begin{bmatrix} 0.0535 + 0.2107\mathrm{i} & -0.0220 - 0.0613\mathrm{i} & 0.0033 + 0.0077\mathrm{i} & -0.0006 - 0.0014\mathrm{i} \end{bmatrix}$$
$$\mathbf{v}_6 = \mathbf{v}_5^*, \quad \mathbf{v}_8 = \mathbf{v}_7^*.$$

It is assumed that the fourth degree of freedom is inaccessible. Then

$$\mathbf{E}_4 \begin{pmatrix} \mathbf{b}_1 \\ \mathbf{b}_2 \end{pmatrix} = \mathbf{0}$$

where

$$\mathbf{E}_4 = \begin{bmatrix} 0 & 0 & 0 & 1 & 0 & 0 & 0 & 0 \\ 0 & 0 & 0 & 0 & 0 & 0 & 0 & 1 \end{bmatrix}.$$

Then

$$\begin{pmatrix} \tilde{\mathbf{b}}_1 \\ \tilde{\mathbf{b}}_2 \end{pmatrix} = \mathbf{N}\boldsymbol{\alpha}, \quad \mathbf{N} = \mathrm{null}\left(\begin{bmatrix} \boldsymbol{\Phi}_1 & \boldsymbol{\Phi}_2 \end{bmatrix} \right), \qquad \boldsymbol{\Phi}_1 = \boldsymbol{\Phi}_{(:,1:3)} \text{ and } \boldsymbol{\Phi}_2 = \boldsymbol{\Phi}_{(:,5:7)}.$$

By choosing $\boldsymbol{\alpha} = \begin{pmatrix} 0.5 & 1 \end{pmatrix}^T$, we obtain

$$\mathbf{b}_1 = \begin{pmatrix} -0.1277 \\ -0.4544 \\ -0.3831 \\ 0 \end{pmatrix}, \qquad \mathbf{b}_2 = \begin{pmatrix} 0.2199 \\ 1.0059 \\ 0.9057 \\ 0 \end{pmatrix}.$$

Also, from

$$\begin{bmatrix} \mathbf{P} \\ \mathbf{E}_3 \\ \mathbf{E}_4 \end{bmatrix} \begin{pmatrix} \mathbf{f} \\ \mathbf{g} \end{pmatrix} = \begin{pmatrix} \tilde{\mathbf{e}} \\ \mathbf{0} \\ \mathbf{0} \end{pmatrix}$$

where

$$\mathbf{P} = \begin{bmatrix} \mu_1 \mathbf{r}_1^T & \mathbf{r}_1^T \\ \mu_2 \mathbf{r}_2^T & \mathbf{r}_2^T \\ \mu_3 \mathbf{r}_3^T & \mathbf{r}_3^T \\ \mu_4 \mathbf{r}_4^T & \mathbf{r}_4^T \end{bmatrix}, \mathbf{r}_1 = \begin{bmatrix} -0.0869 + 0.0672\mathrm{i} \\ -0.1165 + 0.0848\mathrm{i} \\ -0.1399 + 0.0916\mathrm{i} \\ -0.2343 + 0.1512\mathrm{i} \end{bmatrix}, \mathbf{r}_3 = \begin{bmatrix} -0.0547 + 0.0592\mathrm{i} \\ -0.0613 + 0.0615\mathrm{i} \\ -0.0168 + 0.0162\mathrm{i} \\ 0.0278 - 0.0269\mathrm{i} \end{bmatrix},$$

$$\mathbf{r}_2 = \mathbf{r}_1^*, \qquad \mathbf{r}_4 = \mathbf{r}_3^*,$$

$\tilde{\mathbf{e}}^T = \begin{pmatrix} 1 & 1 & 1 & 1 \end{pmatrix}$,

and

$$\mathbf{E}_3 = \begin{bmatrix} 0 & 0 & 1 & 0 & 0 & 0 & 0 & 0 \\ 0 & 0 & 0 & 0 & 0 & 0 & 1 & 0 \end{bmatrix}$$

the control gains are found to be

$$\mathbf{f} = \begin{pmatrix} 0.4784 \\ -4.8277 \\ 0 \\ 0 \end{pmatrix}, \quad \mathbf{g} = \begin{pmatrix} -17.1376 \\ 7.3027 \\ 0 \\ 0 \end{pmatrix}.$$

The last two terms of $\mathbf{g}$ and $\mathbf{f}$ are made zero so that there is one totally inaccessible degree of freedom and a further degree of freedom where there is actuation but no sensor.

Now closed-loop system becomes

$$\left(\mathbf{M} - \mathbf{b}_1\mathbf{f}^T\right)\ddot{\mathbf{x}} + \left(\mathbf{C} - \mathbf{b}_1\mathbf{g}^T - \mathbf{b}_2\mathbf{f}^T\right)\dot{\mathbf{x}} + \left(\mathbf{K} - \mathbf{b}_2\mathbf{g}^T\right)\mathbf{x} = 0$$

with roots given by

$$\mu_{1,2} = -0.03 \pm 1\mathrm{i}$$
$$\mu_{3,4} = -0.1 \pm 2\mathrm{i}$$
$$\mu_{5,6} = -0.1336 \pm 2.5280\mathrm{i}$$
$$\mu_{7,8} = -0.3980 \pm 4.0208\mathrm{i}$$

which are exactly the prescribed eigenvalues.

3.7 The natural frequency modification problem

The *natural frequency modification problem* is the problem of spectrum modification by feedback control in the simplified case when both the open-loop and the closed-loop systems are undamped. Then the open loop eigenvalue problem (3.5) is reduced to

$$\left(\mathbf{K}-\lambda_k\mathbf{M}\right)\mathbf{v}_k=\mathbf{0}, \qquad k=1,2,...,n \tag{3.55}$$

and the closed loop system (3.20) becomes

$$\left(\mathbf{K}-\mu_k\mathbf{M}\right)\mathbf{w}_k=\mathbf{b}\mathbf{g}^T\mathbf{w}_k, \qquad k=1,2,...,n\,. \tag{3.56}$$

and, in terms of the left eigenvectors

$$\boldsymbol{\psi}_k^T\left(\mathbf{K}-\mu_k\mathbf{M}\right)_k=\boldsymbol{\psi}_k^T\mathbf{b}\mathbf{g}^T, \qquad k=1,2,...,n \tag{3.57}$$

We note that (3.56), (3.57) is an eigenvalue problem by *position* feedback control.

Here we want to modify the natural frequencies such that

$$\mu_k=\begin{cases}\mu_k & k=1,2,...,m\\ \lambda_k & k=m+1,m+2,...,n\end{cases} \tag{3.58}$$

where $\{\mu_k\}_{k=1}^m$ is a predefined set of non-negative real eigenvalues.

The condition for inaccessibility of the last p degrees of freedom is

$$\sum_{k=n-p+1}^{n}\left(\left(\mathbf{e}_k^T\mathbf{b}\right)^2+\left(\mathbf{e}_k^T\mathbf{g}\right)^2\right)=0 \tag{3.59}$$

With these definitions Problem 2 is reduced to the following problem.

Problem 3: *Natural frequency modification with inaccessible degrees of freedom*

Given: $\mathbf{M}$, $\mathbf{K}$, $\{\mu_k\}_{k=1}^m$ and $0<p<n$

Find: $\mathbf{b}$, $\mathbf{g}$ such that the poles of (3.56) form the set (3.58) and the condition (3.59) is satisfied.

The no spillover condition $\{\mu_k\}_{k=\tau+1}^n=\{\lambda_k\}_{k=\tau+1}^n$ is imposed by the linear constraint,

$$\boldsymbol{\Phi}\mathbf{b}=\mathbf{0} \tag{3.60}$$

where

$$\mathbf{\Phi} = \begin{bmatrix} \mathbf{v}_{\tau+1}^T \\ \mathbf{v}_{\tau+2}^T \\ \vdots \\ \mathbf{v}_n^T \end{bmatrix} \tag{3.61}$$

The constraint $\{b_k\}_{k=n-p_1+1}^{n} = 0$, which renders the last p_1 degrees of freedom inaccessible to actuation, is imposed by

$$\begin{bmatrix} \mathbf{e}_{n-p_1+1}^T \\ \mathbf{e}_{n-p_1+2}^T \\ \vdots \\ \mathbf{e}_n^T \end{bmatrix} \mathbf{b} = \mathbf{0} \tag{3.62}$$

or

$$\mathbf{E}\mathbf{b} = \mathbf{0}. \tag{3.63}$$

Combining (3.60) and (3.63) leads to

$$\begin{pmatrix} \mathbf{\Phi} \\ \mathbf{E} \end{pmatrix} \mathbf{b} = \mathbf{0} \tag{3.64}$$

There exists a non-trivial solution to equation (3.64) when $\operatorname{rank}\begin{pmatrix} \mathbf{\Phi} \\ \mathbf{E} \end{pmatrix} < n$.

Consequently, equation (3.64) always has a nontrivial solutions when $p_1 \le \tau - 1$.

Then, the non-trivial solution for input vector $\mathbf{b}$ is given by

$$\mathbf{b}_1 = \begin{pmatrix} \tilde{\mathbf{b}}_1 \\ \mathbf{0}_{(p_1 \times 1)} \end{pmatrix}, \quad \tilde{\mathbf{b}}_1 = \mathbf{N}\boldsymbol{\alpha}, \quad \mathbf{N} = \operatorname{null}\left(\mathbf{\Phi}_1\right), \quad \mathbf{\Phi}_1 = \mathbf{\Phi}_{:,(1:n-p_1)}. \tag{3.65}$$

where $\boldsymbol{\alpha}$ is an arbitrary vector.

The terms $\boldsymbol{\alpha}$ should be chosen such that the eigenvalues to be assigned are controllable.

The modification of m eigenvalues is achieved by satisfaction of the linear equations

$$\mathbf{P}\mathbf{g} = \tilde{\mathbf{e}} \tag{3.66}$$

where

$$\mathbf{P}=\begin{bmatrix}\mathbf{r}_1^T\\ \mathbf{r}_2^T\\ \vdots\\ \mathbf{r}_m^T\end{bmatrix},\qquad \mathbf{r}_k=\left(\mathbf{K}-\mu_k\mathbf{M}\right)^{-1}\mathbf{b},\qquad \tilde{\mathbf{e}}=\begin{pmatrix}1\\1\\\vdots\\1\end{pmatrix}\in\mathbb{R}^m \tag{3.67}$$

The no spillover condition $\{\mu_k\}_{k=m+1}^{\tau}=\{\lambda_k\}_{k=m+1}^{\tau}$ is imposed by the linear constraints

$$\mathbf{Qg}=\mathbf{0} \tag{3.68}$$

where

$$\mathbf{Q}=\begin{bmatrix}\mathbf{v}_{m+1}^T\\ \mathbf{v}_{m+2}^T\\ \vdots\\ \mathbf{v}_{\tau}^T\end{bmatrix} \tag{3.69}$$

The control gains $\mathbf{g}$ with p_2 degrees of freedom inaccessible to sensing $\{g_k=0\}_{k=n-p_2+1}^{n}$, are then determined by solving

$$\begin{bmatrix}\mathbf{P}\\ \mathbf{Q}\\ \bar{\mathbf{E}}\end{bmatrix}\mathbf{g}=\begin{pmatrix}\tilde{\mathbf{e}}\\ \mathbf{0}\\ \mathbf{0}\end{pmatrix};\quad \bar{\mathbf{E}}=\begin{bmatrix}\mathbf{e}_{n-p_2+1}^T\\ \mathbf{e}_{n-p_2+2}^T\\ \vdots\\ \mathbf{e}_n^T\end{bmatrix} \tag{3.70}$$

Let

$$\begin{aligned}\mathbf{P}_1&=\mathbf{P}_{(1:m,1:n-p_2)}\\ \mathbf{Q}_1&=\mathbf{Q}_{(1:\tau-m,1:n-p_2)}\end{aligned} \tag{3.71}$$

Equation (3.70) is solvable when $p_2\le n-\tau$ and $\operatorname{rank}\begin{bmatrix}\mathbf{P}_1\\ \mathbf{Q}_1\end{bmatrix}=\operatorname{rank}\begin{bmatrix}\mathbf{P}_1 & \tilde{\mathbf{e}}\\ \mathbf{Q}_1 & \mathbf{0}\end{bmatrix}$.

Similar to the previous analysis in section 3.5, the lower bound on the maximum number of inaccessible actuators is given by $\breve{p}_1=\tau-1$. When equation (3.70) is satisfied for $p_2=\breve{p}_2=n-\tau$, the lower bound on the maximum number of

inaccessible sensors is given by $\breve{p}_2 = n - \tau$. Hence, under the solvability condition, the maximum number of inaccessible degrees of freedom is given by exactly the same analysis as in Section 3.6.

3.7.1 Example 3.2

Consider the five degree-of-freedom mass-spring system shown in Fig. 3.5.

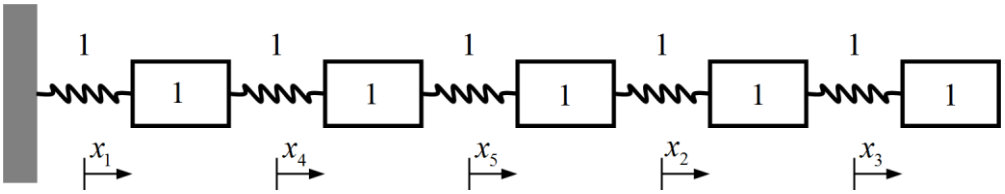

Fig. 3.5 The five degree-of-freedom system

The system matrices are given by

$$\mathbf{M} = \mathbf{I},\ \mathbf{K} = \begin{bmatrix} 2 & & & -1 & \\ & 2 & -1 & & -1 \\ & -1 & 1 & & \\ -1 & & & 2 & -1 \\ & -1 & & -1 & 2 \end{bmatrix}.$$

The open-loop eigenvalues are

$$\lambda_1 = 0.0810,\quad \lambda_2 = 0.6903,\ \lambda_3 = 1.7154,\quad \lambda_4 = 2.8308,\quad \lambda_5 = 3.6825.$$

We wish to assign the first two eigenvalues while the remaining eigenvalues are unchanged

$$\mu_1 = 0.5,\quad \mu_2 = 1.$$

According to the analysis in section 3.6, two inaccessible degrees of freedom are achievable when $\tau = 3$. Hence $p_1 = 2$ and $p_2 = 2$. It will be shown later on that equation (3.70) is solvable. In accessibility of x_4 and x_5 requires that

$$\begin{bmatrix} \mathbf{e}_4^T \\ \mathbf{e}_5^T \end{bmatrix} \mathbf{b} = 0$$

where

$$\mathbf{e}_4^T = \begin{bmatrix} 0 & 0 & 0 & 1 & 0 \end{bmatrix}$$

$$\mathbf{e}_5^T = \begin{bmatrix} 0 & 0 & 0 & 0 & 1 \end{bmatrix}.$$

Also the term $\mathbf{b}$ is required to be orthogonal to of the last two open-loop eigenvectors

$$\begin{bmatrix} \mathbf{v}_4^T \\ \mathbf{v}_5^T \end{bmatrix} \mathbf{b} = \mathbf{0}$$

where

$$\mathbf{v}_4^T = \begin{bmatrix} -0.5485 & -0.5969 & 0.3260 & 0.4557 & 0.1699 \end{bmatrix}$$

$$\mathbf{v}_5^T = \begin{bmatrix} -0.3260 & 0.4557 & -0.1699 & 0.5485 & -0.5969 \end{bmatrix}.$$

Then

$$\tilde{\mathbf{b}}_1 = \mathbf{N}\alpha, \quad \mathbf{N} = \text{null}\left(\mathbf{\Phi}_1\right), \qquad \mathbf{\Phi}_1 = \mathbf{\Phi}_{:,(1:3)}.$$

By choosing $\alpha = -10.3781$, it is found that

$$\mathbf{b} = \begin{pmatrix} 1 \\ 4.2287 \\ 9.4246 \\ 0 \\ 0 \end{pmatrix}.$$

To reassign the first two eigenvalues, $\mathbf{g}$ should satisfy the characteristic equations

$$\begin{bmatrix} \mathbf{r}_1^T \\ \mathbf{r}_2^T \end{bmatrix} \mathbf{g} = \mathbf{0},$$

the no spillover condition $\mu_3 = \lambda_3$ requires that

$$\mathbf{v}_3^T \mathbf{g} = 0,$$

and because the last two degrees of freedom x_4 and x_5 are inaccessible

$$\begin{bmatrix} \mathbf{e}_4^T \\ \mathbf{e}_5^T \end{bmatrix} \mathbf{g} = 0.$$

Hence, by solving

$$\begin{bmatrix} \mathbf{r}_1^T \\ \mathbf{r}_2^T \\ \mathbf{v}_3^T \\ \mathbf{e}_4^T \\ \mathbf{e}_5^T \end{bmatrix} \mathbf{g} = \begin{bmatrix} 1 \\ 1 \\ 0 \\ 0 \\ 0 \end{bmatrix}$$

where

$$\mathbf{r}_1^T = \begin{bmatrix} -14.5759 & -6.7160 & 5.4172 & -22.8638 & -19.7198 \end{bmatrix},$$

$$\mathbf{r}_2^T = \begin{bmatrix} 9.4246 & -9.4246 & -12.6533 & 8.4246 & -1 \end{bmatrix},$$

and

$$\mathbf{v}_3^T = \begin{bmatrix} 0.5969 & -0.3260 & 0.4557 & 0.1699 & -0.5485 \end{bmatrix}$$

it is found that

$$\mathbf{g} = \begin{pmatrix} -0.0330 \\ -0.1005 \\ -0.0287 \\ 0 \\ 0 \end{pmatrix}.$$

Now closed-loop system becomes

$$\mathbf{M}\ddot{\mathbf{x}} + \left(\mathbf{K} - \mathbf{b}\mathbf{g}^T\right)\mathbf{x} = 0$$

with roots given by

$$\mu_1 = 0.5, \quad \mu_2 = 1, \quad \mu_3 = 1.7154, \quad \mu_4 = 2.8308, \quad \mu_5 = 3.6825$$

which are exactly the prescribed eigenvalues.

3.8 Conclusion

A new theory for partial eigenvalue assignment by active vibration control in the presence of inaccessible degrees of freedom is proposed. A new double-input feedback control involved acceleration, velocity and displacement feedback is described. The eigenvalues of the open-loop system, intended to be unchanged, are

maintained in the closed-loop system by the application of orthogonality conditions on the input and feedback gain vectors. The flexibility from the new double-input feedback control and the combination of partial controllability and partial observability allows the simultaneous imposition of zero terms on the input and feedback gains vectors, resulting in the appearance of zero terms in desired locations corresponding to degrees of freedom inaccessible to both actuation and sensing. The methodology is based entirely on linear systems of equations, thereby avoiding the need to use nonlinear optimisation routines. Lower bounds on the maximum numbers of inaccessible actuators and sensors are given and the corresponding conditions are established. By equalising the maximum numbers of inaccessible actuators and sensors, a lower bound on the maximum number of inaccessible degrees of freedom allowed for precise implementation of partial pole placement is given. After simplification of the theory, active natural frequency modification is described. The theory is of practical value to the vibration control of large-dimension structures with many inaccessible degrees of freedom. In the next chapter, multiple-input feedback control will be considered, which allows the closed-loop eigenvectors to be assigned apart from eigenvalues and consequently will produce extra control design freedom.

Chapter 4

Block-decoupling vibration control using eigenstructure assignment

4.1 Introduction

In this chapter, a new block decoupling vibration control algorithm based on eigenstructure assignment using measured receptances is proposed for structural vibration control [129]. Apart from eigenvalue assignment, modal degree of freedom constraints are imposed such that the matrix of closed-loop right eigenvectors is block-diagonalised, leading to block diagonal matrices of the second-order system in physical coordinates. Consequently, the system is decoupled into substructures with desired closed-loop performances. Specifically, the block-diagonal receptance matrix is introduced and eigenstructure assignment by the method of receptances is briefly reviewed. The block decoupling vibration control algorithm for undamped and damped systems with lumped masses is explained. The number of actuators and sensors required in the case of banded damping and stiffness matrices is considered. The methodology is extended to cope with damped systems with inertia coupling using a hybrid block-decoupling vibration control law by the application of acceleration, velocity and displacement feedback control. The merit and performance of the block decoupling control method are exemplified by several numerical examples.

In this chapter we consider from a purely theoretical point of view, the feasibility of decoupling multi-degree of freedom systems to form substructures that are

completely isolated from one another by active vibration control. The research presented is a preliminary study, which might be deemed timely in view of contemporary interest in lightweight and deployable structures, piezo-based actuators and sensors with proven capability and a related literature on active input-output decoupling. For the purpose of simplicity, we limit the investigation in this chapter to the problem of block decoupling to form two independent substructures from a linear multi-degree of freedom system. It is straightforward to show that the approach can be extended to the case of multiple independent substructures and also diagonal decoupling in physical coordinates.

4.2 The closed-loop block-diagonal receptance matrix

The equation of motion of the n degree of freedom linear system may be cast in second-order form as,

$$\mathbf{M}\ddot{\mathbf{x}} + \mathbf{C}\dot{\mathbf{x}} + \mathbf{K}\mathbf{x} = \mathbf{0} \tag{4.1}$$

where $\mathbf{M}, \mathbf{C}$ and $\mathbf{K} \in \mathbb{R}^{n\times n}$ are symmetric matrices, $\mathbf{M}$ is positive definite and $\mathbf{C}$ and $\mathbf{K}$ are positive semi-definite. $\mathbb{R}$ denotes the field of real numbers.

Now, velocity and displacement feedback is applied to decouple and control the system so that the closed-loop system may be written as,

$$\mathbf{M}\ddot{\mathbf{x}} + \left(\mathbf{C} - \mathbf{B}\mathbf{F}^T\right)\dot{\mathbf{x}} + \left(\mathbf{K} - \mathbf{B}\mathbf{G}^T\right)\mathbf{x} = \mathbf{0} \tag{4.2}$$

where $\mathbf{B} \in \mathbb{R}^{n\times q}$ is the force distribution matrix, $\mathbf{F}$ and $\mathbf{G} \in \mathbb{R}^{n\times q}$ are velocity and displacement feedback control gain matrices respectively, q is the number of control inputs.

The dynamic stiffness matrix of the closed-loop system is denoted by,

$$\hat{\mathbf{\Gamma}}(s) = \mathbf{M}s^2 + \left(\mathbf{C} - \mathbf{B}\mathbf{F}^T\right)s + \left(\mathbf{K} - \mathbf{B}\mathbf{G}^T\right) \tag{4.3}$$

Correspondingly, the closed-loop receptance matrix is the inverse of the dynamic stiffness,

$$\hat{\mathbf{H}}(s) = \hat{\mathbf{\Gamma}}^{-1}(s) \tag{4.4}$$

where $(\hat{\bullet})$ denotes the closed-loop system.

A list of integers $(n_1, n_2, \cdots, n_v)$ is called a partition of n if $n_i \geq 1, i=1, 2, \cdots, v$ and $\sum_{i=1}^{v} n_i = n$.

The closed-loop dynamic system is said to be block diagonal with respect to the partition $(n_1, n_2, \cdots, n_v)$ if the receptance matrix takes the form,

$$\hat{\mathbf{H}}(s) = \begin{bmatrix} \hat{\mathbf{H}}_{11}(s) & & & \mathbf{0} \\ & \hat{\mathbf{H}}_{22}(s) & & \\ & & \ddots & \\ \mathbf{0} & & & \hat{\mathbf{H}}_{vv}(s) \end{bmatrix} \tag{4.5}$$

where $\hat{\mathbf{H}}_{ii}(s) \in \mathbb{Q}_p^{n_i \times n_i}(s), i = 1, 2, \cdots, v$, $\mathbb{Q}_p^{n_i \times n_i}(s)$ is the ring of proper rational functions. In the special case when $v = n$ and $n_i = 1$, $i=1, 2, \cdots, v$, the closed-loop system is said to be diagonally decoupled. For a linear system with closed-loop receptance (4.5), the dynamic behaviour may be expressed as,

$$\hat{\mathbf{H}}(s)\mathbf{q}(s) = \mathbf{x}(s) \tag{4.6}$$

where $\mathbf{q}(s)$ and $\mathbf{x}(s)$ are the external forces and displacement responses respectively, indicating that a substructure with receptance matrix $\hat{\mathbf{H}}_{ii}(s)$ is independent of other substructures under the external force $\mathbf{q}(s)$.

In the paper, we show how a multi-degree of freedom linear structure can be decoupled into two independent substructures ($v = 2$ and $n_1 + n_2 = n$) by a new block

decoupling algorithm. The algorithm can be extended straightforwardly to the case of multiple independent substructures and also diagonal decoupling in terms of physical coordinates.

4.3 Pole placement by the method of receptances

Multi-input active vibration control is proposed in this article by pole placement using the method of receptances proposed by Ram and Mottershead [9]. They showed that when the open-loop system is controllable, there exists a solution to the system of equations,

$$\begin{bmatrix} \mu_1\mathbf{w}_1^T & \mathbf{w}_1^T \\ \mu_2\mathbf{w}_2^T & \mathbf{w}_2^T \\ \vdots & \vdots \\ \mu_{2n}\mathbf{w}_{2n}^T & \mathbf{w}_{2n}^T \end{bmatrix} \begin{pmatrix} \mathbf{F} \\ \mathbf{G} \end{pmatrix} = \begin{pmatrix} \boldsymbol{\alpha}_1^T \\ \boldsymbol{\alpha}_2^T \\ \vdots \\ \boldsymbol{\alpha}_{2n}^T \end{pmatrix} \tag{4.7}$$

thereby assigning closed-loop eigenvalues $\{\mu_k\}_{k=1}^{2n}$, closed under conjugation, by the application of displacement and velocity feedback control gains $\mathbf{F}, \mathbf{G}$.

Terms appearing in (4.7) are given by Ram and Mottershead [9] as,

$$\mathbf{w}_k = \alpha_{\mu_k,1}\mathbf{r}_{\mu_k,1} + \alpha_{\mu_k,2}\mathbf{r}_{\mu_k,2} + \cdots + \alpha_{\mu_k,q}\mathbf{r}_{\mu_k,q} = \mathbf{R}_{\mu_k}\boldsymbol{\alpha}_k, \;\; k = 1,2,\cdots,2n \tag{4.8}$$

$$\mathbf{R}_{\mu_k} = \begin{bmatrix} \mathbf{r}_{\mu_k,1} & \mathbf{r}_{\mu_k,2} & \cdots & \mathbf{r}_{\mu_k,q} \end{bmatrix} = \mathbf{H}_{\mu_k}\mathbf{B}; \qquad \mathbf{H}_{\mu_k} = \left[\mathbf{M}\mu_k^{\,2} + \mathbf{C}\mu_k + \mathbf{K}\right]^{-1} \tag{4.9}$$

$$\boldsymbol{\alpha}_k = \begin{bmatrix} \alpha_{\mu_k,1} & \alpha_{\mu_k,2} & \cdots & \alpha_{\mu_k,q} \end{bmatrix}^T \tag{4.10}$$

and $\alpha_{\mu_k,j}$ are arbitrary parameters. $\mathbf{H}_{\mu_k}$ are open-loop receptance matrices which may be measured experimentally and $\mathbf{w}_k$ are the closed-loop right eigenvectors. Constraints may be applied at the j^{th} degree of freedom of the k^{th} mode by the choice of $\alpha_{\mu_k,j}$,

$$\mathbf{e}_j^T\mathbf{w}_k = \mathbf{e}_j^T\mathbf{R}_{\mu_k}\boldsymbol{\alpha}_k = 0 \tag{4.11}$$

where $\mathbf{e}_j$ denotes the j-th unit vector.

It is assumed in the following sections that equation (4.7) is solvable and the closed-loop eigenvalues are closed under conjugation - to ensure strictly real $\mathbf{F}, \mathbf{G}$.

4.4 Block-decoupling control for undamped structures

To illustrate the idea of block-decoupling control, we begin with the problem of undamped systems. The equations of motion of the open-loop and closed-loop n degree-of-freedom undamped systems ($\mathbf{C} = \mathbf{0}$, $\mathbf{F} = \mathbf{0}$) may be written as ,

$$\mathbf{M}\ddot{\mathbf{x}} + \mathbf{K}\mathbf{x} = \mathbf{0} \tag{4.12}$$

and

$$\mathbf{M}\ddot{\mathbf{x}} + \left(\mathbf{K} - \mathbf{B}\mathbf{G}^T\right)\mathbf{x} = \mathbf{0} \tag{4.13}$$

The closed-loop eigenvalue problem is

$$\left(\left(\mathbf{K} - \mathbf{B}\mathbf{G}^T\right) - \mu_k \mathbf{M}\right)\mathbf{w}_k = \mathbf{0}, \quad k = 1, 2, \cdots, n \tag{4.14}$$

or

$$\left(\mathbf{K} - \mathbf{B}\mathbf{G}^T\right)\mathbf{W} - \mathbf{M}\mathbf{W}\mathbf{\Lambda} = \mathbf{0} \tag{4.15}$$

We consider the problem of block decoupling the closed-loop system with respect to the partition $\begin{pmatrix} n_1 & n_2 \end{pmatrix}$. By choice of parameters $\alpha_{\mu_k, j}$ to satisfy equation (4.11), modal degree of freedom constraints may be imposed on right eigenvector $\mathbf{w}_k$,

$$\begin{aligned} w_{jk} &= 0, \qquad j = n_1 + 1, n_1 + 2, \cdots, n, k = 1, 2, \cdots, n_1 \\ w_{jk} &= 0, \qquad j = 1, 2, \cdots, n_1, \; k = n_1 + 1, n_1 + 2, \cdots, n \end{aligned} \tag{4.16}$$

where w_{jk}, is the j^{th} entry of the k^{th} right eigenvector of the closed-loop system. This leads to the block-diagonal matrix of mode shapes,

$$\mathbf{W} = \begin{bmatrix} \mathbf{W}_{11} & \mathbf{0} \\ \mathbf{0} & \mathbf{W}_{22} \end{bmatrix} \tag{4.17}$$

and $\mathbf{W} \in \mathbb{C}^{n \times n}$, $\mathbf{W}_{11} \in \mathbb{C}^{n_1 \times n_1}$, $\mathbf{W}_{22} \in \mathbb{C}^{n_2 \times n_2}$ and zero matrices inside are of proper dimension.

Lemma 4.1: The closed-loop stiffness and receptance matrices will be block diagonal with partition $(n_1 \quad n_2)$ with assigned closed-loop system eigenvalues when the closed-loop right eigenvector matrix $\mathbf{W}$ is block diagonal with the same partition and $\mathbf{M}$ is a lumped mass matrix.

Proof: Since the system is controllable, distinct eigenvalues $\{\mu_1, \mu_2, \cdots, \mu_n\}$ may be assigned with block-diagonal constraints on $\mathbf{W}$ by the method of receptances using equation (4.7) (described in full by Ram and Mottershead [9]). When block-diagonal $\mathbf{W}$ has partition $(n_1 \quad n_2)$, then

$$\mathbf{W}^{-1} = \begin{bmatrix} \mathbf{W}_{11}^{-1} & \mathbf{0} \\ \mathbf{0} & \mathbf{W}_{22}^{-1} \end{bmatrix} \tag{4.18}$$

Hence, from equation (4.15), the closed-loop stiffness matrix

$$\left(\mathbf{K} - \mathbf{B}\mathbf{G}^T\right) = \mathbf{M}\mathbf{W}\mathbf{\Lambda}\mathbf{W}^{-1} \tag{4.19}$$

is block diagonal with respect to the partition $(n_1 \quad n_2)$. Consequently, the closed-loop dynamic stiffness and receptance matrices are block diagonal and the system is block decoupled.

□

Remark 4.1: Equation (4.19) admits the use of a block diagonal mass matrix $\mathbf{M}$ with partition $(n_1 \quad n_2)$. However, for reasons of physical practicality, we discuss only the case of the diagonal (lumped) mass matrix.

□

Therefore, the block-decoupling vibration control algorithm for undamped systems may be summarised as:

1. Decouple the open-loop undamped system to form two uncoupled substructures. This is achieved by the imposition of modal degree of freedom constraints (4.16) on the closed-loop right eigenvectors $\mathbf{w}_k$ by the choice of parameters $\alpha_{\mu_k, j}$ to satisfy equation (4.11).
2. Assign desired eigenvalues $\mathbf{\Lambda}_{11} = diag\left(\mu_k\right)_{k=1}^{n_1}$ and $\mathbf{\Lambda}_{22} = diag\left(\mu_k\right)_{k=n_1+1}^{n}$ to the two substructures by the choice of control gain matrix $\mathbf{G}$ based on the method of receptances using equation (4.7).

The eigenpairs $\{\mathbf{\Lambda}_{11} \quad \mathbf{W}_{11}\}$ and $\{\mathbf{\Lambda}_{22} \quad \mathbf{W}_{22}\}$ are then assigned to the two independent substructures respectively.

If $\mathbf{W}$ is block diagonal with partition $(n_1, n_2, \cdots, n_v)$, then it is straightforward to show that the closed-loop stiffness matrix is also block diagonal with respect to the partition $(n_1, n_2, \cdots, n_v)$. The system becomes strictly diagonal when $v = n$.

4.4.1 Example 4.1

Consider the two degree-of-freedom mass-spring system,

$$\mathbf{M} = \begin{bmatrix} 1 & 0 \\ 0 & 1 \end{bmatrix} \quad \text{and} \quad \mathbf{K} = \begin{bmatrix} 2 & -1 \\ -1 & 1 \end{bmatrix}.$$

The open-loop eigenvalues are,

$\lambda_1 = 0.3820$
$\lambda_2 = 2.6180$

and the eigenvector matrix is,

$$\mathbf{V} = \begin{bmatrix} -0.5257 & -0.8507 \\ -0.8507 & 0.5257 \end{bmatrix}.$$

Now, a two-input proportional feedback controller is used to decouple the system into two independent single-degree-of-freedom systems. The prescribed eigenvalues of the two independent subsystems are

$$\mu_1 = 0.5$$
$$\mu_2 = 3.0.$$

According to the above analysis, modal nodal constraints are imposed to the closed-loop right eigenvectors so that the second entry of the first eigenvector and the first entry of the second eigenvector are zero. The force distribution matrix is chosen as,

$$\mathbf{B} = \begin{bmatrix} \mathbf{b}_1 & \mathbf{b}_2 \end{bmatrix} = \begin{bmatrix} 2 & 2 \\ 2 & 3 \end{bmatrix}.$$

To impose the required modal nodal constraints, the parameters $\alpha_{\mu_k,j}$ are chosen as,

$$\alpha_{\mu_1,1} = -\frac{\mathbf{e}_2^T \mathbf{r}_{\mu_1,2} \alpha_{\mu_1,2}}{\mathbf{e}_2^T \mathbf{r}_{\mu_1,1}};\ \alpha_{\mu_2,1} = -\frac{\mathbf{e}_1^T \mathbf{r}_{\mu_2,2} \alpha_{\mu_2,2}}{\mathbf{e}_1^T \mathbf{r}_{\mu_2,1}}$$

where,

$$\alpha_{\mu_1,2} = \alpha_{\mu_2,2} = 1,\ \mathbf{e}_2^T = \begin{bmatrix} 0 & 1 \end{bmatrix},\ \mathbf{e}_1^T = \begin{bmatrix} 1 & 0 \end{bmatrix}$$

This leads to the matrix of control gains,

$$\mathbf{G} = \begin{bmatrix} 3.25 & -2.5 \\ 0.5 & -1.0 \end{bmatrix}.$$

The resulting closed-loop eigenvalues are found to be,

$$\mu_1 = 0.5$$
$$\mu_2 = 3.0$$

and the eigenvectors are

$$\mathbf{w}_1 = \begin{bmatrix} 1 \\ 0 \end{bmatrix} \text{ and } \mathbf{w}_2 = \begin{bmatrix} 0 \\ 1 \end{bmatrix}.$$

The closed-loop systems matrices are

$$\mathbf{M}_{CL} = \begin{bmatrix} 1 & 0 \\ 0 & 1 \end{bmatrix} \text{ and } \mathbf{K}_{CL} = \begin{bmatrix} 0.5 & 0 \\ 0 & 3.0 \end{bmatrix}.$$

Hence, the closed-loop system is found to be decoupled into two independent single-degree-of-freedom systems with desired eigenvalues.

4.5 Block-decoupling control for damped structures with lumped masses

The closed-loop right- and left-eigenvalue problems may be written as,

$$\left(\mathbf{M}\mu_k^2 + \left(\mathbf{C} - \mathbf{B}\mathbf{F}^T\right)\mu_k + \left(\mathbf{K} - \mathbf{B}\mathbf{G}^T\right)\right)\mathbf{w}_k = \mathbf{0}\,. \tag{4.20}$$

and,

$$\boldsymbol{\psi}_k^T\left(\mathbf{M}\mu_k^2 + \left(\mathbf{C} - \mathbf{B}\mathbf{F}^T\right)\mu_k + \left(\mathbf{K} - \mathbf{B}\mathbf{G}^T\right)\right) = \mathbf{0},\ k = 1, 2, \cdots, 2n \tag{4.21}$$

By combining all the modes into a single expression the right eigenvalue problem (4.20) becomes,

$$\mathbf{M}\mathbf{W}\boldsymbol{\Lambda}^2 + \left(\mathbf{C} - \mathbf{B}\mathbf{F}^T\right)\mathbf{W}\boldsymbol{\Lambda} + \left(\mathbf{K} - \mathbf{B}\mathbf{G}^T\right)\mathbf{W} = \mathbf{0} \tag{4.22}$$

and the left eigenvalue problem (4.21) is,

$$\boldsymbol{\Lambda}^2\boldsymbol{\Psi}^T\mathbf{M} + \boldsymbol{\Lambda}\boldsymbol{\Psi}^T\left(\mathbf{C} - \mathbf{B}\mathbf{F}^T\right) + \boldsymbol{\Psi}^T\left(\mathbf{K} - \mathbf{B}\mathbf{G}^T\right) = \mathbf{0} \tag{4.23}$$

In these expressions $\mathbf{W} \in \mathbb{C}^{n\times 2n}$ is the matrix of right eigenvectors, $\boldsymbol{\Psi} \in \mathbb{C}^{n\times 2n}$ is the matrix of left eigenvectors, $\boldsymbol{\Lambda} = \text{diag}\begin{pmatrix}\mu_1 & \cdots & \mu_{2n}\end{pmatrix} \in \mathbb{C}^{2n\times 2n}$ is the spectral matrix. $\mathbb{C}$ denotes the field of complex numbers.

We partition matrices $\boldsymbol{\Lambda}$, $\mathbf{W}$ and $\boldsymbol{\Psi}$ as follows,

$$\boldsymbol{\Lambda} = \begin{bmatrix} \boldsymbol{\Lambda}_1 & \\ & \boldsymbol{\Lambda}_2 \end{bmatrix} \tag{4.24}$$
$$\boldsymbol{\Lambda}_1 = \text{diag}\begin{pmatrix}\mu_1 & \cdots & \mu_n\end{pmatrix} \in \mathbb{C}^{n\times n};\quad \boldsymbol{\Lambda}_2 = \text{diag}\begin{pmatrix}\mu_{n+1} & \cdots & \mu_{2n}\end{pmatrix} \in \mathbb{C}^{n\times n}$$

$$\begin{aligned}&\mathbf{W}=\begin{bmatrix}\mathbf{W}_{\mathrm{L}} & \mathbf{W}_{\mathrm{R}}\end{bmatrix}\\&\mathbf{W}_{\mathrm{L}}=\begin{bmatrix}\mathbf{w}_1 & \mathbf{w}_2 & \cdots & \mathbf{w}_n\end{bmatrix}\in\mathbb{C}^{n\times n};\quad \mathbf{W}_{\mathrm{R}}=\begin{bmatrix}\mathbf{w}_{n+1} & \mathbf{w}_{n+2} & \cdots & \mathbf{w}_{2n}\end{bmatrix}\in\mathbb{C}^{n\times n}\end{aligned}\tag{4.25}$$

and

$$\begin{aligned}&\boldsymbol{\Psi}=\begin{bmatrix}\boldsymbol{\Psi}_{\mathrm{L}} & \boldsymbol{\Psi}_{\mathrm{R}}\end{bmatrix}\\&\boldsymbol{\Psi}_{\mathrm{L}}=\begin{bmatrix}\boldsymbol{\psi}_1 & \boldsymbol{\psi}_2 & \cdots & \boldsymbol{\psi}_n\end{bmatrix}\in\mathbb{C}^{n\times n};\quad \boldsymbol{\Psi}_{\mathrm{R}}=\begin{bmatrix}\boldsymbol{\psi}_{n+1} & \boldsymbol{\psi}_{n+2} & \cdots & \boldsymbol{\psi}_{2n}\end{bmatrix}\in\mathbb{C}^{n\times n}\end{aligned}\tag{4.26}$$

In the case of complex eigenvalues, $\mu_{n+i}=\mu_n^*$ where $(\bullet)^*$ denotes complex conjugation. Real eigenvalues are grouped equally in $\boldsymbol{\Lambda}_1$ and $\boldsymbol{\Lambda}_2$ at the same diagonal locations.

Then by choice of $\alpha_{\mu_k,j}$ in (4.11), modal degree of freedom constraints on the closed-loop right eigenvectors $\mathbf{w}_k$ may be imposed,

$$\begin{aligned}&w_{jk}=w_{j(k+n)}=0, && j=n_1+1,n_1+2,\cdots,n, && k=1,2,\cdots,n_1\\&w_{jk}=w_{j(k+n)}=0, && j=1,2,\cdots,n_1, && k=n_1+1,n_1+2,\cdots,n\end{aligned}\tag{4.27}$$

Thus, $\mathbf{W}_{\mathrm{L}}$ and $\mathbf{W}_{\mathrm{R}}$ are block diagonalised with respect to the partition $\begin{pmatrix}n_1 & n_2\end{pmatrix}$ as,

$$\mathbf{W}_{\mathrm{L}}=\begin{bmatrix}\mathbf{W}_{\mathrm{L}11} & \mathbf{0}\\ \mathbf{0} & \mathbf{W}_{\mathrm{L}22}\end{bmatrix};\qquad \mathbf{W}_{\mathrm{R}}=\begin{bmatrix}\mathbf{W}_{\mathrm{R}11} & \mathbf{0}\\ \mathbf{0} & \mathbf{W}_{\mathrm{R}22}\end{bmatrix}\tag{4.28}$$

where $\mathbf{W}_{\mathrm{L}11},\mathbf{W}_{\mathrm{R}11}\in\mathbb{C}^{n_1\times n_1}$ and $\mathbf{W}_{\mathrm{L}22},\mathbf{W}_{\mathrm{R}22}\in\mathbb{C}^{n_2\times n_2}$.

We now write equations (4.22) and (4.23) in first-order form as,

$$\mathbf{A}\mathbf{X}=\mathbf{X}\boldsymbol{\Lambda}\tag{4.29}$$

$$\mathbf{Y}^T\mathbf{A}=\boldsymbol{\Lambda}\mathbf{Y}^T\tag{4.30}$$

where (from **Appendix 4.1**),

$$\begin{aligned}&\mathbf{X}=\begin{pmatrix}\mathbf{W}\\ \mathbf{W}\boldsymbol{\Lambda}\end{pmatrix};\quad \mathbf{Y}=\begin{pmatrix}\mathbf{Y}_{\mathrm{U}}\\ \mathbf{Y}_{\mathrm{L}}\end{pmatrix}=\begin{pmatrix}\left(\mathbf{K}-\mathbf{B}\mathbf{G}^T\right)^T\boldsymbol{\Psi}\boldsymbol{\Lambda}^{-1}\\ \mathbf{M}\boldsymbol{\Psi}\end{pmatrix}\\&\mathbf{Y}_{\mathrm{U}}=\begin{bmatrix}\mathbf{y}_{\mathrm{U}1} & \mathbf{y}_{\mathrm{U}2} & \cdots & \mathbf{y}_{\mathrm{U}2n}\end{bmatrix};\quad \mathbf{Y}_{\mathrm{L}}=\begin{bmatrix}\mathbf{y}_{\mathrm{L}1} & \mathbf{y}_{\mathrm{L}2} & \cdots & \mathbf{y}_{\mathrm{L}2n}\end{bmatrix}\end{aligned}\tag{4.31}$$

and,

$$\mathbf{A}=\begin{bmatrix}\mathbf{0} & \mathbf{I}\\ -\mathbf{M}^{-1}\left(\mathbf{K}-\mathbf{B}\mathbf{G}^{T}\right) & -\mathbf{M}^{-1}\left(\mathbf{C}-\mathbf{B}\mathbf{F}^{T}\right)\end{bmatrix} \tag{4.32}$$

Pre-multiplying and post-multiplying equations (4.29) and (4.30) by $\mathbf{Y}^{T}$ and $\mathbf{X}$ respectively lead to,

$$\mathbf{Y}^{T}\mathbf{A}\mathbf{X}=\mathbf{\Lambda}\mathbf{Y}^{T}\mathbf{X}=\mathbf{Y}^{T}\mathbf{X}\mathbf{\Lambda} \tag{4.33}$$

It can be seen from (4.33) that $\mathbf{Y}^{T}\mathbf{X}$ commutes with $\mathbf{\Lambda}$ so that,

$$\mathbf{Y}^{T}\mathbf{X}=\mathbf{D}_{1} \tag{4.34}$$

where $\mathbf{D}_{1}\in\mathbb{C}^{2n\times 2n}$ is diagonal.

Then by normalising the left and right eigenvectors,

$$\mathbf{Y}^{T}\mathbf{X}=\mathbf{I} \tag{4.35}$$

or,

$$\mathbf{Y}^{T}=\mathbf{X}^{-1} \tag{4.36}$$

where $\mathbf{I}$ is the identity matrix.

From equations (4.28) and (4.31),

$$\mathbf{X}=\begin{bmatrix}\mathbf{W}_{\mathrm{L}11} & \mathbf{0} & \mathbf{W}_{\mathrm{R}11} & \mathbf{0}\\ \mathbf{0} & \mathbf{W}_{\mathrm{L}22} & \mathbf{0} & \mathbf{W}_{\mathrm{R}22}\\ \mathbf{W}_{\mathrm{L}11}\mathbf{\Lambda}_{(1)11} & \mathbf{0} & \mathbf{W}_{\mathrm{R}11}\mathbf{\Lambda}_{(2)11} & \mathbf{0}\\ \mathbf{0} & \mathbf{W}_{\mathrm{L}22}\mathbf{\Lambda}_{(1)22} & \mathbf{0} & \mathbf{W}_{\mathrm{R}22}\mathbf{\Lambda}_{(2)22}\end{bmatrix} \tag{4.37}$$

where

$$\mathbf{\Lambda}_{1}=\begin{bmatrix}\mathbf{\Lambda}_{(1)11} & \mathbf{0}\\ \mathbf{0} & \mathbf{\Lambda}_{(1)22}\end{bmatrix};\ \mathbf{\Lambda}_{2}=\begin{bmatrix}\mathbf{\Lambda}_{(2)11} & \mathbf{0}\\ \mathbf{0} & \mathbf{\Lambda}_{(2)22}\end{bmatrix} \tag{4.38}$$

and $\mathbf{\Lambda}_{(1)11}, \mathbf{\Lambda}_{(2)11}\in\mathbb{C}^{n_1\times n_1}$; $\mathbf{\Lambda}_{(1)22}, \mathbf{\Lambda}_{(2)22}\in\mathbb{C}^{n_2\times n_2}$.

The matrix $\mathbf{Y}^{T}$ may be written as

$$\mathbf{Y}^T = \begin{bmatrix} \mathbf{Y}_{\mathrm{U}}^T & \mathbf{Y}_{\mathrm{L}}^T \end{bmatrix} = \begin{bmatrix} \mathbf{Y}_{\mathrm{UL}}^T & \mathbf{Y}_{\mathrm{LL}}^T \\ \mathbf{Y}_{\mathrm{UR}}^T & \mathbf{Y}_{\mathrm{LR}}^T \end{bmatrix} = \begin{bmatrix} \mathbf{Y}_{\mathrm{UL11}}^T & \mathbf{Y}_{\mathrm{UL21}}^T & \mathbf{Y}_{\mathrm{LL11}}^T & \mathbf{Y}_{\mathrm{LL21}}^T \\ \mathbf{Y}_{\mathrm{UL12}}^T & \mathbf{Y}_{\mathrm{UL22}}^T & \mathbf{Y}_{\mathrm{LL12}}^T & \mathbf{Y}_{\mathrm{LL22}}^T \\ \mathbf{Y}_{\mathrm{UR11}}^T & \mathbf{Y}_{\mathrm{UR21}}^T & \mathbf{Y}_{\mathrm{LR11}}^T & \mathbf{Y}_{\mathrm{LR21}}^T \\ \mathbf{Y}_{\mathrm{UR12}}^T & \mathbf{Y}_{\mathrm{UR22}}^T & \mathbf{Y}_{\mathrm{LR12}}^T & \mathbf{Y}_{\mathrm{LR22}}^T \end{bmatrix} \tag{4.39}$$

where

$$\begin{aligned} &\mathbf{Y}_{\mathrm{U}} = \begin{bmatrix} \mathbf{Y}_{\mathrm{UL}} & \mathbf{Y}_{\mathrm{UR}} \end{bmatrix}, \mathbf{Y}_{\mathrm{L}} = \begin{bmatrix} \mathbf{Y}_{\mathrm{LL}} & \mathbf{Y}_{\mathrm{LR}} \end{bmatrix}, \\ &\mathbf{Y}_{\mathrm{UL}} = \begin{bmatrix} \mathbf{Y}_{\mathrm{UL11}} & \mathbf{Y}_{\mathrm{UL12}} \\ \mathbf{Y}_{\mathrm{UL21}} & \mathbf{Y}_{\mathrm{UL22}} \end{bmatrix}, \mathbf{Y}_{\mathrm{LL}} = \begin{bmatrix} \mathbf{Y}_{\mathrm{LL11}} & \mathbf{Y}_{\mathrm{LL12}} \\ \mathbf{Y}_{\mathrm{LL21}} & \mathbf{Y}_{\mathrm{LL22}} \end{bmatrix}, \\ &\mathbf{Y}_{\mathrm{UR}} = \begin{bmatrix} \mathbf{Y}_{\mathrm{UR11}} & \mathbf{Y}_{\mathrm{UR12}} \\ \mathbf{Y}_{\mathrm{UR21}} & \mathbf{Y}_{\mathrm{UR22}} \end{bmatrix}, \ \mathbf{Y}_{\mathrm{LR}} = \begin{bmatrix} \mathbf{Y}_{\mathrm{LR11}} & \mathbf{Y}_{\mathrm{LR12}} \\ \mathbf{Y}_{\mathrm{LR21}} & \mathbf{Y}_{\mathrm{LR22}} \end{bmatrix} \end{aligned} \tag{4.40}$$

with $\mathbf{Y}_{\mathrm{UL}}, \mathbf{Y}_{\mathrm{UR}}, \mathbf{Y}_{\mathrm{LL}}, \mathbf{Y}_{\mathrm{LR}} \in \mathbb{C}^{n \times n}$; $\mathbf{Y}_{\mathrm{UL11}}, \mathbf{Y}_{\mathrm{LL11}}, \mathbf{Y}_{\mathrm{UR11}}, \mathbf{Y}_{\mathrm{LR11}} \in \mathbb{C}^{n_1 \times n_1}$;

$\mathbf{Y}_{\mathrm{UL12}}, \mathbf{Y}_{\mathrm{LL12}}, \mathbf{Y}_{\mathrm{UR12}}, \mathbf{Y}_{\mathrm{LR12}} \in \mathbb{C}^{n_1 \times n_2}$; $\mathbf{Y}_{\mathrm{UL21}}, \mathbf{Y}_{\mathrm{LL21}}, \mathbf{Y}_{\mathrm{UR21}}, \mathbf{Y}_{\mathrm{LR21}} \in \mathbb{C}^{n_2 \times n_1}$;

$\mathbf{Y}_{\mathrm{UL22}}, \mathbf{Y}_{\mathrm{LL22}}, \mathbf{Y}_{\mathrm{UR22}}, \mathbf{Y}_{\mathrm{LR22}} \in \mathbb{C}^{n_2 \times n_2}$.

Lemma 4.2: The closed-loop damping and stiffness matrices will be block diagonal with partition $\begin{pmatrix} n_1 & n_2 \end{pmatrix}$ with assigned closed loop eigenvalues when the closed-loop right eigenvector matrices $\mathbf{W}_{\mathrm{R}}$ and $\mathbf{W}_{\mathrm{L}}$ are block diagonal with the same partition and $\mathbf{M}$ is a lumped mass matrix.

Proof: Since the system is controllable, distinct eigenvalues $\{\mu_1, \mu_2, \cdots, \mu_{2n}\}$, may be assigned with block-diagonal constraints on $\mathbf{W}$ by the method of receptances using equation (4.7), described in full by Ram and Mottershead [9].

By using elementary transformations, the right eigenvector matrix $\mathbf{X}$ may be expressed as,

$$\tilde{\mathbf{X}} = \begin{bmatrix} \mathbf{W}_{\mathrm{L}11} & \mathbf{W}_{\mathrm{R}11} & \mathbf{0} & \mathbf{0} \\ \mathbf{W}_{\mathrm{L}11}\boldsymbol{\Lambda}_{(1)11} & \mathbf{W}_{\mathrm{R}11}\boldsymbol{\Lambda}_{(2)11} & \mathbf{0} & \mathbf{0} \\ \mathbf{0} & \mathbf{0} & \mathbf{W}_{\mathrm{L}22} & \mathbf{W}_{\mathrm{R}22} \\ \mathbf{0} & \mathbf{0} & \mathbf{W}_{\mathrm{L}22}\boldsymbol{\Lambda}_{(1)22} & \mathbf{W}_{\mathrm{R}22}\boldsymbol{\Lambda}_{(2)22} \end{bmatrix} \tag{4.41}$$

The left eigenvector matrix $\mathbf{Y}$ may then be written, using the relationship (4.36), as

$$\begin{aligned} \tilde{\mathbf{Y}} &= \begin{bmatrix} \mathbf{Y}_{\mathrm{UL}11}^T & \mathbf{Y}_{\mathrm{LL}11}^T & \mathbf{Y}_{\mathrm{UL}21}^T & \mathbf{Y}_{\mathrm{LL}21}^T \\ \mathbf{Y}_{\mathrm{UR}11}^T & \mathbf{Y}_{\mathrm{LR}11}^T & \mathbf{Y}_{\mathrm{UR}21}^T & \mathbf{Y}_{\mathrm{LR}21}^T \\ \mathbf{Y}_{\mathrm{UL}12}^T & \mathbf{Y}_{\mathrm{LL}12}^T & \mathbf{Y}_{\mathrm{UL}22}^T & \mathbf{Y}_{\mathrm{LL}22}^T \\ \mathbf{Y}_{\mathrm{UR}12}^T & \mathbf{Y}_{\mathrm{LR}12}^T & \mathbf{Y}_{\mathrm{UR}22}^T & \mathbf{Y}_{\mathrm{LR}22}^T \end{bmatrix} \\ &= \begin{bmatrix} \begin{bmatrix} \mathbf{W}_{\mathrm{L}11} & \mathbf{W}_{\mathrm{R}11} \\ \mathbf{W}_{\mathrm{L}11}\boldsymbol{\Lambda}_{(1)11} & \mathbf{W}_{\mathrm{R}11}\boldsymbol{\Lambda}_{(2)11} \end{bmatrix}^{-1} & \begin{bmatrix} \mathbf{0} & \mathbf{0} \\ \mathbf{0} & \mathbf{0} \end{bmatrix} \\ \begin{bmatrix} \mathbf{0} & \mathbf{0} \\ \mathbf{0} & \mathbf{0} \end{bmatrix} & \begin{bmatrix} \mathbf{W}_{\mathrm{L}22} & \mathbf{W}_{\mathrm{R}22} \\ \mathbf{W}_{\mathrm{L}22}\boldsymbol{\Lambda}_{(1)22} & \mathbf{W}_{\mathrm{R}22}\boldsymbol{\Lambda}_{(2)22} \end{bmatrix}^{-1} \end{bmatrix} \end{aligned} \tag{4.42}$$

so that,

$$\begin{aligned} &\mathbf{Y}_{\mathrm{UL}12}^T = \mathbf{0},\ \mathbf{Y}_{\mathrm{LL}12}^T = \mathbf{0},\ \mathbf{Y}_{\mathrm{UR}12}^T = \mathbf{0},\ \mathbf{Y}_{\mathrm{LR}12}^T = \mathbf{0} \\ &\mathbf{Y}_{\mathrm{UL}21}^T = \mathbf{0},\ \mathbf{Y}_{\mathrm{LL}21}^T = \mathbf{0},\ \mathbf{Y}_{\mathrm{UR}21}^T = \mathbf{0},\ \mathbf{Y}_{\mathrm{LR}21}^T = \mathbf{0} \end{aligned} \tag{4.43}$$

Therefore

$$\mathbf{Y}^T = \begin{bmatrix} \mathbf{Y}_{\mathrm{UL}11}^T & \mathbf{0} & \mathbf{Y}_{\mathrm{LL}11}^T & \mathbf{0} \\ \mathbf{0} & \mathbf{Y}_{\mathrm{UL}22}^T & \mathbf{0} & \mathbf{Y}_{\mathrm{LL}22}^T \\ \mathbf{Y}_{\mathrm{UR}11}^T & \mathbf{0} & \mathbf{Y}_{\mathrm{LR}11}^T & \mathbf{0} \\ \mathbf{0} & \mathbf{Y}_{\mathrm{UR}22}^T & \mathbf{0} & \mathbf{Y}_{\mathrm{LR}22}^T \end{bmatrix} \tag{4.44}$$

with

$$\mathbf{Y}_{\mathrm{LL}}^T = \begin{bmatrix} \mathbf{Y}_{\mathrm{LL}11}^T & \mathbf{0} \\ \mathbf{0} & \mathbf{Y}_{\mathrm{LL}22}^T \end{bmatrix} \text{ and } \mathbf{Y}_{\mathrm{LR}}^T = \begin{bmatrix} \mathbf{Y}_{\mathrm{LR}11}^T & \mathbf{0} \\ \mathbf{0} & \mathbf{Y}_{\mathrm{LR}22}^T \end{bmatrix} \tag{4.45}$$

block diagonal with respect to the partition $\begin{pmatrix} n_1 & n_2 \end{pmatrix}$.

From (4.31),

$$\mathbf{Y}_{\mathrm{LL}} = \mathbf{M}\boldsymbol{\Psi}_{\mathrm{L}};\quad \mathbf{Y}_{\mathrm{LR}} = \mathbf{M}\boldsymbol{\Psi}_{\mathrm{R}} \tag{4.46}$$

Since $\mathbf{M}$ is the lumped mass matrix it follows from equation (4.46) that $\boldsymbol{\Psi}_{\mathrm{L}}$ and $\boldsymbol{\Psi}_{\mathrm{R}}$ are block diagonal with respect to the partition $(n_1 \quad n_2)$.

It is known that the receptance matrix may be expressed as,

$$\begin{aligned}\hat{\mathbf{H}}(s) &= \begin{bmatrix}\mathbf{W}_{\mathrm{L}} & \mathbf{W}_{\mathrm{R}}\end{bmatrix}\begin{bmatrix}(\mathbf{I}_n s - \boldsymbol{\Lambda}_1)^{-1} & \mathbf{0} \\ \mathbf{0} & (\mathbf{I}_n s - \boldsymbol{\Lambda}_2)^{-1}\end{bmatrix}\begin{bmatrix}\boldsymbol{\Psi}_{\mathrm{L}}^T \\ \boldsymbol{\Psi}_{\mathrm{R}}^T\end{bmatrix} \\ &= \mathbf{W}_{\mathrm{L}}(\mathbf{I}_n s - \boldsymbol{\Lambda}_1)^{-1}\boldsymbol{\Psi}_{\mathrm{L}}^T + \mathbf{W}_{\mathrm{R}}(\mathbf{I}_n s - \boldsymbol{\Lambda}_2)^{-1}\boldsymbol{\Psi}_{\mathrm{R}}^T\end{aligned} \tag{4.47}$$

so that $\hat{\mathbf{H}}(s)$ is block diagonal with respect to the partition $(n_1 \quad n_2)$: so too is the dynamic stiffness matrix, i.e. the inverse of $\hat{\mathbf{H}}(s)$.

When $s = 0$,

$$\hat{\boldsymbol{\Gamma}}(0) = \left(\mathbf{K} - \mathbf{B}\mathbf{G}^T\right) \tag{4.48}$$

which shows that the closed-loop stiffness matrix is block diagonal with respect to the partition $(n_1 \quad n_2)$. The dynamic stiffness may be recast as

$$\begin{aligned}\hat{\boldsymbol{\Gamma}}(s) = &\begin{bmatrix}\mathbf{M}_1 & \mathbf{0} \\ \mathbf{0} & \mathbf{M}_2\end{bmatrix}s^2 + \begin{bmatrix}\left(\mathbf{C} - \mathbf{B}\mathbf{F}^T\right)_{11} & \left(\mathbf{C} - \mathbf{B}\mathbf{F}^T\right)_{12} \\ \left(\mathbf{C} - \mathbf{B}\mathbf{F}^T\right)_{21} & \left(\mathbf{C} - \mathbf{B}\mathbf{F}^T\right)_{22}\end{bmatrix}s \\ &+ \begin{bmatrix}\left(\mathbf{K} - \mathbf{B}\mathbf{G}^T\right)_{11} & \mathbf{0} \\ \mathbf{0} & \left(\mathbf{K} - \mathbf{B}\mathbf{G}^T\right)_{22}\end{bmatrix}\end{aligned} \tag{4.49}$$

so that,

$$\left(\mathbf{C} - \mathbf{B}\mathbf{F}^T\right)_{12} s = 0 \text{ and } \left(\mathbf{C} - \mathbf{B}\mathbf{F}^T\right)_{21} s = 0 \tag{4.50}$$

for arbitrary s. Hence the closed-loop damping matrix $\left(\mathbf{C} - \mathbf{B}\mathbf{F}^T\right)$ is block diagonal with respect to the partition $(n_1 \quad n_2)$.

Thus, if the sub-matrices of the right eigenvector, $\mathbf{W}_{\mathrm{L}}$ and $\mathbf{W}_{\mathrm{R}}$, are block diagonal with respect to the partition $(n_1 \quad n_2)$, then the closed-loop damping and stiffness matrices will also be block decoupled with respect to the partition $(n_1 \quad n_2)$.

□

Remark 4.2: Equations (4.46) admit the use of a block diagonal mass matrix **M** with partition $(n_1 \quad n_2)$. For the same reasons as given before, we only consider the case of the diagonal (lumped mass matrix).

□

Therefore, the block-decoupling vibration control algorithm for damped systems may be summarised as:

1. Decouple the open-loop damped system into two uncoupled substructures. This is achieved by the imposition of modal degree of freedom constraints (4.27) on the closed-loop right eigenvectors $\mathbf{w}_k$ by choice of parameters $\alpha_{\mu_k, j}$ to satisfy equation (4.11).
2. Assign desired eigenvalues $\left\{\boldsymbol{\Lambda}_{(1)11} \quad \boldsymbol{\Lambda}_{(2)11}\right\} = \left\{diag\left(\mu_k\right)_{k=1}^{n_1} \quad diag\left(\mu_k\right)_{k=n+1}^{n+n_1}\right\}$ and $\left\{\boldsymbol{\Lambda}_{(1)22} \quad \boldsymbol{\Lambda}_{(2)22}\right\} = \left\{diag\left(\mu_k\right)_{k=n_1+1}^{n} \quad diag\left(\mu_k\right)_{k=n+n_1+1}^{2n}\right\}$ to the two substructures by the choice of control gain matrices $\mathbf{F}, \mathbf{G}$ based on the method of receptances described by (4.7).

The eigenpairs $\left\{\left[\boldsymbol{\Lambda}_{(1)11} \quad \boldsymbol{\Lambda}_{(2)11}\right] \quad \left[\mathbf{W}_{\mathrm{L}11} \quad \mathbf{W}_{\mathrm{R}11}\right]\right\}$ and $\left\{\left[\boldsymbol{\Lambda}_{(1)22} \quad \boldsymbol{\Lambda}_{(2)22}\right] \quad \left[\mathbf{W}_{\mathrm{L}22} \quad \mathbf{W}_{\mathrm{R}22}\right]\right\}$ are then assigned to the two independent substructures respectively.

If $\mathbf{W}_{\mathrm{L}}$ and $\mathbf{W}_{\mathrm{R}}$ are block diagonal with respect to the partition $(n_1, n_2, \cdots, n_v)$, then the closed-loop stiffness and damping matrices are also block diagonal with respect to the partition $(n_1, n_2, \cdots, n_v)$. The system becomes strictly diagonal when $v = n$.

4.5.1 Example 4.2

Consider the three degree-of-freedom system shown in Fig. 4.1.

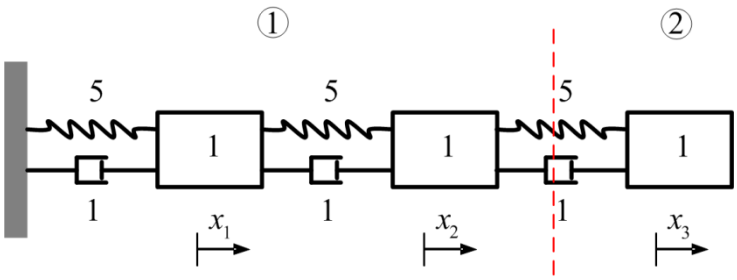

Fig. 4.1 The three degree-of-freedom system

The system matrices of the open-loop system are ,

$$\mathbf{M} = \mathbf{I},\ \mathbf{C} = \begin{bmatrix} 2 & -1 & 0 \\ -1 & 2 & -1 \\ 0 & -1 & 1 \end{bmatrix} \text{ and } \mathbf{K} = \begin{bmatrix} 10 & -5 & 0 \\ -5 & 10 & -5 \\ 0 & -5 & 5 \end{bmatrix}.$$

The open-loop eigenvalues are,

$$\lambda_{1,4} = -0.0990 \pm 0.9902\mathrm{i}$$
$$\lambda_{2,5} = -0.7775 \pm 2.6777\mathrm{i}\,.$$
$$\lambda_{3,6} = -1.6235 \pm 3.6877\mathrm{i}$$

Now, the block decoupling control method is used to decouple the three degree-of-freedom system into two independent substructures as shown in Fig. 4.1 . The eigenvalues of the first substructure are prescribed as,

$$\mu_{1,4} = -0.1 \pm 1.0\mathrm{i}$$
$$\mu_{2,5} = -0.8 \pm 2.8\mathrm{i}$$

and the second substructure

$\mu_{3,6} = -1.6 \pm 3.7\mathrm{i}$.

Modal degree of freedom constraints are imposed on the right eigenvectors of the closed-loop system so that the first two entries of the eigenvectors of the last mode and the last entry of the eigenvectors corresponding to the first two modes are zero. The three inputs are used and the force distribution matrix is chosen as

$$\mathbf{B} = \begin{bmatrix} \mathbf{b}_1 & \mathbf{b}_2 & \mathbf{b}_3 \end{bmatrix} = \begin{bmatrix} 1 & 2 & 3 \\ 0 & 1 & 3 \\ 2 & 0 & 0 \end{bmatrix}.$$

The parameters $\alpha_{\mu_k, j}$ are chosen as,

$$\alpha_{\mu_k,2} = 0.5, \qquad \alpha_{\mu_k,3} = 1, \qquad k = 1,2,4,5$$

$$\alpha_{\mu_k,3} = 1, \qquad k = 3,6$$

$$\alpha_{\mu_k,1} = \mathrm{inv}\left(\mathbf{r}_{\mu_k,1(3)}\right) \times \left(-\mathbf{r}_{\mu_k,2(3)}\alpha_{\mu_k,2} - \mathbf{r}_{\mu_k,3(3)}\alpha_{\mu_k,3}\right), \qquad k = 1,2,4,5$$

$$\begin{pmatrix} \alpha_{\mu_k,1} \\ \alpha_{\mu_k,2} \end{pmatrix} = \mathrm{inv}\left(\mathbf{R}_{\mu_k(1:2,1:2)}\right) \times \left(-\mathbf{r}_{\mu_k,3(1:2)}\alpha_{\mu_k,3}\right), \qquad k = 3,6.$$

and the control gains are found to be,

$$\mathbf{G} = \begin{bmatrix} 0 & 3.0559 & 6.1117 \\ -2.5 & -1.9910 & -3.9820 \\ -5.6250 & 10.6250 & -5.2083 \end{bmatrix} \text{ and } \mathbf{F} = \begin{bmatrix} 0 & 0.6617 & 1.3235 \\ -0.5 & -0.4420 & -0.8840 \\ -1.1000 & 2.1000 & -1.0333 \end{bmatrix}.$$

The closed-loop system is found to have eigenvalues,

$\mu_{1,4} = -0.1 \pm 1.0\mathrm{i}$
$\mu_{2,5} = -0.8 \pm 2.8\mathrm{i}$
$\mu_{3,6} = -1.6 \pm 3.7\mathrm{i}$

and eigenvectors

$$\mathbf{w}_1 = \begin{pmatrix} 0.7122+0.0948\mathrm{i} \\ 0.8198+0.1091\mathrm{i} \\ 0 \end{pmatrix}, \mathbf{w}_2 = \begin{pmatrix} 0.0683+0.1660\mathrm{i} \\ 0.1245+0.2759\mathrm{i} \\ 0 \end{pmatrix}, \mathbf{w}_3 = \begin{pmatrix} 0 \\ 0 \\ -0.1062 - 0.2082\mathrm{i} \end{pmatrix},$$

$$\mathbf{w}_4 = \mathbf{w}_1^*, \mathbf{w}_5 = \mathbf{w}_2^*, \mathbf{w}_6 = \mathbf{w}_3^*$$

The closed-loop system matrices are

$$\mathbf{M}_{CL} = \mathbf{I},\ \mathbf{C}_{CL} = \begin{bmatrix} -3.2939 & 3.0359 & 0 \\ -5.6322 & 5.0939 & 0 \\ 0 & 0 & 3.2000 \end{bmatrix}$$

and

$$\mathbf{K}_{CL} = \begin{bmatrix} -14.4469 & 13.4281 & 0 \\ -26.3910 & 23.9371 & 0 \\ 0 & 0 & 16.2500 \end{bmatrix}$$

which are decoupled to form two independent substructures with desired eigenvalues.

4.6 The number of actuators and sensors

We have seen that the application of modal degree of freedom constraints to block diagonalise the right eigenvector matrix with respect to the partition $(n_1 \quad n_2)$ will cause the closed-loop stiffness and damping matrices to be block decoupled with the same partition. Ram and Mottershead [9] showed that the number of required control inputs should be no less than $1+\max\{n_1, n_2\}$. In this section, it will be shown that the number of required control inputs may be reduced for structures with banded damping and stiffness matrices with semi-bandwidth r.

For practical engineering structures, the connections between components are in general localised. If discretised by finite element methods, it appears that the damping and stiffness matrices are banded with non-zero entries confined to a diagonal band and the coupling in general exists between adjacent degrees of freedom. Hence, the original structure may be decoupled into two independent

substructures if the coupling effect is eliminated in the connection of the two substructures.

Consider a n degree-of-freedom system structure whose dynamic stiffness matrix is banded with equal lower and upper semi-bandwidth r, $1 \le r \le \min\{n_1, n_2\}$, as shown in Fig. 4.2.

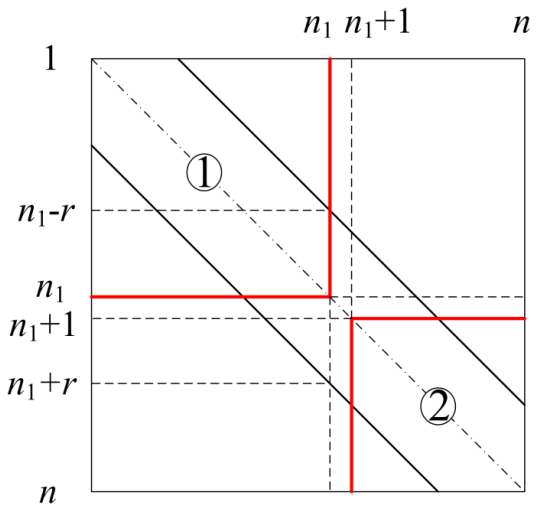

Fig. 4.2 The banded dynamic stiffness matrix

Now, the control objective is to decouple the structure into independent substructure 1 of dimension $n_1 \times n_1$ and substructure 2 of dimension $n_2 \times n_2$. It can be seen that the two substructures are only locally coupled from the $(n_1 - r + 1)^{\text{th}}$ degree of freedom to the $(n_1 + r)^{\text{th}}$ degree of freedom. Hence, the two substructures can be decoupled if the cross-coupling from the $(n_1 - r + 1)^{\text{th}}$ degree of freedom to the $(n_1 + r)^{\text{th}}$ degree of freedom is removed by using feedback control. This may be

achieved by applying neutralising feedback forces from the $(n_1 - r + 1)^{\text{th}}$ degree of freedom to the $(n_1 + r)^{\text{th}}$ degree of freedom.

Lemma 4.3: The n degree of freedom open-loop dynamic system with lumped mass and banded damping and stiffness matrices having equal lower and upper semi-bandwidth $1 \le r \le \min\{n_1, n_2\}$ may always be decoupled into two independent subsystems when $2r$ actuators are located at the coupled degrees of freedom and the number of inputs $q \ge 2r$.

Proof: Let us begin by assuming there are $2r$ actuators at the coupled degrees of freedom. The force distribution matrix $\mathbf{B}$ may then be written as

$$\mathbf{B} = \begin{bmatrix} \mathbf{0}_{(n_1 - r)\times q} \\ \tilde{\mathbf{B}}_{2r\times q} \\ \mathbf{0}_{(n_2 - r)\times q} \end{bmatrix} \text{ and } q \ge 2r \tag{4.51}$$

where $\tilde{\mathbf{B}}_{2r\times q}$ is real parameter matrix chosen so that all open-loop eigenvalues are controllable.

We have seen that the closed-loop damping and stiffness matrices become block diagonal when the right eigenvector matrices $\mathbf{W}_{\mathrm{L}}$ and $\mathbf{W}_{\mathrm{R}}$ are made block diagonal with the same partition $\begin{pmatrix} n_1 & n_2 \end{pmatrix}$ by choice of parameters $\boldsymbol{\alpha}_k \in \mathbb{C}^{q\times 1}$, $k = 1, 2, \cdots, 2n$. From equations (4.9) and (4.27), $\boldsymbol{\alpha}_k$ should be chosen such that,

$$\begin{aligned} &\mathbf{w}_{k(n_1+1:n)} = \mathbf{H}_{\mu_k(n_1+1:n,:)}\mathbf{B}\boldsymbol{\alpha}_k = \mathbf{H}_{\mu_k(n_1+1:n,\, n_1-r+1:n_1+r)}\tilde{\mathbf{B}}_{2r\times q}\boldsymbol{\alpha}_k = \mathbf{0}_{n_2\times 1}, \\ &k = 1, 2, \cdots, n_1, n+1, n+2, \cdots, n+n_1 \end{aligned} \tag{4.52}$$

and

$$\begin{aligned} &\mathbf{w}_{k(1:n_1)} = \mathbf{H}_{\mu_k(1:n_1,:)}\mathbf{B}\boldsymbol{\alpha}_k = \mathbf{H}_{\mu_k(1:n_1,\, n_1-r+1:\, n_1+r)}\tilde{\mathbf{B}}_{2r\times q}\boldsymbol{\alpha}_k = \mathbf{0}_{n_1\times 1}, \\ &k = n_1+1, n_1+2, \cdots, n, n+n_1+1, n+n_1+2, \cdots, 2n \end{aligned} \tag{4.53}$$

Strang and Nguyen [130] showed if a symmetric matrix $[\bullet]$ is banded with semi-bandwidth r, then above the r-th subdiagonal every submatrix of $[\bullet]^{-1}$ has rank $\le r$, and below the r-th superdiagonal every submatrix of $[\bullet]^{-1}$ has rank $\le r$. Therefore

$$\operatorname{rank}\left(\mathbf{H}_{\mu_k(n_1+1:n,\, n_1-r+1:n_1+r)}\right) \le r \tag{4.54}$$

and

$$\operatorname{rank}\left(\mathbf{H}_{\mu_k(1:n_1,\, n_1-r+1:n_1+r)}\right) \le r \tag{4.55}$$

Since

$$\operatorname{rank}\left(\mathbf{H}_{\mu_k(n_1+1:n,\, n_1-r+1:n_1+r)}\tilde{\mathbf{B}}_{2r\times q}\right) \le \operatorname{rank}\left(\mathbf{H}_{\mu_k(n_1+1:n,\, n_1-r+1:n_1+r)}\right) \le r \tag{4.56}$$

and

$$\operatorname{rank}\left(\mathbf{H}_{\mu_k(1:n_1,\, n_1-r+1:n_1+r)}\tilde{\mathbf{B}}_{2r\times q}\right) \le \operatorname{rank}\left(\mathbf{H}_{\mu_k(1:n_1,\, n_1-r+1:n_1+r)}\right) \le r \tag{4.57}$$

it follows that there always exists nontrivial $\boldsymbol{\alpha}_k$ satisfying equations (4.52) and (4.53)

$$\boldsymbol{\alpha}_k = \mathbf{null}\left(\mathbf{H}_{\mu_k(n_1+1:n,\, n_1-r+1:n_1+r)}\tilde{\mathbf{B}}_{2r\times q}\right)\boldsymbol{\gamma},\ \ k = 1,2,\cdots,n_1,n+1,n+2,\cdots,n+n_1 \tag{4.58}$$

and

$$\begin{aligned}&\boldsymbol{\alpha}_k = \mathbf{null}\left(\mathbf{H}_{\mu_k(1:n_1,\, n_1-r+1:n_1+r)}\tilde{\mathbf{B}}_{2r\times q}\right)\boldsymbol{\gamma},\\ &k = n_1+1,n_1+2,\cdots,n,n+n_1+1,n+n_1+2,\cdots,2n\end{aligned} \tag{4.59}$$

where $\boldsymbol{\gamma}$ is an arbitrary non-zero vector.

□

Remark 4.3: It may be proved similarly that if $\min\{n_1,n_2\} < r < \max\{n_1,n_2\}$, then $\min\{n_1,n_2\}+r$ actuators are sufficient for decoupling control of the open-loop system.

□

Lemma 4.4 A necessary condition for block decoupling is that sensors should be placed at the coupled degrees of freedom of the system.

Proof: The force distribution and control gain matrices may be partitioned as

$$\mathbf{B}=\begin{bmatrix}\mathbf{B}_1\\ \mathbf{B}_2\\ \mathbf{B}_3\end{bmatrix},\quad \mathbf{F}=\begin{bmatrix}\mathbf{F}_1\\ \mathbf{F}_2\\ \mathbf{F}_3\end{bmatrix}\ \text{and}\ \mathbf{G}=\begin{bmatrix}\mathbf{G}_1\\ \mathbf{G}_2\\ \mathbf{G}_3\end{bmatrix} \tag{4.60}$$

Let the degrees of freedom associated with $\mathbf{B}_2$, $\mathbf{F}_2$ and $\mathbf{G}_2$ be the coupled degrees of freedom. If there are no sensors placed on the coupled degrees of freedom, then $\mathbf{F}_2=\mathbf{0}$ and $\mathbf{G}_2=\mathbf{0}$ and

$$\mathbf{B}\mathbf{F}^T=\begin{bmatrix}\mathbf{B}_1\mathbf{F}_1^T & \mathbf{B}_1\mathbf{F}_2^T & \mathbf{B}_1\mathbf{F}_3^T\\ \mathbf{0} & \mathbf{0} & \mathbf{0}\\ \mathbf{B}_3\mathbf{F}_1^T & \mathbf{B}_3\mathbf{F}_2^T & \mathbf{B}_3\mathbf{F}_3^T\end{bmatrix}\ \text{and}\ \mathbf{B}\mathbf{G}^T=\begin{bmatrix}\mathbf{B}_1\mathbf{G}_1^T & \mathbf{B}_1\mathbf{G}_2^T & \mathbf{B}_1\mathbf{G}_3^T\\ \mathbf{0} & \mathbf{0} & \mathbf{0}\\ \mathbf{B}_3\mathbf{G}_1^T & \mathbf{B}_3\mathbf{G}_2^T & \mathbf{B}_3\mathbf{G}_3^T\end{bmatrix} \tag{4.61}$$

Consequently, the coupling between the coupled degrees of freedom cannot be eliminated by feedback control.

□

When the mass matrix is diagonal and the damping and stiffness matrices are banded, certain degrees of freedom may be free of actuation and the eigenvalues can be assigned exactly by using full state feedback, which is illustrated in the following example.

4.6.1 Example 4.3

Consider a five-degree-of-freedom system with matrices

$$\mathbf{M}=\mathbf{I},\ \mathbf{C}=\begin{bmatrix}2 & -1 & & & \\ -1 & 2 & -1 & & \\ & -1 & 2 & -1 & \\ & & -1 & 2 & -1\\ & & & -1 & 1\end{bmatrix}\ \text{and}\ \mathbf{K}=\begin{bmatrix}20 & -10 & & & \\ -10 & 15 & -5 & & \\ & -5 & 10 & -5 & \\ & & -5 & 10 & -5\\ & & & -5 & 5\end{bmatrix}.$$

The open-loop eigenvalues are

$$\lambda_{1,6} = -0.0462 \pm 0.7706\text{i}$$
$$\lambda_{2,7} = -0.3550 \pm 2.0897\text{i}$$
$$\lambda_{3,8} = -0.9051 \pm 3.0365\text{i}$$
$$\lambda_{4,9} = -1.6249 \pm 3.7653\text{i}$$
$$\lambda_{5,10} = -1.5688 \pm 5.0190\text{i}$$

The open-loop system is to be decoupled into two uncoupled subsystems. The first subsystem consists of the first three degrees of freedom with prescribed eigenvalues,

$$\mu_{1,6} = -0.05 \pm 0.60\text{i}$$
$$\mu_{2,7} = -0.35 \pm 1.80\text{i}$$
$$\mu_{3,8} = -0.90 \pm 2.80\text{i}$$

and the second subsystem consists of the last two degrees of freedom with prescribed eigenvalues,

$$\mu_{4,9} = -1.42 \pm 3.50\text{i}$$
$$\mu_{5,10} = -1.90 \pm 3.90\text{i}.$$

Modal degree of freedom constraints are imposed on the right eigenvectors so that the first three entries of the eigenvectors corresponding to the last two modes and the last two entries of the eigenvectors corresponding to the first three modes are zero. The semi-bandwidth of the damping and stiffness matrices is one. Hence, it is possible to have the first two and the last degrees of freedom free actuation. Here, two inputs are used and the force distribution matrix is chosen as,

$$\mathbf{B} = \begin{bmatrix} \mathbf{b}_1 & \mathbf{b}_2 \end{bmatrix} = \begin{bmatrix} 0 & 0 \\ 0 & 0 \\ 1 & 2 \\ 5 & 4 \\ 0 & 0 \end{bmatrix}$$

The parameters $\alpha_{\mu_k, j}$ are chosen as,

$$\boldsymbol{\alpha}_k = \mathbf{null}\left(\mathbf{R}_{\mu_k(4:5,1:2)}\right)\mathbf{e}_1, \qquad k = 1,2,3,6,7,8$$

and,

$$\boldsymbol{\alpha}_k = \mathbf{null}\left(\mathbf{R}_{\mu_k(1:3,1:2)}\right)\mathbf{e}_1, \qquad k = 4,5,9,10$$

where $\mathbf{e}_1$ is the 1^{st} unit vector.

The control gains are found to be,

$$\mathbf{F} = \begin{bmatrix} 3.3447 & -4.1809 \\ -0.2537 & 0.3172 \\ -2.6000 & 3.0000 \\ -0.5467 & -0.2267 \\ -2.0508 & 1.0254 \end{bmatrix} \text{ and } \mathbf{G} = \begin{bmatrix} -75.1354 & 93.9193 \\ 63.8172 & -79.7715 \\ -19.7563 & 23.4453 \\ -2.6953 & -1.1523 \\ -10.2043 & 5.1021 \end{bmatrix}$$

and the closed-loop eigenvalues are,

$\mu_{1,6} = -0.05 \pm 0.60\text{i}$
$\mu_{2,7} = -0.35 \pm 1.80\text{i}$
$\mu_{3,8} = -0.90 \pm 2.80\text{i}$
$\mu_{4,9} = -1.42 \pm 3.50\text{i}$
$\mu_{5,10} = -1.90 \pm 3.90\text{i}$

with eigenvectors,

$$\mathbf{w}_1 = \begin{pmatrix} 0.1970 + 0.0071\text{i} \\ 0.3869 + 0.0131\text{i} \\ 0.7384 \\ 0 \\ 0 \end{pmatrix}, \mathbf{w}_2 = \begin{pmatrix} 0.0057 - 0.1784\text{i} \\ -0.0026 - 0.2974\text{i} \\ -0.0630 - 0.3240\text{i} \\ 0 \\ 0 \end{pmatrix}, \mathbf{w}_3 = \begin{pmatrix} -0.0113 - 0.1808\text{i} \\ -0.0651 - 0.2025\text{i} \\ -0.0706 + 0.1435\text{i} \\ 0 \\ 0 \end{pmatrix},$$

$$\mathbf{w}_4 = \begin{pmatrix} 0 \\ 0 \\ 0 \\ -0.0846 - 0.2086\text{i} \\ 0.0452 + 0.1130\text{i} \end{pmatrix}, \mathbf{w}_5 = \begin{pmatrix} 0 \\ 0 \\ 0 \\ -0.0926 + 0.1900\text{i} \\ 0.0340 - 0.0681\text{i} \end{pmatrix}$$

$\mathbf{w}_6 = \mathbf{w}_1^*, \mathbf{w}_7 = \mathbf{w}_2^*, \mathbf{w}_8 = \mathbf{w}_3^*, \mathbf{w}_9 = \mathbf{w}_4^*, \mathbf{w}_{10} = \mathbf{w}_5^*$

The closed-loop system matrices are,

$$\mathbf{M} = \mathbf{I}$$

$$\mathbf{C}_{CL} = \begin{bmatrix} 2 & -1 & 0 & 0 & 0 \\ -1 & 2 & -1 & 0 & 0 \\ 5.0170 & -1.3806 & -1.4000 & 0 & 0 \\ 0 & 0 & 0 & 5.6400 & 5.1525 \\ 0 & 0 & 0 & -1 & 1 \end{bmatrix}$$

$$\mathbf{K}_{CL} = \begin{bmatrix} 20 & -10 & 0 & 0 & 0 \\ -10 & 15 & -5 & 0 & 0 \\ -112.7032 & 90.7257 & -17.1343 & 0 & 0 \\ 0 & 0 & 0 & 28.09 & 25.6128 \\ 0 & 0 & 0 & -5 & 5 \end{bmatrix}$$

Thus, two independent subsystems are achieved as desired with given eigenvalues.

4.7 Decoupling of linear structures with banded mass matrix

In the preceding analysis the mass matrix was assumed to be diagonal (or lumped). This is an unrealistic assumption and in this section we seek to replace it with the more practical representation of a banded mass matrix. The coupling between system degrees of freedom may reasonably be assumed to be localised, as in the case of the finite-element consistent mass matrix. Here we introduce acceleration feedback (in addition to displacement and velocity feedback) to decouple the linear dynamic system with inertia interaction.

In this case, the equations of motion of the closed-loop system may be expressed as,

$$\left(\mathbf{M} - \mathbf{B}\mathbf{D}^T\right)\ddot{\mathbf{x}} + \left(\mathbf{C} - \mathbf{B}\mathbf{F}^T\right)\dot{\mathbf{x}} + \left(\mathbf{K} - \mathbf{B}\mathbf{G}^T\right)\mathbf{x} = \mathbf{0} \tag{4.62}$$

where $\mathbf{D}$, $\mathbf{F}$ and $\mathbf{G} \in \mathbb{R}^{n\times q}$ are the acceleration, velocity and displacement feedback gain matrices respectively. $\mathbf{B} \in \mathbb{R}^{n\times q}$ is the force distribution matrix. If the open-loop dynamic stiffness matrix $\mathbf{\Gamma}(s) = \mathbf{M}s^2 + \mathbf{C}s + \mathbf{K}$ is of semi-bandwidth r ,

$1 \le r \le \min\{n_1, n_2\}$, then the minimum number of inputs is $q = 2r$ and the force distribution matrix may be given by (4.51).

$$\mathbf{B} = \begin{bmatrix} \mathbf{0}_{(n_1-r)\times 2r} \\ \tilde{\mathbf{B}}_{2r\times 2r} \\ \mathbf{0}_{(n_2-r)\times 2r} \end{bmatrix} \tag{4.63}$$

where $\tilde{\mathbf{B}}_{2r\times 2r}$ is chosen to be invertible.

If the acceleration gain matrix is of the form,

$$\mathbf{D} = \begin{bmatrix} \mathbf{0}_{(n_1-r)\times 2r} \\ \tilde{\mathbf{D}}_{2r\times 2r} \\ \mathbf{0}_{(n_2-r)\times 2r} \end{bmatrix} \tag{4.64}$$

then,

$$\mathbf{B}\mathbf{D}^T = \begin{bmatrix} \mathbf{0}_{(n_1-r)\times(n_1-r)} & \mathbf{0}_{(n_1-r)\times 2r} & \mathbf{0}_{(n_1-r)\times(n_2-r)} \\ \mathbf{0}_{2r\times(n_1-r)} & \tilde{\mathbf{B}}_{2r\times 2r}\tilde{\mathbf{D}}^T_{2r\times 2r} & \mathbf{0}_{2r\times(n_2-r)} \\ \mathbf{0}_{(n_2-r)\times(n_1-r)} & \mathbf{0}_{(n_2-r)\times 2r} & \mathbf{0}_{(n_2-r)\times(n_2-r)} \end{bmatrix} \tag{4.65}$$

The open-loop mass matrix may be written as

$$\mathbf{M} = \begin{bmatrix} \mathbf{M}_{(1:n_1-r,\,1:n_1-r)} & \mathbf{M}_{(1:n_1-r,\,n_1-r+1:n_1)} & \mathbf{0}_{(1:n_1-r,\,n_1+1:n_1+r)} & \mathbf{0}_{(1:n_1-r,\,n_1+r+1:n)} \\ \mathbf{M}_{(n_1-r+1:n_1,\,1:n_1-r)} & \begin{bmatrix} \mathbf{M}_{(n_1-r+1:n_1,\,n_1-r+1:n_1)} \\ \mathbf{M}_{(n_1+1:n_1+r,\,n_1-r+1:n_1)} \end{bmatrix} & \begin{matrix} \mathbf{M}_{(n_1-r+1:n_1,\,n_1+1:n_1+r)} \\ \mathbf{M}_{(n_1+1:n_1+r,\,n_1+1:n_1+r)} \end{matrix} & \begin{matrix} \mathbf{0}_{(n_1-r+1:n_1,\,n_1+r+1:n)} \\ \mathbf{M}_{(n_1+1:n_1+r,\,n_1+r+1:n)} \end{matrix} \\ \mathbf{0}_{(n_1+1:n_1+r,\,1:n_1-r)} & & & \\ \mathbf{0}_{(n_1+r+1:n,\,1:n_1-r)} & \mathbf{0}_{(n_1+r+1:n,\,n_1-r+1:n_1)} & \mathbf{M}_{(n_1+r+1:n,\,n_1+1:n_1+r)} & \mathbf{M}_{(n_1+r+1:n,\,n_1+r+1:n)} \end{bmatrix} \tag{4.66}$$

where we denote the central sub-matrix as,

$$\mathbf{M}_1 = \begin{bmatrix} \mathbf{M}_{(n_1-r+1:n_1,\,n_1-r+1:n_1)} & \mathbf{M}_{(n_1-r+1:n_1,\,n_1+1:n_1+r)} \\ \mathbf{M}_{(n_1+1:n_1+r,\,n_1-r+1:n_1)} & \mathbf{M}_{(n_1+1:n_1+r,\,n_1+1:n_1+r)} \end{bmatrix} \tag{4.67}$$

Acceleration feedback is now applied to modify $\mathbf{M}_1$ such that

$$\mathbf{M}_1 - \tilde{\mathbf{M}}_1 = \tilde{\mathbf{B}}\tilde{\mathbf{D}}^T \tag{4.68}$$

where

$$\tilde{\mathbf{M}}_1 = \begin{bmatrix} \tilde{\mathbf{M}}_{(n_1-r+1:\,n_1,\,n_1-r+1:\,n_1)} & \mathbf{0}_{(n_1-r+1:\,n_1,\,n_1+1:\,n_1+r)} \\ \mathbf{0}_{(n_1+1:\,n_1+r,\,n_1-r+1:\,n_1)} & \tilde{\mathbf{M}}_{(n_1+1:\,n_1+r,\,n_1+1:\,n_1+r)} \end{bmatrix} \tag{4.69}$$

is prescribed to be symmetric and to make the closed-loop mass matrix $\mathbf{M}_{CL}$ nonsingular.

$$\mathbf{M}_{CL} = \begin{bmatrix} \mathbf{M}_{(1:\,n_1-r,\,1:\,n_1-r)} & \mathbf{M}_{(1:\,n_1-r,\,n_1-r+1:\,n_1)} & \mathbf{0}_{(1:\,n_1-r,\,n_1+1:\,n_1+r)} & \mathbf{0}_{(1:\,n_1-r,\,n_1+r+1:\,n)} \\ \mathbf{M}_{(n_1-r+1:\,n_1,\,1:\,n_1-r)} & \tilde{\mathbf{M}}_{(n_1-r+1:\,n_1,\,n_1-r+1:\,n_1)} & \mathbf{0}_{(n_1-r+1:\,n_1,\,n_1+1:\,n_1+r)} & \mathbf{0}_{(n_1-r+1:\,n_1,\,n_1+r+1:\,n)} \\ \mathbf{0}_{(n_1+1:\,n_1+r,\,1:\,n_1-r)} & \mathbf{0}_{(n_1+1:\,n_1+r,\,n_1-r+1:\,n_1)} & \tilde{\mathbf{M}}_{(n_1+1:\,n_1+r,\,n_1+1:\,n_1+r)} & \mathbf{M}_{(n_1+1:\,n_1+r,\,n_1+r+1:\,n)} \\ \mathbf{0}_{(n_1+r+1:\,n,\,1:\,n_1-r)} & \mathbf{0}_{(n_1+r+1:\,n,\,n_1-r+1:\,n_1)} & \mathbf{M}_{(n_1+r+1:\,n,\,n_1+1:\,n_1+r)} & \mathbf{M}_{(n_1+r+1:\,n,\,n_1+r+1:\,n)} \end{bmatrix} \tag{4.70}$$

From equation (4.68), the acceleration feedback gain submatrix $\tilde{\mathbf{D}}$ is seen to be given by,

$$\tilde{\mathbf{D}} = \left(\mathbf{M}_1 - \tilde{\mathbf{M}}_1\right)\left(\tilde{\mathbf{B}}^T\right)^{-1} \tag{4.71}$$

Now, the eigenvalue problem associated with the closed-loop linear system becomes

$$\left(\mathbf{M}\mu_k^2 + \mathbf{C}\mu_k + \mathbf{K}\right)\mathbf{w}_k = \mathbf{B}\left(\mu_k^2\mathbf{D}^T + \mu_k\mathbf{F}^T + \mathbf{G}^T\right)\mathbf{w}_k, \quad k = 1,2,\cdots,2n \tag{4.72}$$

Then,

$$\mathbf{w}_k = \alpha_{\mu_k,1}\mathbf{r}_{\mu_k,1} + \alpha_{\mu_k,2}\mathbf{r}_{\mu_k,2} + \cdots + \alpha_{\mu_k,q}\mathbf{r}_{\mu_k,q} = \mathbf{R}_{\mu_k}\boldsymbol{\alpha}_k^T \tag{4.73}$$

where

$$\alpha_{\mu_k,j} = \left(\mu_k^2\mathbf{d}_j^T + \mu_k\mathbf{f}_j^T + \mathbf{g}_j^T\right)\mathbf{w}_k, \;\; k = 1,2,\cdots,2n, \quad j = 1,2,\cdots,q \tag{4.74}$$

$$\mathbf{R}_{\mu_k} = \left(\mathbf{M}\mu_k^2 + \mathbf{C}\mu_k + \mathbf{K}\right)^{-1}\mathbf{B}, \quad k = 1,2,\cdots,2n \tag{4.75}$$

and $\alpha_{\mu_k,j}$ are arbitrary variables and $\boldsymbol{\alpha}_k^T$ are non-zero vectors.

Equations (4.74) may be rewritten as,

$$\xi_{\mu_k,j} = \alpha_{\mu_k,j} - \mu_k^2\mathbf{d}_j^T\mathbf{w}_k = \left(\mu_k\mathbf{f}_j^T + \mathbf{g}_j^T\right)\mathbf{w}_k, \;\; k = 1,2,\cdots,2n, \quad j = 1,2,\cdots,q \tag{4.76}$$

or,

$$\boldsymbol{\xi}_k^T = \boldsymbol{\alpha}_k^T - \mu_k^2 \mathbf{w}_k^T \mathbf{D}, \quad k = 1, 2, \cdots, 2n \tag{4.77}$$

where,

$$\boldsymbol{\xi}_k^T = \begin{bmatrix} \xi_{\mu_k,1} & \xi_{\mu_k,2} & \cdots & \xi_{\mu_k,q} \end{bmatrix} \tag{4.78}$$

Hence, the velocity and displacement feedback control gains are obtained by solving,

$$\mathbf{P} \begin{bmatrix} \mathbf{F} \\ \mathbf{G} \end{bmatrix} = \boldsymbol{\Xi} \tag{4.79}$$

where,

$$\mathbf{P} = \begin{bmatrix} \mu_1 \mathbf{w}_1^T & \mathbf{w}_1^T \\ \mu_2 \mathbf{w}_2^T & \mathbf{w}_2^T \\ \vdots & \vdots \\ \mu_{2n} \mathbf{w}_{2n}^T & \mathbf{w}_{2n}^T \end{bmatrix}, \quad \boldsymbol{\Xi} = \begin{bmatrix} \boldsymbol{\xi}_1^T \\ \boldsymbol{\xi}_2^T \\ \vdots \\ \boldsymbol{\xi}_{2n}^T \end{bmatrix}, \tag{4.80}$$

The closed-loop system will be block decoupled when modal degree of freedom constraints (4.27) are imposed on $\mathbf{w}_k$ in (4.80). It is seen that the decoupling algorithm is basically similar to that presented in Section 4.5 except for the additional of acceleration feedback to generate a block diagonal closed-loop mass matrix.

4.7.1 Example 4.4

Consider the structure shown in Fig. 4.3, which consists of a beam of length $5l = 5\,\text{m}$ fixed at both ends. Assume the cross section of the beam to be rectangular with width $b_s = 2\text{cm}$ and height $h_s = 1\text{cm}$ respectively and the material of the beam to be steel with Young's modulus, $E = 2.0 \times 10^{11}\,\text{Pa}$, and mass density, $\rho_s = 7{,}800\ \text{kg/m}^3$.

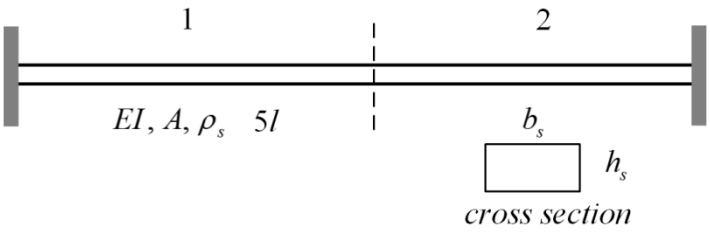

Fig. 4.3 A beam with both ends fixed

The beam is discretised into five beam elements of equal length, with the joints undergoing lateral and rotational displacements. The consistent-mass matrix is employed to include the inertia coupling effect. That is, the mass matrix of each beam element $\mathbf{M}_e$ is

$$\mathbf{M}_e = \frac{\rho_s A l}{420}\begin{bmatrix} 156 & 22l & 54 & -13l \\ 22l & 4l^2 & 13l & -3l^2 \\ 54 & 13l & 156 & -22l \\ -13l & -3l^2 & -22l & 4l^2 \end{bmatrix}.$$

For the sake of illustration, proportional damping $\mathbf{C} = \zeta_1\mathbf{M} + \zeta_2\mathbf{K}$, ($\zeta_1 = 0.001$ and $\zeta_2 = 0.0002$) is assumed.

The open-loop eigenvalues are

$$\lambda_{1,9} = 10^2 \times (-0.0002 \pm 0.1309\mathrm{i}); \quad \lambda_{2,10} = 10^2 \times (-0.0013 \pm 0.3620\mathrm{i});$$
$$\lambda_{3,11} = 10^2 \times (-0.0051 \pm 0.7167\mathrm{i}); \quad \lambda_{4,12} = 10^2 \times (-0.0143 \pm 1.1940\mathrm{i});$$
$$\lambda_{5,13} = 10^2 \times (-0.0402 \pm 2.0045\mathrm{i}); \quad \lambda_{6,14} = 10^2 \times (-0.0891 \pm 2.9830\mathrm{i});$$
$$\lambda_{7,15} = 10^2 \times (-0.1940 \pm 4.4003\mathrm{i}); \quad \lambda_{8,16} = 10^2 \times (-0.3882 \pm 6.2186\mathrm{i}).$$

Now, as shown in Fig. 4.3, the beam is to be decoupled such that beam 1 of length $2.5l$ with prescribed eigenvalues

$$\mu_{1,9} = 10^2 \times (-0.001 \pm 0.12\mathrm{i}); \quad \mu_{2,10} = 10^2 \times (-0.002 \pm 0.38\mathrm{i});$$
$$\mu_{3,11} = 10^2 \times (-0.007 \pm 0.60\mathrm{i}); \quad \mu_{4,12} = 10^2 \times (-0.02 \pm 1.00\mathrm{i});$$

is independent from beam 2 of length $2.5l$ with eigenvalues.

$\mu_{5,13} = 10^2 \times (-0.04 \pm 2.20\mathrm{i})$; $\mu_{6,14} = 10^2 \times (-0.09 \pm 3.50\mathrm{i})$;
$\mu_{7,15} = 10^2 \times (-0.22 \pm 4.00\mathrm{i})$; $\mu_{8,16} = 10^2 \times (-0.40 \pm 6.00\mathrm{i})$.

The closed-loop mass submatrix is given as,

$$\tilde{\mathbf{M}}_1 = \tilde{\mathbf{M}}_{(3:6,3:6)} = \begin{bmatrix} 1.2 & 0.2 & 0 & 0 \\ 0.2 & 0.1 & 0 & 0 \\ 0 & 0 & 1.2 & 0.2 \\ 0 & 0 & 0.2 & 0.1 \end{bmatrix}$$

and the force distribution matrix is chosen to be,

$$\mathbf{B} = \begin{bmatrix} 0 & 0 & 0 & 0 \\ 0 & 0 & 0 & 0 \\ 2 & -18 & -5 & 7 \\ -1 & 8 & 3 & 17 \\ -19 & -9 & -6 & -2 \\ -4 & 1 & 5 & -21 \\ 0 & 0 & 0 & 0 \\ 0 & 0 & 0 & 0 \end{bmatrix}.$$

Then the acceleration feedback gain matrix is found to be

$$\mathbf{D} = \begin{bmatrix} 0 & 0 & 0 & 0 \\ 0 & 0 & 0 & 0 \\ 0.0001 & 0.0126 & -0.0496 & -0.0089 \\ 0.0003 & 0.0178 & -0.0334 & -0.0066 \\ 0.0059 & -0.0065 & -0.0044 & 0.0070 \\ 0.0111 & 0.0066 & -0.0112 & -0.0011 \\ 0 & 0 & 0 & 0 \\ 0 & 0 & 0 & 0 \end{bmatrix}.$$

By using the proposed method, the arbitrary parameters are chosen as

$$\boldsymbol{\alpha}_k = \mathbf{null}\left(\mathbf{R}_{\mu_k(5:8,1:4)}\right)\mathbf{e}_1, \qquad k = 1,\cdots 4,9,\cdots,12$$

and

$$\boldsymbol{\alpha}_k = \mathbf{null}\left(\mathbf{R}_{\mu_k(1:4,1:4)}\right)\mathbf{e}_1, \qquad k = 5,\cdots,8,13,\cdots,16$$

where $\mathbf{e}_1$ is the 1^{st} unit vector.

The velocity and displacement feedback matrices are found to be,

$$\mathbf{F} = \begin{bmatrix} -0.0437 & -0.1278 & 0.3051 & 0.0749 \\ -0.2646 & -1.8709 & 3.3882 & 0.7680 \\ 0.3407 & 2.3008 & -4.0814 & -0.9461 \\ -0.0180 & -0.0095 & 0.1289 & 0.0273 \\ -5.1846 & 18.4621 & -64.9532 & 2.4458 \\ -1.5823 & 4.5051 & -16.0528 & 0.6276 \\ -22.9302 & 66.8830 & -237.2810 & 9.0499 \\ 0.1412 & -0.5029 & 1.7722 & -0.0678 \end{bmatrix}$$

$$\mathbf{G} = 10^5 \times \begin{bmatrix} -0.0012 & 0.0026 & -0.0003 & 0.0003 \\ -0.0014 & 0.0123 & -0.0132 & -0.0023 \\ 0.0030 & -0.0111 & 0.0135 & 0.0012 \\ -0.0004 & 0.0043 & -0.0018 & -0.0005 \\ 0.4696 & -0.1181 & 0.5902 & -0.0221 \\ 0.1085 & -0.0226 & 0.1165 & -0.0031 \\ 1.5801 & -0.4320 & 2.0866 & -0.0720 \\ -0.0121 & 0.0035 & -0.0168 & 0.0006 \end{bmatrix}$$

and the closed-loop matrices are,

$$\mathbf{M}_{CL} = \begin{bmatrix} \mathbf{M}_{CL11} & 0 \\ \mathbf{0} & \mathbf{M}_{CL22} \end{bmatrix}$$

$$\mathbf{M}_{CL11} = \begin{bmatrix} 1.1589 & 0 & 0.2006 & -0.0483 \\ 0 & 0.0297 & 0.0483 & -0.0111 \\ 0.2006 & 0.0483 & 1.2000 & 0.2000 \\ -0.0483 & -0.0111 & 0.2000 & 0.1000 \end{bmatrix}$$

$$\mathbf{M}_{CL22} = \begin{bmatrix} 1.2000 & 0.2000 & 0.2006 & -0.0483 \\ 0.2000 & 0.1000 & 0.0483 & -0.0111 \\ 0.2006 & 0.0483 & 1.1589 & 0 \\ -0.0483 & -0.0111 & 0 & 0.0297 \end{bmatrix}$$

$$\mathbf{K}_{CL} = \begin{bmatrix} \mathbf{K}_{CL11} & \mathbf{0} \\ \mathbf{0} & \mathbf{K}_{CL22} \end{bmatrix}$$

$$\mathbf{K}_{CL11} = 10^6 \times \begin{bmatrix} 0.0080 & 0 & -0.0040 & 0.0020 \\ 0 & 0.0027 & -0.0020 & 0.0007 \\ 0.0006 & 0.0154 & -0.0066 & 0.0072 \\ -0.0006 & -0.0015 & 0.0031 & 0.0005 \end{bmatrix}$$

$$\mathbf{K}_{CL22} = 10^6 \times \begin{bmatrix} 1.1436 & 0.2551 & 3.8470 & -0.0279 \\ -0.1419 & -0.0165 & -0.5212 & 0.0051 \\ -0.0040 & -0.0020 & 0.0080 & 0 \\ 0.0020 & 0.0007 & 0 & 0.0027 \end{bmatrix}$$

$$\mathbf{C}_{CL} = \begin{bmatrix} \mathbf{C}_{CL11} & \mathbf{0} \\ \mathbf{0} & \mathbf{C}_{CL22} \end{bmatrix}$$

$$\mathbf{C}_{CL11} = 10^3 \times \begin{bmatrix} 0.0016 & 0 & -0.0008 & 0.0004 \\ 0 & 0.0005 & -0.0004 & 0.0001 \\ -0.0020 & -0.0220 & 0.0286 & 0.0003 \\ -0.0008 & -0.0084 & 0.0103 & -0.0003 \end{bmatrix}$$

$$\mathbf{C}_{CL22} = 10^3 \times \begin{bmatrix} -0.3156 & -0.0846 & -1.2401 & 0.0091 \\ 0.3369 & 0.0831 & 1.2174 & -0.0091 \\ -0.0008 & -0.0004 & -0.0004 & 0 \\ 0.0004 & 0.0001 & 0 & 0.0005 \end{bmatrix}$$

with the prescribed eigenvalues. The two independent beams are obtained with given eigenvalues.

4.8 Conclusion

In the theoretical study reported here, it is found that block diagonalisation of the system damping and stiffness matrices are achievable by the imposition of modal degree of freedom constraints on right eigenvectors when the open-loop eigenvalues are controllable. In the case of velocity and displacement feedback, the mass matrix is practically restricted to the diagonal (lumped mass) form. This restriction can be lifted to allow for bandedness of the mass matrix when acceleration feedback is

included together with velocity and displacement feedback. In the case of velocity and displacement feedback, the procedure is based on eigenstructure assignment using the method of receptances, while a hybrid method is developed using the receptance and mass matrix when additional acceleration feedback is included. In both cases the closed-loop system is decoupled to form independent substructures and it is demonstrated that eigenvalues can be assigned to the substructures separately. In the case of banded system matrices, the number of actuators required can be reduced to twice of the semi-bandwidth. The theory reported here works well in LTI systems. However, all systems in nature are inherently nonlinear. The presence of nonlinearity will make the dynamic analysis of open-loop systems complicated and linear active vibration control approaches less effective. In the next chapter, a comprehensive investigation of the effects of softening nonlinearity on dynamic responses of aeroelastic systems will be described.

Appendix 4.1: Left eigenvalue problem

From equation (4.30)

$$\mathbf{y}_k^T \begin{bmatrix} \mathbf{0} & \mathbf{I} \\ -\mathbf{M}^{-1}\left(\mathbf{K}-\mathbf{B}\mathbf{G}^T\right) & -\mathbf{M}^{-1}\left(\mathbf{C}-\mathbf{B}\mathbf{F}^T\right) \end{bmatrix} = \mu_k \mathbf{y}_k^T \tag{4.81}$$

where $\mathbf{y}_k^T = \left(\mathbf{y}_{\mathrm{U}k}^T \quad \mathbf{y}_{\mathrm{L}k}^T\right)$. Thus,

$$\left(-\mathbf{y}_{\mathrm{L}k}^T\mathbf{M}^{-1}\left(\mathbf{K}-\mathbf{B}\mathbf{G}^T\right) \quad \mathbf{y}_{\mathrm{U}k}^T - \mathbf{y}_{\mathrm{L}k}^T\mathbf{M}^{-1}\left(\mathbf{C}-\mathbf{B}\mathbf{F}^T\right)\right) = \left(\mu_k\mathbf{y}_{\mathrm{U}k}^T \quad \mu_k\mathbf{y}_{\mathrm{L}k}^T\right) \tag{4.82}$$

$$\mu_k\mathbf{y}_{\mathrm{U}k}^T = -\mathbf{y}_{\mathrm{L}k}^T\mathbf{M}^{-1}\left(\mathbf{K}-\mathbf{B}\mathbf{G}^T\right) \tag{4.83}$$

and

$$\mu_k\mathbf{y}_{\mathrm{L}k}^T = \mathbf{y}_{\mathrm{U}k}^T - \mathbf{y}_{\mathrm{L}k}^T\mathbf{M}^{-1}\left(\mathbf{C}-\mathbf{B}\mathbf{F}^T\right) \tag{4.84}$$

Combining equations (4.83) and (4.84) leads to

$$\left(\mathbf{y}_{\mathrm{L}k}^{T}\mathbf{M}^{-1}\right)\mathbf{M}\mu_k^2+\left(\mathbf{y}_{\mathrm{L}k}^{T}\mathbf{M}^{-1}\right)\left(\mathbf{C}-\mathbf{B}\mathbf{F}^{T}\right)\mu_k+\left(\mathbf{y}_{\mathrm{L}k}^{T}\mathbf{M}^{-1}\right)\left(\mathbf{K}-\mathbf{B}\mathbf{G}^{T}\right)=\mathbf{0} \tag{4.85}$$

Hence $\mathbf{y}_{\mathrm{L}k}^{T}\mathbf{M}^{-1}$ is the left eigenvector associated with μ_k, i.e.

$$\mathbf{y}_{\mathrm{L}k}^{T}\mathbf{M}^{-1}=\boldsymbol{\psi}_k^{T} \tag{4.86}$$

Chapter 5

Aeroelastic systems with softening nonlinearity

5.1 Introduction

All systems in nature are nonlinear. It is well known that linear analysis and active vibration control methodologies have limited performance in nonlinear systems. Therefore, the modelling and performance of the systems can be improved by applying nonlinear analysis methods. A good understanding of open-loop systems is of importance to effective controller design. In this chapter, a comprehensive study of the effects of softening nonlinearity on aeroelastic systems is performed [131]. The nonlinear active flutter control problem is considered in the next chapter.

This chapter aims to investigate the presence of stable and unstable LCO and the conditions under which they may be found in aeroelastic systems with softening nonlinearity. LCO stability criteria, strictly applicable within the limitations of quasilinearisation by sinusoidal-input describing functions, are confirmed by numerical integration in the time domain. Excellent agreement is found at low steady-state amplitudes and even at higher amplitudes the approximation is found to be close to accurate time-domain predictions. Numerical continuation is employed to explore the complete bifurcation behaviour and to confirm the time- and frequency-domain results. The analysis confirms the existence of stable LCO, dependent upon initial conditions, and shows that a softening nonlinearity can destabilise LCO and chaos as well as prohibiting the occurrence of certain predicted LCO. Results are

presented conveniently in the form of graphs of steady-state amplitude versus velocity and as basins of attraction with regions of stability, stable LCO, dynamic instability and static divergence. The boundaries separating the regions of different dynamic behaviour may be simple or non-simple depending upon the parameters of the wing considered.

5.2 Non-dimensional equations

The two-degree-of-freedom wing shown in Fig. 5.1 is considered. It represents a rigid rectangular wing of span s_w and chord c supported at the root with two nonlinear rotational springs having flexural stiffness $K(\kappa)$ and torsional stiffness $K(\theta)$, where κ and θ denote the flap and pitch degrees of freedom respectively. The springs are attached at a distance ec from the aerodynamic centre (on the quarter chord), defining the position of the flexural axis. e is the eccentricity between flexural axis and aerodynamic centre(positive if the spring lies behind the aerodynamic centre). The wing mass per unit area is m_w. It is assumed that the wing has a uniform mass so that the mass axis lies on the mid-chord. Inertial coupling $I_{\kappa\theta}$ is generally present if the wing mass and flexural axes do not coincide.

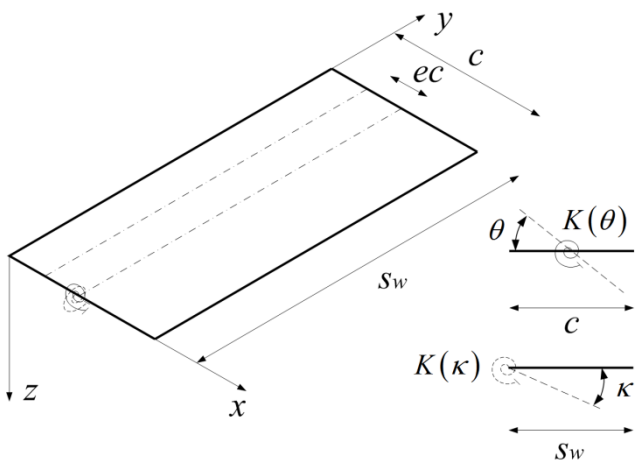

Fig. 5.1 Binary aeroelastic model

The aeroelastic equations of motion with simplified unsteady aerodynamic terms are given by Wright and Cooper [132] for the case of linear root stiffnesses. When nonlinear restoring forces are present they may be re-written as

$$I_\kappa \ddot{\kappa} + I_{\kappa\theta}\ddot{\theta} + \frac{\rho V c s_w^3 a_w}{6}\dot{\kappa} + C_\kappa \dot{\kappa} + \frac{\rho V^2 c s_w^2 a_w}{4}\theta + G(\kappa) = 0 \tag{5.1}$$

$$I_{\kappa\theta}\ddot{\kappa} + I_\theta \ddot{\theta} - \frac{\rho V e c^2 s_w^2 a_w}{4}\dot{\kappa} - \frac{\rho V c^3 s_w M_{\dot{\theta}}}{8}\dot{\theta} + C_\theta \dot{\theta} - \frac{\rho V^2 e c^2 s_w a_w}{2}\theta + M(\theta) = 0 \tag{5.2}$$

where I_κ and I_θ are mass moments of inertia in flap and pitch respectively. $I_{\kappa\theta}$ is the product moment of inertia. C_κ and C_θ are structural damping coefficients in flap and pitch respectively. ρ is the air density. V is the free airflow speed. $M_{\dot{\theta}}$ is an unsteady aerodynamic derivative term accounting for unsteady dynamic behaviour. a_w is the lift curve slope. $G(\kappa)$ and $M(\theta)$ are the nonlinear flap and pitch restoring force and moment, respectively. They may be expressed as $G(\kappa) = K_\kappa \bar{G}(\kappa)$ and $M(\theta) = K_\theta \bar{M}(\theta)$, where K_κ and K_θ are linear stiffness coefficients in the flap and pitch degrees of freedom and $\bar{G}(\kappa)$ and $\bar{M}(\theta)$ are generally nonlinear functions of κ and θ respectively.

Eqs. (5.1) and (5.2) may be cast in non-dimensionalised form

$$\kappa'' + \left(\frac{r_{\kappa\theta}}{r_\kappa}\right)^2 \theta'' + \frac{AR^3 a_w}{3\pi\bar{m}r_\kappa^2}\kappa' + \frac{2\zeta_\kappa}{V^*}\kappa' + \frac{AR^2 a_w}{2\pi\bar{m}r_\kappa^2}\theta + \frac{\tilde{\omega}^2}{(V^*)^2}\bar{G}(\kappa) = 0 \tag{5.3}$$

$$\left(\frac{r_{\kappa\theta}}{r_\theta}\right)^2 \kappa'' + \theta'' - \frac{eAR^2 a_w}{\pi\bar{m}r_\theta^2}\kappa' - \frac{ARM_{\dot{\theta}}}{\pi\bar{m}r_\theta^2}\theta' + \frac{2\zeta_\theta}{V^*}\theta' - \frac{2eARa_w}{\pi\bar{m}r_\theta^2}\theta + \frac{1}{(V^*)^2}\bar{M}(\theta) = 0 \tag{5.4}$$

where $(\bullet)'$ and $(\bullet)''$ are the first and second derivatives of $(\bullet)$ with respect to dimensionless time $\bar{t} = Vt/b$. b is the semi-chord of the wing and $c = 2b$.

$\bar{m} = m_w / \pi\rho b$ is the mass ratio of wing and air. $AR = s_w / b$ is the aspect ratio of the wing. $\omega_\kappa = \sqrt{K_\kappa / I_\kappa}$ and $\omega_\theta = \sqrt{K_\theta / I_\theta}$ are uncoupled flap and pitch natural frequencies respectively. $\tilde{\omega} = \omega_\kappa / \omega_\theta$ is the frequency ratio. $V^* = V / b\omega_\theta$ is the dimensionless free airflow speed. $\zeta_\kappa = C_\kappa / 2\omega_\theta I_\kappa$ and $\zeta_\theta = C_\theta / 2\omega_\theta I_\theta$ are structural viscous damping ratios in flap and pitch respectively. r_κ and r_θ are dimensionless radius of gyration about the flap and pitch axes respectively. $r_{\kappa\theta}$ is a dimensionless quantity corresponding to $I_{\kappa\theta}$. r_κ, r_θ, $r_{\kappa\theta}$ and $\tilde{\omega}$ are functions of system parameters AR, e and $\bar{K}$, and their definitions are given in full in the **Appendix 5.1**.

It can be seen that the dimensionless aeroelastic model is defined by the following eight independent dimensionless quantities AR, $\bar{m}$, e, $\bar{K}$, $M_{\dot{\theta}}$, a_w, ζ_κ, ζ_θ and the dimensionless nonlinear terms $\bar{G}(\kappa)$ and $\bar{M}(\theta)$.

5.3 Limit cycle prediction and stability analysis

It is convenient in this paper to consider a linear spring in flap and a cubic spring in pitch, which conveniently reveals the nature of stability in a softening nonlinear binary aeroelastic system. Then $\bar{G}(\kappa)$ and $\bar{M}(\theta)$ are given by

$$\bar{G}(\kappa) = \kappa \tag{5.5}$$

$$\bar{M}(\theta) = \theta + \bar{K}_{nl}\theta^3 \tag{5.6}$$

where $\bar{K}_{nl} = K_{\theta 3} / K_\theta$ is the ratio of cubic and linear stiffness coefficients. In the case of a softening nonlinearity, $\bar{K}_{nl}$ is negative.

Hence, the dimensionless aeroelastic equations of motion become

$$\kappa'' + \left(\frac{r_{\kappa\theta}}{r_\kappa}\right)^2 \theta'' + \frac{AR^3 a_w}{3\pi\bar{m} r_\kappa^2}\kappa' + \frac{2\zeta_\kappa}{V^*}\kappa' + \frac{AR^2 a_w}{2\pi\bar{m} r_\kappa^2}\theta + \frac{\tilde{\omega}^2}{\left(V^*\right)^2}\kappa = 0 \tag{5.7}$$

$$\begin{aligned}&\left(\frac{r_{\kappa\theta}}{r_\theta}\right)^2 \kappa'' + \theta'' - \frac{eAR^2 a_w}{\pi\bar{m} r_\theta^2}\kappa' - \frac{ARM_{\dot{\theta}}}{\pi\bar{m} r_\theta^2}\theta' + \frac{2\zeta_\theta}{V^*}\theta' \\ &- \frac{2eARa_w}{\pi\bar{m} r_\theta^2}\theta + \frac{1}{\left(V^*\right)^2}\left(\theta + \bar{K}_{nl}\theta^3\right) = 0\end{aligned} \tag{5.8}$$

5.3.1 Limit cycle prediction

A limit cycle prediction method based on describing functions and the Sherman-Morrison formula [53] is proposed here for the dimensionless aeroelastic system already described. In the case of first bifurcation and its post-instability dynamic, the aeroelastic system exhibits a strong filtering property such that the fundamental harmonic is predominant [133]. The nonlinear responses may be assumed to have the following form

$$\kappa = A_\kappa e^{\mathrm{i}(\omega t + \varphi)},\ \theta = A_\theta e^{\mathrm{i}\omega t} \tag{5.9}$$

where A_κ and A_θ are the amplitudes of nonlinear responses in the flap and pitch degrees of freedom respectively and φ is the phase shift in flap response with respect to the pitch response.

The reduced frequency is generally defined as

$$\bar{\omega} = \frac{b}{V}\omega \tag{5.10}$$

so that

$$\kappa = A_\kappa e^{\mathrm{i}(\bar{\omega}\bar{t} + \varphi)},\ \theta = A_\theta e^{\mathrm{i}\bar{\omega}\bar{t}} \tag{5.11}$$

and the dimensionless Laplacian argument is given by

$$\bar{s} = \frac{b}{V}s \tag{5.12}$$

Laplace transformation and application of the sinusoidal-input describing function leads to the quasi-linearised equations corresponding to Eqs. (5.7) and (5.8)

$$\left[\bar{\mathbf{M}}\bar{s}^2+\left(\bar{\mathbf{C}}+\bar{\mathbf{C}}_A\right)\bar{s}+\bar{\mathbf{K}}_A+\bar{\mathbf{K}}_1+\bar{\mathbf{K}}_3\left(A_\theta\right)\right]\mathbf{x}\left(s\right)=\mathbf{0} \tag{5.13}$$

where the matrices $\bar{\mathbf{M}}$, $\bar{\mathbf{C}}$, $\bar{\mathbf{C}}_A$, $\bar{\mathbf{K}}_A$, $\bar{\mathbf{K}}_1$, $\bar{\mathbf{K}}_3\left(A_\theta\right)$ and $\mathbf{x}\left(s\right)$ are given in full in the **Appendix 5.1**.

The Sherman-Morrison formula allows the receptance matrix of the quasilinearised system to be determined as

$$\hat{\bar{\mathbf{H}}}\left(\bar{s}\right)=\bar{\mathbf{H}}\left(\bar{s}\right)-\frac{\bar{N}\left(A_\theta\right)\bar{\mathbf{H}}\left(\bar{s}\right)\mathbf{e}_f\mathbf{e}_f^T\bar{\mathbf{H}}\left(\bar{s}\right)}{1+\bar{N}\left(A_\theta\right)\mathbf{e}_f^T\bar{\mathbf{H}}\left(\bar{s}\right)\mathbf{e}_f} \tag{5.14}$$

when the receptance of the underlying linear system

$$\bar{\mathbf{H}}\left(\bar{s}\right)=\left(\bar{\mathbf{M}}\bar{s}^2+\left(\bar{\mathbf{C}}+\bar{\mathbf{C}}_A\right)\bar{s}+\bar{\mathbf{K}}_A+\bar{\mathbf{K}}_1\right)^{-1} \tag{5.15}$$

and the describing function

$$\bar{N}\left(A_\theta\right)=\frac{1}{\left(V^*\right)^2}\frac{3A_\theta^2}{4}\bar{K}_{nl} \tag{5.16}$$

are both known and $\mathbf{e}_f=\begin{bmatrix}0 & 1\end{bmatrix}^T$ is a vector that defines the location of the nonlinearity.

The characteristic equation is given by

$$P\left(A_\theta,\bar{s}\right)=1+\bar{N}\left(A_\theta\right)\mathbf{e}_f^T\bar{\mathbf{H}}\left(\bar{s}\right)\mathbf{e}_f \tag{5.17}$$

Limit cycle oscillations are undamped, neutrally-stable oscillations. Mathematically, the eigenvalues corresponding to limit cycle oscillations are purely imaginary numbers, denoted as $\pm\mathrm{i}\bar{\omega}$. Therefore the limit cycle equations are

$$\mathrm{Re}\left(1+\bar{N}\left(A_\theta\right)\mathbf{e}_f^T\bar{\mathbf{H}}\left(\bar{s}\right)\mathbf{e}_f\,\Big|_{\bar{s}=\pm\mathrm{i}\bar{\omega}}\right)=0 \tag{5.18}$$

$$\mathrm{Im}\left(\mathbf{e}_f^T \bar{\mathbf{H}}(\bar{s}) \mathbf{e}_f \Big|_{\bar{s} = \pm \mathrm{i}\bar{\omega}} \right) = 0 \tag{5.19}$$

It is evident that Eq.(5.19) is an equation in the non-dimensional frequency $\bar{\omega}$ only. If there exist limit cycles, we can derive the frequency $\bar{\omega}$ from Eq.(5.19), substitute $\bar{\omega}$ into Eq.(5.18) and then solve it for the amplitude A_g. Therefore, it is unnecessary to solve coupled equations in the amplitude A_g and frequency $\bar{\omega}$, which reduces the computation effort and makes the limit cycle prediction process very straightforward.

5.3.2 Stability of LCO

A limit cycle stability criterion may be used to determine the stability of LCO in the presence of amplitude and/or frequency perturbations and is derived here for the dimensionless aeroelastic system already described.

If there exists a limit cycle with amplitude A_0 and eigenvalue $\bar{s}_0 = \mathrm{i}\bar{\omega}$, the following equation holds

$$P(A_0, \bar{s}_0) = 1 + \bar{N}(A_0) \mathbf{e}_f^T \bar{\mathbf{H}}(\bar{s}_0) \mathbf{e}_f = 0 \tag{5.20}$$

Small perturbations in the limit cycle amplitude and eigenvalue are introduced by making the following changes to Eq.(5.20)

$$\begin{aligned} A_0 &\longrightarrow A_0 + \Delta A, \\ \bar{s}_0 &\longrightarrow \bar{s}_0 + \Delta\bar{s} = \bar{s}_0 + \Delta\sigma + \mathrm{i}\Delta\bar{\omega} \end{aligned} \tag{5.21}$$

Then

$$P(A_0 + \Delta A, \bar{s}_0 + \Delta\sigma + \mathrm{i}\Delta\bar{\omega}) = 0 \tag{5.22}$$

and by expanding Eq. (5.22) in a Taylor series around the equilibrium state $(A_0, \bar{s}_0)$ it is found that

$$P\left(A_0+\Delta A,\bar{s}_0+\Delta\sigma+\mathrm{i}\Delta\bar{\omega}\right)=P\left(A_0,\bar{s}_0\right)+\frac{\partial P}{\partial A}\Delta A+\frac{\partial P}{\partial \bar{s}}\Delta\sigma \\ +\mathrm{i}\frac{\partial P}{\partial \bar{s}}\Delta\bar{\omega}+O\left(\Delta A\right)+O\left(\Delta s\right)=0 \tag{5.23}$$

Subtracting Eq. (5.20) from Eq. (5.23) and eliminating the high-order terms leads to

$$\frac{\partial P}{\partial A}\Delta A+\frac{\partial P}{\partial \bar{s}}\Delta\sigma+\mathrm{i}\frac{\partial P}{\partial \bar{s}}\Delta\bar{\omega}=0 \tag{5.24}$$

Satisfaction of Eq. (5.24) requires that the real and imaginary parts are separately equal to zero

$$\mathrm{Re}\left(\frac{\partial P}{\partial A}\right)\Delta A+\mathrm{Re}\left(\frac{\partial P}{\partial \bar{s}}\right)\Delta\sigma+\mathrm{Re}\left(\mathrm{i}\frac{\partial P}{\partial \bar{s}}\right)\Delta\bar{\omega}=0 \tag{5.25}$$

$$\mathrm{Im}\left(\frac{\partial P}{\partial A}\right)\Delta A+\mathrm{Im}\left(\frac{\partial P}{\partial \bar{s}}\right)\Delta\sigma+\mathrm{Im}\left(\mathrm{i}\frac{\partial P}{\partial \bar{s}}\right)\Delta\bar{\omega}=0 \tag{5.26}$$

But,

$$\mathrm{Re}\left(\frac{\partial P}{\partial \bar{s}}\right)=\mathrm{Im}\left(\mathrm{i}\frac{\partial P}{\partial \bar{s}}\right) \tag{5.27}$$

$$\mathrm{Im}\left(\frac{\partial P}{\partial \bar{s}}\right)=-\mathrm{Re}\left(\mathrm{i}\frac{\partial P}{\partial \bar{s}}\right) \tag{5.28}$$

so that Eqs. (5.25) and (5.26) may be cast as

$$\mathrm{Re}\left(\frac{\partial P}{\partial A}\right)\Delta A+\mathrm{Re}\left(\frac{\partial P}{\partial \bar{s}}\right)\Delta\sigma-\mathrm{Im}\left(\frac{\partial P}{\partial \bar{s}}\right)\Delta\bar{\omega}=0 \tag{5.29}$$

$$\mathrm{Im}\left(\frac{\partial P}{\partial A}\right)\Delta A+\mathrm{Im}\left(\frac{\partial P}{\partial \bar{s}}\right)\Delta\sigma+\mathrm{Re}\left(\frac{\partial P}{\partial \bar{s}}\right)\Delta\bar{\omega}=0 \tag{5.30}$$

Eliminating $\Delta\bar{\omega}$ then leads to

$$\mathrm{Re}\left(conj\left(\frac{\partial P}{\partial A}\right)\bullet\frac{\partial P}{\partial \bar{s}}\right)=\left(\left(\mathrm{Re}\left(\frac{\partial P}{\partial \bar{s}}\right)\right)^2+\left(\mathrm{Im}\left(\frac{\partial P}{\partial \bar{s}}\right)\right)^2\right)\left(-\frac{\Delta\sigma}{\Delta A}\right) \tag{5.31}$$

The first term on the right-hand-side is strictly non-negative. The null value is the case of the unchanging characteristic equation with frequency and damping, which is not of interest. Therefore, if the left-hand-side is positive, then $\Delta\sigma/\Delta A<0$. A positive

amplitude perturbation ($\Delta A > 0$) results in the eigenvalue moving to the left-hand side of the complex plane. This is a stable system configuration, in which energy is dissipated until the amplitude decays to its unperturbed value. Similarly, negative amplitude perturbation ($\Delta A < 0$) requires an unstable system whose eigenvalue moves to the right-hand side of the complex plane($\Delta\sigma > 0$) causing the amplitude to grow until the unperturbed LCO is again attained. This condition, $\Delta\sigma/\Delta A<0$, defines a stable LCO. Similarly, $\Delta\sigma/\Delta A>0$, defines an unstable LCO.

Based the above perturbation analysis, for a stable limit cycle

$$\mathrm{Re}\left(conj\left(\frac{\partial P}{\partial A} \right) \bullet \frac{\partial P}{\partial \bar{s}} \right) > 0 \tag{5.32}$$

at $A = A_0$ and $\bar{s} = \bar{s}_0$.

And for an unstable limit cycle,

$$\mathrm{Re}\left(conj\left(\frac{\partial P}{\partial A} \right) \bullet \frac{\partial P}{\partial \bar{s}} \right) < 0 \tag{5.33}$$

at $A = A_0$ and $\bar{s} = \bar{s}_0$.

5.4 Softening nonlinearity: Examples, results and discussion

For softening nonlinearity, static divergence is a common occurrence and therefore it is of importance to estimate the static instability boundary when investigating the nature of the instability. The softening stiffness nonlinearity is located in the pitch degree of freedom so that the nonlinear restoring moment is expressed as,

$$M(\theta) = \frac{1}{\left(V^*\right)^2}\left(\theta + \bar{K}_{nl}\theta^3\right) - \frac{2eARa_w}{\pi \bar{m} r_\theta^2}\theta \tag{5.34}$$

The nonlinear restoring moment first grows with increasing pitch angle but then decreases. When the pitch angle reaches a critical value the nonlinear restoring

moment becomes zero, which indicates that the nonlinear system has lost its restoring capability and the system is statically divergent. The negative nonlinear restoring moment is not admissible for a physical engineering structure. Therefore, a static divergence boundary is achieved for the softening nonlinear system for the entire flight speed range.

The LCO prediction method described above is used to determine the amplitudes of steady-state responses for the two-degree-of-freedom aeroelastic system with softening cubic nonlinearity in pitch. Results are compared to time-domain results obtained by using the built-in MATLAB solver ODE45, which is an adaptive step-size solver based on the explicit Runge-Kutta(4,5) formula, the Dorman-Prince pair [134]. Results from two typical numerical examples are presented here.

Before carrying out the nonlinear aeroelastic response analysis, the linear flutter speed for each case is computed by selecting $\bar{K}_{nl} = 0$ and then increasing V^* until the real part of one pair of eigenvalues becomes positive.

5.4.1 Example 5.1

5.4.1.1 LCO prediction and stability analysis

The softening nonlinear system has model parameters $\bar{m} = 26,\ e = 0.23,\ \bar{K} = 14,$ $\bar{K}_{nl} = -15,\ M_{\dot{\theta}} = -1.2,\ a_w = 2\pi,\ \zeta_\kappa = 0$ and $\zeta_\theta = 0$. The chosen value of $\bar{K}_{nl}$ leads to small steady-state aeroelastic response amplitudes (approx. $\theta < 15°$) so that linear aerodynamic assumption is satisfied [104]. Limit cycle amplitudes and frequencies over the airflow speed range from 0 to 3.0 may be determined by the proposed limit cycle prediction method. The resultant LCO amplitudes versus speed and LCO frequency against speed curves are shown in Figs. 5.2 and 5.3. The stability of the

obtained LCO is determined by the inequalities (5.32) and (5.33). For instance, at speed $V^* = 1.2$, there exist two LCOs. One LCO has amplitude $A_{\theta 1} = 0.1969$ and frequency $\bar{\omega}_1 = 0.5751$. Based on the LCO stability criterion it is found that

$$\mathrm{Re}\left(conj\left(\frac{\partial P}{\partial A} \right) \bullet \frac{\partial P}{\partial \bar{s}} \right) \Bigg|_{\substack{A = 0.1969 \\ \bar{s} = \pm \mathrm{i}0.5751}} = -9.3338 < 0 \tag{5.35}$$

which indicates the LCO is an unstable one. The other LCO has amplitude $A_{\theta 2} = 0.2314$ and frequency $\bar{\omega}_2 = 0.5092$ so that

$$\mathrm{Re}\left(conj\left(\frac{\partial P}{\partial A} \right) \bullet \frac{\partial P}{\partial \bar{s}} \right) \Bigg|_{\substack{A = 0.2314 \\ \bar{s} = \pm \mathrm{i}0.5092}} = 34.2899 > 0 \tag{5.36}$$

and is found to be stable.

As shown in Fig. 5.2, at the same speed, the amplitude of the stable LCO is larger than that of the unstable one. However, it can be seen in Fig. 5.3 that the frequency of the stable LCO is smaller than the unstable LCO frequency. This result is to be expected because stiffness reduces with amplitude so low amplitude vibrations will have higher frequencies.

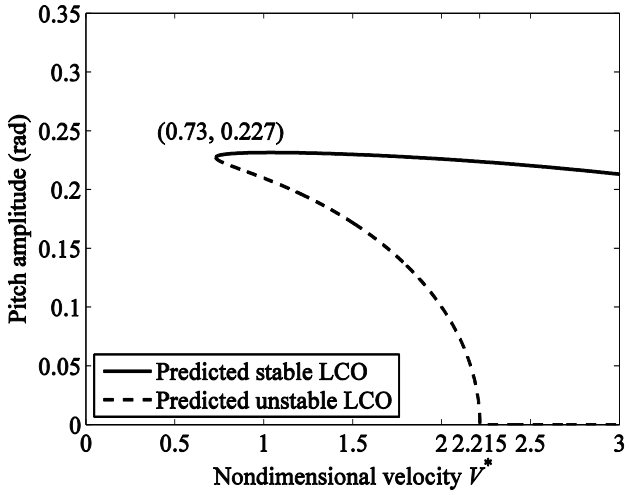

Fig. 5.2 Predicted LCO amplitude versus dimensionless velocity

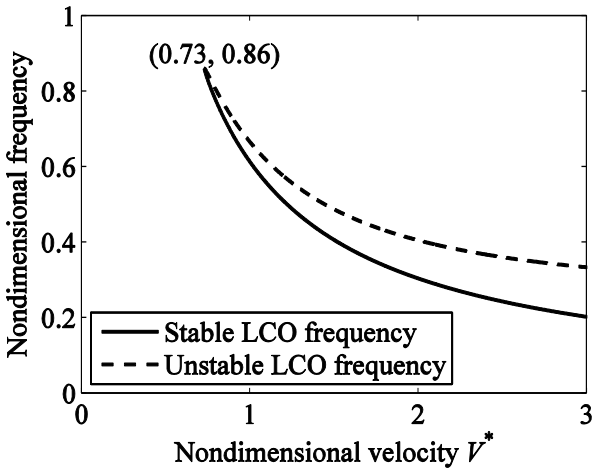

Fig. 5.3 Predicted LCO frequency against dimensionless velocity

It is seen that LCO is predicted to start to occur at a speed $V^* = 0.73$, much below the linear flutter boundary at $V^* = 2.215$, so that the Hopf-bifurcation is subcritical. Beyond the linear flutter boundary, the unstable LCO amplitude is zero, which indicates that the initial equilibrium state is an unstable attractor and any disturbance will cause the system to move away from this state. This is exactly the characteristic of the corresponding linear system after the Hopf-bifurcation point, which confirms the correctness of predicted results in terms of the linear flutter boundary. It is, however, well known that the accuracy of the describing-function approximation diminishes with increase in amplitude. Thus it is necessary to confirm the results of frequency domain analysis by detailed analysis (without approximation) in the time domain.

5.4.1.2 Time-domain response

Time-domain responses over the speed range of interests are calculated by numerical integration of Eqs. (5.7) and (5.8). To compute the time history, any initial condition may be chosen as a combination of initial state variables. Obviously, it would not be possible in this research to explore every combination. It is convenient however to use the pitch angle as the only non-zero initial condition, because (1) the static

divergence boundary can be computed analytically in terms of the pitch angle and (2) the describing function technique is also able to directly produce the LCO pitch amplitude. This facilitates the direct comparison of LCO amplitude in the pitch degree of freedom with both the static divergence boundary in terms of pitch angle and the initial pitch angle. And, the subsequent stability analysis can be carried out entirely in the pitch degree of freedom. Hence, unless otherwise stated a single initial condition is placed on the pitch angle, $\begin{bmatrix}\kappa & \theta & \kappa' & \theta'\end{bmatrix} = \begin{bmatrix}0 & \theta_0 & 0 & 0\end{bmatrix}$. The resulting steady-state time-domain responses are summarized in Fig. 5.4.

At velocities less than 0.73 with the initial pitch angle below static divergence boundary the aeroelastic system is always stable, characterised by a decaying time-domain response. However, when the initial pitch angle is slightly above the static divergence boundary, the time-domain response is divergent and the system experiences static instability. Two time series at the same speed, $V^* = 0.4$, are given in Figs. 5.5 and 5.6 to illustrate this behaviour.

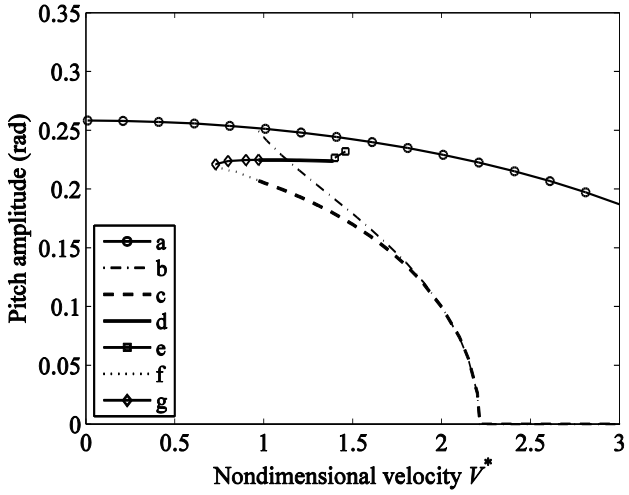

Fig. 5.4 Time-domain LCO amplitude and initial condition against velocity. a-static divergence boundary; b-initial condition for unstable LCO; c-unstable LCO; d-stable LCO; e-asymmetric stable LCO; f-unstable LCO (nonzero initial flap velocity); g-stable LCO (nonzero initial flap velocity)

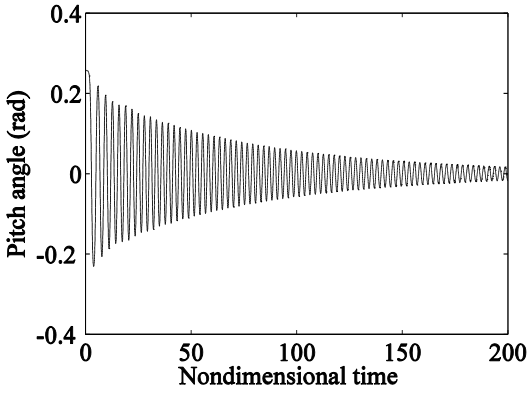

Fig. 5.5 Pitch time series at $V^* = 0.4$

$\left(\kappa(0), \theta(0), \dot{\kappa}(0), \dot{\theta}(0)\right) = (0, 0.2570, 0, 0)$

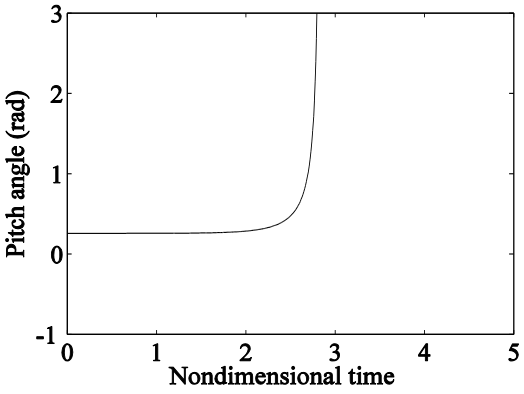

Fig. 5.6 Pitch time series at $V^* = 0.4$

$\left(\kappa(0), \theta(0), \dot{\kappa}(0), \dot{\theta}(0)\right) = (0, 0.2571, 0, 0)$

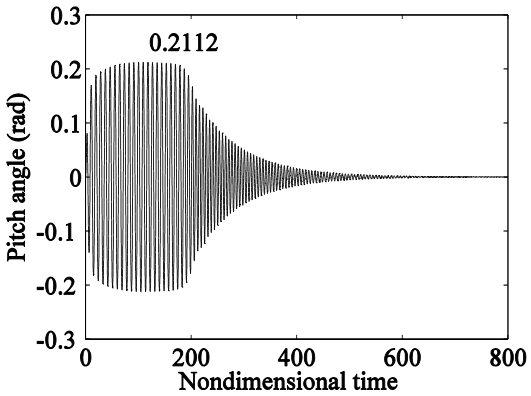

Fig. 5.7 Pitch time series at $V^* = 0.9$

$\left(\kappa(0), \theta(0), \dot{\kappa}(0), \dot{\theta}(0)\right) =$
$(0, 0, 0.17602430952544202702 45, 0)$

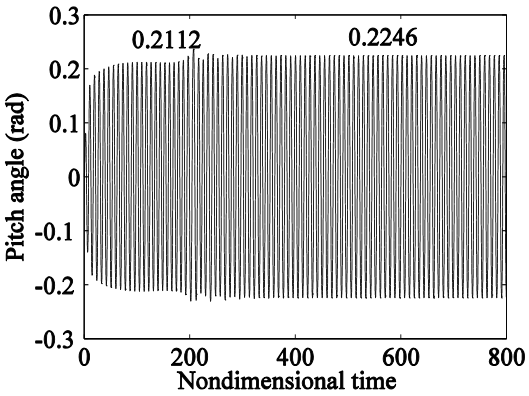

Fig. 5.8 Pitch time series at $V^* = 0.9$

$\left(\kappa(0), \theta(0), \dot{\kappa}(0), \dot{\theta}(0)\right) =$
$(0, 0, 0.17602430952544202702 46, 0)$

Over speeds ranging from approximately 0.73 to 0.972, the system experiences similar responses to those at speeds less than 0.73 when the only initial condition is a nonzero pitch angle, $\left[\kappa \quad \theta \quad \kappa' \quad \theta'\right] = \left[0 \quad \theta_0 \quad 0 \quad 0\right]$. However, both stable and unstable LCO can be achieved under initial excitation by the flap velocity only, $\left[\kappa \quad \theta \quad \kappa' \quad \theta'\right] = \left[0 \quad 0 \quad \kappa_0' \quad 0\right]$, as depicted in the curves 'f' and 'g' in Fig. 5.4. The time series at $V^* = 0.9$ are given in Figs. 5.7 and 5.8. Neither stable nor unstable LCO could be found in this region when the only initial condition was on the pitch angle – this is thought to be due to the close proximity of the initial condition to the static divergence boundary.

For $0.972 < V^* < 1.39$, the system exhibits decaying responses when the initial pitch angle is less than an initial condition boundary for unstable LCO, denoted by curve 'b' in Fig. 5.4. Above this initial condition boundary quite different system responses are obtained. In order to illustrate the features of responses in this region clearly, the aeroelastic system at speed $V^* = 1.2$ is analysed thoroughly and its responses are represented here. At the initial condition boundary, $\left(\kappa(0), \theta(0), \dot{\kappa}(0), \dot{\theta}(0)\right) = (0, 0.2157308904, 0, 0)$, critical initial displacement excitation results in oscillations first with constant amplitude, which later decay gradually, shown in Figs. 5.9 and 5.10. When the initial pitch angle is very slightly changed ($\left(\kappa(0), \theta(0), \dot{\kappa}(0), \dot{\theta}(0)\right) = (0, 0.2157308905, 0, 0)$), the system oscillates with constant amplitude at the beginning and subsequently moves to another motion state with greater amplitude. Eventually, it encounters a dramatic climb and undergoes unbounded motion, demonstrated in Figs. 5.11 and 5.12. After further tiny increase of initial excitation, so that $\left(\kappa(0), \theta(0), \dot{\kappa}(0), \dot{\theta}(0)\right) = (0, 0.2157308906, 0, 0)$, the time-domain response depicted in Figs. 5.13 and 5.14 shows a stable limit cycle oscillation after a preliminary-stage vibration with the same limited-amplitude as that in Figs. 5.9 – 5.12. Referring to Figs. 5.9 – 5.14, it is clear that the system first experiences an unstable limit cycle oscillation sensitive to any small perturbation. It may die away as a point attractor [135] as in Figs. 5.9 and 5.10. If a slight change happens, the motion starting with constant amplitude may grow and become statically divergent as in Figs. 5.11 and 5.12. Alternatively a stable LCO, or periodic attractor [135], such as depicted in Figs. 5.13 and 5.14 may be found. Further searching reveals unstable limit cycle oscillations for $0.73 < V^* < 3$, with amplitudes

denoted by curves ‘c’ and ‘f’ in Fig. 5.4. The occurrence of unstable LCO depends on the initial condition.

When the initial pitch angle is close to the amplitude of the stable LCO, the unstable LCO tends to disappear, and the system experiences stable LCO, shown typically in Figs. 5.15 and 5.16. The stable LCO is characterised by local stability. That is to say the stable LCO has its own basin of attraction. This can be illustrated by the fact that when the initial pitch angle is larger than the stable LCO amplitude, the system may be attracted directly to the zero-amplitude equilibrium state rather than the periodic attractor of the stable LCO, as shown in Figs. 5.17 and 5.18.

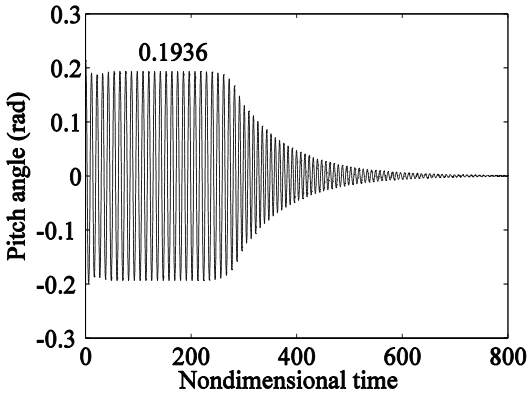

Fig. 5.9 Pitch time series at $V^* = 1.2$

$(\kappa(0), \theta(0), \dot{\kappa}(0), \dot{\theta}(0)) = (0, 0.2157308904, 0, 0)$

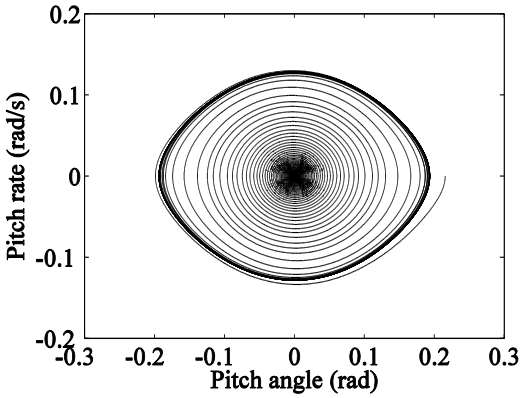

Fig. 5.10 Phase plane $V^* = 1.2$

$(\kappa(0), \theta(0), \dot{\kappa}(0), \dot{\theta}(0)) = (0, 0.2157308904, 0, 0)$

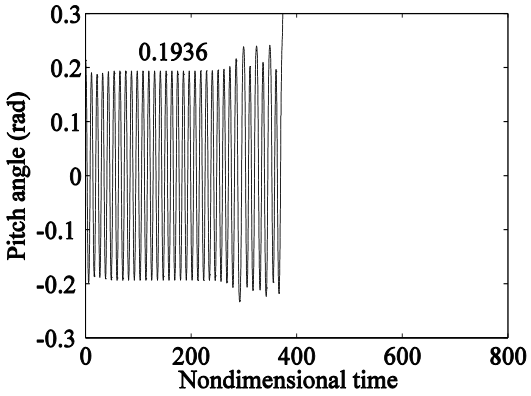

Fig. 5.11 Pitch time series at $V^* = 1.2$

$(\kappa(0), \theta(0), \dot{\kappa}(0), \dot{\theta}(0)) = (0, 0.2157308905, 0, 0)$

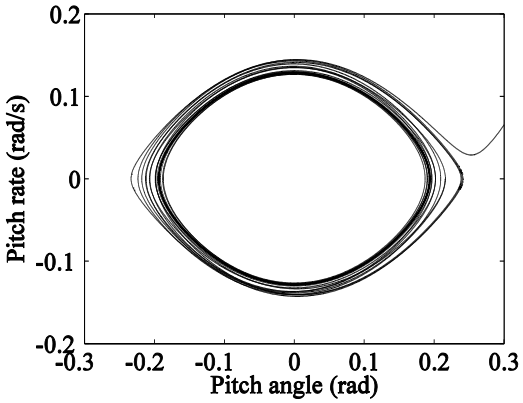

Fig. 5.12 Phase plane $V^* = 1.2$

$(\kappa(0), \theta(0), \dot{\kappa}(0), \dot{\theta}(0)) = (0, 0.2157308905, 0, 0)$

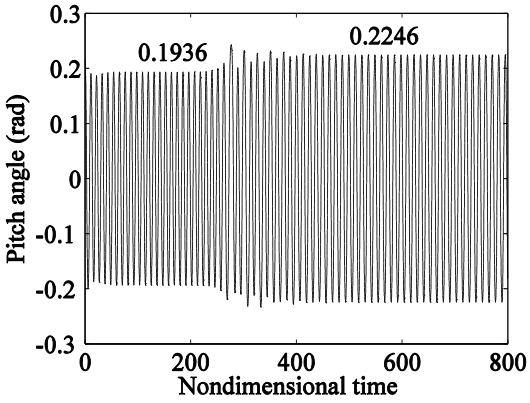

Fig. 5.13 Pitch time series at $V^* = 1.2$

$(\kappa(0), \theta(0), \dot{\kappa}(0), \dot{\theta}(0)) = (0, 0.2157308906, 0, 0)$

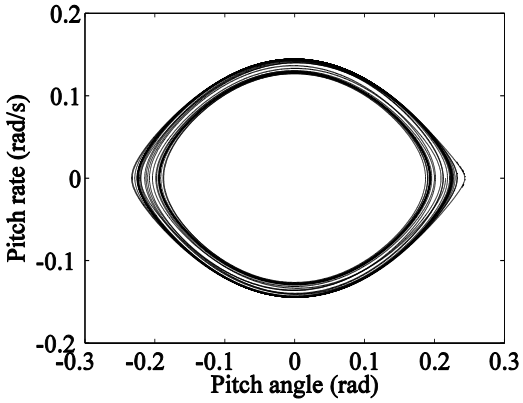

Fig. 5.14 Phase plane at $V^* = 1.2$

$(\kappa(0), \theta(0), \dot{\kappa}(0), \dot{\theta}(0)) = (0, 0.2157308906, 0, 0)$

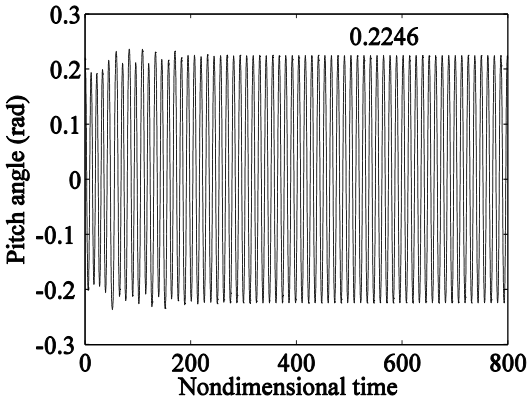

Fig. 5.15 Pitch time series at $V^* = 1.2$

$(\kappa(0), \theta(0), \dot{\kappa}(0), \dot{\theta}(0)) = (0, 0.2204, 0, 0)$

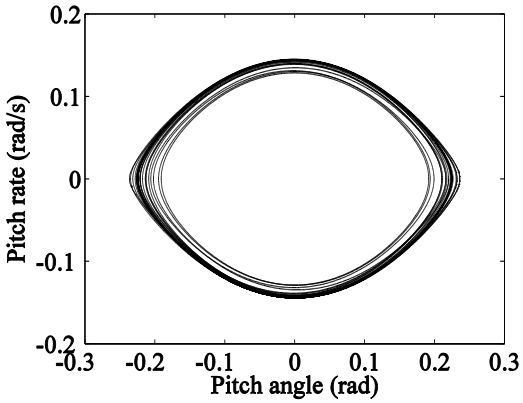

Fig. 5.16 Phase plane at $V^* = 1.2$

$(\kappa(0), \theta(0), \dot{\kappa}(0), \dot{\theta}(0)) = (0, 0.2204, 0, 0)$

Furthermore, after disturbing the unstable LCO the response of the system may become unbounded directly rather than arrive at the stable LCO as shown in Figs. 5.13 and 5.14. This can be understood by comparing Figs. 5.15 and 5.16 to Figs. 5.19 and 5.20, where the system is subjected to very slightly different initial excitations.

In the speed range $1.4 < V^* < 1.46$, the stable LCO responses, denoted by curve 'e' in Fig. 5.4, seem to be offset and lose their symmetry. A mirrored time-domain response, about $\theta = 0$ axis, can be obtained for a different initial condition – both are illustrated in Figs. 5.21 and 5.22. For $1.47 < V^* < 1.476$, the steady-state response

remains periodic and asymmetric about the about $\theta = 0$ axis, but the magnitude is not constant anymore and several amplitudes appear in turn.

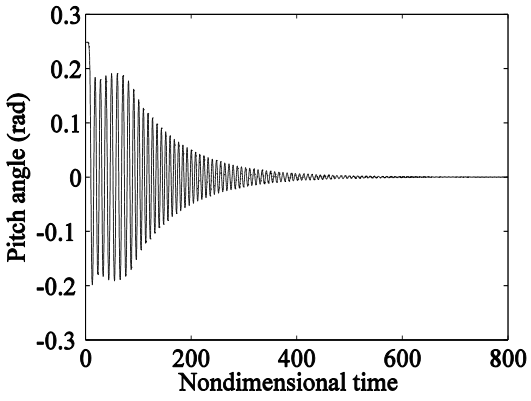

Fig. 5.17 Pitch time series at $V^* = 1.2$

$(\kappa(0), \theta(0), \dot{\kappa}(0), \dot{\theta}(0)) = (0, 0.24785, 0, 0)$

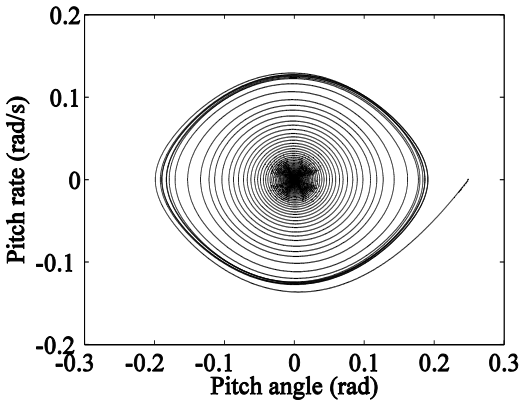

Fig. 5.18 Phase plane at $V^* = 1.2$

$(\kappa(0), \theta(0), \dot{\kappa}(0), \dot{\theta}(0)) = (0, 0.24785, 0, 0)$

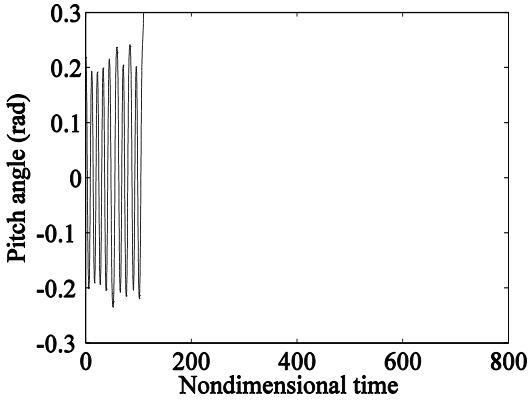

Fig. 5.19 Pitch time series at $V^* = 1.2$

$(\kappa(0), \theta(0), \dot{\kappa}(0), \dot{\theta}(0)) = (0, 0.2203, 0, 0)$

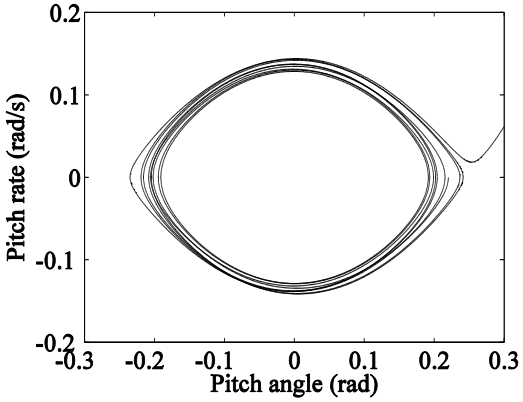

Fig. 5.20 Phase plane at $V^* = 1.2$

$(\kappa(0), \theta(0), \dot{\kappa}(0), \dot{\theta}(0)) = (0, 0.2203, 0, 0)$

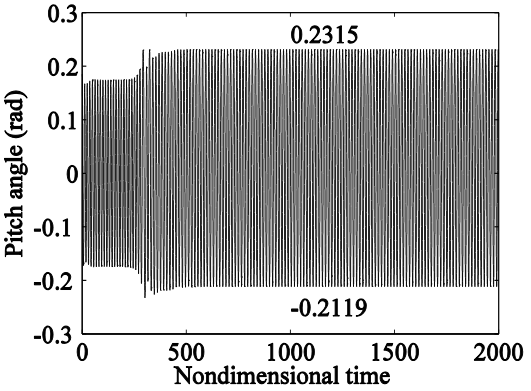

Fig. 5.21 Pitch time series at $V^* = 1.45$

$(\kappa(0), \theta(0), \dot{\kappa}(0), \dot{\theta}(0)) = (0, 0.1851375901, 0, 0)$

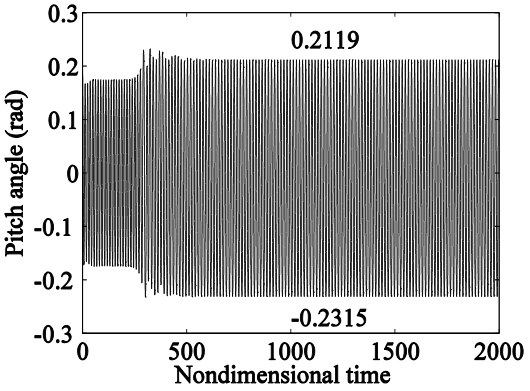

Fig. 5.22 Pitch time series at $V^* = 1.45$

$(\kappa(0), \theta(0), \dot{\kappa}(0), \dot{\theta}(0)) = (0, 0.18513759011, 0, 0)$

For $1.477 < V^* < 1.49$, LCO cannot be obtained. Instead, the time series is offset about the $\theta = 0$ axis up and down alternately before the occurrence of static divergence. An example of this sort of response when $V^* = 1.48$ is given in Fig. 5.23. Also, different ODE solvers (MATLAB ODE45 and stiff solver ODE23s as well as the standard fourth order Runge-Kutta algorithm) with various maximum step sizes have been used to integrate the equations of motion, with similar time series achieved. This confirms that the response is genuine and not caused by numerical instability. Furthermore, similar time-domain responses were achieved in an aeroelastic system with hardening nonlinearity by Price et al. [136]. They concluded that time series of this sort were chaotic. To check if the time history obtained is indeed chaotic, the Lyapunov exponent is calculated using a numerical scheme given in [137], originating from the works of Shimada and Nagashima [138] and Benettin et al. [139]. The Lyapunov exponent is used to measure the rate of divergence of nearby orbits in the phase space and a positive Lyapunov exponent indicates chaotic motion. The limit cycle oscillation corresponds to a zero Lyapunov exponent and the negative exponent denotes a stable response. The system response, also at $V^* = 1.48$, but with a different initial condition was obtained by numerical integration using a fourth order Runge-Kutta scheme with a fixed time step $\Delta t = 0.01$. Once again similar time series results are obtained as shown in Fig. 5.24. The resultant Lyapunov exponent for time series shown in Fig. 5.24 (prior to static divergence) is 0.0635, indicating that the system experiences chaos before static instability.

It can be seen from Figs. 5.23 and 5.24 that the chaotic motion is destroyed by static divergence. For speeds ranging from 1.49 to 2.145, neither LCO nor chaotic motions are obtained. The system undergoes dynamic instability followed by static instability,

which is probably due to the magnitude of the dynamic response becoming close to the static divergence boundary.

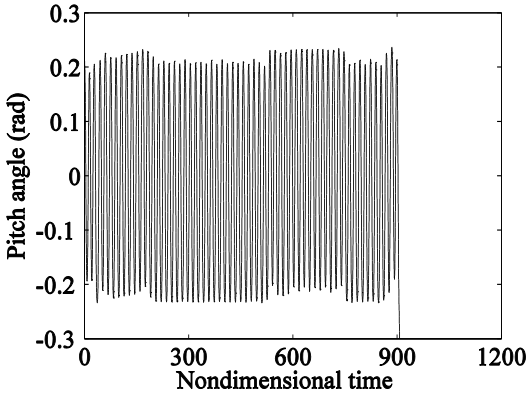

Fig. 5.23 Pitch time series at $V^* = 1.48$

$(\kappa(0), \theta(0), \dot{\kappa}(0), \dot{\theta}(0)) =$
$(0, 0.21199993099996, 0, 0)$

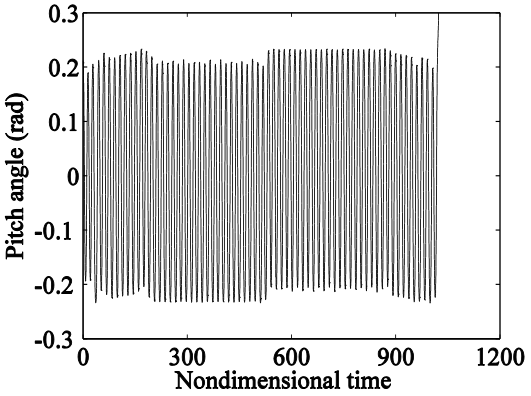

Fig. 5.24 Pitch time series at $V^* = 1.48$

$(\kappa(0), \theta(0), \dot{\kappa}(0), \dot{\theta}(0)) =$
$(0, 00.211999930929051, 0, 0)$

When the flight speed is beyond the linear flutter boundary, the system is always unstable. The response depends upon the initial displacement. When the initial displacement in the pitch degree of freedom is less than the critical value for static divergence, the time series first shows oscillatory growth and then a sharp non-oscillatory increase. A typical time-domain response of this type is presented in Fig. 5.25. When the initial condition is equal to or exceeds the static divergence boundary the responses are always non-oscillatory and increase dramatically as in Fig. 5.26.

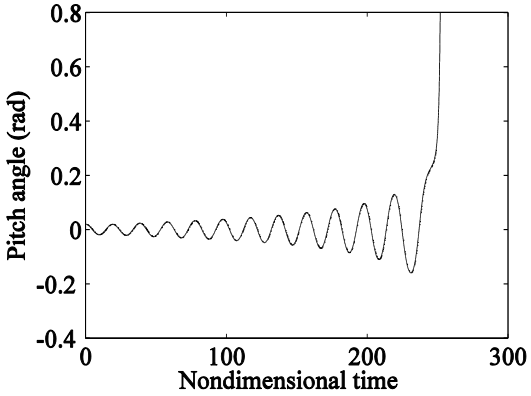

Fig. 5.25 Pitch time series at $V^* = 2.5$

$(\kappa(0), \theta(0), \dot{\kappa}(0), \dot{\theta}(0)) = (0, 0.02, 0, 0)$

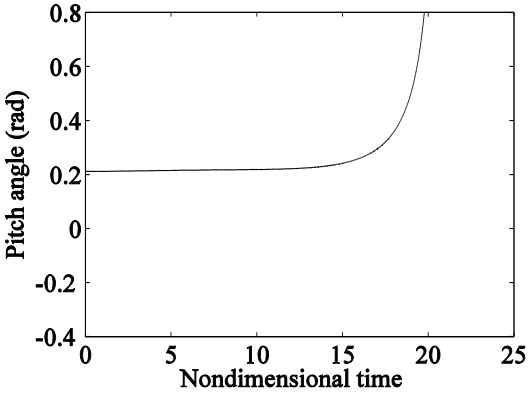

Fig. 5.26 Pitch time series at $V^* = 2.5$

$(\kappa(0), \theta(0), \dot{\kappa}(0), \dot{\theta}(0)) = (0, 0.2113, 0, 0)$

5.4.1.3 Comparison of frequency-domain and time-domain results

Fig. 5.27 is obtained by superimposing Fig. 5.2 on Fig. 5.4 and allows time-domain steady-state responses to be compared with those predicted by using describing functions and the Sherman-Morrison formula. It can be seen that the unstable LCO achieved in time domain agree with those predicted by frequency-domain method, especially in flight regime where the amplitude of unstable LCO is relatively small. In terms of stable LCO, it is seen that frequency-domain (describing function) approach results in a slight amplitude overestimate for the softening nonlinearity, especially in the region of the fold bifurcation. Never-the-less the frequency domain prediction remains accurate enough for most engineering purposes, but is not able to predict the stable LCO with offset or chaos. Also, it can be seen that the static divergence boundary intersects the curve of predicted stable LCO at $V^* = 2.145$. It is understandable that neither LCO nor chaos can be found after the intersection because the static instability occurs before stable LCO or chaos. Furthermore, the softening nonlinearity may have a destabilising effect on stable LCO or chaos and prohibit the appearance of these phenomena when initial pitch angles required for their appearance are close to the static divergence boundary. This is thought likely to account for the absence of time-domain stable LCO (initial condition on the pitch angle only) when $0.73 < V^* < 0.972$. It might also be the reason why neither chaos nor stable LCOs are found in the range $1.49 < V^* < 2.145$ although stable LCO are predicted by the frequency domain approach. Further analysis using numerical continuation codes allows for a more complete understanding of the bifurcation behaviour of the system.

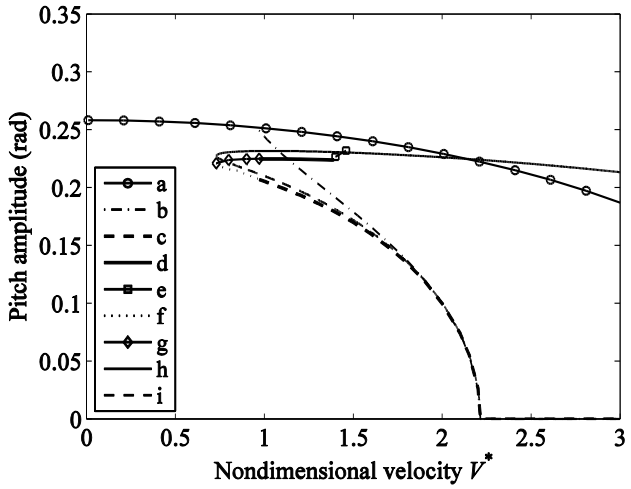

Fig. 5.27 Comparison of results of time-domain and frequency-domain. a-static divergence boundary; b-initial condition for unstable LCO; c-unstable LCO; d-stable LCO; e-asymmetric stable LCO; f-unstable LCO (initial flap velocity); g-stable LCO (initial flap velocity); h-predicted stable LCO; i-predicted unstable LCO

5.4.1.4 Complete bifurcation analysis

To fully understand the nonlinear behaviour of aeroelastic systems with softening nonlinearity, complete bifurcation analysis is explored using the numerical continuation software package MATCONT [140]. Two equilibrium curves are obtained, denoted by 'a' and 'b' in Fig. 5.28. Curve 'a' represents zero equilibrium with two Hopf-bifurcation points 'A' ($V^* = 2.215$) and 'C' ($V^* = 6.916$) and a branch point 'B' ($V^* = 4.351$). Hopf-bifurcation 'A' is subcritical, indicated by a positive first Lyapunov coefficient. The limit cycle arising from this bifurcation point is unstable, as are the equilibrium points on segment 'AC'. On the other hand, the Hopf-bifurcation 'C' is supercritical because it has a negative first Lyapunov coefficient. It can be seen from Fig. 5.28 that the branch point is actually the intersection of the two equilibrium curves. Apart from the branch point 'B', equilibrium branch 'b' includes a subcritical Hopf-bifurcation point 'D' ($V^* = 4.038$). By comparison, the equilibrium branch 'b' coincides with the

computed static divergence boundary shown in Fig. 5.4. As would be expected the static divergence boundary represents an equilibrium condition of the system.

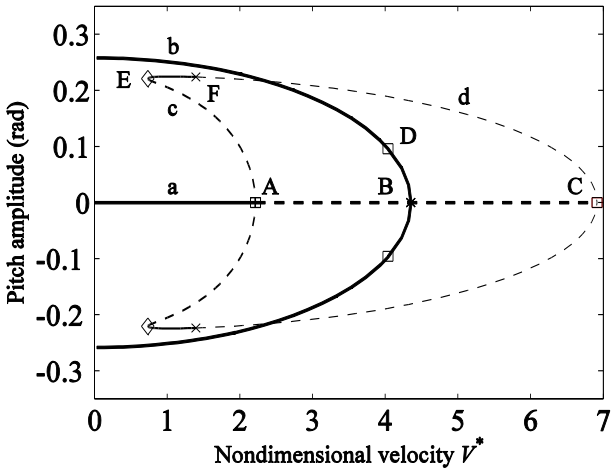

Fig. 5.28 Equilibrium and primary LCO branches

From any of the two Hopf-bifurcation points, numerical continuation of limit cycles can be computed, thereby generating primary LCO branches, shown by curves ‘c’ and ‘d’ in Fig. 5.28. On the primary LCO curves, a fold bifurcation (limit point of cycles (LPC)), which generically corresponds to a turning point of a curve of limit cycles, occurs at ‘E’ ($V^* = 0.73$). At this position two cycles collide and merge into a critical cycle with two Floquet multipliers equal to 1. From this it follows that a stable primary branch ‘d’ occurs after the LPC point. Therefore, the primary LCO branch ‘c’ between the LCP point and the first Hopf-bifurcation ‘A’ is unstable and the other branch ‘d’ is stable, which agrees with the results from frequency-domain stability analysis. For $0.73 < V^* < 1.4$, the LCO branch ‘d’ is stable and symmetric. However, at $V^* = 1.4$, the primary LCO branch encounters a branch point ‘F’ with one real Floquet multiplier exiting the unit cycle at +1, which is actually a symmetry-breaking bifurcation [141]. Subsequently, the LCO branch ‘d’ becomes unstable, shown as dashed curve ‘FC’, and two stable asymmetric sub-branches are created on either side. This bifurcation is also known as supercritical pitchfork bifurcation of

limit cycles [141, 142]. Afterwards, at $V^* = 1.405$, a Neimark-Sacker bifurcation point of limit cycles appears. However, at this point, the periodic solution has real multipliers $\mu_1\mu_2 = 1$ and consequently the Neimark-Sacker bifurcation point turns into a neutral saddle, which is a not bifurcation point [143].

Further branch-following numerical continuation on the periodic LCO solutions are shown in Fig. 5.29. Starting from the branch point 'F' on the primary LCO, two sub-branches of LCO around the primary LCO branch 'd', i.e., lower branch 'e' and upper branch 'f', are obtained. The upper branch 'f' undergoes a period doubling bifurcation (flip bifurcation) at $V^* = 1.47$ with a negative normal form coefficient indicating the appearance of stable double-period cycles, and ends at the Hopf-bifurcation point 'D' of the equilibrium branch 'b', which is subcritical with a positive first Lyapunov coefficient. It indicates that the segment from the period doubling bifurcation point 'H' to the Hopf-bifurcation point 'D' is unstable. The lower branch 'e' also experiences a period doubling bifurcation 'G' at $V^* = 1.47$ with a negative normal form coefficient, followed by an unstable segment. Neither sub-branch 'e' nor 'f' are symmetric in terms of the zero equilibrium branch. However, sub-branches 'e' and 'f' are mirror images of each other, which is in accordance with the mirrored time domain responses computed by the adaptive step size Runge-Kutta algorithm over the speed range $1.4 < V^* < 1.46$, as shown in Figs. 21 and 22.

Following the sub-branch 'e', a new branch of LCO emerges at the period doubling point 'G', shown as branch 'g'. This is a bifurcation to a branch of periodic orbits of double period. This can be confirmed by the phase plane at $V^* = 1.475$ shown in Fig. 5.30, exhibiting the doubled period and obtained by using the adaptive step-size Runge-Kutta algorithm. Increasing the flight speed leads to the phenomenon of

stable single-period oscillation on sub-branch ‘e’ that splits into stable double-period oscillations on branch ‘g’. The features of stable double-period oscillations also agree with that of the time domain responses over the speed range $1.47 < V^* < 1.476$. Branch ‘g’ remains stable until further period doubling occurs at $V^* = 1.476$, denoted by point ‘I’. Similarly, branch ‘f’ undergoes period doubling at the same velocity, shown as ‘H’**,** where a new branch ‘h’ arises. Also, it can be seen that new branch ‘h’ encounters a further period doubling bifurcation ‘J’.

From Fig. 5.29, the emanating branch of periodic orbits undergoes a sequence of period doublings, one of the possible routes to chaos [142]. Based on the above complete bifurcation analysis, the computed time domain responses and Lyapunov exponent, it is confidently concluded that the aeroelastic system with softening nonlinearity undergoes chaos at speed range beyond $V^* = 1.477$ and a sequence of period doubling is the route to chaos. However, it can be seen from Fig. 5.29 that the amplitude of potential chaotic behaviour approaches the static divergence boundary, so that the static divergence boundary prohibits the appearance of stable chaos in the time domain.

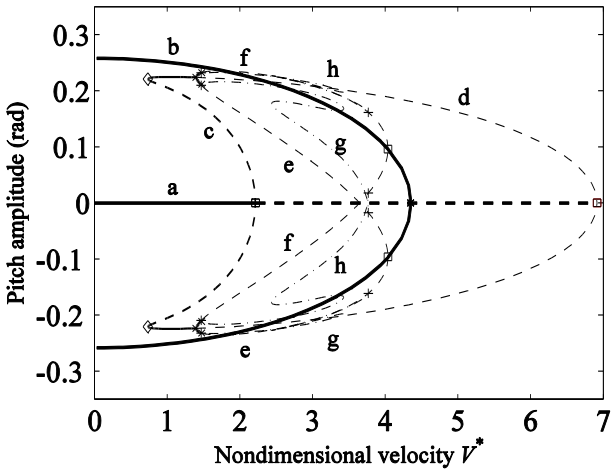

(a)

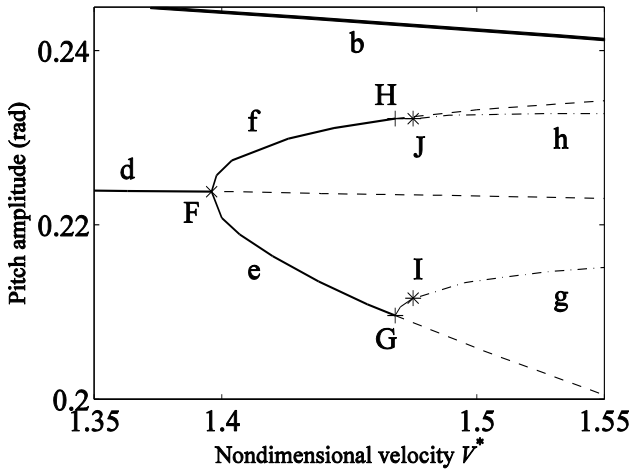

(b)

Fig. 5.29 Complete bifurcation branches obtained via MATCONT. a-zero equilibrium branch; b-static divergence boundary; c-unstable primary branch of LCO; d-stable primary branch of LCO; e-lower sub-branch; f- upper sub-branch; g-period-doubling branch of e; h-period-doubling branch of f

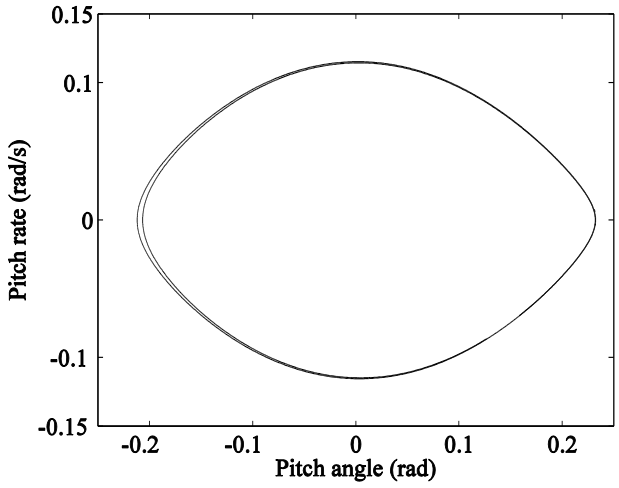

Fig. 5.30 Phase plane of LCO at $V^* = 1.475$

The time-domain responses achieved by the adaptive step size Runge-Kutta algorithm (stable and unstable symmetric LCO, asymmetric LCO, and LCO with doubled period) coincide with the LCO obtained by numerical continuation techniques.

5.4.1.5 Two-dimensional section of the basin of attraction

The preceding time-domain analysis confirms that the stability of the system is sensitive to initial conditions. To fully appreciate the dependence of stability on starting values a thorough time domain response calculation is carried out in a two-dimensional section with $0.01 < V^* < 3.0$ and $0 < \theta_0 < 0.35$. The steps for non-dimensional velocity and starting pitch angle are 0.01 and 0.0001 respectively. The other initial state variables are zero. That is, the initial condition is $\begin{bmatrix} \kappa & \theta & \kappa' & \theta' \end{bmatrix} = \begin{bmatrix} 0 & \theta_0 & 0 & 0 \end{bmatrix}$. Actually, the basin of attraction is five dimensional. The stability of each point in the two-dimensional section is indexed and depicted in Fig. 5.31. Within region 3 the system is statically unstable. The boundary between this and other regions is the static divergence boundary. In region 2 the system first undergoes dynamical instability followed by static divergence. The time histories are convergent if initial values are located in region 1 and the system is absolutely stable. The majority of region 1 is located under the static divergence boundary and to the left of region 2. However, we can see that many isolated small regions denoted by '+' exist within region 2 where they are entirely surrounded by instability. This shows that there exists no simple boundary which separates the stable and unstable regions as indicated previously [104, 106]. The time histories show unstable LCO for a while before bifurcating to other sorts of motion (stable oscillation, stable LCO or dynamic instability) if appropriate initial values are chosen near the boundaries between region 1 and region 2 or between region 1 and region 4. Most interestingly, the regions of stable limit cycle oscillation are defined and shown in black. They appear not to form a single connected region, though they are seen to be present as predicted by frequency domain analysis, close to the nose the

unstable/stable LCO curve (curves 'h' and 'i' in Fig. 5.27) and below the static divergence boundary.

To summarise, the aeroelastic system with softening nonlinearity defined in Example 1, shows regions of stable (convergent), neutrally stable (unstable or stable LCO) and unstable responses within a two-dimensional section of the basin of attraction. Above the static divergence boundary, the system experiences static instability. The occurrence of convergent responses, unstable and stable LCO, dynamic instability and subsequent static divergence are all very sensitive to initial conditions. The boundaries between the regions are generally not simple.

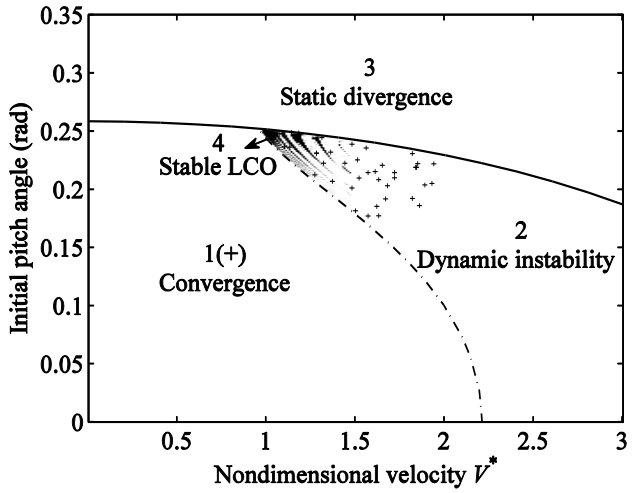

Fig. 5.31 Two-dimensional section of the basin of attraction (Example 5.1). Region 1-convergence; Region 2-dynamical instability followed by static divergence; Region 3-static divergence; Region 4-stable LCO.

5.4.2 Example 5.2

Another softening nonlinear system with the same model parameters $\bar{m}$, $\bar{K}_{nl}$, $M_{\dot{\theta}}$, a_w, ζ_κ and ζ_θ as Example 5.1 but different $AR = 9$, $e = 0.24$ and $\bar{K} = 6$ is used. The stable and unstable LCO are predicted by the frequency-domain method and the speed at which the unstable LCO disappears is found to agree with the linear flutter speed. The global bifurcation point occurs at $V^* = 0.26$, far below the linear flutter

speed $V^* = 2.697$. However, this case is different from the previous one in that the static divergence boundary intersects with the unstable LCO branch predicted by describing functions, as shown in Fig. 5.32 . Hence, the system is expected to experience static instability before the appearance of predicted stable LCO. Indeed, no stable LCO is achieved in time domain over the whole flight regime. However, it is known that the frequency-domain prediction, based on describing function is likely to be slightly inaccurate in the region of the of the fold bifurcation. Therefore is in necessary to carry out a complete bifurcation analysis in order to achieve a comprehensive understanding of the nonlinear dynamics of the system.

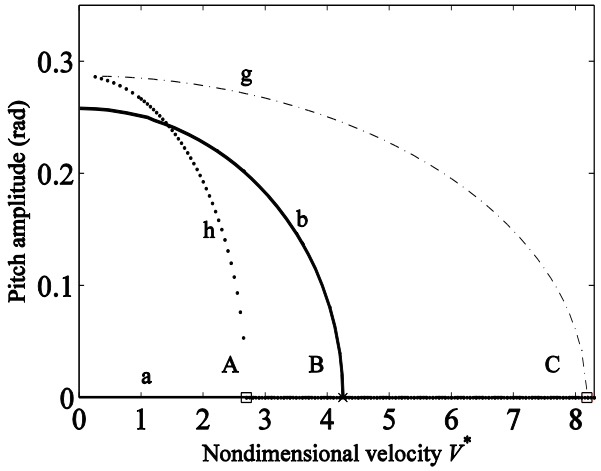

Fig. 5.32 Comparison of static divergence boundary and predicted LCO. a-zero equilibrium branch; b-static divergence boundary; g-predicted stable LCO; h-predicted unstable LCO

Using numerical continuation, complete bifurcation branches are obtained as shown in Fig. 5.33. It can be seen that the zero equilibrium branch has two Hopf-bifurcation points 'A' ($V^* = 2.697$) and 'C' ($V^* = 8.186$), which are subcritical and supercritical indicated by positive and negative first Lyapunov coefficient respectively. Also, it has branch point 'B' ($V^* = 4.252$), at the intersection with equilibrium branch 'b'. Apart from the branch point 'B', branch 'b' includes two subcritical Hopf-bifurcation points 'D' and 'E' ($V^* = 3.692$). As before, branch 'b' denotes the static divergence

boundary. Starting from the subcritical Hopf-bifurcation point ‘A’, an unstable LCO branch ‘c’ emerges and encounters a branch point ‘G’ ($V^* = 0.404$) and a fold bifurcation at ‘F’ ($V^* = 0.318$). A stable LCO branch ‘d’ continues from point ‘F’ without further branch points and eventually ends at the supercritical Hopf-bifurcation point ‘C’. Two sub-branches (‘e’ and ‘f’) emerge from the branch point ‘G’ on the unstable LCO branch ‘c’, and are mirror images of each other, finally ending at the two subcritical Hopf-bifurcation points ‘D’ and ‘E’ of branch ‘b’ respectively, which indicates that these two sub-branches are unstable.

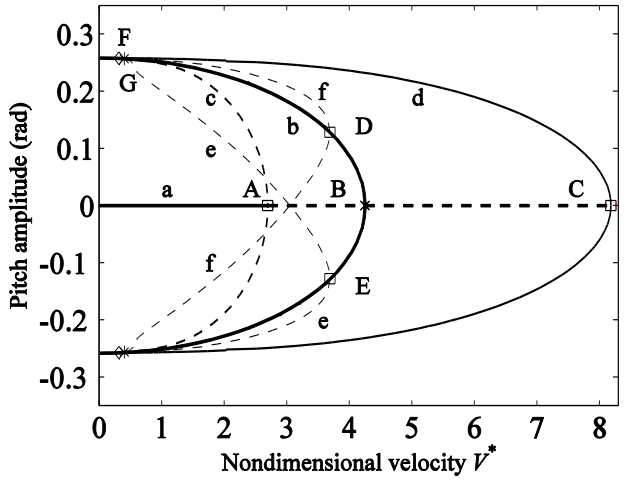

(a)

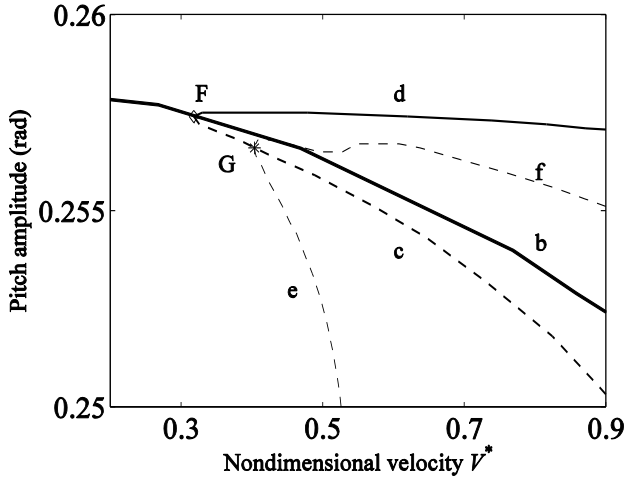

(b)

Fig. 5.33 Complete bifurcation branches obtained via MATCONT. a-zero equilibrium branch; b-static divergence boundary; c-unstable primary branch of LCO; d-stable primary branch of LCO; e-lower sub-branch; f- upper sub-branch

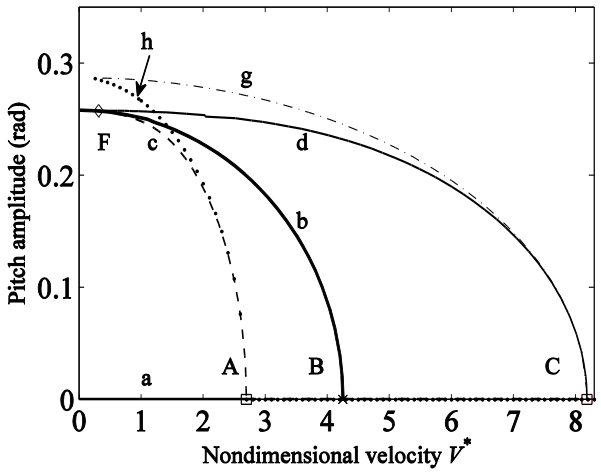

Fig. 5.34 Comparison of bifurcation branches obtained via the describing functions and MATCONT. a-zero equilibrium branch; b-static divergence boundary; c-unstable branch of LCO; d-stable branch of LCO; g-predicted stable LCO; h-predicted unstable LCO

According to the preceding complete bifurcation analysis, it can be seen that the static divergence boundary passes exactly through the fold bifurcation point 'F' and has stable and unstable LCO branches above and below respectively. Consequently LCO on the stable branch are prohibited by the static divergence boundary. Comparison of the bifurcation branches obtained via the describing functions and by MATCONT, shown in Fig. 5.34, reveals that although the describing function approach is an approximation, especially in the region of the fold bifurcation, it produces regions of system stability almost coincident with those determined from numerical continuation. That is, the system experiences static instability before the occurrence of stable LCO, which is prohibited.

The stability of the system with softening nonlinearity described in Example 5.2 is very sensitive to initial conditions with regions of convergence, dynamic instability and static divergence shown in Fig. 5.35. The boundaries between the regions in this case are simple.

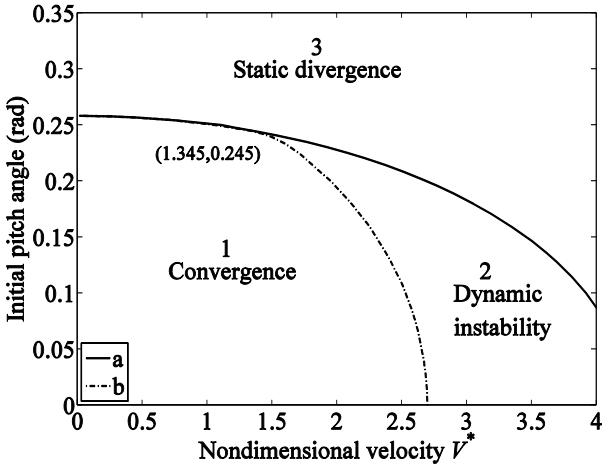

Fig. 5.35 Two-dimensional section of the basin of attraction (Example 5.2). a-static divergence boundary; b-initial condition for unstable LCO

5.5 Conclusion

A comprehensive study of the effects of softening structural nonlinearity is presented including stable and unstable LCO, static divergence and chaos. Complex dynamic behaviour is demonstrated using the illustration of a nonlinear binary flutter model with a cubic stiffness in the pitch degree of freedom. A limit cycle prediction method based on describing functions and Sherman-Morrison formula is proposed to predict LCO in frequency domain, which avoids solving coupled equations about limit cycle frequency and amplitude and makes the limit cycle prediction procedure considerably straightforward. The stability of predicted LCO is determined by proposed stability criteria. The frequency domain methods are confirmed by numerical integration of the governing differential equations in the time domain. In addition, new dynamic responses, including asymmetric LCO and chaos, are revealed in time domain. Aeroelastic stability in the presence of softening structural nonlinearity is found to be strongly dependent upon initial conditions. LCO and chaos may be destabilised when the amplitude of oscillation approaches the static divergence boundary and predicted stable LCO are prohibited. Complete bifurcation analysis by the use of numerical continuation techniques and two-dimensional

sections of the basin of attraction allow the nature of stability occurring over the whole speed range to be explained. It is demonstrated the aeroelastic systems with softening nonlinearity are characterised by Hopf, fold, pitchfork (symmetry-breaking) and period doubling (flip) bifurcations. In some circumstances, the basins of attractions are not singly connected regions, so that the boundaries between different dynamic regimes are not simple. Dependent upon the wing parameters, regions may appear where the predicted stable LCO are free from the destabilising effect of softening nonlinearity. With a sound understanding of the effects of softening nonlinearity presented here, in conjunction with well-known effects of hardening nonlinearity, a new active vibration control approach will be presented in the next chapter for aeroelastic systems with softening or hardening nonlinearity.

Appendix 5.1 Coefficients in Eqs.(5.3) , (5.4) and (5.13)

The following non-dimensional terms are defined:

$$r_\kappa = \sqrt{\frac{I_\kappa}{m_w b^4}} = \sqrt{\frac{2AR^3}{3}},\ r_\theta = \sqrt{\frac{I_\theta}{m_w b^4}} = \sqrt{AR\left(\frac{7}{6} - 4e + 8e^2\right)},$$

$$r_{\kappa\theta} = \sqrt{\frac{I_{\kappa\theta}}{m_w b^4}} = \sqrt{AR^2\left(\frac{1}{2} - 2e\right)},\ \tilde{\omega} = \frac{\omega_\kappa}{\omega_\theta} = \sqrt{\bar{K}}\sqrt{\frac{1}{AR^2}\left(\frac{7}{4} - 6e + 12e^2\right)},$$

$$\bar{K} = K_\kappa / K_\theta\ ,\ \mathbf{x}(s) = \begin{bmatrix} \kappa(s) \\ \theta(s) \end{bmatrix},$$

$$\bar{\mathbf{M}} = \begin{bmatrix} 1 & \left(\frac{r_{\kappa\theta}}{r_\kappa}\right)^2 \\ \left(\frac{r_{\kappa\theta}}{r_\theta}\right)^2 & 1 \end{bmatrix},\ \bar{\mathbf{C}} = \begin{bmatrix} \frac{2\zeta_\kappa}{V^*} & 0 \\ 0 & \frac{2\zeta_\theta}{V^*} \end{bmatrix},\ \bar{\mathbf{C}}_A = \begin{bmatrix} \frac{AR^3 a_w}{3\pi\bar{m}r_\kappa^2} & 0 \\ -\frac{eAR^2 a_w}{\pi\bar{m}r_\theta^2} & -\frac{ARM_{\dot{\theta}}}{\pi\bar{m}r_\theta^2} \end{bmatrix},$$

$$\bar{\mathbf{K}}_A = \begin{bmatrix} 0 & \dfrac{AR^2 a_w}{2\pi \bar{m} r_\kappa^2} \\ 0 & -\dfrac{2eARa_w}{\pi \bar{m} r_\theta^2} \end{bmatrix},\ \bar{\mathbf{K}}_1 = \begin{bmatrix} \left(\dfrac{\tilde{\omega}}{V^*}\right)^2 & 0 \\ 0 & \dfrac{1}{\left(V^*\right)^2} \end{bmatrix},\ \bar{\mathbf{K}}_3\left(A_\theta\right) = \begin{bmatrix} 0 & 0 \\ 0 & \dfrac{1}{\left(V^*\right)^2}\dfrac{3A_\theta^2}{4}\bar{K}_{nl} \end{bmatrix},$$

Chapter 6

Robust passivity-based continuous sliding-mode control for under-actuated nonlinear wing sections

6.1 Introduction

The purpose of this chapter is to develop a robust passivity-based continuous sliding-mode control approach, which can globally stabilise all the degrees of freedom of an under-actuated nonlinear prototypical wing section with matched and mismatched uncertainty and input disturbance. The approach makes good use of the robustness of sliding-mode control to large matched uncertainty and large input disturbances. To deal with mismatched uncertainty in under-actuated systems, a robust passivity-based control method is used for the design of globally exponentially stable nonlinear sliding surfaces. Moreover, a proposed continuous sliding-mode control is able to alleviate the chattering which occurs in the process of discontinuous sliding-mode control. The sufficient conditions for global asymptotic stability and global stability of under-actuated two-degree-of-freedom nonlinear aeroelastic systems are provided.

6.2 Nonlinear aeroelastic model

The under-actuated nonlinear system in question takes the form of a generic two-dimensional wing section with trailing-edge control surface, as depicted in Fig. 6.1. This example was used previously for classic aeroelastic analysis and control design

[117]. The wing section with chord $c = 2b$ and unit span $s_w = 1$ is supported by a linear spring with stiffness K_h in plunge and a nonlinear torsional spring with stiffness $K_\theta(\theta)$ in pitch. The springs are attached at a distance $a_h b$ from the midchord, defining the elastic axis. The centre of mass is at a distance $r_{cg} = x_\theta b$ from the elastic axis.

The governing equations of motion of the model were given by Ko et al. [117] ,

$$m_t \ddot{h} + m_w x_\theta b \ddot{\theta} + C_h \dot{h} + K_h h = -L \tag{6.1}$$

$$m_w x_\theta b \ddot{h} + I_\theta \ddot{\theta} + C_\theta \dot{\theta} + K_\theta(\theta)\theta = M \tag{6.2}$$

where h and θ denote plunge and pitch displacements respectively; m_t is the total mass of wing and its supporting structure; m_w is the mass of wing; I_θ is the mass moment of inertia about the elastic axis; and C_h and C_θ are structural damping coefficients in plunge and pitch respectively.

L and M are the aerodynamic lift and moment about the elastic axis. Quasi-steady aerodynamic forces [144] are employed such that,

$$L = \rho V^2 b C_{L_\theta}\left(\theta + \frac{\dot{h}}{V} + \left(\frac{1}{2} - a_h\right) b \frac{\dot{\theta}}{V}\right) + \rho V^2 b C_{L_\beta}\beta \tag{6.3}$$

$$M = \rho V^2 b^2 C_{M_\theta}\left(\theta + \frac{\dot{h}}{V} + \left(\frac{1}{2} - a_h\right) b \frac{\dot{\theta}}{V}\right) + \rho V^2 b^2 C_{M_\beta}\beta \tag{6.4}$$

where ρ is the air density; V is the free airflow speed; β is the trailing-edge control surface deflection; C_{L_θ} and C_{L_β} are aerodynamic lift coefficients due to the angle of attack and the deflection of trailing-edge control surface; and C_{M_θ} and C_{M_β} are the aerodynamic moment coefficients.

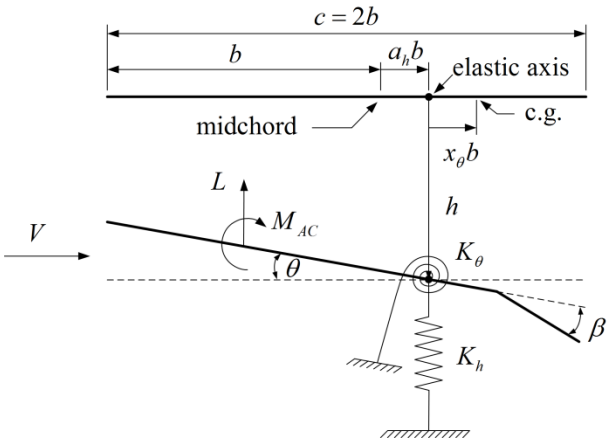

Fig. 6.1 The aeroelastic model with pitch and plunge degrees of freedom

In this chapter, bounded nonlinear torsional uncertainty and control input disturbance are considered. Then by combining equations (6.1)-(6.4) and introducing the nonlinear uncertainty and input disturbance, it is found that,

$$\mathbf{M}\ddot{\mathbf{x}}+\left(\mathbf{C}+\mathbf{C}_A\right)\dot{\mathbf{x}}+\left(\mathbf{K}+\mathbf{K}_A\right)\mathbf{x}+\mathbf{\Delta K x}=\mathbf{b}\left(\beta+\Delta\beta\right) \tag{6.5}$$

where

$$\mathbf{M}=\begin{bmatrix} m_t & m_w x_\theta b \\ m_w x_\theta b & I_\theta \end{bmatrix},\ \mathbf{C}_A=\begin{bmatrix} \rho V b C_{L_\theta} & \rho V b^2 C_{L_\theta}\left(1/2-a_h\right) \\ -\rho V b^2 C_{M_\theta} & -\rho V b^3 C_{M_\theta}\left(1/2-a_h\right) \end{bmatrix},$$

$$\mathbf{C}=\begin{bmatrix} C_h & 0 \\ 0 & C_\theta \end{bmatrix},\ \mathbf{K}_A=\begin{bmatrix} 0 & \rho V^2 b C_{L_\theta} \\ 0 & -\rho V^2 b^2 C_{M_\theta} \end{bmatrix},\ \mathbf{K}=\begin{bmatrix} K_h & 0 \\ 0 & K_\theta\left(\theta\right) \end{bmatrix},$$

$$\mathbf{\Delta K}=\begin{bmatrix} 0 & 0 \\ 0 & \Delta K_\theta\left(\theta\right) \end{bmatrix},\ \mathbf{x}=\begin{pmatrix} h \\ \theta \end{pmatrix},\ \mathbf{b}=\begin{pmatrix} -\rho V^2 b C_{L_\beta} \\ \rho V^2 b^2 C_{M_\beta} \end{pmatrix}.$$

and $\Delta K_\theta\left(\theta\right)$ and $\Delta\beta$ represent the nonlinear torsional uncertainty and input disturbance respectively.

If $\begin{bmatrix} h & \theta & \dot{h} & \dot{\theta} \end{bmatrix}^T=\begin{bmatrix} \overline{x}_1 & \overline{x}_2 & \overline{x}_3 & \overline{x}_4 \end{bmatrix}^T=\overline{\mathbf{x}}^T$, then Equations in (6.5) may be cast in state-space form

$$\dot{\bar{\mathbf{x}}} = \bar{\mathbf{f}}\left(\bar{\mathbf{x}}\right) + \bar{\mathbf{g}}\left(\beta + \Delta\beta\right) + \boldsymbol{\delta} \tag{6.6}$$

where

$$\bar{\mathbf{f}}\left(\bar{\mathbf{x}}\right) = \begin{pmatrix} \bar{x}_3 \\ \bar{x}_4 \\ -k_1\bar{x}_1 - \left(k_2 V^2 + p\left(\bar{x}_2\right)\right)\bar{x}_2 - c_1\bar{x}_3 - c_2\bar{x}_4 \\ -k_3\bar{x}_1 - \left(k_4 V^2 + q\left(\bar{x}_2\right)\right)\bar{x}_2 - c_3\bar{x}_3 - c_4\bar{x}_4 \end{pmatrix}, \quad \bar{\mathbf{g}} = \begin{pmatrix} 0 \\ 0 \\ g_3 \\ g_4 \end{pmatrix},$$

$\boldsymbol{\delta} = \mathbf{t}\Delta K_\theta\left(\bar{x}_2\right)\bar{x}_2$, $\mathbf{t} = \begin{bmatrix} 0 & 0 & t_3 & t_4 \end{bmatrix}^T$,

$d = m_t I_\theta - m_w^2 x_\theta^2 b^2$, $k_1 = I_\theta K_h / d$, $k_2 = \left(I_\theta \rho b C_{L_\theta} + m_w x_\theta \rho b^3 C_{M_\theta}\right)/d$,

$k_3 = -m_w x_\theta b K_h / d$, $k_4 = -\left(m_w x_\theta \rho b^2 C_{L_\theta} + m_t \rho b^2 C_{M_\theta}\right)/d$,

$p\left(\bar{x}\right) = -m_w x_\theta b K_\theta\left(\bar{x}\right)/d$, $q\left(\bar{x}\right) = m_t K_\theta\left(\bar{x}\right)/d$,

$c_1 = \left[I_\theta\left(C_h + \rho V b C_{L_\theta}\right) + m_w x_\theta \rho V b^3 C_{M_\theta}\right]/d$,

$c_3 = \left[-m_w x_\theta b\left(C_h + \rho V b C_{L_\theta}\right) - m_t \rho V b^2 C_{M_\theta}\right]/d$,

$c_2 = \left[I_\theta \rho V b^2 C_{L_\theta}\left(1/2 - a_h\right) - m_w x_\theta b C_\theta + m_w x_\theta \rho V b^4 C_{M_\theta}\left(1/2 - a_h\right)\right]/d$,

$c_4 = \left[m_t\left(C_\theta - \rho V b^3 C_{M_\theta}\left(1/2 - a_h\right)\right) - m_w x_\theta \rho V b^3 C_{L_\theta}\left(1/2 - a_h\right)\right]/d$,

$g_3 = -V^2\left(I_\theta \rho b C_{L_\beta} + m_w x_\theta \rho b^3 C_{M_\beta}\right)/d$, $g_4 = V^2\left(m_w x_\theta \rho b^2 C_{L_\beta} + m_t \rho b^2 C_{M_\beta}\right)/d$,

$t_3 = m_w x_\theta b / d$ and $t_4 = -m_t / d$.

6.3 Normal form

The pitch angle is here selected as the output feedback variable,

$$y_o = \bar{x}_2 = \theta \tag{6.7}$$

The relative degree of the system, denoted by r_d, is determined by the number of times the output can be differentiated until the input appears explicitly in the expression for the r_d^{th} time derivative. In the present case,

$$
\begin{aligned}
y_o &= \bar{x}_2 \\
\dot{y}_o &= \frac{\mathrm{d}y_o}{\mathrm{d}\bar{\mathbf{x}}}.\frac{\mathrm{d}\bar{\mathbf{x}}}{\mathrm{d}t} = \frac{\mathrm{d}y_o}{\mathrm{d}\bar{\mathbf{x}}}\cdot\left(\bar{\mathbf{f}}\left(\bar{\mathbf{x}}\right)+\bar{\mathbf{g}}\cdot\left(\beta+\Delta\beta\right)+\boldsymbol{\delta}\right) \\
&= \begin{bmatrix}0 & 1 & 0 & 0\end{bmatrix}\begin{pmatrix} \bar{x}_3 \\ \bar{x}_4 \\ -k_1\bar{x}_1-\left(k_2V^2+p\left(\bar{x}_2\right)\right)\bar{x}_2-c_1\bar{x}_3-c_2\bar{x}_4 \\ -k_3\bar{x}_1-\left(k_4V^2+q\left(\bar{x}_2\right)\right)\bar{x}_2-c_3\bar{x}_3-c_4\bar{x}_4 \end{pmatrix} = \bar{x}_4 \\
\ddot{y}_o &= \frac{\mathrm{d}\dot{y}_o}{\mathrm{d}\bar{\mathbf{x}}}.\frac{\mathrm{d}\bar{\mathbf{x}}}{\mathrm{d}t} = \frac{\mathrm{d}\bar{x}_4}{\mathrm{d}\bar{\mathbf{x}}}\cdot\left(\bar{\mathbf{f}}\left(\bar{\mathbf{x}}\right)+\bar{\mathbf{g}}\cdot\left(\beta+\Delta\beta\right)+\boldsymbol{\delta}\right) \\
&= \begin{bmatrix}0 & 0 & 0 & 1\end{bmatrix}\cdot\left(\bar{\mathbf{f}}\left(\bar{\mathbf{x}}\right)+\bar{\mathbf{g}}\cdot\left(\beta+\Delta\beta\right)+\boldsymbol{\delta}\right) \\
&= -k_3\bar{x}_1-\left(k_4V^2+q\left(\bar{x}_2\right)\right)\bar{x}_2-c_3\bar{x}_3-c_4\bar{x}_4+g_4\left(\beta+\Delta\beta\right)+\delta_2
\end{aligned}
\tag{6.8}
$$

where $\delta_2 = t_4\Delta K_\theta\left(\bar{x}_2\right)\bar{x}_2$.

Since the input $g_4\left(\beta+\Delta\beta\right)$ appears in the expression for $\ddot{y}_o$ it is apparent that relative degree $r_d = 2$. The significance of this is that the nonlinear system may be divided into an external sub-system of dimension r_d, generally with nonlinear input, and a sub-system of $2n-r_d$ nonlinear equations known as the internal dynamics, where n is the number of degrees of freedom. In the present case both subsystems are of order 2. This arrangement of equations is known as the normal form, which in the present case may be obtained by means of the transformation,

$$
\mathbf{z} = \mathbf{T}\bar{\mathbf{x}} \text{ or } \begin{pmatrix} z_1 \\ z_2 \\ z_3 \\ z_4 \end{pmatrix} = \begin{bmatrix} -g_4 & g_3 & 0 & 0 \\ 0 & 1 & g_4/\varphi_4 & -g_3/\varphi_4 \\ 0 & 1 & 0 & 0 \\ 0 & 0 & 0 & 1 \end{bmatrix}\begin{pmatrix} \bar{x}_1 \\ \bar{x}_2 \\ \bar{x}_3 \\ \bar{x}_4 \end{pmatrix} \tag{6.9}
$$

where $\varphi_4 = g_3c_1+g_4c_2-c_3\,g_3^2/g_4-c_4g_3 \neq 0$, such that $\frac{dz_1}{d\bar{\mathbf{x}}}\bar{\mathbf{g}} = 0$, $\frac{dz_2}{d\bar{\mathbf{x}}}\bar{\mathbf{g}} = 0$ to ensure that the input does not appear explicitly in the equations of the internal dynamics. The matrix $\mathbf{T}$, being invertible, is a global diffeomorphism.

Application of equation (6.9), in (6.6) leads to the normal form,

$$\dot{\mathbf{z}}_{(1-2)} = \mathbf{f}_1\left(\mathbf{z}_{(1-2)}\right) + \mathbf{f}_2\left(\mathbf{z}_{(1-2)}, z_3\right) z_3 + \boldsymbol{\delta}_1 \tag{6.10}$$

$$\dot{z}_3 = z_4 \tag{6.11}$$

$$\dot{z}_4 = f_b\left(\mathbf{z}\right) + g_4 \cdot \left(\beta + \Delta\beta\right) + \delta_2 \tag{6.12}$$

where

$$\mathbf{f}_1\left(\mathbf{z}_{(1-2)}\right) = \mathbf{S}\mathbf{z}_{(1-2)} = \begin{bmatrix} 0 & -\varphi_4 \\ -\varphi_1/\varphi_4 & \varphi_2 \end{bmatrix} \mathbf{z}_{(1-2)} \tag{6.13}$$

$$\mathbf{f}_2\left(\mathbf{z}_{(1-2)}, z_3\right) = \begin{pmatrix} \varphi_4 \\ \left(-\dfrac{1}{\varphi_4}\right)\left(\varphi_2\varphi_4 + \varphi_{31} + \varphi_{32} K_\theta\left(z_3\right)\right) \end{pmatrix} \tag{6.14}$$

$$f_b\left(\mathbf{z}\right) = \varphi_7 z_1 + \varphi_4\varphi_8\left(z_3 - z_2\right) + \varphi_{91} z_3 + \varphi_{92} K_\theta\left(z_3\right) z_3 + \varphi_{10} z_4 \tag{6.15}$$

$$\mathbf{z}_{(1-2)} = \begin{pmatrix} z_1 \\ z_2 \end{pmatrix},\ \boldsymbol{\delta}_1 = \tilde{\mathbf{t}}\Delta K_\theta\left(z_3\right) z_3,\ \tilde{\mathbf{t}} = \begin{pmatrix} 0 \\ \tilde{t}_2 \end{pmatrix} = \begin{pmatrix} 0 \\ \dfrac{g_4 m_w x_\theta b + g_3 m_t}{\varphi_4 d} \end{pmatrix} \tag{6.16}$$

$$\varphi_1 = k_3\left(g_3/g_4\right) - k_1,\ \varphi_{31} = g_3 k_1 + g_4 k_2 V^2 - k_3\left(g_3^2/g_4\right) - g_3 k_4 V^2 \tag{6.17}$$

$$\varphi_2 = c_3\left(g_3/g_4\right) - c_1,\ \varphi_{32} = -\left(g_4 m_w x_\theta b + g_3 m_t\right)/d,\ \varphi_7 = k_3/g_4,\ \varphi_8 = c_3/g_4 \tag{6.18}$$

$$\varphi_{91} = -\left(k_3\left(g_3/g_4\right) + k_4 V^2\right),\ \varphi_{92} = -m_t/d \ \text{ and } \ \varphi_{10} = -\left(c_3\left(g_3/g_4\right) + c_4\right) \tag{6.19}$$

In the new coordinate system, equations (6.11) and (6.12) comprise the chain of simple integrators whereas the internal dynamics, determined by equation (6.10), are not directly affected by the control input. Together, equations (6.10)-(6.12) define a cascaded system of equations in the normal form.

The zero dynamics of the system (6.10)-(6.12), without uncertainty and disturbance, are given by the linear system,

$$\dot{\mathbf{z}}_{(1-2)} = \mathbf{f}_1\left(\mathbf{z}_{(1-2)}\right) = \mathbf{S}\mathbf{z}_{(1-2)} \tag{6.20}$$

when the output is set to zero, $y_o = z_3 = 0$, which in turn causes z_4 to vanish, i.e. $z_4 = 0$. The zero dynamics in nonlinear systems is equivalent to the zero dynamics in

LTI systems in that stability of the zero dynamics means that the system is minimum phase. In feedback linearisation, the global exponential stability of the zero dynamics is a necessary condition for the global asymptotic stability of the overall system, the sufficient condition being that the internal dynamics is input-to-state stable [21]. The nonlinear system is globally minimum phase if the zero dynamics has a global, asymptotically-stable equilibrium point.

In this paper, we will employ sliding-mode control to globally stabilise the nonlinear system (6.10)-(6.12). The idea of sliding-mode control is to design a control input β to force the system states to move toward a desired stable sliding surface S and maintain the states on it. Once on the sliding surface, all the states will move along the sliding surface and converge to zero. On the sliding surface, the behaviour of the system is determined by the prescribed sliding surface. It will be shown later that the design of a stable sliding-mode surface will stabilise the internal dynamics.

Due to the form of equations (6.10)-(6.12) it is convenient to choose a nonlinear sliding surface as,

$$S = z_4 - \Phi_1\left(\mathbf{z}_{(1-3)}\right) = 0 \tag{6.21}$$

where $\mathbf{z}_{(1-3)} = \left[\mathbf{z}_{(1-2)}^T, z_3\right]^T$ and $\Phi_1\left(\mathbf{z}_{(1-3)}\right)$ is an unknown function to be designed with the requirement that the origin of the dynamics of the reduced-order model,

$$\dot{\mathbf{z}}_{(1-2)} = \mathbf{f}_1\left(\mathbf{z}_{(1-2)}\right) + \mathbf{f}_2\left(\mathbf{z}_{(1-2)}, z_3\right) z_3 + \boldsymbol{\delta}_1 \tag{6.22}$$

$$\dot{z}_3 = \Phi_1\left(\mathbf{z}_{(1-3)}\right) \tag{6.23}$$

confined to the sliding surface, shall be globally asymptotically stable. The design of $\Phi_1\left(\mathbf{z}_{(1-3)}\right)$ amounts to solving a stabilisation problem for the system (6.22)-(6.23) with $z_4 = \Phi_1\left(\mathbf{z}_{(1-3)}\right)$ viewed as the control input.

In view of its importance, the stability properties of the zero dynamics of system (6.10)-(6.12) will now be considered. Suppose the origin of zero dynamics $\dot{\mathbf{z}}_{(1-2)} = \mathbf{f}_1\left(\mathbf{z}_{(1-2)}\right) = \mathbf{S}\mathbf{z}_{(1-2)}$ is globally asymptotically stable, then $\mathbf{S}$ is Hurwitz, $\det\left(\mathbf{S} - \lambda\mathbf{I}\right) = \lambda^2 - \varphi_2\lambda - \varphi_1$ so that $\varphi_1, \varphi_2 < 0$. Hence, for any given positive definite symmetric matrix $\bar{\mathbf{Q}}$, there exists a positive definite symmetric matrix $\bar{\mathbf{P}}$ that satisfies the Lyapunov equation,

$$\bar{\mathbf{P}}\mathbf{S} + \mathbf{S}^T\bar{\mathbf{P}} = -\bar{\mathbf{Q}} \tag{6.24}$$

Correspondingly, there exists a continuously differentiable, radially unbounded storage function[1] $W\left(\mathbf{z}\right)$ satisfying

$$\lambda_{\min}\left(\bar{\mathbf{P}}\right)\left\|\mathbf{z}_{(1-2)}\right\|_2^2 \le W\left(\mathbf{z}_{(1-2)}\right) = \mathbf{z}_{(1-2)}^T\bar{\mathbf{P}}\mathbf{z}_{(1-2)} \le \lambda_{\max}\left(\bar{\mathbf{P}}\right)\left\|\mathbf{z}_{(1-2)}\right\|_2^2 \tag{6.25}$$

and

$$\dot{W}\left(\mathbf{z}_{(1-2)}\right) = \frac{\mathrm{d}W\left(\mathbf{z}_{(1-2)}\right)}{\mathrm{d}\mathbf{z}_{(1-2)}}\mathbf{f}_1\left(\mathbf{z}_{(1-2)}\right) = -\mathbf{z}_{(1-2)}{}^T\bar{\mathbf{Q}}\mathbf{z}_{(1-2)} \le -\lambda_{\min}\left(\bar{\mathbf{Q}}\right)\left\|\mathbf{z}_{(1-2)}\right\|_2^2 \tag{6.26}$$

for $\forall\mathbf{z}_{(1-2)} \in \mathbb{R}^{2\times 1}$, where $\dot{W}\left(\mathbf{z}_{(1-2)}\right)$ and $\mathrm{d}W\left(\mathbf{z}_{(1-2)}\right)\big/\mathrm{d}\mathbf{z}_{(1-2)}$ are the differentials of $W\left(\mathbf{z}_{(1-2)}\right)$ with respect to time t and $\mathbf{z}_{(1-2)}$ respectively, $\lambda_{\min}\left(\bullet\right)$ and $\lambda_{\max}\left(\bullet\right)$ are

[1] A radially unbounded function is a function $W\left(\mathbf{z}\right)$ for which $\left\|\mathbf{z}\right\| \to \infty \Rightarrow W\left(\mathbf{z}\right) \to \infty$.

minimum and maximum eigenvalues of $(\bullet)$, and $\|(\bullet)\|_2$ is the Euclidean norm of $(\bullet)$ [21].

In the analysis above, positive-definite $\bar{\mathbf{Q}}$ may be chosen arbitrarily, but in this paper is taken to be,

$$\bar{\mathbf{Q}} = \begin{bmatrix} q_1 & 0 \\ 0 & q_2 \end{bmatrix}, \; q_1 > 0, \; q_2 > 0 \tag{6.27}$$

Then $\bar{\mathbf{P}}$ is found as,

$$\bar{\mathbf{P}} = \begin{bmatrix} p_{11} & p_{12} \\ p_{12} & p_{22} \end{bmatrix} = \begin{bmatrix} \dfrac{\varphi_1 q_2}{2\varphi_2 \varphi_4^2} - \dfrac{q_1}{2\varphi_2} + \dfrac{\varphi_2 q_1}{2\varphi_1} & \dfrac{\varphi_4 q_1}{2\varphi_1} \\ \dfrac{\varphi_4 q_1}{2\varphi_1} & -\dfrac{q_2}{2\varphi_2} + \dfrac{\varphi_4^2 q_1}{2\varphi_1 \varphi_2} \end{bmatrix} \tag{6.28}$$

which is indeed a positive-definite, symmetric matrix. Since the zero dynamics are linear they are not only globally asymptotically stable but converge to zero exponentially.

6.4 Nonlinear aeroelastic system with control input disturbance

First, we consider the case where the only uncertainty is the control input disturbance,

$$\boldsymbol{\delta}_1 = \mathbf{0}, \; \delta_2 = 0 \text{ and } \Delta\beta \neq 0 \tag{6.29}$$

Then the system (6.10)-(6.12) becomes,

$$\dot{\mathbf{z}}_{(1-2)} = \mathbf{f}_1\left(\mathbf{z}_{(1-2)}\right) + \mathbf{f}_2\left(\mathbf{z}_{(1-2)}, z_3\right) z_3 \tag{6.30}$$

$$\dot{z}_3 = z_4 \tag{6.31}$$

$$\dot{z}_4 = f_b(\mathbf{z}) + g_4 \cdot (\beta + \Delta\beta) \tag{6.32}$$

6.4.1 Passivity-based sliding surface design

Consider the system (6.30) and (6.31). z_4 may be viewed as the input to the system and z_3 the output variable. According to the definition of passivity [21, 145], the

system (6.30) and (6.31) is said to be strictly passive if there exists a differentiable and positive definite storage function $U_1\left(\mathbf{z}_{(1-3)}\right)$ such that

$$\dot{U}_1 < z_3 z_4, \ \forall z_3, z_4 \in \mathbb{R}, \ \forall z_3 \neq 0. \tag{6.33}$$

This may be understood physically as follows. If $U_1\left(\mathbf{z}_{(1-3)}\right)$ represents the energy of the system, then inequality (6.33) indicates that the system (6.30) and (6.31) is dissipative because the energy storage rate is less than the external energy supply rate $z_3 z_4$, with the difference being the energy dissipation rate. If z_4 is designed such that $\dot{U}_1 < 0$ with $\forall z_3 \neq 0$, then the system can be stabilised with input z_4. Here, the feedback passivity property [21, 145] is used to design $z_4 = \Phi_1\left(\mathbf{z}_{(1-3)}\right)$ such that global stability of the system (6.30), (6.31) is obtained.

Lemma 6.1 Suppose the origin of the zero dynamics $\dot{\mathbf{z}}_{(1-2)} = \mathbf{f}_1\left(\mathbf{z}_{(1-2)}\right) = \mathbf{S}\mathbf{z}_{(1-2)}$ is globally exponentially stable, then the origin of the system (6.30)-(6.31) can be globally exponentially stabilised by,

$$z_4 = \Phi_1\left(z_{(1-3)}\right) = -\frac{dW\left(\mathbf{z}_{(1-2)}\right)}{d\mathbf{z}_{(1-2)}}\mathbf{f}_2 - \chi z_3, \ \chi > 0 \tag{6.34}$$

Proof: Take a storage function candidate,

$$U_1\left(\mathbf{z}_{(1-3)}\right) = W\left(\mathbf{z}_{(1-2)}\right) + \frac{1}{2}z_3^2 \tag{6.35}$$

for the system (6.30)-(6.31), where $W\left(\mathbf{z}_{(1-2)}\right)$ satisfies (6.25) and (6.26). It may be shown that,

$$\min\left(\lambda_{\min}\left(\bar{\mathbf{P}}\right), \frac{1}{2}\right)\left\|\mathbf{z}_{(1-3)}\right\|_2^2 \leq U_1\left(\mathbf{z}_{(1-3)}\right) \leq \max\left(\lambda_{\max}\left(\bar{\mathbf{P}}\right), \frac{1}{2}\right)\left\|\mathbf{z}_{(1-3)}\right\|_2^2 \tag{6.36}$$

The derivative of U_1 is,

$$\dot{U}_1 = \frac{\mathrm{d}U_1}{\mathrm{d}\mathbf{z}_{(1-3)}}\dot{\mathbf{z}}_{(1-3)} = \begin{bmatrix} \dfrac{\mathrm{d}W\left(\mathbf{z}_{(1-2)}\right)}{\mathrm{d}\mathbf{z}_{(1-2)}} & z_3 \end{bmatrix} \begin{bmatrix} \dot{\mathbf{z}}_{(1-2)} \\ \dot{z}_3 \end{bmatrix} \tag{6.37}$$

Substitution (6.30) and (6.31) into (6.37) leads to,

$$\begin{aligned} \dot{U}_1 &= \frac{\mathrm{d}W\left(\mathbf{z}_{(1-2)}\right)}{\mathrm{d}\mathbf{z}_{(1-2)}}\mathbf{f}_1 + z_3\frac{\mathrm{d}W\left(\mathbf{z}_{(1-2)}\right)}{\mathrm{d}\mathbf{z}_{(1-2)}}\mathbf{f}_2 + z_3 z_4 \\ &= \frac{\mathrm{d}W\left(\mathbf{z}_{(1-2)}\right)}{\mathrm{d}\mathbf{z}_{(1-2)}}\mathbf{f}_1 + z_3\left(\frac{\mathrm{d}W\left(\mathbf{z}_{(1-2)}\right)}{\mathrm{d}\mathbf{z}_{(1-2)}}\mathbf{f}_2 + z_4\right) \end{aligned} \tag{6.38}$$

and applying the feedback control (6.34) gives,

$$\dot{U}_1 = \frac{\mathrm{d}W\left(\mathbf{z}_{(1-2)}\right)}{\mathrm{d}\mathbf{z}_{(1-2)}}\mathbf{f}_1 - \chi z_3^2 \le -\min\left(\lambda_{\min}\left(\bar{\mathbf{Q}}\right), \chi\right)\left\|\mathbf{z}_{(1-3)}\right\|_2^2 \tag{6.39}$$

Then by invoking Theorem 4.10 [21] with inequalities (6.36) and (6.39) , the origin of the system (6.30), (6.31) is found to be globally exponentially stable.

□

Now, considering the reduced-order model (6.30)-(6.31), supposing the zero dynamics to be globally exponentially stable, a nonlinear sliding surface may be chosen as

$$S = z_4 - \Phi_1\left(\mathbf{z}_{(1-3)}\right) = z_4 - \left(-\frac{\mathrm{d}W\left(\mathbf{z}_{(1-2)}\right)}{\mathrm{d}\mathbf{z}_{(1-2)}}\mathbf{f}_2 - \chi z_3\right) = 0 \tag{6.40}$$

which is globally exponentially stable. The stable sliding surface guarantees the stability of the internal dynamics (6.30). However, it is still necessary to determine the input β that ensures that the states of the system are attracted to the sliding surface and remain upon it.

6.4.2 Sliding mode control design

The sliding-mode control input aims to compel the states of the system, starting away from the sliding surface S, to move toward it (i.e., the reaching phase) and then to be maintained upon it (i.e., sliding phase). In this way the sliding surface S is made globally attractive. Here, an approach based on Lyapunov stability theory is used for the design of a sliding-mode control input. If a candidate Lyapunov function is selected as

$$U_2(S) = \frac{S^2}{2} \tag{6.41}$$

then the control input should be designed such that

$$\dot{U}_2 = S\dot{S} < 0, \ \forall S \neq 0 \tag{6.42}$$

By differentiating equation (6.40) and combining this with equations (6.30)-(6.32), and (6.13)-(6.15), the derivative of S may be determined as,

$$\dot{S} = \dot{z}_4 - \dot{\Phi}_1\left(\mathbf{z}_{(1-3)}\right) = \Phi_2(\mathbf{z}) + g_4 \cdot (\beta + \Delta\beta) \tag{6.43}$$

where $\Phi_1\left(\mathbf{z}_{(1-3)}\right)$ and $\Phi_2(\mathbf{z})$ are given in **Appendix 6.1**.

The term on the left-hand-side of inequality (6.42) becomes,

$$\dot{U}_2 = S\left(\Phi_2(\mathbf{z}) + g_4(\beta + \Delta\beta)\right) \tag{6.44}$$

To ensure inequality (6.42) is satisfied globally, a discontinuous sliding-mode control input may be applied according to,

$$\beta = \left(-\frac{\Phi_2(\mathbf{z})}{g_4} - \frac{\xi}{g_4}\operatorname{sgn}(S) - \frac{\upsilon}{g_4}S\right) \tag{6.45}$$

where $\xi, \upsilon > 0$. The term $-\Phi_2(\mathbf{z})/g_4$, a continuous control input, is used to neutralise the known term $\Phi_2(\mathbf{z})$ in equation (6.44). The other two terms in (6.45)

both have negative signs, so that deviation of the dynamic response from $S = 0$ leads to an input that returns the system to the sliding surface. Specifically, $-(\xi / g_4)\mathrm{sgn}(S)$ is used to compensate the input disturbance and $-(\upsilon / g_4)S$ is an exponential approaching law that guarantees an exponential convergence rate in the reaching phase and consequently reduces the approaching time to the sliding surface.

Substituting (6.45) into (6.44) leads to,

$$\begin{aligned} \dot{U}_2 &= S\left(-\xi \mathrm{sgn}(S) + g_4 \Delta\beta - \upsilon S\right) \\ &= -\xi |S| + S\left(g_4 \Delta\beta\right) - \upsilon S^2 \\ &\le -\left(\xi - |g_4 \Delta\beta|\right)|S| - \upsilon S^2 \end{aligned} \tag{6.46}$$

It is assumed that,

$$|g_4 \Delta\beta| \le \eta_0 \xi \tag{6.47}$$

where η_0, ξ are chosen based upon an estimate of the input uncertainty $\Delta\beta$ and the known g_4 while $0 \le \eta_0 < 1$.

Then, inequality (6.46) becomes,

$$\dot{U}_2 \le -(1 - \eta_0)\xi |S| - \upsilon S^2 \le 0 \tag{6.48}$$

which indicates that the discontinuous sliding control input (6.45) is able to force the system states to move toward the sliding surface (6.40) if the control input disturbance satisfies (6.47). Once the states are restricted the sliding surface, they exponentially converge to zero as time approaches infinity because the sliding surface (6.40) is designed to be globally exponentially stable. It is however well known that a discontinuous sliding control will result in chattering, which presents an obstacle to the practical application of sliding-mode control [146].

The continuous sliding-mode approach is commonly used to overcome the problem of chattering caused by the signum function in equation (6.45). Here, the signum function $\mathrm{sgn}(S)$ is replaced by a saturation function,

$$\mathrm{sat}\left(\frac{S}{\varepsilon}\right)=\begin{cases}\mathrm{sgn}(S) & |S|>\varepsilon \\ \dfrac{S}{\varepsilon} & |S|\le\varepsilon\end{cases} \tag{6.49}$$

where ε is a small constant that defines a boundary layer of constant width neighbouring the sliding surface at $S=0$.

Then the continuous sliding-mode control input becomes,

$$\beta=\left(-\frac{\Phi_2(\mathbf{z})}{g_4}-\frac{\xi}{g_4}\mathrm{sat}\left(\frac{S}{\varepsilon}\right)-\frac{\upsilon}{g_4}S\right) \tag{6.50}$$

If the zero dynamics are exponentially stable and the input disturbance is bounded by (6.47) , then the system can be globally stabilised by using the continuous sliding mode control input (6.50) and the trajectories are shown in **Appendix 6.2** to reach the positively invariant set,

$$\Omega_\varepsilon=\left\{U_1\left(\mathbf{z}_{(1-3)}\right)\le U_3(\varepsilon)\right\}\bigcap\left\{|S|\le\varepsilon\right\} \tag{6.51}$$

close to the sliding surface defined by a boundary layer of thickness ε and an associated energy term $U_3(\varepsilon)$ defined in the **Appendix 6.2**. Thus the application of continuous sliding-mode control generally results in the sliding phase never being reached, but the states are instead restricted to the thin boundary layer close to it.

□

Remark 6.1: The analysis above, and in **Appendix 6.2**, does not imply an assumption of smallness of the input disturbance. The controller is able to admit

large input disturbances under the practical limitation of the control surface deflection.

Remark 6.2: The analysis above, and in **Appendix 6.2**, does not imply an assumption that the structural nonlinearity is hardening or softening. Hence with known bounded input disturbance, the controller is able to globally stabilise under-actuated wing sections with hardening or softening nonlinearity.

6.4.3 Example 6.1

A two-degree-of-freedom plunging and pitching prototypical wing section with torsional nonlinearity [117] is used here for the purposes of demonstration. The system parameters are given in Table 6.1. The nonlinear torsional stiffness is

$$K_\theta(\theta) = \sum_{i=1}^{5} k_{\theta i}\theta^{i-1}$$
$$= 6.8614\left(1 + 1.1438\theta + 96.6696\theta^2 + 9.5134\theta^3 - 727.6641\theta^4\right)(\text{N.m/rad})$$

which is a softening nonlinearity.

Table 6.1 System parameters

Parameters	Value	Parameters	Value
m_t	12.3870 Kg	C_{M_θ}	$\left(0.5 + a_h\right)C_{L_\theta}$
m_w	2.0490 Kg	C_{L_β}	3.358
b	0.135 m	C_{M_β}	-1.94
ρ	1.225 Kg/m^3	K_h	2844.4 N/m
r_{cg}	$0.0873 - \left(b + a_h b\right)$ m	C_h	27.43 Kg/s
I_θ	$m_w r_{cg}^2 + 0.0517$ kgm^2	C_θ	0.036 Kgm^2/s
s_w	0.6 m	a_h	-0.6847
C_{L_θ}	2π		

The linear flutter boundary of the open-loop system is found to be 11.5 m/s and at velocity 16m/s, the nonlinear responses are given in Fig. 6.2.

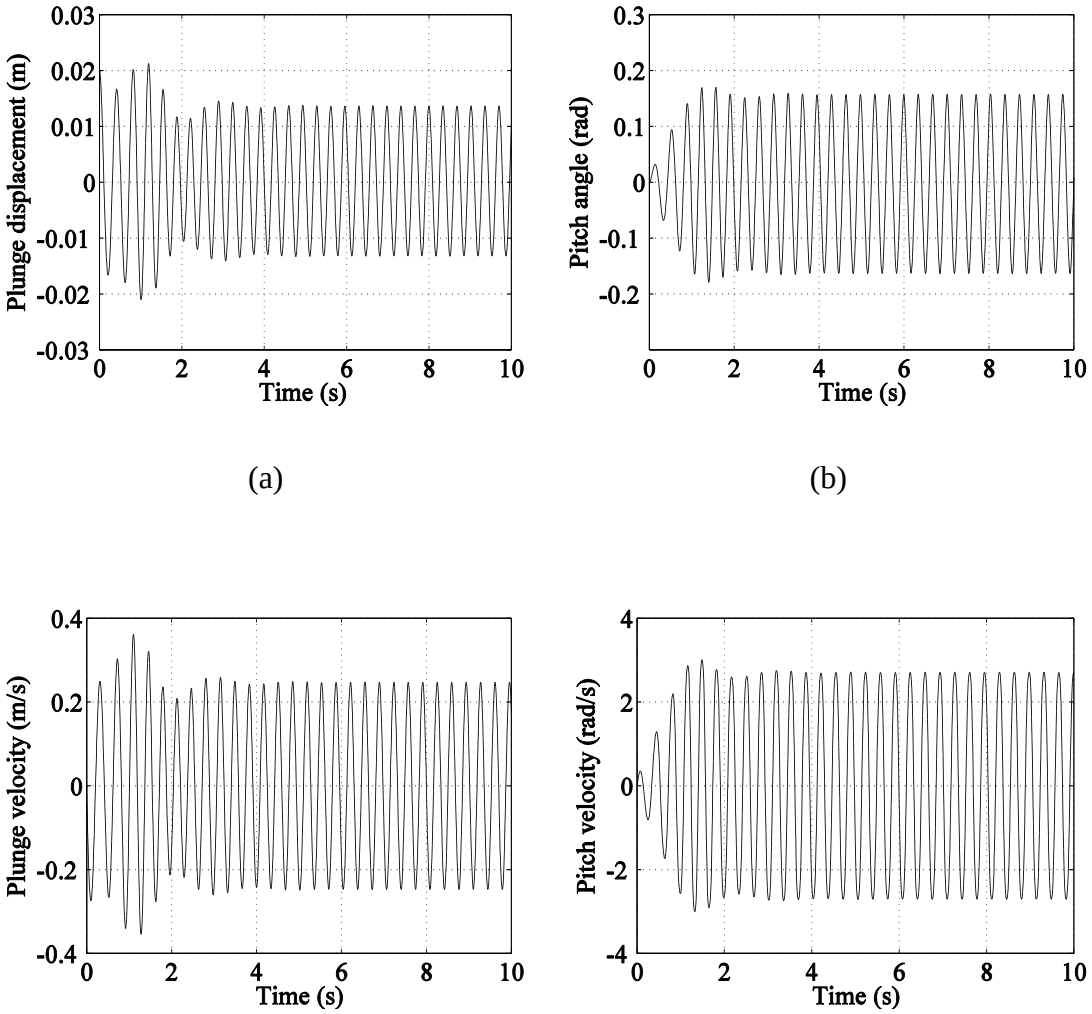

Fig. 6.2 The open-loop time histories with initial condition
$\left[h(0) \quad \theta(0) \quad \dot{h}(0) \quad \dot{\theta}(0)\right]^T = [0.02 \quad 0 \quad 0 \quad 0]^T$

In this example, a sinusoidal input disturbance $g_4 \Delta\beta = 0.1\sin(50t)$, which satisfies the matching condition, is considered. In principle, $\bar{\mathbf{Q}}$ may be any positive-definite matrix, χ and υ may be chosen as any positive real numbers, ξ and η_0 as arbitrarily chosen nonnegative real numbers satisfying (6.47) and $0 \le \eta_0 < 1$, but in practice are

limited by the trailing-edge control surface angle of an experimental rig. In this example the following parameters are selected,

$$\bar{\mathbf{Q}} = \begin{bmatrix} 1/8 & 0 \\ 0 & 1/2 \end{bmatrix},\ \chi = 550,\ \xi = 0.2,\ \eta_0 = 0.5,\ \upsilon = 47 \text{ and } \varepsilon = 0.02$$

for illustration. The closed-loop responses in Fig. 6.3 show the complete state of closed-loop system to be stable and in Fig. 6.4 a sinusoidal response of very low amplitude is shown to exist. Fig. 6.5 confirms that the responses are bounded in a small region around the origin, as explained by (6.51). Also, the control input, shown in Fig. 6.6 is sinusoidal with low amplitude. Despite the presence of very low amplitude sinusoidal response, the large-amplitude open-loop responses have been constrained into a very small positively invariant set around origin, which significantly alleviates effects of nonlinear flutter.

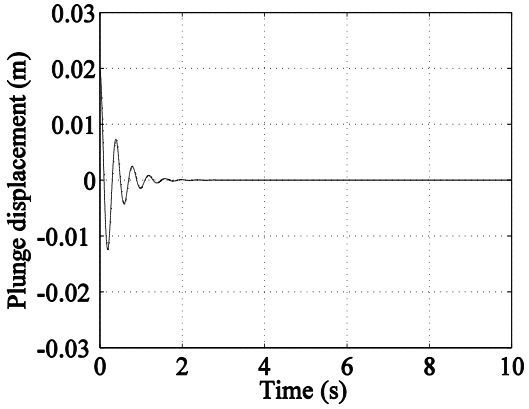

(a)

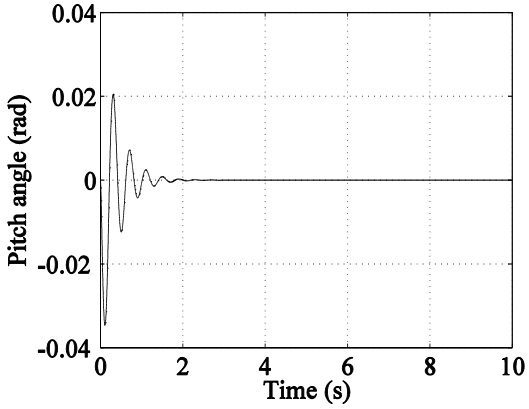

(b)

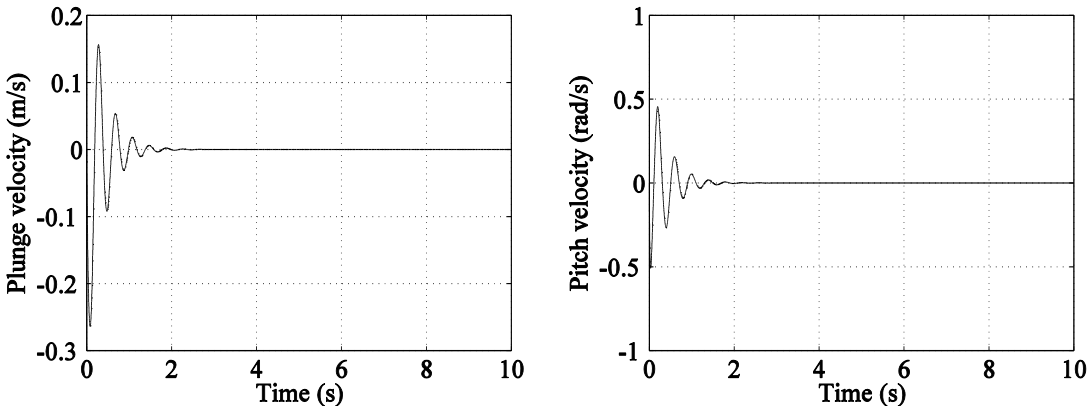

(c) (d)

Fig. 6.3 The closed-loop time histories with initial condition
$\left[h(0) \quad \theta(0) \quad \dot{h}(0) \quad \dot{\theta}(0)\right]^T = [0.02 \quad 0 \quad 0 \quad 0]^T$

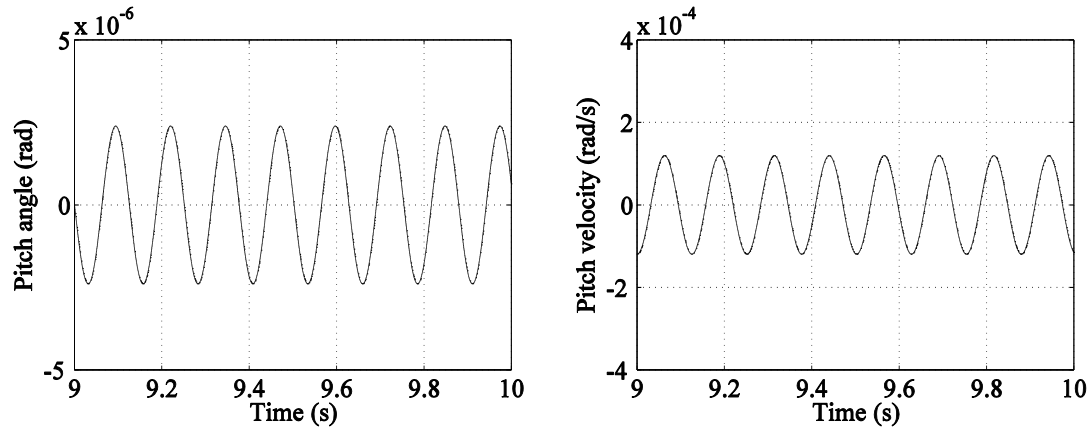

(a) (b)

Fig. 6.4 The zoomed closed-loop time histories with initial condition
$\left[h(0) \quad \theta(0) \quad \dot{h}(0) \quad \dot{\theta}(0)\right]^T = [0.02 \quad 0 \quad 0 \quad 0]^T$

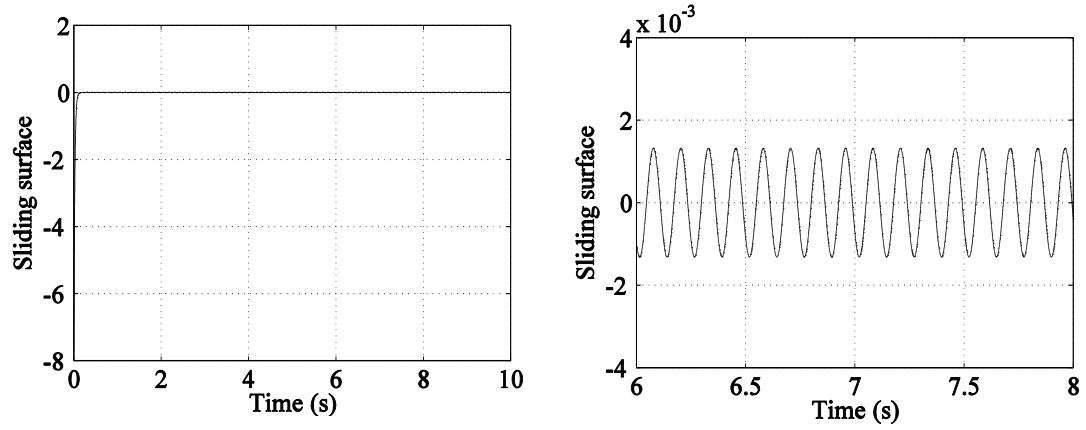

(a) (b)

Fig. 6.5 Sliding surface

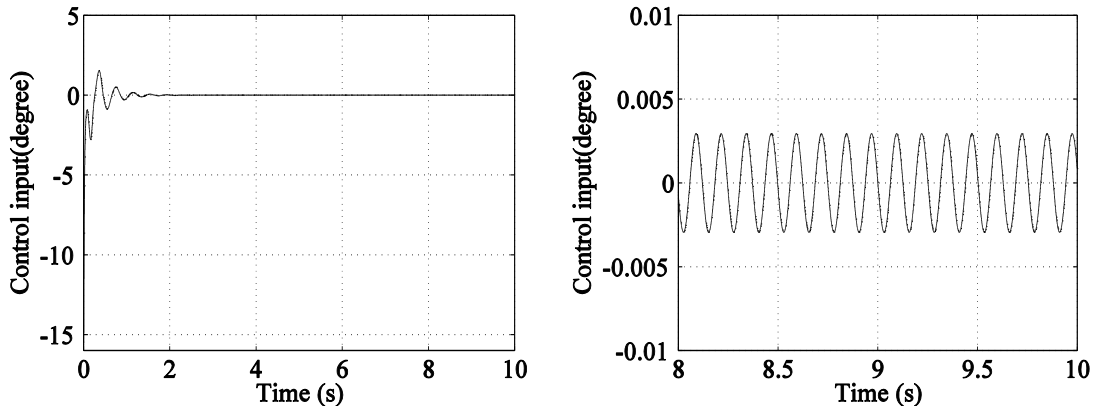

(a) (b)

Fig. 6.6 Trailing-edge control surface angle

6.5 Nonlinear aeroelastic systems with bounded torsional nonlinear uncertainty

In general structural nonlinearity is identified experimentally. There unavoidably exist measuring and identification errors, which produce unmatched and matched uncertainties $\boldsymbol{\delta}_1 \neq \mathbf{0}$ and $\delta_2 \neq 0$ respectively.

It is assumed that the structural nonlinearity uncertainty is bounded by

$$\left|\Delta K_\theta(\theta)\theta\right| = \left|\Delta K_\theta(z_3)z_3\right| \le \left|n(z_3)z_3\right| \tag{6.52}$$

where $n(z_3)$, differentiable with respect to z_3, is a known upper bound of the uncertain nonlinearity stiffness.

The case of uncertain structural torsional nonlinearity is considered whereby the overall system (6.10)-(6.12) is re-written as,

$$\dot{\mathbf{z}}_{(1-2)} = \mathbf{f}_1\left(\mathbf{z}_{(1-2)}\right) + \mathbf{f}_2\left(\mathbf{z}_{(1-2)}, z_3\right)z_3 + \boldsymbol{\delta}_1 \tag{6.53}$$

$$\dot{z}_3 = z_4 \tag{6.54}$$

$$\dot{z}_4 = f_b(\mathbf{z}) + g_4\beta + \delta_2 \tag{6.55}$$

6.5.1 Robust passivity-based sliding surface design

In this case, a robust passivity-based control technique [147] is used to design a stable nonlinear sliding surface. According to the definition [147], the system (6.53) and (6.54) , with z_3 and z_4 viewed as output variable and input respectively, is said to be robust strictly passive if there exists a differentiable positive-definite function $U_1\left(\mathbf{z}_{(1-3)}\right)$ such that,

$$\dot{U}_1 = \frac{dU_1\left(\mathbf{z}_{(1-3)}\right)}{d\mathbf{z}_{(1-3)}}\begin{pmatrix}\mathbf{f}_1\left(\mathbf{z}_{(1-2)}\right) + \mathbf{f}_2\left(\mathbf{z}_{(1-2)}, z_3\right)z_3 + \boldsymbol{\delta}_1 \\ z_4\end{pmatrix} < z_3 z_4, \ \forall z_3 \neq 0 \tag{6.56}$$

holds for any $\boldsymbol{\delta}_1$ subjected to the constraint (6.52). In what follows, it will be shown how z_4 will be chosen such that the system (6.53) and (6.54) can be stabilised.

Lemma 6.2 Suppose the origin of the zero dynamics $\dot{\mathbf{z}}_{(1-2)} = \mathbf{f}_1\left(\mathbf{z}_{(1-2)}\right) = \mathbf{S}\mathbf{z}_{(1-2)}$ is globally exponentially stable and let $W\left(\mathbf{z}_{(1-2)}\right)$ be a continuously differentiable,

radially unbounded Lyapunov function candidate satisfying (6.25) and(6.26). Then there exists a positive real constant ϑ such that,

$$\frac{dW\left(\mathbf{z}_{(1-2)}\right)}{d\mathbf{z}_{(1-2)}}\mathbf{f}_1+\frac{\vartheta}{2}\left(\frac{dW\left(\mathbf{z}_{(1-2)}\right)}{d\mathbf{z}_{(1-2)}}\tilde{\mathbf{t}}\right)^2<-\gamma_1\left\|\mathbf{z}_{(1-2)}\right\|_2^2 \tag{6.57}$$

where γ_1 is a positive constant.

Proof: Since $\dot{\mathbf{z}}_{(1-2)}=\mathbf{f}_1\left(\mathbf{z}_{(1-2)}\right)=\mathbf{S}\mathbf{z}_{(1-2)}$ is globally exponentially stable, there exists a continuously differentiable, radially unbounded Lyapunov function $W\left(\mathbf{z}_{(1-2)}\right)$ satisfying (6.25) and (6.26). Thus,

$$\frac{dW\left(\mathbf{z}_{(1-2)}\right)}{d\mathbf{z}_{(1-2)}}\tilde{\mathbf{t}}=2\mathbf{z}_{(1-2)}^T\bar{\mathbf{P}}\tilde{\mathbf{t}}=2\tilde{t}_2\left(z_1p_{12}+z_2p_{22}\right) \tag{6.58}$$

Therefore,

$$\begin{aligned}&\frac{dW\left(\mathbf{z}_{(1-2)}\right)}{d\mathbf{z}_{(1-2)}}\mathbf{f}_1+\frac{\vartheta}{2}\left(\frac{dW\left(\mathbf{z}_{(1-2)}\right)}{d\mathbf{z}_{(1-2)}}\tilde{\mathbf{t}}\right)^2\\&=\frac{dW\left(\mathbf{z}_{(1-2)}\right)}{d\mathbf{z}_{(1-2)}}\mathbf{f}_1+2\vartheta\tilde{t}_2^2\left(z_1p_{12}+z_2p_{22}\right)^2\end{aligned} \tag{6.59}$$

Then, due to (6.26) and the expression,

$$\left(z_1p_{12}+z_2p_{22}\right)^2\le 2\left(z_1p_{12}\right)^2+2\left(z_2p_{22}\right)^2\le 2\max\left(p_{12}^2,p_{22}^2\right)\left(z_1^2+z_2^2\right) \tag{6.60}$$

equation (6.59) becomes,

$$\begin{aligned}&\frac{dW\left(\mathbf{z}_{(1-2)}\right)}{d\mathbf{z}_{(1-2)}}\mathbf{f}_1+\frac{\vartheta}{2}\left(\frac{dW\left(\mathbf{z}_{(1-2)}\right)}{d\mathbf{z}_{(1-2)}}\tilde{\mathbf{t}}\right)^2\\&\le-\left[\lambda_{\min}\left(\bar{\mathbf{Q}}\right)-4\vartheta\tilde{t}_2^2\max\left(p_{12}^2,p_{22}^2\right)\right]\left\|\mathbf{z}_{(1-2)}\right\|_2^2\\&=-\gamma_1\left\|\mathbf{z}_{(1-2)}\right\|_2^2\end{aligned} \tag{6.61}$$

where $\gamma_1>0$ provided that $\vartheta<\dfrac{\lambda_{\min}\left(\bar{\mathbf{Q}}\right)}{4\tilde{t}_2^2\max\left(p_{12}^2,p_{22}^2\right)}$.

□

Lemma 6.3 Suppose the origin of the zero dynamics $\dot{\mathbf{z}}_{(1-2)} = \mathbf{f}_1\left(\mathbf{z}_{(1-2)}\right) = \mathbf{S}\mathbf{z}_{(1-2)}$ is globally exponentially stable, then the origin of the uncertain subsystem (6.53)-(6.54) can be globally exponentially stabilised by

$$z_4 = \Phi_3\left(\mathbf{z}_{(1-3)}\right) = -\frac{dW\left(\mathbf{z}_{(1-2)}\right)}{d\mathbf{z}_{(1-2)}}\mathbf{f}_2 - \frac{1}{2\vartheta}n^2\left(z_3\right)z_3 - \chi z_3, \;\; \chi > 0 \tag{6.62}$$

where $W\left(\mathbf{z}_{(1-2)}\right)$ is a radially unbounded, positive-definite Lyapunov function satisfying (6.25) and (6.26) and ϑ satisfies (6.57).

Proof: Suppose the origin of the zero dynamics $\dot{\mathbf{z}}_{(1-2)} = \mathbf{f}_1\left(\mathbf{z}_{(1-2)}\right) = \mathbf{S}\mathbf{z}_{(1-2)}$ is globally exponentially stable and there exist a radially unbounded, positive definite Lyapunov function $W\left(\mathbf{z}_{(1-2)}\right)$ satisfying (6.25) and (6.26).

Take a storage function candidate,

$$U_1\left(\mathbf{z}_{(1-3)}\right) = W\left(\mathbf{z}_{(1-2)}\right) + \frac{1}{2}z_3^2 \tag{6.63}$$

for the uncertain subsystem (6.53)-(6.54), which satisfies (6.36).

The derivate of U_1 is,

$$\dot{U}_1 = \frac{\mathrm{d}U_1}{\mathrm{d}\mathbf{z}_{(1-3)}}\dot{\mathbf{z}}_{(1-3)} = \begin{bmatrix} \dfrac{\mathrm{d}W\left(\mathbf{z}_{(1-2)}\right)}{\mathrm{d}\mathbf{z}_{(1-2)}} & z_3 \end{bmatrix}\begin{bmatrix} \dot{\mathbf{z}}_{(1-2)} \\ \dot{z}_3 \end{bmatrix} \tag{6.64}$$

Substitution (6.53) and (6.54) in (6.64), in conjugation with (6.16), leads to,

$$\begin{aligned}\dot{U}_1 &= \frac{dW\left(\mathbf{z}_{(1-2)}\right)}{d\mathbf{z}_{(1-2)}}\mathbf{f}_1 + z_3\frac{dW\left(\mathbf{z}_{(1-2)}\right)}{d\mathbf{z}_{(1-2)}}\mathbf{f}_2 + \frac{dW\left(\mathbf{z}_{(1-2)}\right)}{d\mathbf{z}_{(1-2)}}\boldsymbol{\delta}_1 + z_3 z_4 \\ &\le \frac{dW\left(\mathbf{z}_{(1-2)}\right)}{d\mathbf{z}_{(1-2)}}\mathbf{f}_1 + z_3\frac{dW\left(\mathbf{z}_{(1-2)}\right)}{d\mathbf{z}_{(1-2)}}\mathbf{f}_2 + z_3 z_4 + \left|\frac{dW\left(\mathbf{z}_{(1-2)}\right)}{d\mathbf{z}_{(1-2)}}\tilde{\mathbf{t}}\right|\left|\Delta K_\theta\left(z_3\right)z_3\right|\end{aligned} \tag{6.65}$$

and using the bound on the nonlinearity (6.52),

$$\dot{U}_1 \le \frac{dW\left(\mathbf{z}_{(1-2)}\right)}{d\mathbf{z}_{(1-2)}}\mathbf{f}_1 + z_3\frac{dW\left(\mathbf{z}_{(1-2)}\right)}{d\mathbf{z}_{(1-2)}}\mathbf{f}_2 + z_3 z_4 + \left|\frac{dW\left(\mathbf{z}_{(1-2)}\right)}{d\mathbf{z}_{(1-2)}}\tilde{\mathbf{t}}\right|\left|n\left(z_3\right)z_3\right| \tag{6.66}$$

Since

$$\begin{aligned}\left|\frac{dW\left(\mathbf{z}_{(1-2)}\right)}{d\mathbf{z}_{(1-2)}}\tilde{\mathbf{t}}\right|\left|n\left(z_3\right)z_3\right| &= \left(\left|\frac{dW\left(\mathbf{z}_{(1-2)}\right)}{d\mathbf{z}_{(1-2)}}\tilde{\mathbf{t}}\right|\sqrt{\vartheta}\right)\left(\frac{1}{\sqrt{\vartheta}}\left|n\left(z_3\right)z_3\right|\right) \\ &\le \frac{1}{2}\left(\left|\frac{dW\left(\mathbf{z}_{(1-2)}\right)}{d\mathbf{z}_{(1-2)}}\tilde{\mathbf{t}}\right|\sqrt{\vartheta}\right)^2 + \frac{1}{2}\left(\frac{1}{\sqrt{\vartheta}}\left|n\left(z_3\right)z_3\right|\right)^2 \\ &= \frac{\vartheta}{2}\left(\frac{dW\left(\mathbf{z}_{(1-2)}\right)}{d\mathbf{z}_{(1-2)}}\tilde{\mathbf{t}}\right)^2 + \frac{1}{2\vartheta}n^2\left(z_3\right)z_3^2\end{aligned} \tag{6.67}$$

inequality (6.66) becomes,

$$\dot{U}_1 \le \frac{dW\left(\mathbf{z}_{(1-2)}\right)}{d\mathbf{z}_{(1-2)}}\mathbf{f}_1 + z_3\frac{dW\left(\mathbf{z}_{(1-2)}\right)}{d\mathbf{z}_{(1-2)}}\mathbf{f}_2 + z_3 z_4 + \frac{\vartheta}{2}\left(\frac{dW\left(\mathbf{z}_{(1-2)}\right)}{d\mathbf{z}_{(1-2)}}\tilde{\mathbf{t}}\right)^2 + \frac{1}{2\vartheta}n^2\left(z_3\right)z_3^2 \tag{6.68}$$

Then, by using feedback control (6.62),

$$\begin{aligned}\dot{U}_1 &= -\chi z_3^2 + \frac{dW\left(\mathbf{z}_{(1-2)}\right)}{d\mathbf{z}_{(1-2)}}\mathbf{f}_1 + \frac{\vartheta}{2}\left(\frac{dW\left(\mathbf{z}_{(1-2)}\right)}{d\mathbf{z}_{(1-2)}}\tilde{\mathbf{t}}\right)^2 \\ &\le -\chi z_3^2 - \gamma_1\left\|\mathbf{z}_{(1-2)}\right\|_2^2 \\ &\le -\gamma_2\left\|\mathbf{z}_{(1-3)}\right\|_2^2\end{aligned} \tag{6.69}$$

where $\gamma_2 = \min\left(\chi, \gamma_1\right) > 0$.

Hence, by invoking Theorem 4.10 [21] with inequalities (6.36) and (6.69), the origin of the system (6.53) and (6.54) is found to be globally exponentially stable.

□

Now considering the reduced order system defined by equations (6.53) and (6.54), if the zero dynamics, $\dot{\mathbf{z}}_{(1-2)} = \mathbf{f}_1\left(\mathbf{z}_{(1-2)}\right) = \mathbf{S}\mathbf{z}_{(1-2)}$, is globally exponentially stable, in the presence of bounded nonlinear torsional uncertainty, the nonlinear sliding-mode surface may be chosen as,

$$S = z_4 - \Phi_3\left(\mathbf{z}_{(1-3)}\right) = 0 \tag{6.70}$$

to ensure that the reduced-order uncertain system is robustly exponentially stable.

6.5.2 Sliding mode control input design

Similarly to the analysis in Section 6.4.2, a sliding control input is to be designed such that the sliding manifold $S = 0$ is globally attractive. If a candidate Lyapunov function is selected as,

$$U_2\left(S\right) = \frac{S^2}{2} \tag{6.71}$$

then the control input should be designed such that,

$$\dot{U}_2 = S\dot{S} < 0, \ \forall S \neq 0 \tag{6.72}$$

By differentiating equation (6.70) and combining this with equations (6.85), (6.53)-(6.55), and (6.13)-(6.16), the derivative of S may be determined as,

$$\dot{S} = \Phi_4\left(\mathbf{z}\right) + \Phi_5\left(\mathbf{z}\right)\Delta K_\theta\left(z_3\right)z_3 + g_4\beta \tag{6.73}$$

where $\Phi_4(\mathbf{z}) = \Phi_2(\mathbf{z}) + \frac{1}{2\vartheta}\frac{\partial\left(n^2(z_3)z_3\right)}{\partial z_3}z_4$ with $\Phi_2(\mathbf{z})$ given by equation (6.86) in **Appendix 6.1** and

$$\Phi_5(\mathbf{z}) = \left[t_4 + \tilde{t}_2\left(q_2 + \left(\frac{q_2}{\varphi_2\varphi_4} - \frac{\varphi_4 q_1}{\varphi_1\varphi_2}\right)\left(\varphi_{31} + \varphi_{32}K_\theta(z_3)\right)\right)\right] \tag{6.74}$$

Then,

$$\dot{U}_2 = S\Phi_4(\mathbf{z}) + S\Phi_5(\mathbf{z})\Delta K_\theta(z_3)z_3 + Sg_4\beta \tag{6.75}$$

To ensure (6.72) is satisfied globally, a discontinuous sliding-mode control input may be applied in the form,

$$\beta = \left(-\frac{\Phi_4(\mathbf{z})}{g_4} - \frac{\xi(\mathbf{z})}{g_4}\mathrm{sgn}(S) - \frac{\upsilon}{g_4}S\right) \tag{6.76}$$

where $\xi(\mathbf{z}), \upsilon > 0$.

Substituting (6.76) into (6.75) leads to,

$$\dot{U}_2 \le \left|\Phi_5(\mathbf{z})\right| \times \left|n(z_3)z_3\right| \times |S| - \xi(\mathbf{z})|S| - \upsilon S^2 \tag{6.77}$$

It is assumed that,

$$\left|\Phi_5(\mathbf{z})\right| \times \left|n(z_3)z_3\right| \le \eta(\mathbf{z}) + \eta_0\xi(\mathbf{z}) \tag{6.78}$$

where $\eta(\mathbf{z}) \ge 0$ is a continuous function, and $0 \le \eta_0 < 1$.

Then by combining (6.77) and (6.78) it is found that,

$$\dot{U}_2 \le -(1-\eta_0)\xi_0|S| - \upsilon S^2 \le 0 \tag{6.79}$$

provided that $\xi(\mathbf{z}) \ge \frac{\eta(\mathbf{z})}{1-\eta_0} + \xi_0$ and $\xi_0 > 0$.

Inequality (6.78) shows that the discontinuous control input (6.76) is able to compel the states of the system, with bounded torsional nonlinearity uncertainty satisfying

(6.78), to move toward the sliding surface (6.70). Once the states are restricted the sliding surface (6.70), they exponentially converge to zero as time approaches infinity because the sliding surface (6.70) is designed to be globally exponentially stable.

Similarly to previous analysis in section 6.4.2, chatter may be alleviated by replacing the control input (6.75) with a continuous control input,

$$\beta = \left(-\frac{\Phi_4(\mathbf{z})}{g_4} - \frac{\xi(\mathbf{z})}{g_4}\text{sat}\left(\frac{S}{\varepsilon}\right) - \frac{\upsilon}{g_4}S \right) \tag{6.80}$$

If the zero dynamics are exponentially stable, the nonlinearity uncertainty is bounded by (6.52) and satisfies the condition (6.78) then the system can be globally stabilised by using the continuous sliding mode control input (6.80) and the trajectories are shown in **Appendix 6.3** to reach the positively invariant set,

$$\Omega_\varepsilon = \left\{ U_1\left(\mathbf{z}_{(1-3)}\right) \le U_4(\varepsilon) \right\} \bigcap \left\{ |S| \le \varepsilon \right\} \tag{6.81}$$

close to the sliding surface defined by a boundary layer of thickness ε and an associated energy term $U_4(\varepsilon)$ defined in the **Appendix 6.3**.

The system (6.53)-(6.54) with $z_4 = \Phi_3\left(\mathbf{z}_{(1-3)}\right)$ is globally exponentially stable. If $\eta(\mathbf{0}) = 0$ and $\eta_0 = 0$, then for a small enough ε, the origin of the full closed-loop system is shown in **Appendix 6.3** to be globally asymptotically stable.

Remark 6.3: The analysis above, and in **Appendix 6.3**, does not imply an assumption of smallness of the torsional nonlinear uncertainty. Hence the controller is able to admit large matched and mismatched uncertainties under the practical limitation of the control surface deflection.

Remark 6.4: The analysis above, and in **Appendix 6.3**, does not imply an assumption that the structural nonlinearity is hardening or softening. Hence with known bounded nonlinearity uncertainty, the controller is able to globally stabilise under-actuated wing sections with hardening or softening nonlinearity.

6.5.3 Example 6.2

The system with the same parameters described in section 6.4.3, except that the nonlinearity is hardening, is considered,

$$\begin{aligned} K_\theta(\theta) &= \sum_{i=1}^{5} k_{\theta i}\theta^{i-1} \\ &= 6.8614\left(1+1.1438\theta+96.6696\theta^2+9.5134\theta^3+727.6641\theta^4\right)\left(\text{N.m/rad}\right) \end{aligned} \tag{6.82}$$

with globally bounded uncertainty,

$$\left\|\Delta K_\theta(\theta)\theta\right\| \le \left\|n(\theta)\theta\right\| = \left\|0.1K_\theta(\theta)\theta\right\| \tag{6.83}$$

Suppose that the coefficients in (6.82), $k_{\theta 1}$, $k_{\theta 3}$ and $k_{\theta 5}$ are 8%, 7% and 9% underestimated respectively, and $k_{\theta 2}$ and $k_{\theta 4}$ are 2% and 5% overestimated respectively. The nonlinear uncertainty $\Delta K_\theta(\theta)\theta = 0.08k_{\theta 1}\theta - 0.02k_{\theta 2}\theta^2 + 0.07k_{\theta 3}\theta^3 - 0.05k_{\theta 4}\theta^4 + 0.09k_{\theta 5}\theta^5$ is found to satisfy the inequality (6.83).

The responses of the real open-loop system, with uncertainty included, shown in Fig. 6.7 are in limit cycle oscillation.

Let

$$\bar{\mathbf{Q}} = \begin{bmatrix} 1/8 & 0 \\ 0 & 1/2 \end{bmatrix},\ \vartheta = \frac{0.9\lambda_{\min}\left(\bar{\mathbf{Q}}\right)}{4\tilde{t}_2^2 \max\left(p_{12}^2, p_{22}^2\right)},\ \chi = 80000\quad \upsilon = 52.2,$$

$$\xi(\mathbf{z}) = \frac{\eta(\mathbf{z})}{1-\eta_0} + \xi_0,\ \eta_0 = 0,\ \xi_0 = 0.01,\ \eta(\mathbf{z}) = \left|\Phi_5(\mathbf{z})\right| \times \left|n(z_3)z_3\right|$$

Using the proposed robust continuous sliding-mode controller designed based on the nominal open-loop system, the closed-loop responses at $V = 16$ m/s are shown in Fig. 6.8, demonstrating the asymptotic stability of the closed-loop system. The matrix $\bar{\mathbf{Q}}$ may be any positive definite matrix, ϑ, χ and υ are arbitrarily chosen positive real numbers and $\xi(\mathbf{z})$, $\eta(\mathbf{z})$ and ξ_0 are arbitrarily

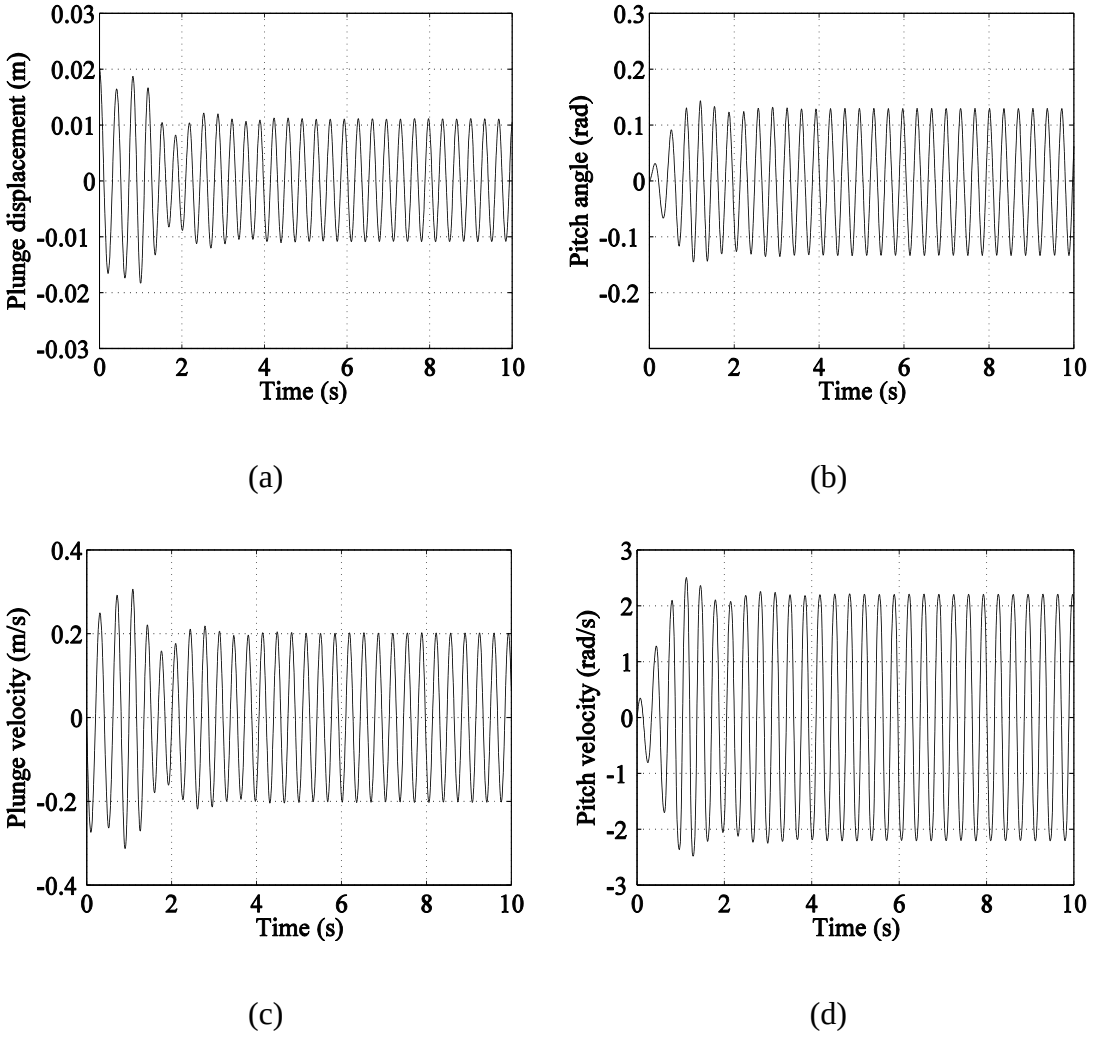

Fig. 6.7 The open-loop time histories with initial condition
$\left[h(0) \quad \theta(0) \quad \dot{h}(0) \quad \dot{\theta}(0)\right]^T = [0.02 \quad 0 \quad 0 \quad 0]^T$

chosen such that (6.78) and $\xi(\mathbf{z}) \geq \dfrac{\eta(\mathbf{z})}{1-\eta_0} + \xi_0$ are satisfied within the limitations of the control input level.

The sliding surface is depicted in Fig. 6.9, where it can be seen to begin away from the boundary layer. It firstly achieves the positively invariant set (6.81) and then stabilises asymptotically to the origin. This is because the origin of the reduced-order system is globally exponentially stable and $\eta(\mathbf{0}) = 0$ and $\eta_0 = 0$ for the current aerofoil with torsional nonlinear uncertainty. The control input in Fig. 6.10 is seen to be smooth with low-amplitude.

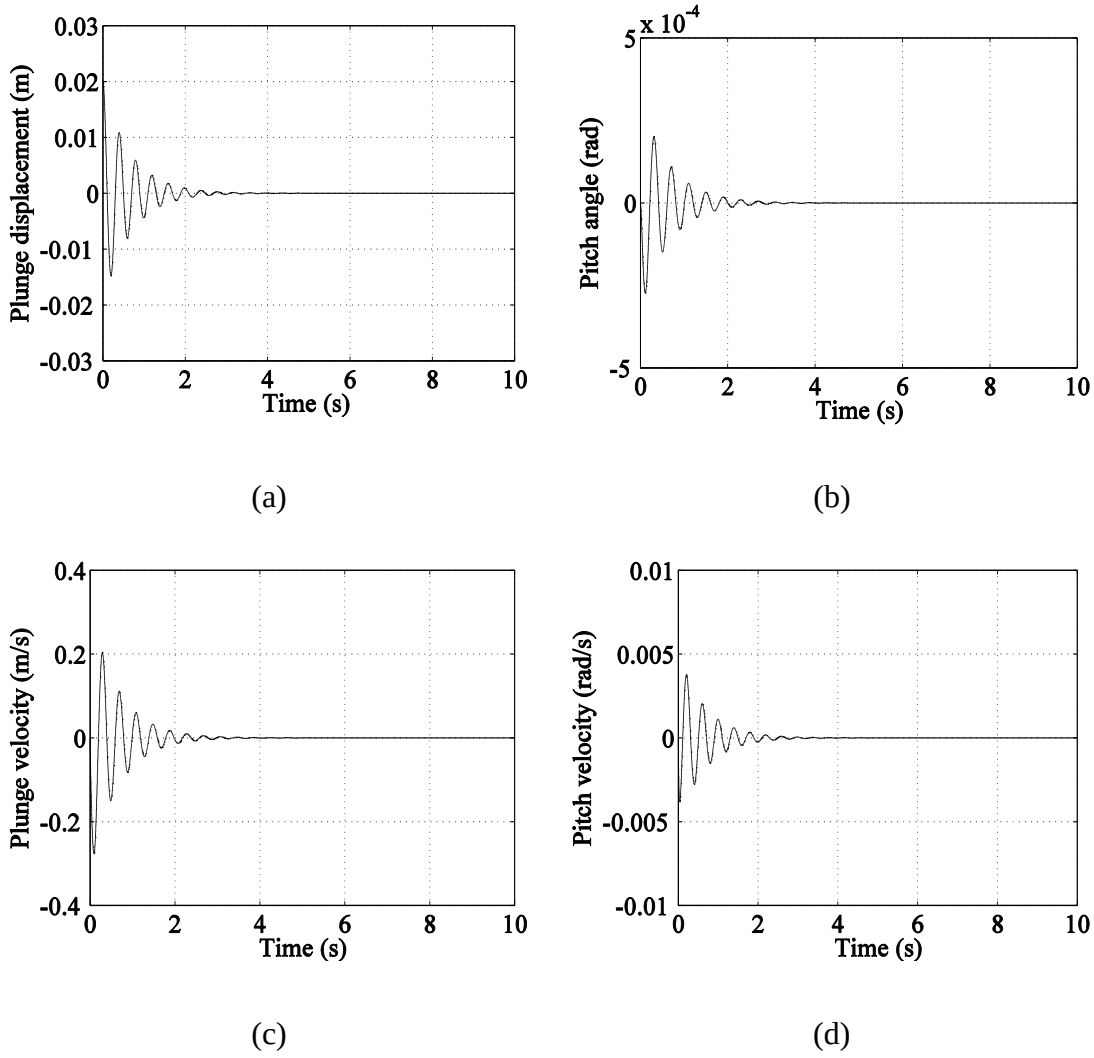

Fig. 6.8 The closed-loop time histories with initial condition $\left[h(0) \quad \theta(0) \quad \dot{h}(0) \quad \dot{\theta}(0)\right]^T = \left[0.02 \quad 0 \quad 0 \quad 0\right]^T$

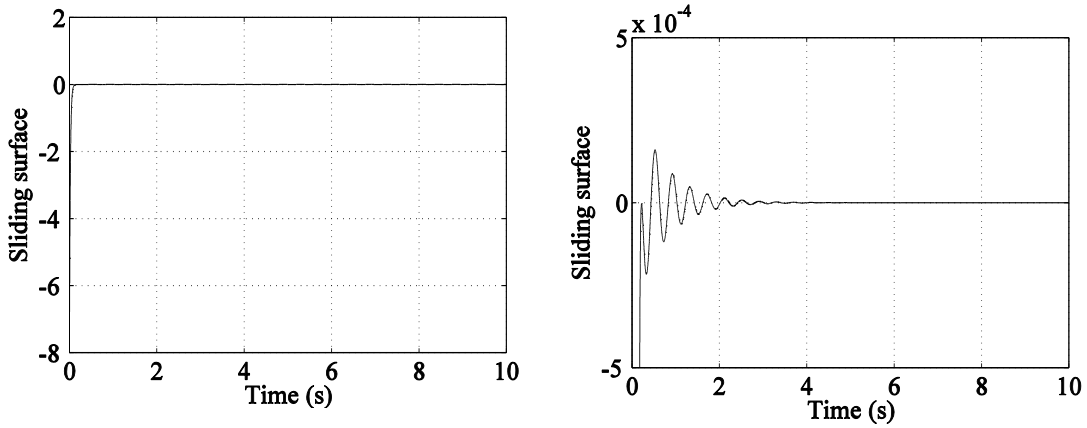

(a) (b)

Fig. 6.9 Sliding surface

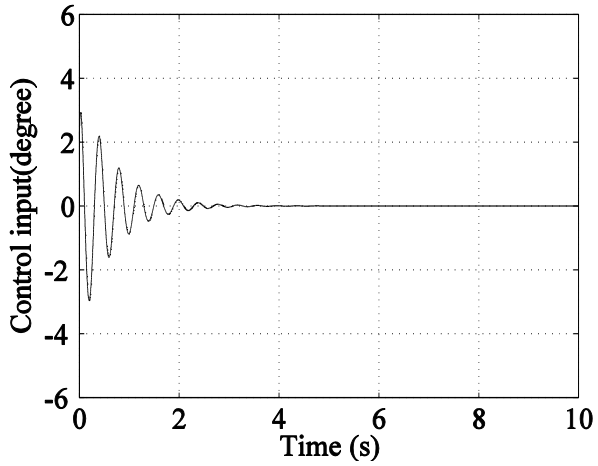

Fig. 6.10 Trailing edge control surface angle

6.5.4 Example 6.3

The system with softening nonlinearity described in section 6.4.3 is considered. Suppose that the coefficients $k_{\theta 1}$ and $k_{\theta 3}$ are 8% and 7% underestimated respectively, and $k_{\theta 2}$, $k_{\theta 4}$ and $k_{\theta 5}$ are 2%, 5% and 9% overestimated respectively. The nonlinearity uncertainty is $\Delta K_\theta(\theta)\theta = 0.08k_{\theta 1}\theta - 0.02k_{\theta 2}\theta^2 + 0.07k_{\theta 3}\theta^3 - 0.05k_{\theta 4}\theta^4 - 0.09k_{\theta 5}\theta^5$. There exists a differentiable upper bound function

$$n(\theta)\theta = \left(0.1k_{\theta 1} + 0.1k_{\theta 2}\theta + 0.1k_{\theta 3}\theta^2 + 0.1k_{\theta 4}\theta^3 - 0.1k_{\theta 5}\theta^4\right)\theta \tag{6.84}$$

which globally satisfies $\left\|\Delta K_\theta(\theta)\theta\right\| \le \left\|n(\theta)\theta\right\|$.

The responses of the real open-loop system, with uncertainty included, shown in Fig. 6.11, are statically divergent under the given initial condition due to the presence of softening nonlinearity.

Let

$$\bar{\mathbf{Q}} = \begin{bmatrix} 1/8 & 0 \\ 0 & 1/2 \end{bmatrix},\ \vartheta = \frac{0.9\lambda_{\min}\left(\bar{\mathbf{Q}}\right)}{4\tilde{t}_2^2 \max\left(p_{12}^2, p_{22}^2\right)},\ \chi = 80000 \quad \upsilon = 52.2,$$

$$\xi(\mathbf{z}) = \frac{\eta(\mathbf{z})}{1-\eta_0} + \xi_0,\ \eta_0 = 0,\ \xi_0 = 0.01,\ \eta(\mathbf{z}) = \left|\Phi_5(\mathbf{z})\right| \times \left|n(z_3) z_3\right|$$

Using the proposed robust continuous sliding-mode controller designed based on the nominal open-loop system, the closed-loop responses at $V = 16$ m/s are shown in Fig. 6.12, demonstrating the asymptotic stability of the closed-loop system under the same initial condition.

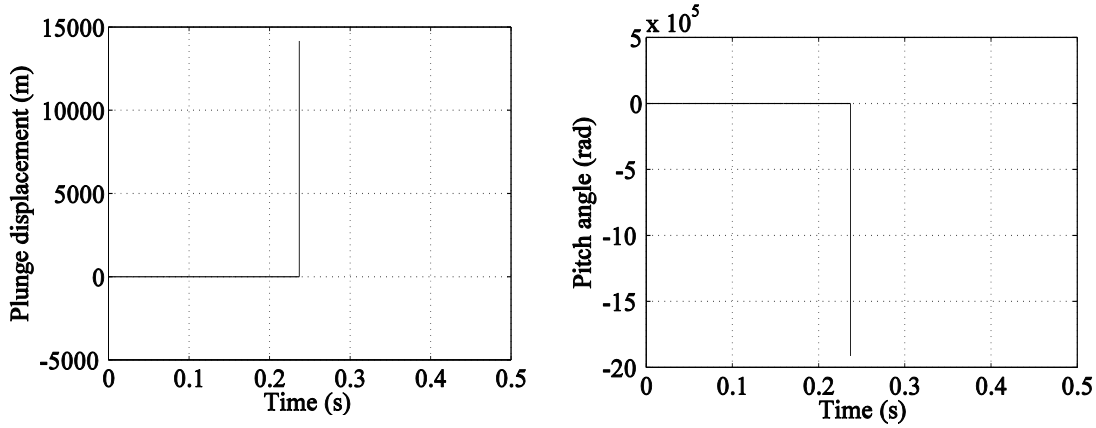

(a) (b)

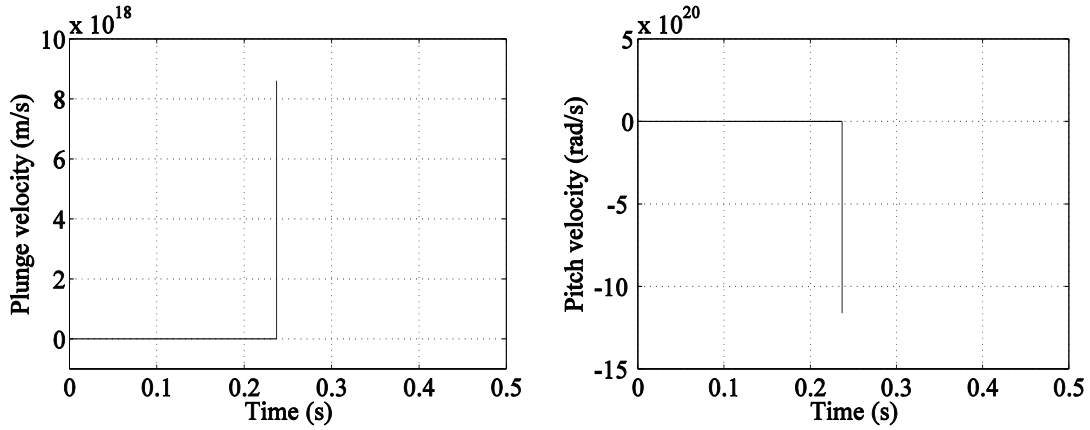

(c) (d)

Fig. 6.11 The open-loop time histories with initial condition
$\left[h(0) \quad \theta(0) \quad \dot{h}(0) \quad \dot{\theta}(0)\right]^T = \left[0.3 \quad 0 \quad 0 \quad 0\right]^T$

The sliding surface is depicted in Fig. 6.13, where it can be seen to begin away from the boundary layer. It firstly achieves the positively invariant set (6.81) and then stabilises asymptotically to the origin. This is because the origin of the reduced-order system is globally exponentially stable and $\eta(\mathbf{0}) = 0$ and $\eta_0 = 0$ for the current aerofoil with torsional nonlinear uncertainty. The control input in Fig. 6.14 seen to be smooth. Hence, the robust passivity-based sliding mode controller is able to globally stabilise the under-actuated wing section with softening nonlinearity in the face of nonlinearity uncertainty.

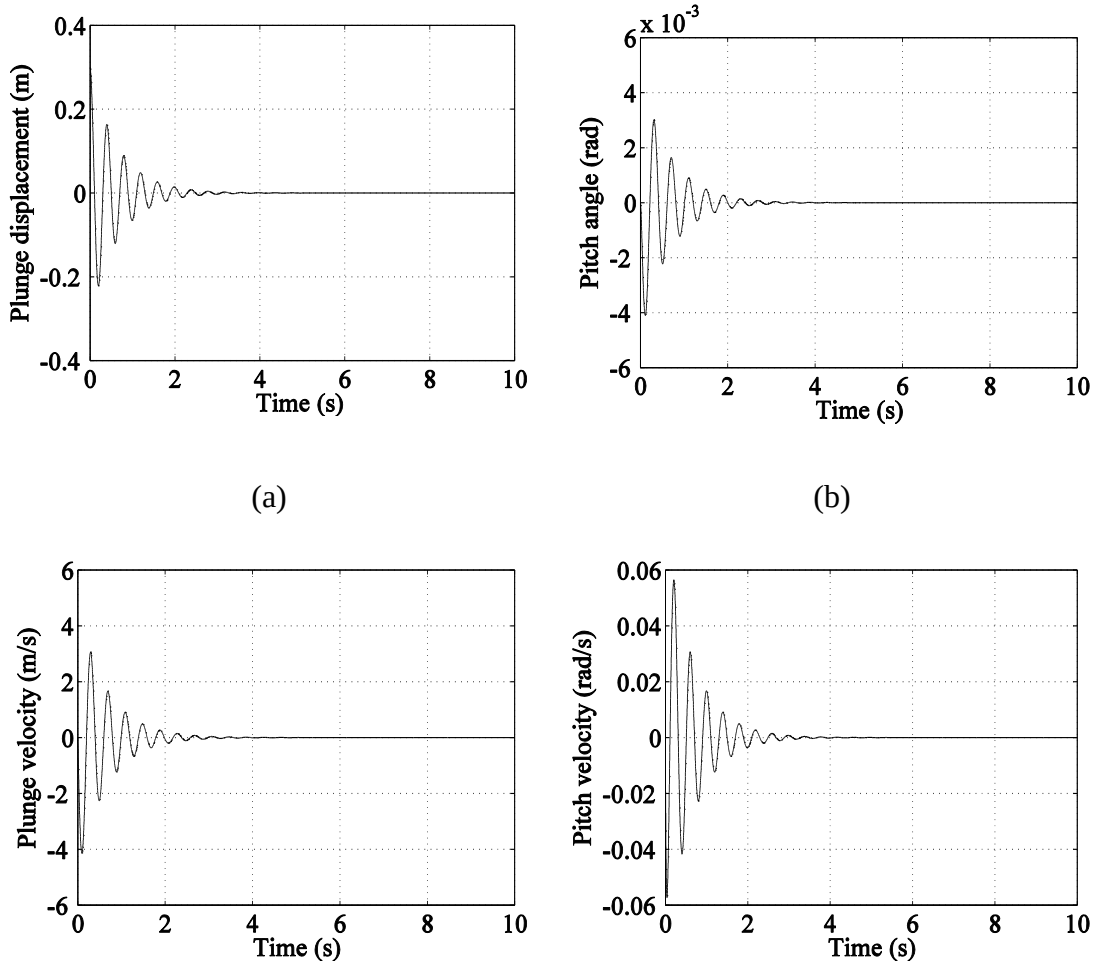

Fig. 6.12 The closed-loop time histories with initial condition

$$\left[h(0) \quad \theta(0) \quad \dot{h}(0) \quad \dot{\theta}(0)\right]^T = \left[0.3 \quad 0 \quad 0 \quad 0\right]^T$$

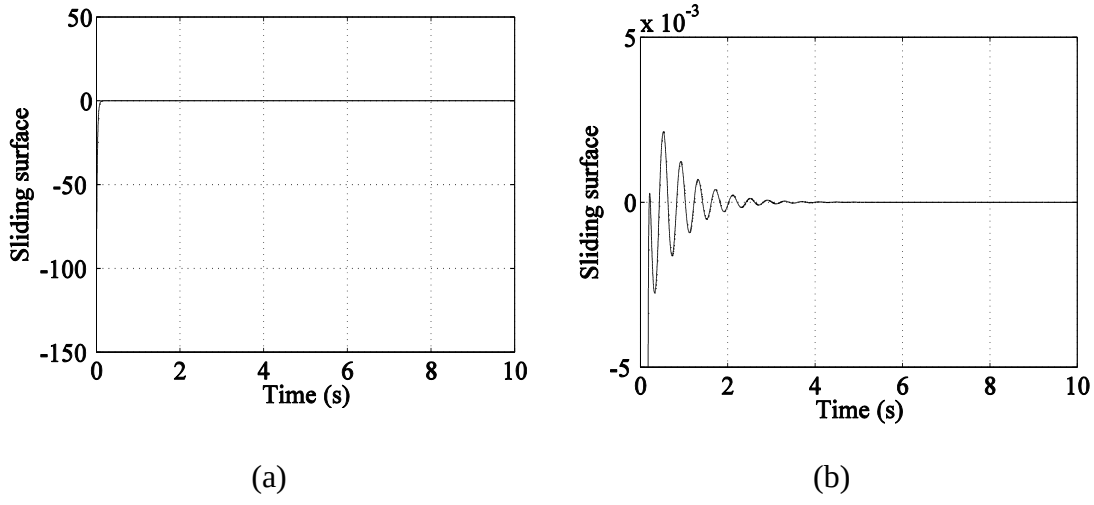

Fig. 6.13 Sliding surface

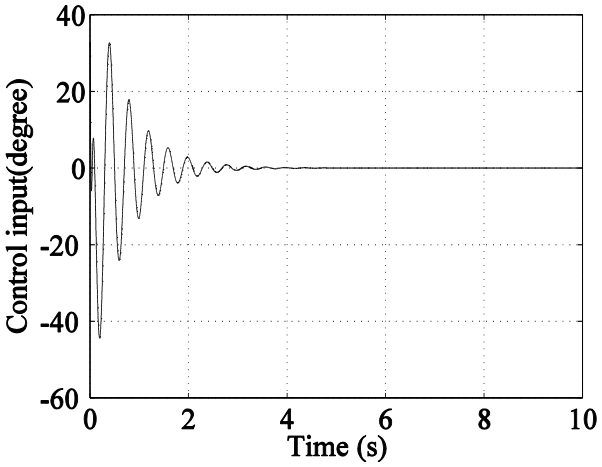

Fig. 6.14 Trailing edge control surface angle

6.6 Conclusion

A new approach is developed for the suppression of flutter instability in an under-actuated prototypical wing section with torsional nonlinearity. Passivity-based control is used to design a nonlinear sliding-mode surface in the presence of matched uncertainty and input disturbance, while robust passivity-based control is employed in the presence of mismatched uncertainty. A continuous sliding-mode control input, designed by the use of an approach based on Lyapunov stability theory, is employed to stabilise the overall system. With known bounds on both the input disturbance and nonlinear uncertainty, the controller is able to globally stabilise the overall system with softening or hardening torsional nonlinearity, when the zero dynamics are globally exponentially stable. The controller is able to admit large nonlinearity uncertainty and input disturbance under the practical limitation of the control surface deflection. Application of the controller is demonstrated by means of a series of example problems.

Appendix 6.1: **Expressions for $\Phi_1\left(\mathbf{z}_{(1-3)}\right)$ and $\Phi_2\left(\mathbf{z}\right)$**

$\Phi_1\left(\mathbf{z}_{(1-3)}\right)$ may be determined using (6.25) , (6.28) and (6.14) as,

$$\begin{aligned}\Phi_1\left(\mathbf{z}_{(1-3)}\right) &= -\frac{dW\left(\mathbf{z}_{(1-2)}\right)}{d\mathbf{z}_{(1-2)}}\mathbf{f}_2 - \chi z_3 \\ &= -\frac{d}{d\mathbf{z}_{(1-2)}}\left(\mathbf{z}_{(1-2)}^T\bar{\mathbf{P}}\mathbf{z}_{(1-2)}\right)\mathbf{f}_2 - \chi z_3 = -2\mathbf{z}_{(1-2)}^T\bar{\mathbf{P}}\mathbf{f}_2 - \chi z_3 \\ &= -\left[\left(\frac{\varphi_1 q_2}{\varphi_2\varphi_4^2} - \frac{q_1}{\varphi_2}\right)\varphi_4 - \frac{q_1}{\varphi_1}\left(\varphi_{31} + \varphi_{32}K_\theta\left(z_3\right)\right)\right]z_1 \\ &\quad -\left[q_2 + \left(\frac{q_2}{\varphi_2\varphi_4} - \frac{\varphi_4 q_1}{\varphi_1\varphi_2}\right)\left(\varphi_{31} + \varphi_{32}K_\theta\left(z_3\right)\right)\right]z_2 - \chi z_3\end{aligned} \tag{6.85}$$

$\Phi_2\left(\mathbf{z}\right)$ may be determined using (6.43), (6.85) and (6.13)-(6.16) as

$$\begin{aligned}\Phi_2\left(\mathbf{z}\right) &= \varphi_7 z_1 + \varphi_4\varphi_8\left(z_3 - z_2\right) + \varphi_{91}z_3 + \varphi_{92}K_\theta\left(z_3\right)z_3 + \varphi_{10}z_4 \\ &\quad + \left[\left(\frac{\varphi_1 q_2}{\varphi_2\varphi_4^2} - \frac{q_1}{\varphi_2}\right)\varphi_4 - \frac{q_1}{\varphi_1}\left(\varphi_{31} + \varphi_{32}K_\theta\left(z_3\right)\right)\right]\varphi_4\left(z_3 - z_2\right) \\ &\quad + \left[q_2 + \left(\frac{q_2}{\varphi_2\varphi_4} - \frac{\varphi_4 q_1}{\varphi_1\varphi_2}\right)\left(\varphi_{31} + \varphi_{32}K_\theta\left(z_3\right)\right)\right] \\ &\quad \times\left(-\frac{1}{\varphi_4}\right)\left[\varphi_1 z_1 + \varphi_4\varphi_2\left(z_3 - z_2\right) + \varphi_{31}z_3 + \varphi_{32}K_\theta\left(z_3\right)z_3\right] \\ &\quad + \left[-\frac{\varphi_{32}q_1}{\varphi_1}z_1 + \varphi_{32}\left(\frac{q_2}{\varphi_2\varphi_4} - \frac{\varphi_4 q_1}{\varphi_1\varphi_2}\right)z_2\right]\frac{\partial K_\theta\left(z_3\right)}{\partial z_3}z_4 + \chi z_4\end{aligned} \tag{6.86}$$

Appendix 6.2: **- Continuous sliding-mode control design – robustness to input disturbance**.

The motion during continuous sliding-mode control generally consists only of a *reaching phase*, during which trajectories, starting away from the sliding surface $S = 0$, move towards it and are then confined to a thin boundary layer close to it.

There is generally no sliding phase because the states never reach the sliding surface exactly.

In the reaching phase, i.e., $S = z_4 - \Phi_1\left(\mathbf{z}_{(1-3)}\right) \neq 0$, the system (6.30)-(6.31) becomes,

$$\dot{\mathbf{z}}_{(1-2)} = \mathbf{f}_1\left(\mathbf{z}_{(1-2)}\right) + \mathbf{f}_2\left(\mathbf{z}_{(1-2)}, z_3\right) z_3 \tag{6.87}$$

$$\dot{z}_3 = \Phi_1\left(\mathbf{z}_{(1-3)}\right) + S \tag{6.88}$$

Equations (6.87)-(6.88) define a reduced order system with S viewed as input. The saturation function in equation (6.49) allows the behaviour under two different input levels, outside the boundary layer $\left(|S| > \varepsilon\right)$ and inside the boundary layer $\left(|S| \leq \varepsilon\right)$, to be considered separately.

Outside the boundary layer, $|S| > \varepsilon$:

The substitution of equation (6.50) into (6.44) leads to,

$$\dot{U}_2 = S\left(-\xi \text{sat}\left(\frac{S}{\varepsilon}\right) + g_4 \Delta\beta - \upsilon S \right) \tag{6.89}$$

Then by combing this expression with the inequalities (6.49) and (6.47) it is found that,

$$\begin{aligned} \dot{U}_2 &= -\xi|S| + S\left(g_4 \Delta\beta\right) - \upsilon S^2 \\ &\leq -\left(\xi - |g_4 \Delta\beta|\right)|S| - \upsilon S^2 \\ &\leq -\left(1 - \eta_0\right)\xi|S| - \upsilon S^2 \leq 0 \end{aligned} \tag{6.90}$$

Inequality (6.90) implies that whenever $|S(0)| > \varepsilon$, $|S(t)|$ will decrease until it reaches in the boundary layer $\left(|S| \leq \varepsilon\right)$ and afterwards remain there. The boundary layer $\left\{|S| \leq \varepsilon\right\}$ is a positively invariant set.

Inside the boundary layer, $|S| \leq \varepsilon$:

The behaviour of the overall closed-loop system can be further examined by investigating the behaviour of the system (6.87)-(6.88) with S, $|S| \le \varepsilon$, viewed as the input.

Taking $U_1\left(\mathbf{z}_{(1-3)}\right)$ given by (6.35) as a Lyapunov function candidate for the system (6.87)-(6.88),

$$\dot{U}_1 = \frac{\mathrm{d}U_1}{\mathrm{d}\mathbf{z}_{(1-3)}}\dot{\mathbf{z}}_{(1-3)} = \begin{bmatrix} \dfrac{\mathrm{d}W\left(\mathbf{z}_{(1-2)}\right)}{\mathrm{d}\mathbf{z}_{(1-2)}} & z_3 \end{bmatrix} \begin{bmatrix} \dot{\mathbf{z}}_{(1-2)} \\ \dot{z}_3 \end{bmatrix} \tag{6.91}$$

combining with equations (6.87)-(6.88),

$$\dot{U}_1 = \frac{\mathrm{d}W\left(\mathbf{z}_{(1-2)}\right)}{\mathrm{d}\mathbf{z}_{(1-2)}}\mathbf{f}_1 + z_3\frac{\mathrm{d}W\left(\mathbf{z}_{(1-2)}\right)}{\mathrm{d}\mathbf{z}_{(1-2)}}\mathbf{f}_2 + z_3\Phi_1\left(\mathbf{z}_{(1-3)}\right) + z_3 S \tag{6.92}$$

and with (6.34), leads to,

$$\dot{U}_1 = \frac{\mathrm{d}W\left(\mathbf{z}_{(1-2)}\right)}{\mathrm{d}\mathbf{z}_{(1-2)}}\mathbf{f}_1 - \chi z_3^2 + z_3 S \tag{6.93}$$

Now, introducing the inequality (6.26),

$$\dot{U}_1 \le -\lambda_{\min}\left(\bar{\mathbf{Q}}\right)\left\|\mathbf{z}_{(1-2)}\right\|_2^2 - \chi z_3^2 + |z_3||S| \tag{6.94}$$

and separating χz_3^2 into two parts, $\chi\left(1-\varsigma_1\right)z_3^2$ and $\chi\varsigma_1 z_3^2$, then,

$$\begin{aligned} \dot{U}_1 = &-\left(1-\varsigma_2\right)\lambda_{\min}\left(\bar{\mathbf{Q}}\right)\left\|\mathbf{z}_{(1-2)}\right\|_2^2 - \frac{\varsigma_2}{2}\lambda_{\min}\left(\bar{\mathbf{Q}}\right)\left\|\mathbf{z}_{(1-2)}\right\|_2^2 - \frac{\varsigma_2}{2}\lambda_{\min}\left(\bar{\mathbf{Q}}\right)\left\|\mathbf{z}_{(1-2)}\right\|_2^2 \\ &-\chi\left(1-\varsigma_1\right)z_3^2 - \chi\varsigma_1 z_3^2 + |z_3||S| \end{aligned} \tag{6.95}$$

where $0 < \varsigma_1, \varsigma_2 < 1$.

It is readily seen that $|z_1| \le \left\|\mathbf{z}_{(1-2)}\right\|_2^2$ and $|z_2| \le \left\|\mathbf{z}_{(1-2)}\right\|_2^2$, in which case,

$$\begin{aligned}\dot{U}_1 \le & -(1-\varsigma_2)\lambda_{\min}(\bar{\mathbf{Q}})\left\|\mathbf{z}_{(1-2)}\right\|_2^2 - \chi(1-\varsigma_1)z_3^2 - \frac{\varsigma_2}{2}\lambda_{\min}(\bar{\mathbf{Q}})|z_1| \\ & -\frac{\varsigma_2}{2}\lambda_{\min}(\bar{\mathbf{Q}})|z_2| - \chi\varsigma_1 z_3^2 + |z_3||S|\end{aligned} \tag{6.96}$$

If $|S|/(\chi\varsigma_1) < |z_3|$, such that,

$$-\chi\varsigma_1 z_3^2 + |z_3||S| < 0 \tag{6.97}$$

then,

$$\begin{aligned}\dot{U}_1 &\le -(1-\varsigma_2)\lambda_{\min}(\bar{\mathbf{Q}})\left\|\mathbf{z}_{(1-2)}\right\|_2^2 - \chi(1-\varsigma_1)z_3^2 - \frac{\varsigma_2}{2}\lambda_{\min}(\bar{\mathbf{Q}})|z_1| - \frac{\varsigma_2}{2}\lambda_{\min}(\bar{\mathbf{Q}})|z_2| \\ &\le -(1-\varsigma_2)\lambda_{\min}(\bar{\mathbf{Q}})\left\|\mathbf{z}_{(1-2)}\right\|_2^2 - \chi(1-\varsigma_1)z_3^2 \\ &\le -\min\left((1-\varsigma_2)\lambda_{\min}(\bar{\mathbf{Q}}), \chi(1-\varsigma_1)\right)\left\|\mathbf{z}_{(1-3)}\right\|_2^2 \\ &\le 0\end{aligned} \tag{6.98}$$

Also, if

$$|z_3| \le |S|/(\chi\varsigma_1) \quad \text{and} \quad 2|S|^2/\left(\varsigma_2\chi\varsigma_1\lambda_{\min}(\bar{\mathbf{Q}})\right) \le |z_1| \tag{6.99}$$

or

$$|z_3| \le |S|/(\chi\varsigma_1) \quad \text{and} \quad 2|S|^2/\left(\varsigma_2\chi\varsigma_1\lambda_{\min}(\bar{\mathbf{Q}})\right) \le |z_2| \tag{6.100}$$

then,

$$-\frac{\varsigma_2}{2}\lambda_{\min}(\mathbf{Q})|z_1| + |z_3||S| \le 0 \ \text{ or } \ -\frac{\varsigma_2}{2}\lambda_{\min}(\bar{\mathbf{Q}})|z_2| + |z_3||S| \le 0 \tag{6.101}$$

and

$$\begin{aligned}\dot{U}_1 &\le -(1-\varsigma_2)\lambda_{\min}(\bar{\mathbf{Q}})\left\|\mathbf{z}_{(1-2)}\right\|_2^2 - \chi(1-\varsigma_1)z_3^2 - \chi\varsigma_1 z_3^2 \\ &\le -(1-\varsigma_2)\lambda_{\min}(\bar{\mathbf{Q}})\left\|\mathbf{z}_{(1-2)}\right\|_2^2 - \chi(1-\varsigma_1)z_3^2 \\ &\le -\min\left((1-\varsigma_2)\lambda_{\min}(\bar{\mathbf{Q}}), \chi(1-\varsigma_1)\right)\left\|\mathbf{z}_{(1-3)}\right\|_2^2 \\ &\le 0\end{aligned} \tag{6.102}$$

By combining the conditions (6.97), (6.99) and (6.100) on the inequalities (6.98) and (6.102), the dynamics of the system is found to be stable under the single condition that there exists a positive real number γ_3 such that,

$$\gamma_3 \left\| \mathbf{z}_{(1-3)} \right\|_2 \geq \left\| \mathbf{z}_{(1-3)} \right\|_\infty \geq \mathcal{K}_1\left(|S|\right) = \max\left\{ |S| / \left(\chi \varsigma_1\right),\ 2|S|^2 \Big/ \left(\varsigma_2 \chi \varsigma_1 \lambda_{\min}\left(\bar{\mathbf{Q}}\right)\right) \right\} \tag{6.103}$$

where $\left\| (\bullet) \right\|_\infty$ is the infinity norm of $(\bullet)$ and $\forall \mathbf{z}_{(1-3)} \in \mathbb{R}^{3\times 1}$. It can be seen that $\mathcal{K}_1\left(|S|\right)$ a strictly increasing function of $|S|$ with $\mathcal{K}_1(0) = 0$.

Then by invoking Theorem 4.19 [21] with inequalities (6.36), (6.98) , (6.102) and (6.103) the subsystem (6.87)-(6.88) is found to be input-to-state stable so that the states are bounded under bounded input.

Lemma A2.1 If the origin of the zero dynamics of subsystem (6.30)-(6.31) is globally exponentially stable and (6.47) is satisfied, then by using the continuous sliding-mode controller (6.50), the trajectory of the full closed-loop system will be bounded for all $t \geq 0$ reaching the positively invariant set $\Omega_\varepsilon = \left\{ U_1\left(\mathbf{z}_{(1-3)}\right) \leq U_3\left(\varepsilon\right) \right\} \bigcap \left\{ |S| \leq \varepsilon \right\}$ determined by a small design parameter ε.

Proof*:* The preceding analysis shows that whenever $|S(0)| > \varepsilon$, $|S(t)|$ will decrease until it reaches the boundary layer $\left(|S| \leq \varepsilon\right)$ and remain inside thereafter. The boundary layer is a positively invariant set $\left\{ |S| \leq \varepsilon \right\}$.

Remembering that $\mathcal{K}_1\left(|S|\right)$ is a strictly increasing function of $|S|$, we now choose $|S| = \varepsilon$ as the upper limit of $|S|$ within the boundary layer. Then U_3 may be introduced as a strictly increasing function of ε as,

$$U_3\left(\varepsilon\right) = \max\left(\lambda_{\max}\left(\bar{\mathbf{P}}\right), \frac{1}{2} \right) \left(\frac{1}{\gamma_3} \mathcal{K}_1\left(\varepsilon\right) \right)^2 \tag{6.104}$$

where $|S| \leq \varepsilon$.

Let us assume that $U_1\left(\mathbf{z}_{(1-3)}\right) \geq U_3(\varepsilon)$. Then by combining (6.36) and (6.104) it is found that,

$$U_3(\varepsilon) = \max\left(\lambda_{\max}\left(\bar{\mathbf{P}}\right), \frac{1}{2}\right)\left(\frac{1}{\gamma_3}\mathcal{K}_1(\varepsilon)\right)^2 \leq U_1\left(\mathbf{z}_{(1-3)}\right) \leq \max\left(\lambda_{\max}\left(\bar{\mathbf{P}}\right), \frac{1}{2}\right)\left\|\mathbf{z}_{(1-3)}\right\|_2^2 \quad (6.105)$$

which means that,

$$\left(\frac{1}{\gamma_3}\mathcal{K}_1(\varepsilon)\right)^2 \leq \left\|\mathbf{z}_{(1-3)}\right\|_2^2 \text{ or } \frac{1}{\gamma_3}\mathcal{K}_1(\varepsilon) \leq \left\|\mathbf{z}_{(1-3)}\right\|_2 \quad (6.106)$$

Since $|S| \leq \varepsilon$, inequality (6.106) becomes,

$$\left\|\mathbf{z}_{(1-3)}\right\|_2 \geq \frac{1}{\gamma_3}\mathcal{K}_1(\varepsilon) \geq \frac{1}{\gamma_3}\mathcal{K}_1(|S|) \quad (6.107)$$

This result confirms the inequality (6.103). Thus, inside the boundary layer, if

$$U_1\left(\mathbf{z}_{(1-3)}\right) \geq U_3(\varepsilon) \quad (6.108)$$

then $\dot{U}_1 \leq 0$, so that the system is globally stable under the condition,

$$\Omega_\varepsilon = \left\{U_1\left(\mathbf{z}_{(1-3)}\right) \leq U_3(\varepsilon)\right\} \cap \left\{|S| \leq \varepsilon\right\} \quad (6.109)$$

where $\cap$ denotes the intersection.

Thus, whenever $|S(0)| > \varepsilon$, $|S(t)|$ will decrease until it reaches the boundary layer and eventually the positively invariant set (6.109) and remains inside the boundary layer thereafter.

□

Appendix 6.3: **Continuous sliding-mode control design – robustness to nonlinear uncertainty**.

In the reaching phase, i.e., $S = z_4 - \Phi_3\left(\mathbf{z}_{(1-3)}\right) \neq 0$, the system (6.53)-(6.54) becomes,

$$\dot{\mathbf{z}}_{(1-2)} = \mathbf{f}_1\left(\mathbf{z}_{(1-2)}\right) + \mathbf{f}_2\left(\mathbf{z}_{(1-3)}\right) z_3 + \boldsymbol{\delta}_1 \tag{6.110}$$

$$\dot{z}_3 = \Phi_3\left(\mathbf{z}_{(1-3)}\right) + S \tag{6.111}$$

Equations (6.110)-(6.111) define a reduced order system with S viewed as input. The saturation function in equation (6.80) allows the behaviour under two different input levels, outside the boundary layer $\left(|S| > \varepsilon\right)$ and inside the boundary layer $\left(|S| \le \varepsilon\right)$, to be considered separately.

Outside the boundary layer, $|S| > \varepsilon$:

The substitution of equation (6.80) into (6.75) leads to,

$$\dot{U}_2 = S\Phi_5\left(\mathbf{z}\right)\Delta K_\theta\left(z_3\right) z_3 - S\xi\left(\mathbf{z}\right)\text{sat}\left(\frac{S}{\varepsilon}\right) - \upsilon S^2 \tag{6.112}$$

Then by combining this expression with the inequalities (6.49) and (6.78) it is found that,

$$\dot{U}_2 \le -\left(1-\eta_0\right)\xi_0|S| - \upsilon S^2 \le 0 \tag{6.113}$$

Inequality (6.113) implies that whenever $|S(0)| > \varepsilon$, $|S(t)|$ will decrease until it reaches in the boundary layer $\left(|S| \le \varepsilon\right)$ and afterwards remain there. The boundary layer $\left(|S| \le \varepsilon\right)$ is a positively invariant set.

Inside the boundary layer, $|S| \le \varepsilon$:

The behaviour of the overall closed-loop system can be further examined by investigating the behaviour of the system (6.110)-(6.111) with S, $|S| \le \varepsilon$, viewed as the input.

Taking $U_1\left(\mathbf{z}_{(1-3)}\right)$ given by (6.35) as a Lyapunov function candidate for the system (6.110)-(6.111),

$$\dot{U}_1 = \frac{\mathrm{d}U_1}{\mathrm{d}\mathbf{z}_{(1-3)}}\dot{\mathbf{z}}_{(1-3)} = \begin{bmatrix} \dfrac{\mathrm{d}W\left(\mathbf{z}_{(1-2)}\right)}{\mathrm{d}\mathbf{z}_{(1-2)}} & z_3 \end{bmatrix} \begin{bmatrix} \dot{\mathbf{z}}_{(1-2)} \\ \dot{z}_3 \end{bmatrix} \tag{6.114}$$

combining with equations (6.110)-(6.111), (6.62), and (6.57) leads to,

$$\dot{U}_1 \le -(1-\varsigma_2)\gamma_1 \left\|\mathbf{z}_{(1-2)}\right\|_2^2 - \chi(1-\varsigma_1)z_3^2 - \frac{\varsigma_2}{2}\gamma_1|z_1| - \frac{\varsigma_2}{2}\gamma_1|z_2| - \chi\varsigma_1 z_3^2 + |z_3||S| \tag{6.115}$$

where $0 < \varsigma_1, \varsigma_2 < 1$.

If $|S|/(\chi\varsigma_1) < |z_3|$, such that,

$$-\chi\varsigma_1 z_3^2 + |z_3||S| < 0 \tag{6.116}$$

and separately, if

$$|z_3| \le |S|/(\chi\varsigma_1) \quad \text{and} \quad 2|S|^2/(\varsigma_2\chi\varsigma_1\gamma_1) \le |z_1| \tag{6.117}$$

or

$$|z_3| \le |S|/(\chi\varsigma_1) \quad \text{and} \quad 2|S|^2/(\varsigma_2\chi\varsigma_1\gamma_1) \le |z_2| \tag{6.118}$$

it may be shown that,

$$\dot{U}_1 \le -\min\left((1-\varsigma_2)\gamma_1, \chi(1-\varsigma_1)\right)\left\|\mathbf{z}_{(1-3)}\right\|_2^2 \le 0 \tag{6.119}$$

By combining the conditions (6.116), (6.117) and (6.118) on the inequality (6.119), the dynamics of the system is found to be stable under the single condition that there exists a positive real number γ_4 such that,

$$\gamma_4\left\|\mathbf{z}_{(1-3)}\right\|_2 \ge \left\|\mathbf{z}_{(1-3)}\right\|_\infty \ge \mathcal{K}_2\left(|S|\right) = \max\left\{|S|/(\chi\varsigma_1),\ 2|S|^2/(\varsigma_2\chi\varsigma_1\gamma_1)\right\},\ \forall\mathbf{z}_{(1-3)} \in \mathbb{R}^{3\times 1} \tag{6.120}$$

It can be seen that $\mathcal{K}_2\left(|S|\right)$ a strictly increasing function of $|S|$ with $\mathcal{K}_2(0) = 0$.

Then by invoking Theorem 4.19 [21] with inequalities (6.36) , (6.119) and (6.120) the subsystem (6.110)-(6.111) is found to be input-to-state stable so that the states are bounded under bounded input.

Lemma A3.1 Consider the system (6.53)-(6.55). Suppose the zero dynamics $\dot{\mathbf{z}} = \mathbf{f}_1(\mathbf{z}) = \mathbf{S}\mathbf{z}$ are globally exponentially stable and inequalities (6.52) and (6.78) are satisfied. Then using the continuous sliding-mode controller (6.80), the trajectory of the full closed-loop system will be bounded for all $t \geq 0$ and reaches a positively invariant set (6.125) controlled by the design parameter ε . Moreover, if $\eta(\mathbf{0}) = 0$ and $\eta_0 = 0$, then there exists $\varepsilon^* > 0$ such that for all $0 < \varepsilon < \varepsilon^*$, the origin of the full closed-loop system will be globally asymptotically stable.

Proof: We choose $|S| = \varepsilon$ as the upper limit of $|S|$ within the boundary layer. Then U_4 may be introduced as a strictly increasing function of ε as,

$$U_4(\varepsilon) = \max\left(\lambda_{\max}(\bar{\mathbf{P}}), \frac{1}{2}\right)\left(\frac{1}{\gamma_4}\mathcal{K}_2(\varepsilon)\right)^2 \tag{6.121}$$

where $|S| \leq \varepsilon$.

Let us assume that $U_1\left(\mathbf{z}_{(1-3)}\right) \geq U_4(\varepsilon)$. Then by combining (6.36) and (6.121) it is found that,

$$U_4(\varepsilon) = \max\left(\lambda_{\max}(\bar{\mathbf{P}}), \frac{1}{2}\right)\left(\frac{1}{\gamma_4}\mathcal{K}_2(\varepsilon)\right)^2 \leq U_1\left(\mathbf{z}_{(1-3)}\right) \leq \max\left(\lambda_{\max}(\bar{\mathbf{P}}), \frac{1}{2}\right)\left\|\mathbf{z}_{(1-3)}\right\|_2^2 \tag{6.122}$$

which means that,

$$\frac{1}{\gamma_4}\mathcal{K}_2(\varepsilon) \leq \left\|\mathbf{z}_{(1-3)}\right\|_2 \tag{6.123}$$

Since $|S| \leq \varepsilon$, inequality (6.123) becomes,

$$\left\|\mathbf{z}_{(1-3)}\right\|_2 \geq \frac{1}{\gamma_4}\mathcal{K}_2(\varepsilon) \geq \frac{1}{\gamma_4}\mathcal{K}_2(|S|) \tag{6.124}$$

This result confirms the inequality (6.120). Thus, inside the boundary layer, if $\left\{U_1\left(z_{(1-3)}\right) \geq U_4(\varepsilon)\right\}$, then $\dot{U}_1 \leq 0$, so that the system is globally stable under the condition,

$$\Omega_\varepsilon = \left\{U_1\left(\mathbf{z}_{(1-3)}\right) \leq U_4(\varepsilon)\right\} \cap \{|S| \leq \varepsilon\} \tag{6.125}$$

where $\cap$ denotes the intersection.

Thus, whenever $|S(0)| > \varepsilon$, $|S(t)|$ will decrease until it reaches the boundary layer $(|S| \leq \varepsilon)$ and afterwards remain there. Eventually, the trajectory of the full closed-loop system is found to be bounded for all $t \geq 0$ and reaches a positively invariant set (6.125) controlled by the design parameter ε. Moreover, the system (6.53)-(6.54) with $z_4 = \Phi_3\left(\mathbf{z}_{(1-3)}\right)$ is globally exponentially stable. If $\eta(\mathbf{0}) = 0$ and $\eta_0 = 0$, then according to Theorem 14.2 [21], then there exists ε^* such that for all $0 < \varepsilon < \varepsilon^*$, the origin of the full closed-loop system will be globally asymptotically stable.

□

Chapter 7

Conclusion and future work

7.1 Conclusion

In this research basic theoretical solutions to several intellectual challenges in active vibration control in linear time invariant systems and nonlinear aeroelastic systems are presented. The method of receptances based on eigenvalue assignment, which was developed for vibration suppression in linear systems [8, 9], is further developed for linear systems with inaccessible degrees of freedom and large flexible structures requiring block decoupling vibration control. Also, a comprehensive investigation of aeroelastic systems with softening nonlinearity and robust active flutter suppression in under-actuated wing sections with softening or hardening nonlinearity is presented.

Partial pole placement is of practical value in vibration suppression and stabilisation of large-dimension structures. It is found not infrequently in practice that there exist certain degrees of freedom inaccessible to actuation and sensing simultaneously. In Chapter 3, a new theory for partial pole assignment using measured receptances in the presence of inaccessible degrees of freedom is proposed [128]. A new double-input feedback control involving displacement, velocity and acceleration feedback is described. The eigenvalues of the open-loop system, intended to be unchanged, are maintained in the closed-loop system by utilising both partial controllability and partial observability conditions such that both input and feedback gain vectors are unknown. Extra null constraints on desired entries in the input and feedback gain

vectors results in the appearance of degrees of freedom inaccessible to both actuation and sensing. The methodology is based entirely on linear systems of equations, thereby avoiding the need to use nonlinear optimisation routines. A lower bound on the maximum number of inaccessible degrees of freedom allowed for precise implementation of partial pole placement is given. The simplification of the theory results in active natural frequency modification, which is also described.

Large flexible structures are very difficult in terms of isolating one substructure from the vibration of anther since the rigid body assumption in convectional vibration isolation techniques is invalid. It is not infrequent that large flexible structures are disturbed by multiple excitations. Even though one of the disturbances has been isolated, isolated substructures are still prone to oscillations with large amplitude in the face of other disturbances. To address this problem, a new block decoupling vibration control algorithm based on eigenstructure assignment using measured receptances is proposed for simultaneous active vibration isolation and suppression in Chapter 4 [129]. It is found that independent substructures with desired eigenvalues assigned separately are achievable by assigning eigenvalues and adding modal degree of freedom constraints on right eigenvectors when the open-loop system is controllable. The restriction to the block diagonal mass matrix in the case of velocity and displacement feedback can be lifted to allow for bandedness of the mass matrix when additional acceleration feedback is included for inertial decoupling. In the case of banded system matrices, the number of actuators required can be reduced to twice of the semi-bandwidth. The algorithm lays a preliminary theoretical foundation for simultaneous vibration isolation and suppression in large flexible structure subjected to multiple excitations.

All systems in nature are nonlinear. A good understanding of the effects of nonlinearity improves the active vibration control design in nonlinear systems. A comprehensive study of the effects of softening structural nonlinearity in aeroelastic systems is presented in Chapter 5 [131], which sheds new light on to topic that is not completely understood. Complex dynamic behaviour is demonstrated using the illustration of a nonlinear binary flutter model with a cubic stiffness in the pitch degree of freedom. The identification and stability analysis of limit cycles in the frequency domain using describing functions and the receptances of the underlying linear system are carried out. Numerical integration of the governing differential equations in the time domain confirms the frequency domain results and also reveals new behaviour, including asymmetric LCO and chaos. Also, aeroelastic stability in the presence of softening structural nonlinearity is found to be strongly dependent upon initial conditions. LCO and chaos may be destabilised when the amplitude of oscillation approaches the static divergence boundary and predicted stable LCO are prohibited. Bifurcation analysis using numerical continuation methods are undertaken to demonstrate that the aeroelastic systems with softening nonlinearity are characterised by Hopf, fold, pitchfork and period doubling bifurcations. Complete bifurcation analysis and two-dimensional sections of the basin of attraction allow the nature of stability occurring over the whole speed range to be explained. In some circumstances, the basins of attractions are not singly connected regions, so that the boundaries between different dynamic regimes are not simple. Dependent upon the wing parameters, regions may appear where the predicted stable LCO are free from the destabilising effect of softening nonlinearity.

Due to the effects of nonlinearity, linear active control techniques exhibit limited success in flutter suppression in nonlinear aeroelastic systems. Nonlinear active

vibration control methodologies are preferred. The global stability of under-actuated nonlinear aeroelastic systems is a challenging research topic of importance to the problem of the actuator failure and in the development of next-generation flight vehicles constrained by weight and cost. Since there are unavoidable modelling errors and external disturbances, the global stability of under-actuated aeroelastic system becomes more complicated. In Chapter 6, a robust passivity-based sliding mode control approach is developed for globally stabilising an under-actuated prototypical wing section with torsional nonlinearity, softening or hardening [148]. Passivity-based control is used to design a nonlinear sliding-mode surface in the presence of matched uncertainty and input disturbance, while robust passivity-based control is employed in the presence of mismatched uncertainty. A continuous sliding-mode control input is employed to stabilise the overall system. With known bounds on both the input disturbance and nonlinear uncertainty, the controller is able to globally stabilise the overall system when the zero dynamics are globally exponentially stable and the trajectories will reach a positively invariant set determined by the thickness of a boundary layer. Large nonlinearity uncertainty and large input disturbance can be admitted under the practical limitation of control surface deflection. Furthermore, the overall system will be globally asymptotically stable provided that certain conditions (described in section 6.5.2) are satisfied.

The research reported here offers sound theoretical solutions to several intellectual challenges in the development and the application of active vibration control techniques in linear time invariant systems and nonlinear aeroelastic systems. Also, the research sheds new light on to the effects of softening nonlinearity in aeroelastic systems, which is not completely understood. The methods and outcomes have

significant applications to not only aerospace engineering stressed in the preceding chapters but also other industries including automotive and civil.

7.2 Future work

The research has potential applications in many industries and can be developed further into many directions of research. The basic theories for partial pole placement with inaccessible degrees of freedom and block decoupling vibration control in linear time invariant systems, and global robust flutter suppression in under-actuated nonlinear aeroelastic systems are developed and presented in this thesis. Also, semi-analytical and numerical investigation of the effects of softening nonlinearity on aeroelastic systems is presented. Other aspects that can be considered as further work may be summarised here:

1. The method of receptances, originally developed in [8, 9] and further developed in this thesis [128, 129], is based on the assumption of distinct eigenvalues in both open- and closed-loop systems. In practice, systems with closely spaced eigenvalues, which are close to being defective, are common. Developing the method of receptances in defective systems is an interesting line of research.
2. Experiments for block decoupling vibration control in large flexible smart structures with embedded piezo-based actuators and sensors may be carried out.
3. The Boeing Joined-Wing SensorCraft is a concept proposed to serve as a next-generation, high altitude, long endurance reconnaissance unmanned aircraft. Buckling is considered to be a critical constraint for its aeroelastic performance [149]. It is of significant importance to comprehensively

investigate the effects of softening nonlinearity experimentally, due to buckling of the aerodynamic responses of joined-wing sensor-crafts.

4. Experiments for robust passivity-based sliding mode control may be carried out on a nonlinear wing section at the University of Liverpool.

References

[1] C.M. Denegri, Limit cycle oscillation flight test results of a fighter with external stores, Journal of Aircraft, 37 (2000) 761-769.

[2] Denegri C.M, Jr., M.R. Johnson, Limit cycle oscillation prediction using artificial neural networks, Journal of Guidance, Control, and Dynamics, 24 (2001) 887-895.

[3] J. Croft, Airbus elevator flutter: Annoying or dangerous?, Aviation Week & Space Technology, 155 (2001) 41.

[4] L. Librescu, G. Chiocchia, P. Marzocca, Implications of cubic physical/aerodynamic non-linearities on the character of the flutter instability boundary, International Journal of Non-Linear Mechanics, 38 (2003) 173-199.

[5] O. Cuvalci, A. Ertas, S. Ekwaro-Osire, I. Cicek, Nonlinear-linear vibration absorber for a system under sinusoidal and random excitation: experiments, Journal of Sound and Vibration, 249 (2002) 701-718.

[6] Y.S. Lee, A.F. Vakakis, L.A. Bergman, D.M. McFarland, G. Kerschen, Suppressing aeroelastic instability using broadband passive targeted energy transfers, part 1:Theory, AIAA Journal, 45 (2007) 693-711.

[7] Y.S. Lee, G. Kerschen, D. Michael McFarland, W. Joel Hill, C. Nichkawde, T.W. Strganac, L.A. Bergman, A.F. Vakakis, Suppressing aeroelastic instability using broadband passive targeted energy transfers, part 2: Experiments, AIAA Journal, 45 (2007) 2391-2400.

[8] Y.M. Ram, J.E. Mottershead, Receptance method in active vibration control, AIAA Journal, 45 (2007) 562-567.

[9] Y.M. Ram, J.E. Mottershead, Multiple-input active vibration control by partial pole placement using the method of receptances, Mechanical Systems and Signal Processing, 40 (2013) 727-735.

[10] E.H. Dowell, D. Tang, Nonlinear aeroelasticity and unsteady aerodynamics, AIAA Journal, 40 (2002) 1697-1707.

[11] Y.Q. Tu, G.T. Zheng, On the vibration isolation of flexible structures, Journal of Applied Mechanics, 74 (2006) 415-420.

[12] P. Gardonio, S.J. Elliott, R.J. Pinnington, Active isolation of structural vibration on a multiple-degree-of-freedom system, Part 1: The dynamics of the system, Journal of Sound and Vibration, 207 (1997) 61-93.

[13] P. Gardonio, S.J. Elliott, R.J. Pinnington, Active isolation of structural vibration on a multiple-degree-of-freedom system, Part II: Effectiveness of active control strategies, Journal of Sound and Vibration, 207 (1997) 95-121.

[14] P. Gardonio, S.J. Elliott, Passive and active isolation of structural vibration transmission between two plates connected by a set of mounts, Journal of Sound and Vibration, 237 (2000) 483-511.

[15] B.H.K. Lee, S.J. Price, Y.S. Wong, Nonlinear aeroelastic analysis of airfoils: bifurcation and chaos, Progress in Aerospace Sciences, 35 (1999) 205-334.

[16] D.S. Woolston, H.L. Runyan, T.A. Byrdsong, Some effects of system nonlinearities in the problem of aircraft flutter, in: NACA TN-3539, 1955.

[17] J.S. Vipperman, J.M. Barker, R.L. Clark, G.J. Balas, Comparison of mu- and H2-Synthesis Controllers on an experimental typical section, Journal of Guidance, Control, and Dynamics, 22 (1999) 278-285.

[18] J.J. Block, T.W. Strganac, Applied active control for a nonlinear aeroelasticstructure, Journal of Guidance, Control, and Dynamics, 21 (1998) 838-845.

[19] L. Yang, Y. Hongnian, H. Yu, Y. Liu, A survey of underactuated mechanical systems, IET Control Theory & Applications, 7 (2013) 921-935.

[20] R. Xu, Ü. Özgüner, Sliding mode control of a class of underactuated systems, Automatica, 44 (2008) 233-241.

[21] H.K. Khalil, Nonlinear systems, Upper Saddle River, N.J. : Prentice Hall, 2002.

[22] R. Alkhatib, M.F. Golnaraghi, Active structural vibration control: A review, Shock and Vibration Digest, 35 (2003) 367-383.

[23] J.E. Mottershead, Y.M. Ram, Inverse eigenvalue problems in vibration absorption: Passive modification and active control, Mechanical Systems and Signal Processing, 20 (2006) 5-44.

[24] W.M. Wonham, On pole assignment in multi-input controllable linear systems, Automatic Control, IEEE Transactions on, 12 (1967) 660-665.

[25] E.J. Davison, On pole assignment in linear systems with incomplete state feedback, Automatic Control, IEEE Transactions on, 15 (1970) 348-351.

[26] H. Kimura, Pole assignment by gain output feedback, Automatic Control, IEEE Transactions on, 20 (1975) 509-516.

[27] E.Y. Shapiro, J.C. Chung, Application of eigenvalue/eigenvector assignment by constant output feedback to flight control system design, in: 15th Annual Conference on Information Sciences and Systems,, Johns Hopkins University, Baltimore, Maryland, 1981, pp. 164-169.

[28] A.N. Andry, E.Y. Shapiro, J.C. Chung, eigenstructure assignment for linear systems, Aerospace and Electronic Systems, IEEE Transactions on, AES-19 (1983) 711-729.

[29] L.R. Fletcher, J.F. Magni, Exact pole assignment by output feedback. Part 1, International Journal of Control, 45 (1987) 1995-2007.

[30] L.R. Fletcher, Exact pole assignment by output feedback. Part 2, International Journal of Control, 45 (1987) 2009-2019.

[31] J.F. Magni, Exact pole assignment by output feedback. Part 3, International Journal of Control, 45 (1987) 2021-2033.

[32] R. Byers, S.G. Nash, Approaches to robust pole assignment, International Journal of Control, 49 (1989) 97-117.

[33] J. Kautsky, N.K. Nichols, E.K.W. Chu, Robust pole assignment in singular control systems, Linear Algebra and Its Applications, 121 (1989) 9-37.

[34] J. Kautsky, N.K. Nichols, P. Van Dooren, Robust pole assignment in linear state feedback, International Journal of Control, 41 (1985) 1129-1155.

[35] E.K. Chu, B.N. Datta, Numerically robust pole assignment for second-order systems, International Journal of Control, 64 (1996) 1113-1127.

[36] E.K. Chu, Pole assignment for second-order systems, Mechanical Systems and Signal Processing, 16 (2002) 39-59.

[37] Y. Saad, Projection and deflation method for partial pole assignment in linear state feedback, Automatic Control, IEEE Transactions on, 33 (1988) 290-297.

[38] B.N. Datta, S. Elhay, Y.M. Ram, Orthogonality and partial pole assignment for the symmetric definite quadratic pencil, Linear Algebra and its Applications, 257 (1997) 29-48.

[39] Y.M. Ram, S. Elhay, Pole assignment in vibratory systems by multi-input control, Journal of Sound and Vibration, 230 (2000) 309-321.

[40] B.N. Datta, D.R. Sarkissian, Multi-input partial eigenvalue assignment for the symmetric quadratic pencil, in: Proceedings of the 1999 American Control Conference (99ACC), IEEE, San Diego, CA, USA, 1999, pp. 2244-2247.

[41] B.N. Datta, L. Wen-Wei, W. Jenn-Nan, Robust partial pole assignment for vibrating systems with aerodynamic effects, Automatic Control, IEEE Transactions on, 51 (2006) 1979-1984.

[42] S. Xu, J. Qian, Orthogonal basis selection method for robust partial eigenvalue assignment problem in second-order control systems, Journal of Sound and Vibration, 317 (2008) 1.

[43] S. Brahma, B. Datta, An optimization approach for minimum norm and robust partial quadratic eigenvalue assignment problems for vibrating structures, Journal of Sound and Vibration, 324 (2009) 471-489.

[44] Z.-J. Bai, B.N. Datta, J. Wang, Robust and minimum norm partial quadratic eigenvalue assignment in vibrating systems: A new optimization approach, Mechanical Systems and Signal Processing, 24 (2010) 766-783.

[45] C.A. Guzzardo, S.S. Pang, Y.M. Ram, Optimal actuation in vibration control, Mechanical Systems and Signal Processing, 35 (2013) 279-290.

[46] Y.M. Ram, J.E. Mottershead, M.G. Tehrani, Partial pole placement with time delay in structures using the receptance and the system matrices, Linear Algebra and its Applications, 434 (2011) 1689-1696.

[47] Z.-J. Bai, M.-X. Chen, J.-K. Yang, A multi-step hybrid method for multi-input partial quadratic eigenvalue assignment with time delay, Linear Algebra and its Applications, 437 (2012) 1658-1669.

[48] K.V. Singh, R. Dey, B.N. Datta, Partial eigenvalue assignment and its stability in a time delayed system, Mechanical Systems and Signal Processing, (In press) (2013).

[49] J.E. Mottershead, M.G. Tehrani, S. James, Y.M. Ram, Active vibration suppression by pole-zero placement using measured receptances, Journal of Sound and Vibration, 311 (2008) 1391-1408.

[50] M. Ghandchi Tehrani, R.N.R. Elliott, J.E. Mottershead, Partial pole placement in structures by the method of receptances: Theory and experiments, Journal of Sound and Vibration, 329 (2010) 5017-5035.

[51] J.E. Mottershead, M.G. Tehrani, S. James, P. Court, Active vibration control experiments on an AgustaWestland W30 helicopter airframe, Proceedings of the Institution of Mechanical Engineers, Part C: Journal of Mechanical Engineering Science, 226 (2012) 1504-1516.

[52] E. Papatheou, X. Wei, S. Jiffri, M.G. Tehrani, S. Bode, K.V. Singh, J.E. Mottershead, J.E. Cooper, Flutter control using vibration test data: theory, rig design and preliminary results., in: International Conference on Noise and Vibration Engineering., KU Leuven, Leuven, 2012, pp. Paper No. 424.

[53] X. Wei, J. Mottershead, Limit cycle assignment in nonlinear aeroelastic systems using describing functions and the receptance method, in: R. Allemang, J. De Clerck, C. Niezrecki, A. Wicks (Eds.) Topics in Modal Analysis, Volume 7, Springer New York, 2014, pp. 701-713.

[54] K.V. Singh, L.A. McDonough, R. Kolonay, J.E. Cooper, Receptance-based active aeroelastic control using multiple control surfaces, Journal of Aircraft, 51 (2014) 335-342.

[55] B.C. Moore, On the flexibility offered by state feedback in multivariable systems beyond closed loop eigenvalue assignment, in: Decision and Control including the 14th Symposium on Adaptive Processes, 1975 IEEE Conference on, 1975, pp. 207-214.

[56] G. Klein, B.C. Moore, Eigenvalue-generalized eigenvector assignment with state feedback, Automatic Control, IEEE Transactions on, 22 (1977) 140-141.

[57] M. Fahmy, J. O'Reilly, On eigenstructure assignment in linear multivariable systems, Automatic Control, IEEE Transactions on, 27 (1982) 690-693.

[58] S. Srinathkumar, Eigenvalue/eigenvector assignment using output feedback, Automatic Control, IEEE Transactions on, 23 (1978) 79-81.

[59] D.J. Inman, A. Kress, Eigenstructure assignment using inverse eigenvalue methods, Journal of Guidance, Control, and Dynamics, 18 (1995) 625-627.

[60] B.N. Datta, S. Elhay, Y.M. Ram, D.R. Sarkissian, Partial eigenstructure assignment for the quadratic pencil, Journal of Sound and Vibration, 230 (2000) 101-110.

[61] W.M. Wonham, Linear multivariable control: A geometric approach (2nd ed.), Springer-Verlag, New York, 1979.

[62] K.M. Sobel, E.Y. Shapiro, Application of eigensystem assignment to lateral translation and yaw pointing flight control, in: Decision and Control, 1984. The 23rd IEEE Conference on, 1984, pp. 1423-1428.

[63] K. Sobel, E. Shapiro, Eigenstructure assignment for design of multimode flight control systems, Control Systems Magazine, IEEE, 5 (1985) 9-15.

[64] B.-K. Song, S. Jayasuriya, Active vibration control using eigenvector assignment for mode localization, in: American Control Conference, 1993, 1993, pp. 1020-1024.

[65] F.J. Shelley, W.W. Clark, Closed-loop mode localization for vibration control in flexible structures, in: American Control Conference, 1994, 1994, pp. 1826-1830 vol.1822.

[66] F.J. Shelley, W.W. Clark, Experimental application of feedback control to localize vibration, Journal of Vibration and Acoustics, 122 (1996) 143-150.

[67] F.J. Shelley, W.W. Clark, Active mode localization in distributed parameter systems with consideration of limited actuator placement, Part 1: Theory, Journal of Vibration and Acoustics, 122 (2000) 160-164.

[68] F.J. Shelley, W.W. Clark, Active mode localization in distributed parameter systems with consideration of limited actuator placement, Part 2: Simulations and experiments, Journal of Vibration and Acoustics, 122 (2000) 165-168.

[69] Q. Zhang, G.L. Slater, R.J. Allemang, Suppression of undesired inputs of linear systems by eigenspace assignment, Journal of Guidance, Control, and Dynamics, 13 (1990) 330-336.

[70] J.W. Choi, J.G. Lee, Y. Kim, T. Kang, Design of an effective controller via disturbance accommodating left eigenstructure assignment, Journal of Guidance, Control, and Dynamics, 18 (1995) 347-354.

[71] T.Y. Wu, K.W. Wang, Vibration control via disturbance rejection through left eigenvector assignment, in: Proceedings of SPIE - The International Society for Optical Engineering, 2005, pp. 378-389.

[72] J.W. Choi, A simultaneous assignment methodology of right/left eigenstructures, IEEE Transactions on Aerospace and Electronic Systems, 34 (1998) 625-634.

[73] T.Y. Wu, K.W. Wang, Active vibration isolation via simultaneous left-right eigenvector assignment, Smart Materials and Structures, 17 (2008).

[74] B. Morgan, Jr., The synthesis of linear multivariable systems by state-variable feedback, Automatic Control, IEEE Transactions on, 9 (1964) 405-411.

[75] P.L. Falb, W. Wolovich, Decoupling in the design and synthesis of multivariable control systems, Automatic Control, IEEE Transactions on, 12 (1967) 651-659.

[76] E. Gilbert, The decoupling of multivariable systems by state feedback, SIAM Journal on Control, 7 (1969) 50-63.

[77] J. Descusse, J.F. Lafay, M. Malabre, Solution to Morgan's problem, Automatic Control, IEEE Transactions on, 33 (1988) 732-739.

[78] P.N. Paraskevopoulos, F.N. Koumboulis, A new approach to the decoupling problem of linear time-invariant systems, Journal of the Franklin Institute, 329 (1992) 347-369.

[79] J.W. Howze, Necessary and sufficient conditions for decoupling using output feedback, Automatic Control, IEEE Transactions on, 18 (1973) 44-46.

[80] M.J. Denham, A necessary and sufficient condition for decoupling by output feedback, Automatic Control, IEEE Transactions on, 18 (1973) 535-536.

[81] J. Descusse, A necessary and sufficient condition for decoupling using output feedback, International Journal of Control, 31 (1980) 833-840.

[82] A. Morse, W. Wonham, Decoupling and Pole Assignment by Dynamic Compensation, SIAM Journal on Control, 8 (1970) 317-337.

[83] M.M. Bayoumi, T. Duffield, Output feedback decoupling and pole placement in linear time-invariant systems, Automatic Control, IEEE Transactions on, 22 (1977) 142-143.

[84] P.N. Paraskevopoulos, F.N. Koumboulis, Decoupling and pole assignment in generalised state space systems, Control Theory and Applications, IEE Proceedings D, 138 (1991) 547-560.

[85] S. Sato, P.V. Lopresti, On the generalization of state feedback decoupling theory, Automatic Control, IEEE Transactions on, 16 (1971) 133-139.

[86] P.N. Paraskevopoulos, S.G. Tzafestas, Group decoupling theory for a generalized linear multivariable control system, International Journal of Systems Science, 6 (1975) 239-248.

[87] H. Hikita, Block decoupling and arbitrary pole assignment for a linear right-invertible system by dynamic compensation, International Journal of Control, 45 (1987) 1641-1653.

[88] J. Descusse, Block noninteracting control with (non)regular static state feedback: A complete solution, Automatica, 27 (1991) 883-886.

[89] G. Basile, G. Marro, A state space approach to noninteracting controls, Ricerchi di Automatica, 1 (1970) 68-77.

[90] S.M. Sato, P.V. Lopresti, New results in multivariable decoupling theory, Automatica, 7 (1971) 499-508.

[91] M. Malabre, J.A. Torres-Munoz, Block decoupling by precompensation revisited, IEEE Transactions on Automatic Control, 52 (2007) 922-926.

[92] M.L.J. Hautus, M. Heymann, Linear feedback decoupling-Transfer function analysis, IEEE Transactions on Automatic Control, AC-28 (1983) 823-832.

[93] C. Commault, J.M. Dion, J.A. Torres, Minimal structure in the block decoupling problem with stability, Automatica, 27 (1991) 331-338.

[94] Q.-G. Wang, Decoupling with internal stability for unity output feedback systems, Automatica, 28 (1992) 411-415.

[95] Q.-G. Wang, Y. Yang, Transfer function matrix approach to decoupling problem with stability, Systems & Control Letters, 47 (2002) 103-110.

[96] Q.-G. Wang, Decoupling Control, Heidelberg : Springer, 2006.

[97] L. Ching-An, Necessary and sufficient conditions for existence of decoupling controllers, Automatic Control, IEEE Transactions on, 42 (1997) 1157-1161.

[98] Q.-G. Wang, Decoupling control, Springer, Heidelberg, 2006.

[99] E.C. Zacharenakis, Input-output decoupling and disturbance rejection problems in structural analysis, Computers & Structures, 55 (1995) 441-451.

[100] E.C. Zacharenakis, On the input-output decoupling with simultaneous disturbance attenuation and $h\infty$ optimization problem in structural analysis, Computers & Structures, 60 (1996) 627-633.

[101] Q.S. Li, J.Q. Fang, A.P. Jeary, D.K. Liu, Decoupling control law for structural control implementation, International Journal of Solids and Structures, 38 (2001) 6147-6162.

[102] D.J. Inman, Active modal control for smart structures, Philosophical Transactions of the Royal Society A: Mathematical, Physical and Engineering Sciences, 359 (2001) 205-219.

[103] B.N. Datta, F. Rincón, Feedback stabilization of a second-order system: A nonmodal approach, Linear Algebra and its Applications, 188–189 (1993) 135-161.

[104] B.H.K. Lee, L.Y. Jiang, Y.S. Wong, Flutter of an airfoil with a cubic restoring force, Journal of Fluids and Structures, 13 (1999) 75-101.

[105] J.K. Liu, H.C. Chan, Limit cycle oscillations of a wing section with a tip mass, Nonlinear Dynamics, 23 (2000) 259-270.

[106] G. Dimitriadis, G. Vio, J. Cooper, Stability and limit cycle oscillation amplitude prediction for simple nonlinear aeroelastic systems, in: 45th AIAA/ASME/ASCE/AHS/ASC Structures, Structural Dynamics and Materials Conference AIAA, Palm Springs, California, 2004, pp. 2001-2014.

[107] B. Ghadiri, M. Razi, Limit cycle oscillations of rectangular cantilever wings containing cubic nonlinearity in an incompressible flow, Journal of Fluids and Structures, 23 (2007) 665-680.

[108] B. Stanford, P. Beran, Direct flutter and limit cycle computations of highly flexible wings for efficient analysis and optimization, Journal of Fluids and Structures, 36 (2013) 111-123.

[109] R.W. Bunton, C.M. Denegri Jr, Limit cycle oscillation characteristics of fighter aircraft, Journal of Aircraft, 37 (2000) 916-918.

[110] T. L, W. L, Y. R, Active aeroelastic oscillation control on the F/A-18 aircraft, in: Guidance, Navigation and Control Conference, American Institute of Aeronautics and Astronautics, 1985.

[111] P.M. Hartwich, S.K. Dobbs, A.E. Arslan, S.C. Kim, Navier-Stokes computations of limit-cycle oscillations for a B-1-like configuration, Journal of Aircraft, 38 (2001) 239-247.

[112] S. Jacobson, R. Britt, D. Freim, P. Kelly, Residual pitch oscillation (RPO) flight test and analysis on the B-2 bomber, in: 39th AIAA/ASME/ASCE/AHS/ASC Structures, Structural Dynamics, and Materials Conference and Exhibit, American Institute of Aeronautics and Astronautics, 1998.

[113] K.D. Frampton, R.L. Clark, Experiments on Control of Limit-Cycle Oscillations in a Typical Section, Journal of Guidance, Control, and Dynamics, 23 (2000) 956-960.

[114] J. Ko, A.J. Kurdila, T.W. Strganac, Nonlinear control of a prototypical wing section with torsional nonlinearity, Journal of Guidance, Control, and Dynamics, 20 (1997) 1181-1189.

[115] J.W. Ko, T.W. Strganac, A.J. Kurdila, Stability and control of a structurally nonlinear aeroelastic system, Journal of Guidance Control and Dynamics, 21 (1998) 718-725.

[116] J. Ko, T.W. Strganac, A.J. Kurdila, Adaptive feedback linearization for the control of a typical wing section with structural nonlinearity, Nonlinear Dynamics, 18 (1999) 289.

[117] J. Ko, T.W. Strganac, J.L. Junkins, M.R. Akella, A.J. Kurdila, Structured model reference adaptive control for a wing section with structural nonlinearity, Journal of Vibration and Control, 8 (2002) 553-573.

[118] A. Behal, P. Marzocca, V.M. Rao, A. Gnann, Nonlinear adaptive control of an aeroelastic two-dimensional lifting surface, Journal of Guidance, Control, and Dynamics : A Publication of the American Institute of Aeronautics and Astronautics Devoted to the Technology of Dynamics and Control, 29 (2006) 382.

[119] W. Xing, S.N. Singh, Adaptive output feedback control of a nonlinear aeroelastic structure, Journal of Guidance, Control, and Dynamics, 23 (2000) 1109-1116.

[120] K.W. Lee, S.N. Singh, Global robust control of an aeroelastic system using output feedback, Journal of Guidance, Control, and Dynamics, 30 (2007) 271-275.

[121] F. Zhang, D. Soffker, Active flutter suppression of a nonlinear aeroelastic system using PI-observer, in: H. Ulbrich, L. Ginzinger (Eds.) Motion and Vibration Control, Springer Netherlands, 2009, pp. 367-376.

[122] T. Degaki, S. Suzuki, Sliding mode control application for two-dimensional active flutter suppression, Transactions of the Japan Society for Aeronautical and Space Sciences, 43 (2001) 174-181.

[123] C.L. Chen, C.C. Peng, H.T. Yau, High-order sliding mode controller with backstepping design for aeroelastic systems, Communications in Nonlinear Science and Numerical Simulation, 17 (2012) 1813-1823.

[124] K.W. Lee, S.N. Singh, Robust higher-order sliding-mode finite-time control of aeroelastic systems, Journal of Guidance, Control, and Dynamics, 37 (2014) 1664-1671.

[125] C. Chieh-Li, C. Chung-Wei, Y. Her-Terng, Design of dynamic sliding mode controller to aeroelastic systems, Applied Mathematics & Information Sciences, 6 (2012) 89-98.

[126] B.-H. Lee, J.-h. Choo, S. Na, P. Marzocca, L. Librescu, Sliding mode robust control of supersonic three degrees-of-freedom airfoils, International Journal of Control, Automation and Systems, 8 (2010) 279-288.

[127] S. Gujjula, S.N. Singh, Variable structure control of unsteady aeroelastic system with partial state information, Journal of Guidance, Control, and Dynamics, 28 (2005) 568-573.

[128] X. Wei, J.E. Mottershead, Y.M. Ram, Partial pole placement by feedback control with inaccessible degrees of freedom, Mechanical Systems and Signal Processing, (submitted) (2015).

[129] X. Wei, J.E. Mottershead, Block-decoupling vibration control using eigenstructure assignment, Mechanical Systems and Signal Processing, In press (2015).

[130] G. Strang, T. Nguyen, The interplay of ranks of submatrices, SIAM Review, 46 (2004) 637-646.

[131] X. Wei, J.E. Mottershead, Aeroelastic systems with softening nonlinearity, AIAA Journal, 52 (2014) 1915-1927.

[132] J.R. Wright, J.E. Cooper, Introduction to aircraft aeroelasticity and loads, John Wiley, Chichester, 2007.

[133] S.F. Shen, An approximate analysis of nonlinear flutter problems, Journal of the Aerospace Sciences 26 (1959) 25-32.

[134] J. Dormand, P. Prince, A family of embedded Runge-Kutta formulae, Journal of Computational and Applied Mathematics, 6 (1980) 19-26.

[135] J.M.T. Thompson, H.B. Stewart, Nonlinear dynamics and chaos: geometrical methods for engineers and scientists, Wiley, Chichester, 1986.

[136] S.J. Price, H. Alighanbari, B.H.K. Lee, The aeroelastic response of a two-dimensional airfoil with bilinear and cubic structural nonlinearities, Journal of Fluids and Structures, 9 (1995) 175-193.

[137] F.C. Moon, Chaotic vibrations: an introduction for applied scientists and engineers, Wiley, New York, 1987.

[138] I. Shimada, T. Nagashima, A numerical approach to ergodic problem of dissipative dynamical systems, Progress of Theoretical Physics, 61 (1979) 1605-1616.

[139] G. Benettin, L. Galgani, A. Giorgilli, J.-M. Strelcyn, Lyapunov Characteristic Exponents for smooth dynamical systems and for hamiltonian systems; A method for computing all of them. Part 2: Numerical application, Meccanica, 15 (1980) 21-30.

[140] A. Dhooge, W. Govaerts, Y.A. Kuznetsov, MATCONT : A MATLAB package for numerical bifurcation analysis of ODEs, ACM Transactions on Mathematical Software, 29 (2003) 141.

[141] G. Dimitriadis, Shooting-based complete bifurcation prediction for aeroelastic systems with freeplay, Journal of Aircraft, 48 (2011) 1864-1877.

[142] R. Seydel, Practical bifurcation and stability analysis, 3rd ed., Springer, New York, 2010.

[143] Y.A. Kuznetsov, Elements of applied bifurcation theory, Springer, New York, 1998.

[144] Y.C. Fung, An introduction to the theory of aeroelasticity, Wiley, New York, 1955.

[145] C.I. Byrnes, A. Isidori, J.C. Willems, Passivity, feedback equivalence, and the global stabilization of minimum phase nonlinear systems, Automatic Control, IEEE Transactions on, 36 (1991) 1228-1240.

[146] K.D. Young, V.I. Utkin, U. Ozguner, A control engineer's guide to sliding mode control, IEEE Transactions on Control Systems Technology, 7 (1999) 328-342.

[147] W. Lin, T. Shen, Robust passivity and feedback design for minimum-phase nonlinear systems with structureal uncertainty, Automatica, 35 (1999) 35-47.

[148] X. Wei, J.E. Mottershead, Robust passivity-based continuous sliding-mode control for under-actuated nonlinear wing sections, Journal of Guidance, Control, and Dynamics, (submitted) (2015).

[149] C.C. Rasmussen, R.A. Canfield, M. Blair, Joined-wing sensor-craft configuration design, Journal of Aircraft, 43 (2006) 1470-1478.